

U.S. DEPARTMENT OF COMMERCE  
National Technical Information Service

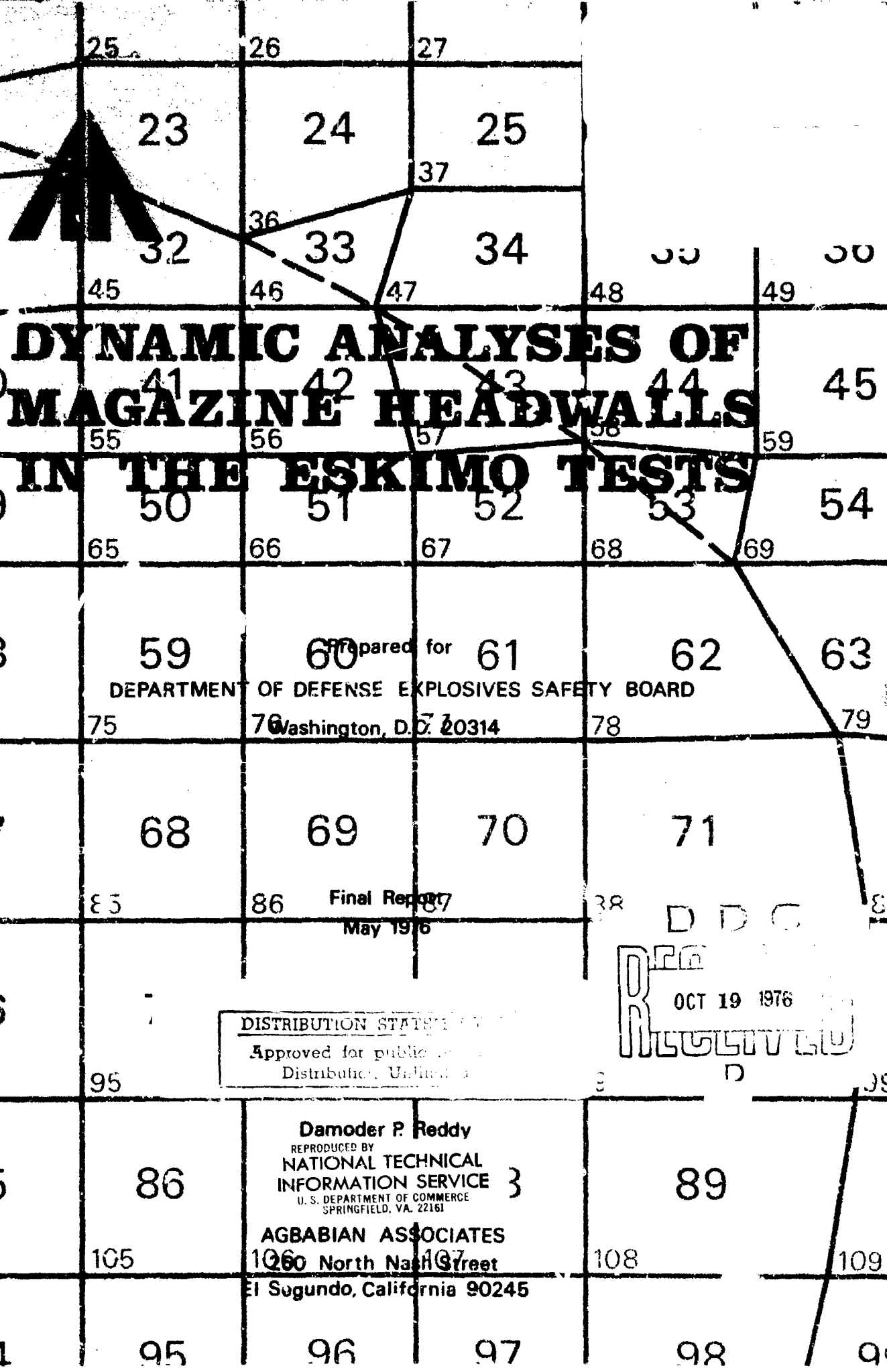
AD-A030 885

DYNAMIC ANALYSES OF MAGAZINE HEADWALLS  
IN THE ESKIMO TESTS

AGBABIAN ASSOCIATES,  
EL SEGUNDO, CALIFORNIA

MAY 1976

AD A 030885  
294064



**DYNAMIC ANALYSES OF  
MAGAZINE HEADWALLS  
IN THE ESKIMO TESTS**

Prepared for  
DEPARTMENT OF DEFENSE EXPLOSIVES SAFETY BOARD  
Washington, D.C. 20314

Final Report  
May 1976

DDC  
OCT 19 1976  
RECEIVED

DISTRIBUTION STATEMENT  
Approved for public release  
Distribution Unlimited

**Damoder P. Reddy**  
REPRODUCED BY  
NATIONAL TECHNICAL  
INFORMATION SERVICE }  
U. S. DEPARTMENT OF COMMERCE  
SPRINGFIELD, VA. 22161  
**AGABIAN ASSOCIATES**  
1060 North North Street  
El Segundo, California 90245



SECURITY CLASSIFICATION OF THIS PAGE (When Data Entered)

| REPORT DOCUMENTATION PAGE   |                       | READ INSTRUCTIONS<br>BEFORE COMPLETING FORM  |
|---|-----------------------|--|
| 1. REPORT NUMBER<br>R-7556-1-4182   | 2. GOVT ACCESSION NO. | 3. RECIPIENT'S CATALOG NUMBER  |
| 4. TITLE (and Subtitle)<br>Dynamic Analyses of Magazine Headwalls<br>in the ESKIMO Tests  |                       | 5. TYPE OF REPORT & PERIOD COVERED<br>FINAL<br>May 1975 to May 1976                  |
|   |                       | 6. PERFORMING ORG. REPORT NUMBER<br>R-7556-1-4182                                    |
| 7. AUTHOR(s)<br>Ramoder P. Reddy  |                       | 8. CONTRACT OR GRANT NUMBER(s)<br>DAAB09-75-C-0025                                   |
| 9. PERFORMING ORGANIZATION NAME AND ADDRESS<br>Agbabian Associates<br>250 N. Nash Street<br>El Segundo, California 90245  |                       | 10. PROGRAM ELEMENT, PROJECT, TASK<br>AREA & WORK UNIT NUMBERS<br>RDT&E 4A765J02M857 |
| 11. CONTROLLING OFFICE NAME AND ADDRESS<br>Department of Defense Explosives Safety Board<br>Washington, D.C. 20314  |                       | 12. REPORT DATE<br>May 1976  |
|   |                       | 13. NUMBER OF PAGES<br>214   |
| 14. MONITORING AGENCY NAME & ADDRESS (if different from Controlling Office)   |                       | 15. SECURITY CLASS. (of this report)<br>Unclassified                                 |
|   |                       | 15a. DECLASSIFICATION/DOWNGRADING<br>SCHEDULE  |
| 16. DISTRIBUTION STATEMENT (of this Report)<br><br>Approved for public release; distribution unlimited.   |                       |  |
| 17. DISTRIBUTION STATEMENT (of the abstract entered in Block 20, if different from Report)  |                       |  |
| 18. SUPPLEMENTARY NOTES   |                       |  |
| 19. KEY WORDS (Continue on reverse side if necessary and identify by block number)<br>Magazine Headwall Response      Nonlinear Finite Element<br>Dynamic Finite Element          ESKIMO Test<br>Nonlinear Slabs                    Igloo Storage Magazine<br>Explosive Blast                    Nonlinear Soils  |                       |  |
| 20. ABSTRACT (Continue on reverse side if necessary and identify by block number)<br><br>This report describes the results of dynamic response analyses of magazine headwalls in three tests, namely, ESKIMO I, II, and IV. The finite element models of the headwalls were subjected to blast loadings selected on the basis of measured data and theoretical investigations. The responses of the headwalls were obtained using the INSLAB code, a nonlinear, dynamic finite element computer program. The behavior of the headwall material was described by a bilinear<br><br>(continued on other side) |                       |  |

## 20. ABSTRACT (continue.)

moment-curvature relationship, and the supporting soil was simulated by a series of nonlinear springs and linear dampers. The results of the calculations were compared with available test data. In general, the predicted behavior of the headwalls agreed very well with their observed behavior. The present analysis of the south headwall in ESKIMO I, using the refined finite element mesh, showed better agreement with the test results than those from the previous analysis, which used a coarse mesh. The results for the east headwall, ESKIMO II, showed that the computed permanent displacement contours are quite similar in shape to those measured. The results for the northeast headwall, ESKIMO III, indicated that the concrete beams around the doorway were effective in reducing the maximum displacement of the headwall and that the biparting and sliding type of door was superior to the double-leaf and hinged type for resisting blast loads. The computed motions of the northeast headwall, ESKIMO IV, compared very well with the corresponding test data.



R-7556-1-4182

## PREFACE

This technical report is submitted by Agbabian Associates as part of the work required under Contract No. DAAB09-75-C-0025 with the Department of Defense Explosives Safety Board. Project Manager for Agbabian Associates and Principal Investigator for the preparation of this report is D. P. Reddy. Major contributions to the study have been made by D. Van Dillen, H. S. Ts'ao, B. Barclay, and J. W. Workman of the Agbabian Associates staff. Technical monitor of the contract for the Department of Defense Explosives Safety Board is Dr. T. A. Zaker.



## SUMMARY

This report describes the results of dynamic response analyses of magazine headwalls in three tests, namely, ESKIMO I, II, and IV. The finite element models of the headwalls were subjected to blast loadings selected on the basis of measured data and theoretical investigations. The responses of the headwalls were obtained using the INSLAB code, a nonlinear, dynamic finite element computer program. The behavior of the headwall material was described by a bilinear moment-curvature relationship, and the supporting soil was simulated by a series of nonlinear springs and linear dampers. The results of the calculations were compared with available test data. In general, the predicted behavior of the headwalls agreed very well with their observed behavior. The present analysis of the south headwall in ESKIMO I, using the refined finite element mesh, showed better agreement with the test results than those from the previous analysis, which used a coarse mesh. The results for the east headwall, ESKIMO II, showed that the computed permanent displacement contours are quite similar in shape to those measured. The results for the northeast headwall, ESKIMO II, indicated that the concrete beams around the doorway were effective in reducing the maximum displacement of the headwall and that the biparting and sliding type of door was superior to the double-leaf and hinged type for resisting blast loads. The computed motions of the northeast headwall, ESKIMO IV, compared very well with the corresponding test data.



## CONTENTS

| <u>Section</u> |  | <u>Page</u> |
|----------------|--|-------------|
| 1              | INTRODUCTION AND BACKGROUND . . . . .  | 1           |
|                | 1.1 Description of ESKIMO I Test . . . . .                                   | 1           |
|                | 1.2 Description of ESKIMO II Test . . . . .                                  | 7           |
|                | 1.3 Description of ESKIMO III Test . . . . .                                 | 10          |
|                | 1.4 Description of ESKIMO IV Test . . . . .                                  | 12          |
|                | 1.5 Objectives and Scope . . . . .   | 16          |
| 2              | PRESSURE LOADING ON HEADWALLS . . . . .                                      | 17          |
|                | 2.1 Pressure Histories for ESKIMO I Test . . . . .                           | 17          |
|                | 2.2 Pressure Histories for ESKIMO II Test . . . . .                          | 20          |
|                | 2.3 Pressure Loading History for ESKIMO IV Test . . . . .                    | 22          |
| 3              | STRUCTURAL MODEL OF HEADWALL AND DOOR SYSTEM . . . . .                       | 31          |
|                | 3.1 Structural Model, ESKIMO I Test . . . . .                                | 31          |
|                | 3.2 Structural Models of Headwalls in ESKIMO II . . . . .                    | 58          |
|                | 3.3 Structural Model of Igloo B (Northeast)<br>Headwall, ESKIMO IV . . . . . | 64          |
| 4              | INSTRUMENTATION FOR ESKIMO IV . . . . .                                      | 71          |
|                | 4.1 Pressure Gages . . . . .   | 71          |
|                | 4.2 Accelerometers . . . . .   | 75          |
|                | 4.3 Linear Motion Transducers . . . . .                                      | 75          |
| 5              | DYNAMIC RESPONSE OF HEADWALLS IN ESKIMO TESTS . . . . .                      | 79          |
|                | 5.1 Introduction . . . . .   | 79          |
|                | 5.2 Response of South Headwall, ESKIMO I . . . . .                           | 79          |
|                | 5.3 Response of East Headwall, ESKIMO II . . . . .                           | 89          |
|                | 5.4 Response of Northeast Headwall, ESKIMO II . . . . .                      | 93          |
|                | 5.5 Response of Northeast Headwall, ESKIMO IV . . . . .                      | 99          |



## CONTENTS (CONTINUED)

| <u>Section</u>  |  | <u>Page</u> |
|-----------------|--|-------------|
| 6               | CONCLUSIONS AND RECOMMENDATIONS . . . . .  | 181         |
| 6.1             | Conclusions . . . . .  | 181         |
| 6.2             | Recommendations . . . . .  | 183         |
| 7               | REFERENCES . . . . .   | 185         |
| <u>Appendix</u> |  |             |
| A               | INCLUSION OF NONLINEAR SPRINGS IN INSLAB CODE . .  | 187         |
| B               | PROCEDURE FOR CALCULATING YIELD MOMENTS FOR A<br>REINFORCED-CONCRETE SECTION . . . . .   | 195         |
| C               | PROCEDURE FOR COMPUTING EQUIVALENT MODULI FOR<br>A REINFORCED CONCRETE SECTION . . . . . | 199         |

## ILLUSTRATIONS

| <u>Figure</u> |   |    |
|---------------|---|----|
| 1-1           | Layout of Test Structures for ESKIMO I . . . . .                                  | 3  |
| 1-2           | Steel-Arch, Earth-Mounded Igloo Storage . . . . .                                 | 4  |
| 1-3           | Layout of Test Structures for ESKIMO II Magazine<br>Separation Test . . . . .     | 8  |
| 1-4           | Layout of Test Structures for ESKIMO III Magazine<br>Separation Test . . . . .    | 13 |
| 1-5           | Layout of Test Structures for ESKIMO IV Magazine<br>Separation Test . . . . .     | 15 |
| 2-1           | Reflected Overpressure on South Igloo, ESKIMO I .                                 | 18 |
| 2-2           | Headwall Blast-Pressure Loading Zones,<br>ESKIMO I . . . . .                      | 19 |
| 2-3           | Proposed Pressure Histories for Northeast and<br>East Igloos, ESKIMO II . . . . . | 21 |



## CONTENTS (CONTINUED)

| <u>Figure</u> |   | <u>Page</u> |
|---------------|---|-------------|
| 2-4           | Placement of Pressure Gages, Igloo B (Northeast Igloo) of ESKIMO IV . . . . .   | 23          |
| 2-5           | Comparison of Pressure Histories for a Vertical Array of Gages, Igloo B of ESKIMO IV . . . . .  | 25          |
| 2-6           | Comparison of Pressure Histories to Test Uniformity of Pressure Loading across Width of Headwall, Igloo B of ESKIMO IV . . . . .                              | 26          |
| 2-7           | Free-Field Ground Level and Reflected Headwall Pressure Pulses for Analysis of Igloo B, ESKIMO IV . . . . .   | 27          |
| 2-8           | Comparison of Pressure Histories for a Vertical Array of Gages with the Proposed Loading Pulse for Response Analysis of Igloo B, ESKIMO IV . . . . .          | 28          |
| 2-9           | Comparison of Headwall Pressure Pulse for Analysis of Igloo B (ESKIMO IV) with Estimated Reflected Pulse and Measured Free-Field Ground Level Pulse . . . . . | 29          |
| 3-1           | Coarse Finite Element Model of South Headwall, ESKIMO I . . . . .   | 32          |
| 3-2           | Refined Finite Element Model of South Headwall, ESKIMO I . . . . .  | 33          |
| 3-3           | Door Details for South igloo, ESKIMO I . . . . .  | 36          |
| 3-4           | Details of Headwall Construction for South Igloo, ESKIMO I . . . . .  | 37          |
| 3-5           | Dynamic Stiffness of Soil . . . . .   | 41          |
| 3-6           | Test Problems to Determine a Suitable Model to Represent Soil . . . . .   | 44          |
| 3-7           | Case A: Displacement-Time Histories of the Headwall . . . . .   | 45          |
| 3-8           | Case B: Displacement-Time Histories of the Headwall . . . . .   | 46          |



## CONTENTS (CONTINUED)

| <u>Figure</u> |  | <u>Page</u> |
|---------------|--|-------------|
| 3-9           | Case B: Velocity-Time Histories of the Headwall  | 47          |
| 3-10          | Case C: Displacement-Time Histories of the Headwall . . . . .                                  | 48          |
| 3-11          | Case C: Velocity-Time Histories of the Headwall  | 49          |
| 3-12          | Axial Stiffness of Steel Arch . . . . .  | 53          |
| 3-13          | Movement of Headwall of North Acceptor Igloo, ESKIMO I . . . . .                               | 56          |
| 3-14          | Headwall of North Igloo, ESKIMO I . . . . .  | 57          |
| 3-15          | Igloo C (Northeast) Headwall, ESKIMO II . . . . .  | 59          |
| 3-16          | Finite Element Mesh of Igloo B (Northeast) Headwall, ESKIMO II . . . . .                       | 61          |
| 3-17          | Configuration of Steel Door for Igloo B (Northeast), ESKIMO II . . . . .                       | 63          |
| 3-18          | Finite Element Model of Northeast Headwall, ESKIMO IV . . . . .                                | 65          |
| 3-19          | Configuration of Steel Door for Igloo B (Northeast) Headwall, ESKIMO IV . . . . .              | 67          |
| 3-20          | Regions of Different Material Properties for Igloo B (Northeast) Headwall, ESKIMO IV . . . . . | 68          |
| 4-1           | Placement of Pressure Gages on Northeast (B) Igloo, ESKIMO IV . . . . .                        | 73          |
| 4-2           | Placement of Pressure Gages on East (D) and West (E) Igloos, ESKIMO IV . . . . .               | 74          |
| 4-3           | Placement of Accelerometers on Headwall of Northeast Igloo, ESKIMO IV . . . . .                | 76          |
| 4-4           | Placement of LVDT Transducers on Headwall of Northeast Igloo, ESKIMO IV . . . . .              | 78          |



## CONTENTS (CONTINUED)

| <u>Figure</u> |   | <u>Page</u> |
|---------------|---|-------------|
| 5-1           | Computed Motion of South and West Igloos at Node 1 . . . . .                                  | 107         |
| 5-2           | Computed Motion of South and West Igloos at Node 19 . . . . .                                 | 108         |
| 5-3           | Computed Motion of South and West Igloos at Node 46 . . . . .                                 | 109         |
| 5-4           | Computed Motion of South and West Igloos at Node 49 . . . . .                                 | 110         |
| 5-5           | Computed Motion of South and West Igloos at Node 50 . . . . .                                 | 111         |
| 5-6           | Computed Motion of South and West Igloos at Node 73 . . . . .                                 | 112         |
| 5-7           | Computed Motion of South and West Igloos at Node 76 . . . . .                                 | 113         |
| 5-8           | Computed Motion of South and West Igloos at Node 77 . . . . .                                 | 114         |
| 5-9           | Computed Motion of South and West Igloos at Node 100 . . . . .                                | 115         |
| 5-10          | Computed Displacements along Edges of Headwalls of South and West Igloos . . . . .            | 116         |
| 5-11          | Computed Displacements along ^ . h Line of Headwalls of South and West Igloos . . . . .       | 117         |
| 5-12          | Computed Displacement at Ground Level of Several Locations on South and West Igloos . . . . . | 118         |
| 5-13          | Computed Motion from Prior Calculation Corresponding to Node 1 . . . . .                      | 119         |
| 5-14          | Computed Motion from Prior Calculation Corresponding to Node 19 . . . . .                     | 120         |
| 5-15          | Computed Motion from Prior Calculation Corresponding to Node 77 . . . . .                     | 121         |



## CONTENTS (CONTINUED)

| <u>Figure</u> |   | <u>Page</u> |
|---------------|---|-------------|
| 5-16          | Computed Motion from Prior Calculation<br>Corresponding to Node 46 . . . . .  | 122         |
| 5-17          | Computed Motion from Prior Calculation<br>Corresponding to Node 49 . . . . .  | 123         |
| 5-18          | Computed Motion from Prior Calculation<br>Corresponding to Node 76 . . . . .  | 124         |
| 5-19          | Computed Motion from Prior Calculation<br>Corresponding to Node 73 . . . . .  | 125         |
| 5-20          | Computed Motion from Prior Calculation<br>Corresponding to Node 103 . . . . .   | 126         |
| 5-21          | Movement of Headwall of South Acceptor Igloo . .  | 127         |
| 5-22          | Movement of Headwall of West Acceptor Igloo . . .   | 127         |
| 5-23          | Computed Displacements (in hundredths of a foot)<br>of the Headwalls of the South and West Igloos,<br>ESKIMO I, 0.22 Sec after Arrival of the Blast<br>Wave . . . . .           | 128         |
| 5-24          | Computed Displacements (in hundredths of a foot)<br>with a Rigid Body Displacement of 0.25 Ft Added<br>in for the Sake of Comparison with the West<br>Igloo, ESKIMO I . . . . . | 129         |
| 5-25          | Computed Displacements (in hundredths of a foot)<br>of the Headwalls of the South and West Igloos,<br>ESKIMO I, 0.22 Sec after Arrival of the Blast . .                         | 130         |
| 5-26          | Computed Motion of East Headwall (ESKIMO II) at<br>Node 1 . . . . .   | 131         |
| 5-27          | Computed Motion of East Headwall (ESKIMO II) at<br>Node 9 . . . . .   | 132         |
| 5-28          | Computed Motion of East Headwall (ESKIMO II) at<br>Node 19 . . . . .  | 133         |
| 5-29          | Computed Motion of East Headwall (ESKIMO II) at<br>Node 21 . . . . .  | 134         |



## CONTENTS (CONTINUED)

| <u>Figure</u> |   | <u>Page</u> |
|---------------|---|-------------|
| 5-30          | Computed Motion of East Headwall (ESKIMO II) at Node 46 . . . . .           | 135         |
| 5-31          | Computed Motion of East Headwall (ESKIMO II) at Node 49 . . . . .           | 136         |
| 5-32.         | Computed Motion of East Headwall (ESKIMO II) at Node 50 . . . . .           | 137         |
| 5-33          | Computed Motion of East Headwall (ESKIMO II) at Node 73 . . . . .           | 138         |
| 5-34          | Computed Motion of East Headwall (ESKIMO II) at Node 76 . . . . .           | 139         |
| 5-35          | Computed Motion of East Headwall (ESKIMO II) at Node 77 . . . . .           | 140         |
| 5-36          | Computed Motion of East Headwall (ESKIMO II) at Node 103 . . . . .          | 141         |
| 5-37          | Permanent Displacement Contours of East Headwall, ESKIMO II . . . . .       | 142         |
| 5-38          | Computed Displacement Contours of East Headwall at $t = 145$ msec . . . . . | 143         |
| 5-39 .        | Computed Displacement Contours of East Headwall at $t = 157$ msec . . . . . | 144         |
| 5-40          | Computed Motion of Northeast Igloo (ESKIMO II) at Node 9 . . . . .          | 145         |
| 5-41          | Computed Motion of Northeast Igloo (ESKIMO II) at Node 16 . . . . .         | 146         |
| 5-42          | Computed Motion of Northeast Igloo (ESKIMO II) at NODE 22 . . . . .         | 147         |
| 5-43          | Computed Motion of Northeast Igloo (ESKIMO II) at Node 39 . . . . .         | 148         |
| 5-44          | Computed Motion of Northeast Igloo (ESKIMO II) at Node 42 . . . . .         | 149         |



## CONTENTS (CONTINUED)

| <u>Figure</u> |  | <u>Page</u> |
|---------------|--|-------------|
| 5-45          | Computed Motion of Northeast Igloo (ESKIMO II) at Node 45 . . . . .                            | 150         |
| 5-46          | Computed Motion of Northeast Igloo (ESKIMO II) at Node 60 . . . . .                            | 151         |
| 5-47          | Computed Motion of Northeast Igloo (ESKIMO II) at Node 72 . . . . .                            | 152         |
| 5-48          | Computed Motion of Northeast Igloo (ESKIMO II) at Node 75 . . . . .                            | 153         |
| 5-49          | Computed Motion of Northeast Igloo (ESKIMO II) at Node 77 . . . . .                            | 154         |
| 5-50          | Computed Motion of Northeast Igloo (ESKIMO II) at Node 79 . . . . .                            | 155         |
| 5-51          | Computed Motion of Northeast Igloo (ESKIMO II) at Node 81 . . . . .                            | 156         |
| 5-52          | Computed Motion of Northeast Igloo (ESKIMO II) at Node 101 . . . . .                           | 157         |
| 5-53          | Computed Motion of Northeast Igloo (ESKIMO II) at Node 105 . . . . .                           | 158         |
| 5-54          | Computed Motion of Northeast Igloo (ESKIMO II) at Node 108 . . . . .                           | 159         |
| 5-55          | Computed Motion of Northeast Igloo (ESKIMO II) at Node 115 . . . . .                           | 160         |
| 5-56          | Permanent Movements of Northeast Headwall of ESKIMO II as Measured (in hundredths of feet) . . | 161         |
| 5-57          | Computed Permanent Displacements of Northeast Headwall of ESKIMO III (in hundredths of feet) . | 162         |
| 5-58          | Computed Motion of Northeast Igloo (ESKIMO IV) at Node 21 . . . . .                            | 163         |
| 5-59          | Computed Motion of Northeast Igloo (ESKIMO IV) at Node 24 . . . . .                            | 164         |



## CONTENTS (CONTINUED)

| <u>Figure</u> |   | <u>Page</u> |
|---------------|---|-------------|
| 5-60          | Computed Motion of Northeast Igloo (ESKIMO IV) at Node 61 . . . . .   | 165         |
| 5-61          | Computed Motion of Northeast Igloo (ESKIMO IV) at Node 64 . . . . .   | 166         |
| 5-62          | Computed Motion of Northeast Igloo (ESKIMO IV) at Node 69 . . . . .   | 167         |
| 5-63          | Computed Motion of Northeast Igloo (ESKIMO IV) at Node 91 . . . . .   | 168         |
| 5-64          | Computed Motion of Northeast Igloo (ESKIMO IV) at Node 94 . . . . .   | 169         |
| 5-65          | Computed Motion of Northeast Igloo (ESKIMO IV) at Node 97 . . . . .   | 170         |
| 5-66          | Computed Motion of Northeast Igloo (ESKIMO IV) at Node 99 . . . . .   | 171         |
| 5-67          | Computed Motion of Northeast Igloo (ESKIMO IV) at Node 119 . . . . .  | 172         |
| 5-68          | Computed Motion of Northeast Igloo (ESKIMO IV) at Node 121 . . . . .  | 173         |
| 5-69          | Computed Motion of Northeast Igloo (ESKIMO IV) at Node 124 . . . . .  | 174         |
| 5-70          | Measured Permanent Displacement Contours of Northeast Headwall of ESKIMO IV (in hundredths of feet) . . . . .   | 175         |
| 5-71          | Computed Displacement Contours of Northeast Headwall of ESKIMO IV at 158 msec (in hundredths of feet) . . . . . | 176         |
| 5-72          | Measured Acceleration Time Histories of Northeast Headwall of ESKIMO IV . . . . .                               | 177         |
| 5-73          | Measured Displacement Time Histories of Northeast Headwall in ESKIMO IV . . . . .                               | 179         |



## CONTENTS (CONTINUED)

## TABLES

| <u>Table</u> |  | <u>Page</u> |
|--------------|--|-------------|
| 1-1          | Details of Igloos in ESKIMO II . . . . .   | 9           |
| 1-2          | Details of Igloos in ESKIMO III . . . . .  | 11          |
| 3-1          | Comparison of Coarse and Refined Finite Element Meshes . . . . .                         | 34          |
| 3-2          | Soil Stiffness from Test in North Igloo . . . . .  | 40          |
| 3-3          | Properties of Headwall and Wingwall Sections of Igloo B (Northeast), ESKIMO II . . . . . | 64          |
| 3-4          | Material Properties for Igloo B (Northeast) Headwall, ESKIMO IV . . . . .                | 69          |
| 4-1          | Schedule of Gages for Measurement of Air Blast, ESKIMO IV . . . . .                      | 72          |
| 4-2          | Schedule of Accelerometers for Northeast Igloo, ESKIMO IV . . . . .                      | 77          |
| 5-1          | Motion of South Headwall (ESKIMO I) above Center of Door . . . . .                       | 83          |
| 5-2          | Peak Velocities of Upper Corner of Door . . . . .  | 83          |
| 5-3          | Peak Deflection of Center of Doorway . . . . .   | 84          |
| 5-4          | Peak Acceleration of Base of Headwall . . . . .  | 85          |
| 5-5          | Motion of East Headwall (ESKIMO II) above Center of Doorway . . . . .                    | 92          |
| 5-6          | Computed Maximum and Permanent Displacement of Northeast Headwall, ESKIMO II . . . . .   | 95          |
| 5-7          | Comparison of Computed Maximum Displacements for ESKIMO II . . . . .                     | 96          |
| 5-8          | Motion of Northeast Headwall, ESKIMO II, above Center of Doorway . . . . .               | 98          |



## CONTENTS (CONCLUDED)

| <u>Table</u> |  | <u>Page</u> |
|--------------|--|-------------|
| 5-9          | Comparison of Maximum Displacements of Northeast Headwalls of ESKIMO II and ESKIMO IV Igloos . . . | 101         |
| 5-10         | Comparison of Maximum and Permanent Displacements of Northeast Igloo, ESKIMO IV . . . . .          | 104         |
| 5-11         | Comparison of Maximum Acceleration of Northeast Igloo, ESKIMO IV . . . . .                         | 106         |



## SECTION 1

## INTRODUCTION AND BACKGROUND

This report covers a part of a general program sponsored by the Department of Defense Explosives Safety Board (DDESB) to determine safe inter-magazine separation distances for various orientations of magazines for storing chemical explosives. The main objective of the program is to determine the minimum intermagazine separation distances so that an explosion in one magazine (donor) will not cause an explosion in an adjacent magazine (acceptor). This report describes a study to predict analytically the behavior of magazine headwalls and to compare analytical and test data.

Preliminary tests had indicated that specifications for minimum separation distances between magazines were excessively conservative for some orientations. Increasing land costs and siting problems made it desirable to justify reducing the rear-to-front separation distance. Earlier tests had indicated that earth-covered, steel-arch igloo magazines can be safely spaced side by side at a distance in feet of  $1.25 W^{1/3}$ , in which  $W$  is the weight in pounds of the high explosives in storage. On the other hand, very few test data had been developed for determining the minimum safe distances for other magazine orientations.

Starting in 1971, the DDESB sponsored a series of large-scale magazine explosion experiments, called the ESKIMO series, for the purpose of establishing minimum separation distances for earth-covered, steel-arch magazines. To date, four tests designated as ESKIMO I, ESKIMO II, ESKIMO III, AND ESKIMO IV have been conducted. These tests are described briefly in the following sections.

### 1.1 DESCRIPTION OF ESKIMO I TEST

ESKIMO I was a large-scale magazine explosion experiment conducted on 8 December 1971 at the Randsburg Wash Test Range of the Naval Weapons Center, China Lake, California. Four earth-covered, steel-arch magazines were exposed to the explosion of the contents of a similar magazine. The donor magazine



contained 200,000 lb of high explosives. The four acceptor igloos faced the donor and were located at various distances ranging from 73 ft to 161 ft, as shown in Figure 1-1. The distances 73 ft and 161 ft correspond to  $1.25 W^{1/3}$  and  $2.75 W^{1/3}$ , respectively, where  $W$  is the weight in pounds of the explosive in the donor magazine. Two concrete block structures simulating one particular type of Air Force aboveground magazine were also placed in the area at distances of 117 ft ( $2 W^{1/3}$ ) from the donor igloo, as shown in Figure 1-1.

The four acceptor steel-arch igloos were built in accordance with the standard drawing shown in Figure 1-2. Each of the igloos was 25 ft wide by 14 ft high, with the length limited to 20 ft. Steel wing walls were used in the test in lieu of concrete. The igloos were covered by a 90%-compacted earth surcharge to a depth of 2 ft at the top of the arch.

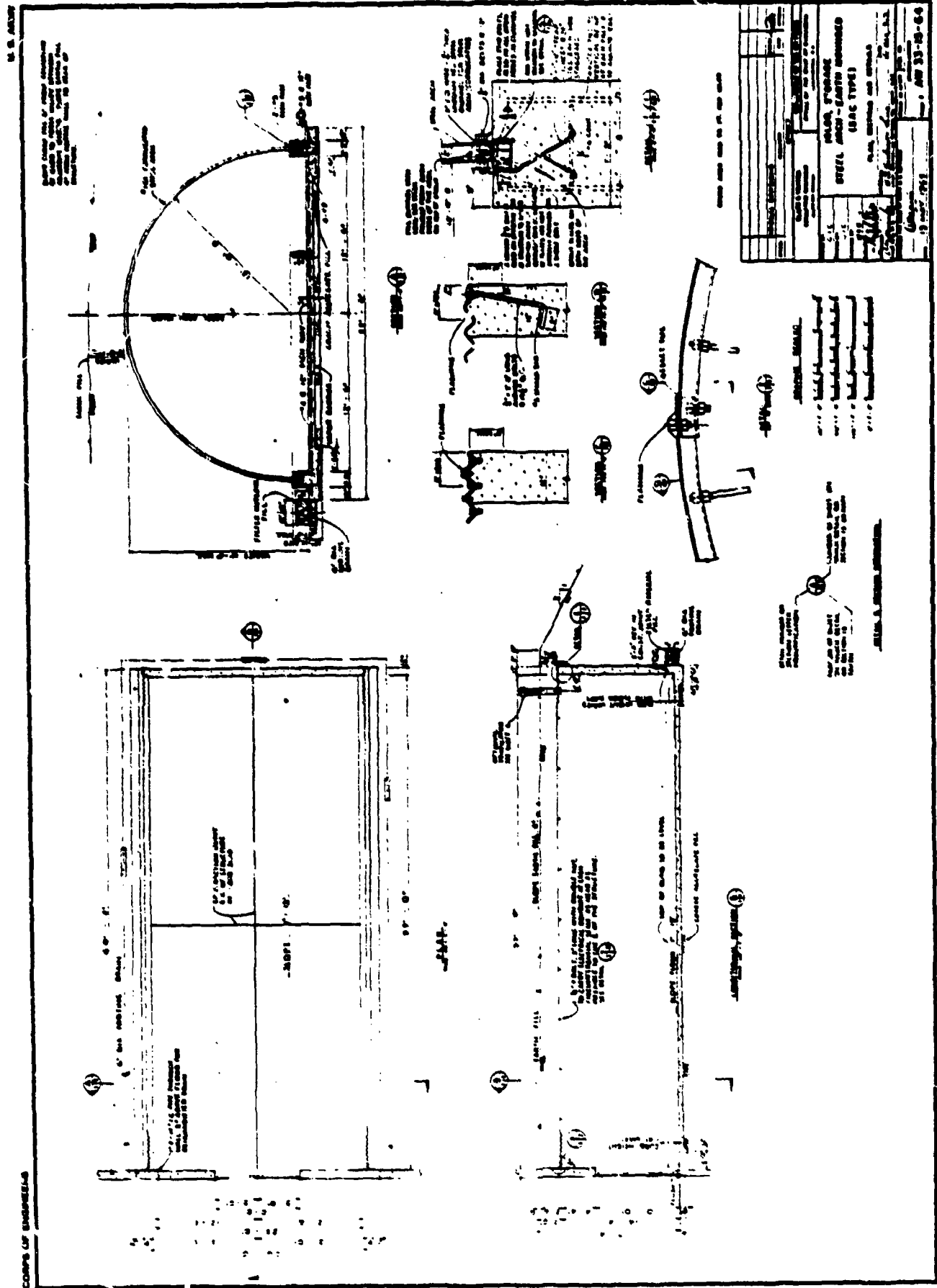
The primary objective of this test was to establish a safe, practicable minimum-separation distance between steel-arch magazines for face-on exposures. Another major objective of the test was to determine the fragment and debris hazard from mass detonation of explosive-filled projectiles in an earth-covered magazine.

The damage to structures varied from minor headwall damage at the south igloo to complete destruction of the concrete block structures. The status of the acceptor charges after the test indicated a range from no explosion or burning in the south igloo to complete explosion or detonation of all charges in the east igloo.

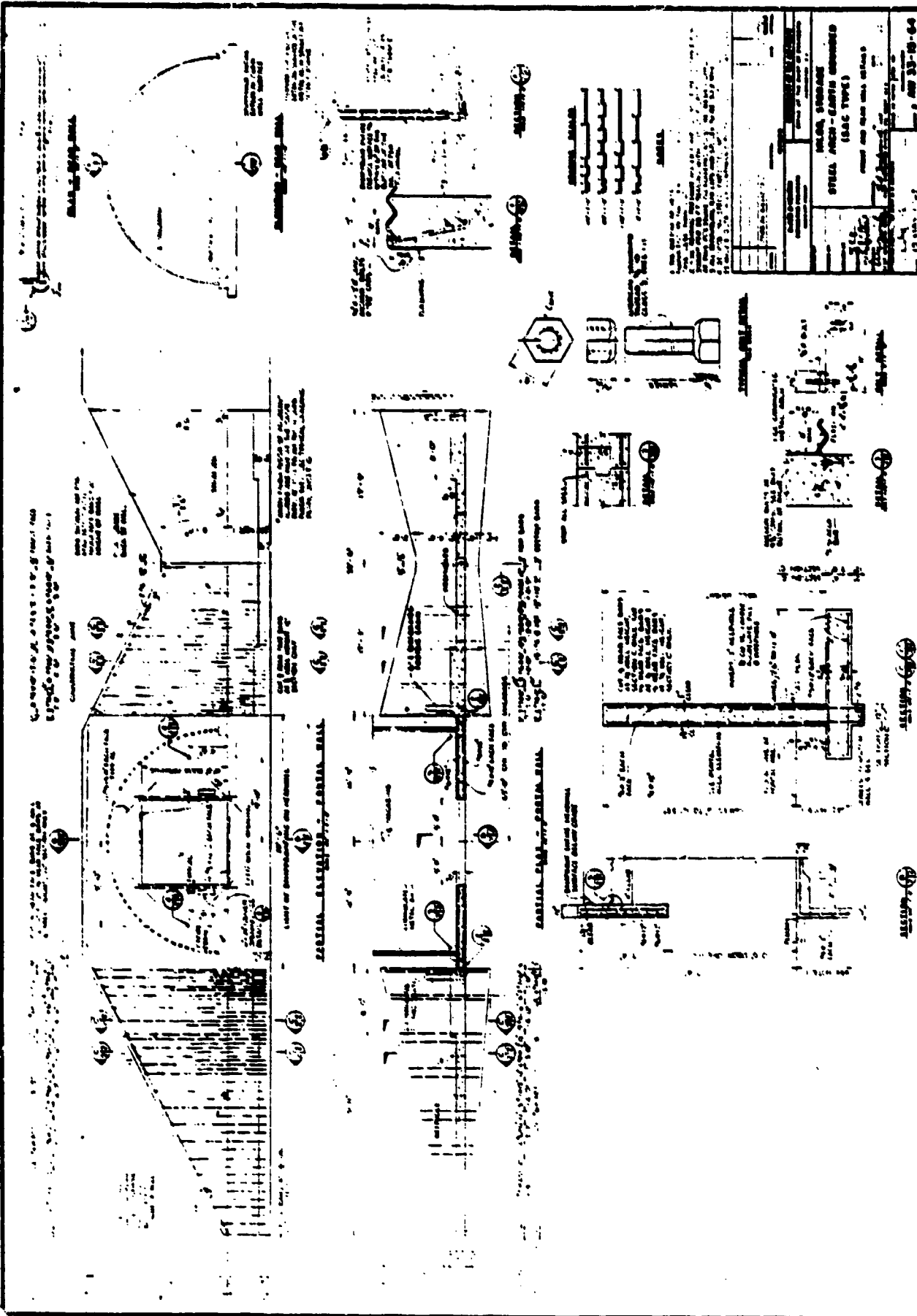
Permanent deflections of the order of several inches, accompanied by yield-line formation, have been noted in some of the surviving headwalls. On the other hand, photographic evidence indicates that the steel plate doors in the igloos were driven in with considerable velocity before coming to rest, while remaining partially attached to frames. In the forward exposure, complete failure of the hinges occurred, and the doors were driven violently against the rear wall of that magazine (20-ft depth, wall to wall).



Copy available to DDG does not permit fully legible reproduction



(a) Plan, sections, and details

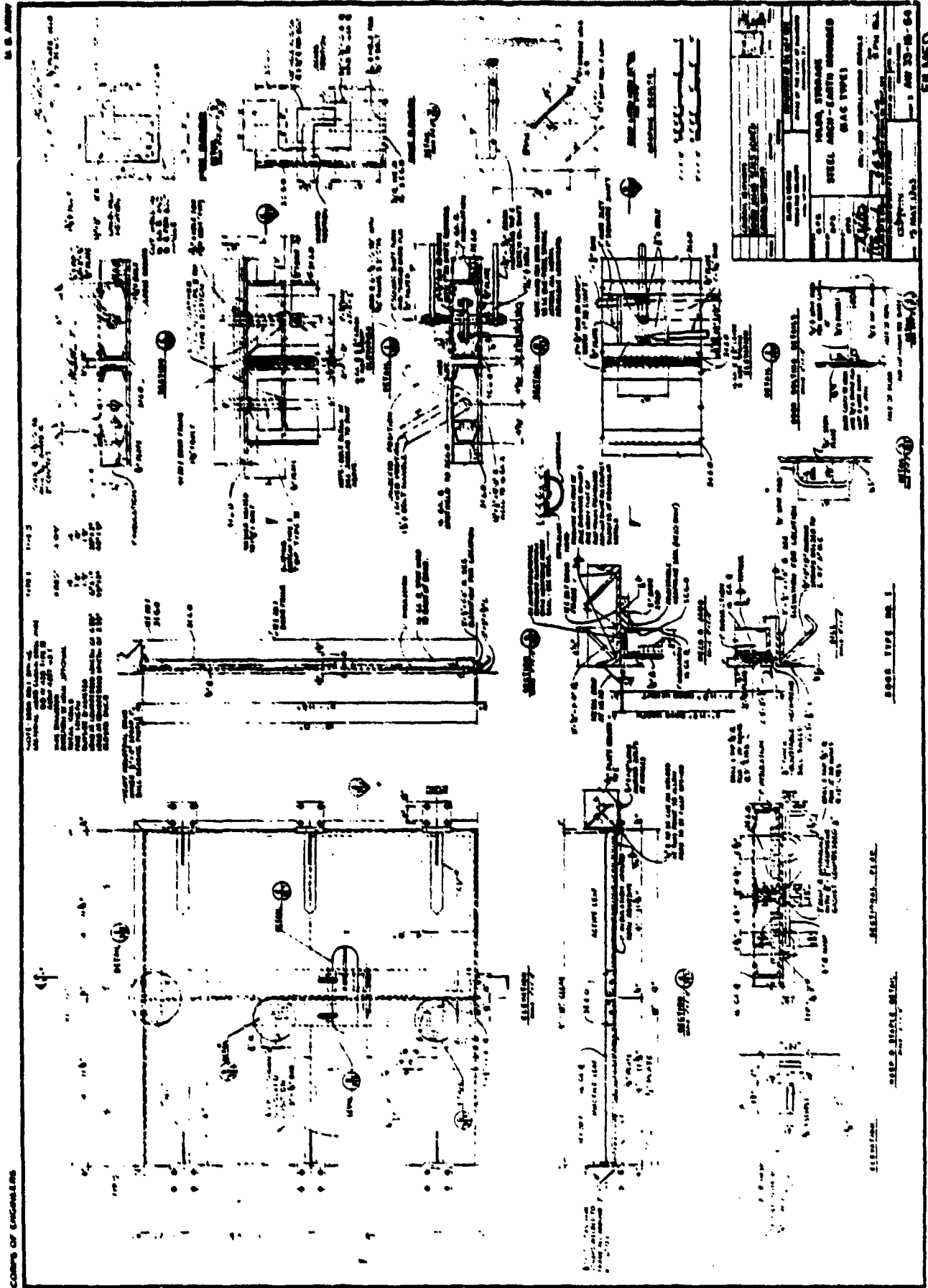


(b) Front and rear wall details

FIGURE 1-2. (CONTINUED)

Copy available to DDC does not permit fully legible reproduction

Copy available to DDC does not permit fully legible reproduction



(c) Door and miscellaneous details



Reference 1 includes a detailed description and the conclusions of the ESKIMO I test. Test results indicated that formerly applicable separation distances could be significantly reduced.

Agbabian Associates (AA) performed dynamic response analyses of the headwalls in the ESKIMO I test, using a finite element model of the headwall (Ref. 2). The analyses were performed with the INSLAB code, a nonlinear finite element computer program (Ref. 3). The objective of the analyses was to understand the behavior of the reinforced concrete headwalls subjected to blast loading and to use this knowledge in reducing reliance on full-scale proof testing.

## 1.2 DESCRIPTION OF ESKIMO II TEST

The ESKIMO II test was conducted on 22 May 1973 at the Randsburg Wash Test Range of the Naval Weapons Center, China Lake, California. Five earth-covered, steel-arch magazines were exposed face-on all at the same distance from the explosion source, as shown in Figure 1-3. The igloos to the north, south, and west were those remaining from the ESKIMO I test. However, the igloos to the south and west were fitted with new door designs. All the magazine structures were earth-covered, semicircular corrugated steel arches except the northeast igloo, which was constructed with a new type of noncircular steel arch. Table 1-1 shows details of all igloos in the ESKIMO II test.

The explosion source consisted of 72 tritonal-filled, 750-lb bombs in two triangular stacks, in base-to-base contact. This source, containing 27,000 lb of explosives, had an expected TNT equivalent weight of approximately 24,000 lb. The source was designed to produce an impulse load of 1100 psi msec on the headwalls of the test magazines located at 147 ft from the source. This was the value of impulse estimated to act on the lowest third of an acceptor igloo from explosion of an earth-covered magazine filled to capacity (i.e., 500,000 lb net explosive weight permitted in one igloo by the current standards) at a rear-to-front separation distance of  $2.0 \times W^{1/3}$ , or 159 ft, where  $W$  is the weight (lb) of charge in the magazine filled to capacity. Subsequently, however, free-field measurements made to the rear of the ESKIMO III donor magazine, and loadings observed in ESKIMO IV, have indicated an impulse load

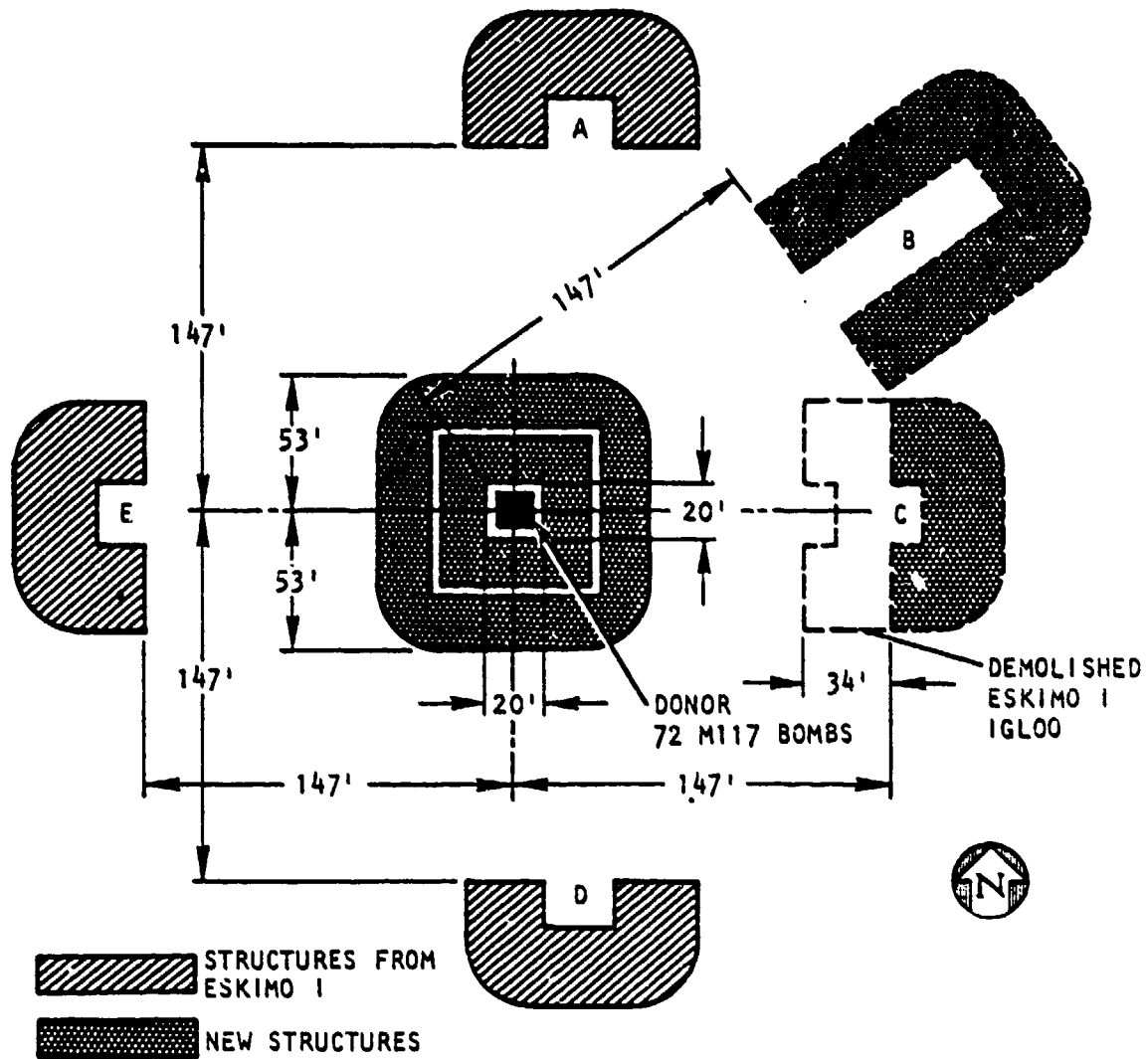


FIGURE 1-3. LAYOUT OF TEST STRUCTURES FOR ESKIMO I  
MAGAZINE SEPARATION TEST



TABLE 1-1. DETAILS OF IGLOOS IN ESKIMO II

| Igloo Designation | Position Relative to the Donor | Length, ft | New or Existing Construction | Type of Arch       | Headwall Type | Door Construction     |           |  |
|-------------------|--------------------------------|------------|------------------------------|--------------------|---------------|-----------------------|-----------|--|
|                   |                                |            |                              |                    |               | Nominal Door Size, ft | Door Type |  |
|                   |                                | Height     | Width                        |                    |               |                       |           |  |
| A                 | North                          | 20         | Remaining from ESKIMO I      | Semi-circular      | Navy Type II  | 10                    | 8         | Double leaf, hinged  |
| B                 | Northeast                      | 80         | New construction             | Noncircular (oval) | Stradley      | 10                    | 10        | 8parting, sliding  |
| C                 | East                           | 10         | New construction*            | Semi-circular      | Army Standard | 10                    | 10        | Double leaf, hinged  |
| D                 | South                          | 20         | Remaining from ESKIMO I      | Semi-circular      | Army Standard | 10                    | 10        | Single leaf, sliding                                       |
| E                 | West                           | 20         | Remaining from ESKIMO I      | Semi-circular      | Army Standard | 10                    | 10        | Double leaf, hinged, with removable steel beam reinforcing |

\*This igloo is identical in every respect to the igloos used in ESKIMO I.

AA 7584



of about 1200 psi msec from only 350,000 lb detonated in an igloo at this scaled distance. In ESKIMO IV, this level of loading was produced 147 ft from a bare TNT hemisphere weighing 37,000 lb.

Piezoelectric and strain-gage pressure transducers were positioned in and near the headwalls of the test magazines. Accelerometers and linear motion transducers were mounted on the doors and headwalls of the structures. Self-recording mechanical pressure gages were placed at distant stations. Door motions were observed by a high-speed camera in the interior of each of the magazines.

Because the near-field blast loading exceeded that planned, the igloo structures were subjected to an overtest. Despite this overtest, the large, single-leaf sliding door on Igloo D (south) withstood the blast loading without breakup or severe distortions. Likewise, the Stradley-type headwall used for Igloo B (northeast) incurred only an acceptable degree of damage. The test reaffirmed the need for achieving a balance in the strength of headwalls and doors.

Reference 4 includes a detailed description of the ESKIMO II test.

### 1.3 DESCRIPTION OF ESKIMO III TEST

The ESKIMO III test was conducted on 12 June 1974 at the Randsburg Wash Test Range of the Naval Weapons Center, China Lake, California. Five earth-covered, steel-arch magazines were exposed in the test to the explosion of the contents of a similar magazine, as shown in Figure 1-4. Igloos B, D, and E were those remaining from the ESKIMO II test. Igloo A and the donor magazine were new structures. Igloo A structure substituted a less expensive, light-gage, deep-corrugated arch in place of heavy structural plate; otherwise, it was identical to the standard steel-arch igloo. This igloo would furnish a test of the opinion that the earth cover is the most important factor in preventing explosion communication. In addition, this igloo was intended to provide a direct qualification test of the lightweight igloo. The donor magazine was built to the same specifications as Igloo A. Table 1-2 shows details of all igloos in the ESKIMO III test.



R-7556-1-4182

TABLE 1-2. DETAILS OF IGLOOS IN ESKIMO III

| Igloo Designation | New or Existing Construction | Type of Arch                               | Nominal Distance from Donor (W = Weight of Explosion Source in Pounds) | Exposure Type           | Door type  | Headwall Type           |
|-------------------|------------------------------|--|--|-------------------------|--|-------------------------|
| A                 | New                          | Semicircular, lightweight, deep-corrugated | $1.25 W^{1/3}$   | Side-to-side            | Two-leaf hinged  | Army Standard*          |
| B                 | Old, from ESKIMO II          | Oval                                       | $1.25 W^{1/3}$   | Side-to-side            | Refitted with single-leaf sliding, spanning horizontally | Modified Stradley-type† |
| C                 | Old, from 1963 test          | Semicircular                               | $2.75 W^{1/3}$   | Front-to-side           | Single-leaf sliding                                      | Army Standard*          |
| D                 | Old, from ESKIMO II          | Semicircular                               | $2.55 W^{1/3}$   | Side-to-side and angled | Two-leaf hinged  | Army Standard*          |
| E                 | Old, from ESKIMO I and II    | Semicircular                               | $3.70 W^{1/3}$   | Front-to-front          | Two-leaf hinged  | Army Standard*          |
| Donor             | New                          | Semicircular, lightweight, deep-corrugated | --   | --                      | Two-leaf hinged  | Army Standard*          |

AA 7585

1 Built to OCE Drawing 33-15-64

1 Built to OCE Drawing 33-15-73



The explosion source consisted of 350,000 lb of tritonal in 750-lb bombs in the donor igloo shown in Figure 1-4.

Incident peak pressure was measured at the ground surface in front of each acceptor igloo. Reflected peak pressure was measured from face-on blast gages set in each headwall. A row of surface gages measured the incident peak pressure over the earth on the oval arch igloo and on the light-gage circular arch magazine. Acceleration and displacement measurements were made on the arches of these igloos so that should they fail, the rapidity of failure could be used to estimate whether there would have been a risk of explosion communication to the contents. Detailed damage surveys and permanent displacement measurements were made after the test.

The main objective of the ESKIMO III test was to expose an earth-covered, noncircular, corrugated steel arch magazine (Igloo B) and a new circular, light-gage, deep-corrugated steel arch magazine (Igloo A) to explosion of an adjacent magazine at the minimum side-to-side spacing now permitted by standards. In addition, magazine headwall and door structures were tested at several other distances and orientations of interest.

A preliminary inspection of the structures after the test showed that the doors of Igloos A, B, D, and E were all blown open. The headwall of Igloo E experienced the most severe damage, and permanent inward displacements were as much as 1.5 ft. Except for local damage near one edge of the door opening, the headwall of Igloo D experienced generally slight damage. The remaining headwalls showed only minor damage. Additional details on the test are provided in Reference 5.

#### 1.4 DESCRIPTION OF ESKIMO IV TEST

The ESKIMO IV test was conducted on 10 September 1975, also at the Randsburg Wash Test Range, Naval Weapons Center, China Lake, California. Its principal objective was to demonstrate the resistance of a newly designed headwall-and-door combination to explosive blast loading from detonation of the contents of another magazine.



R-7556-1-4182

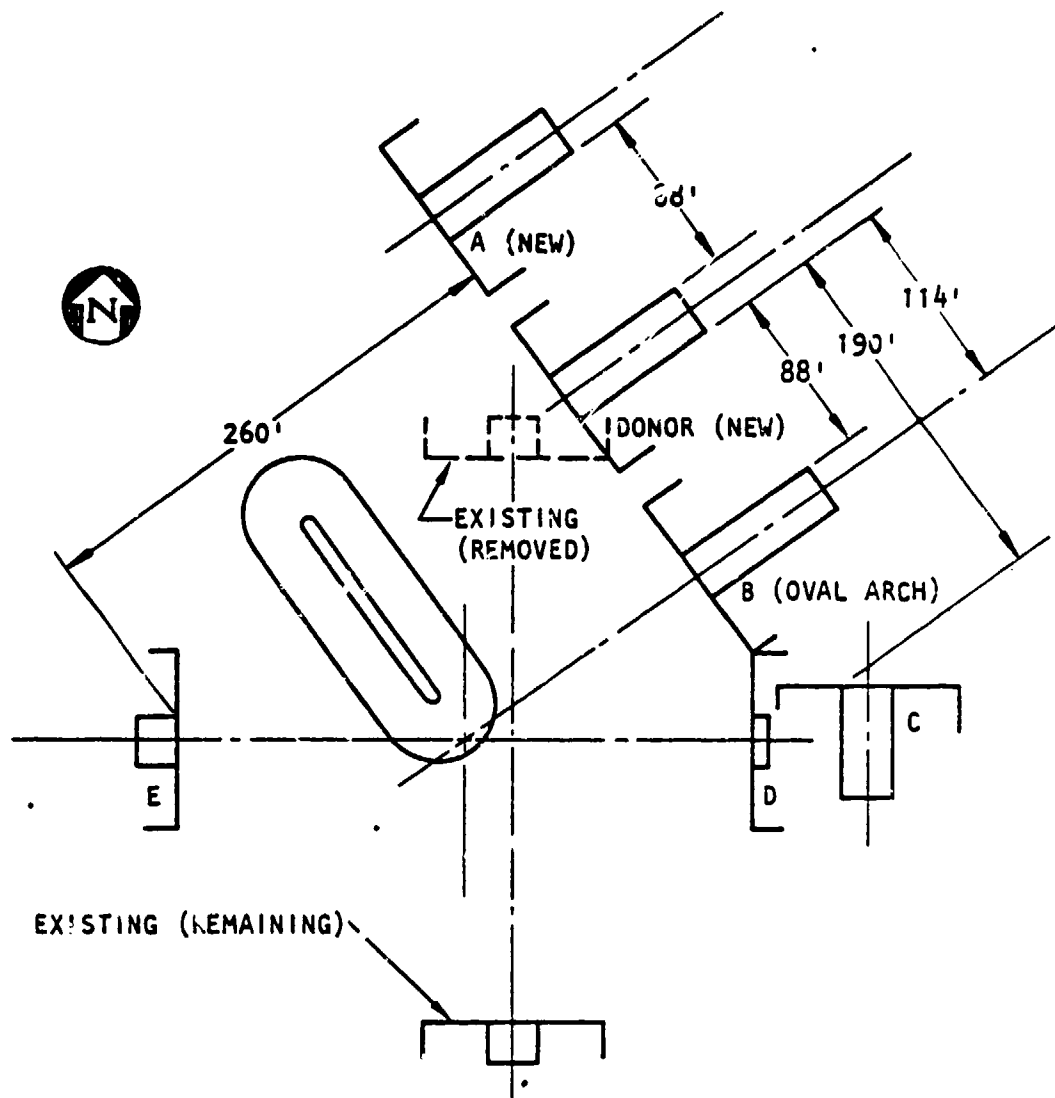


FIGURE 1-4. LAYOUT OF TEST STRUCTURES FOR ESKIMO III MAGAZINE SEPARATION TEST



The ESKIMO IV test array consisted of three magazine structures each facing the explosion source 147 ft away, as shown in Figure 1-5. The primary target structure was Igloo B to the northeast, consisting of a single-leaf sliding door, horizontally spanned, mounted on a modified headwall of the standard Stradley magazine.

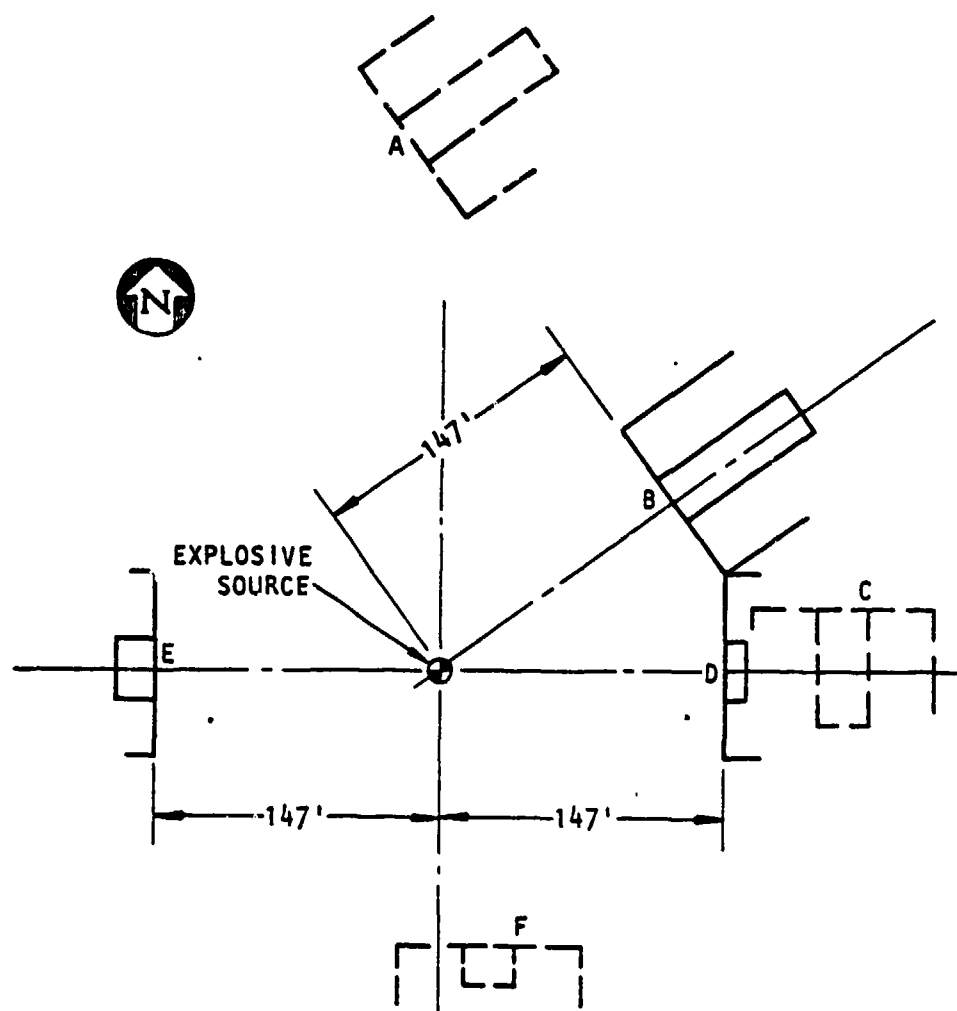
Igloo D (east) was rebuilt with the two-leaf, hinged, steel-plate door and the headwall of the standard circular steel arch magazine. Exposed to the same level of loading as the primary target, it served as a control structure to demonstrate directly the relative strength of the primary target (Igloo B).

Igloo E to the west was rebuilt with the headwall of the standard circular steel arch magazine, but fitted with a single-leaf sliding door. This combination was tested inconclusively in ESKIMO II, but the test had indicated a serious imbalance in strength between the door and headwall.

The test utilized a nearly ideal explosion source to generate blast loadings. It afforded the opportunity for more extensive source diagnostics and dynamic response measurements on the target structures than in previous tests of the ESKIMO series. This in turn would enable an extensive correlation between measured and calculated responses.

The explosion source consisted of 8-lb rectangular blocks of TNT stacked in the form of a hemisphere, containing a total of 37,000 lb of TNT. The explosives were left exposed, rather than surrounded by an earth cover or barriers.

Pressure gages were installed in the headwalls and in the ground nearby to measure blast pressures on the headwalls. Accelerometers and linear displacement transducers (LVDTs) were used to measure structure-response time histories of the headwalls. Self-recording pressure gages were installed to measure pressure loading at the far-field stations. Details on the locations of the pressure gages, accelerometers, and LVDTs are discussed in Section 4.



NOTE: IGLOOS A, C, AND F WERE OLD STRUCTURES FROM THE PREVIOUS ESKIMO TESTS THAT WERE NOT CONSIDERED IN ESKIMO IV.

FIGURE 1-5. LAYOUT OF TEST STRUCTURES FOR ESKIMO IV MAGAZINE SEPARATION TEST



Preliminary results (Ref. 6) showed that the doors of Igloos D and E were blown in. The headwall of Igloo E sustained extensive damage. The headwalls of Igloos B and D and the door of Igloo B sustained little or no damage.

### 1.5 OBJECTIVES AND SCOPE

The overall objective of the present study was to develop confidence in analytical techniques for predicting the dynamic response of concrete headwalls and steel-door structures to air-blast overpressures resulting from explosion of the contents of an adjacent magazine. To achieve the objective, the analytically predicted responses of the headwalls were compared with experimental data from the ESKIMO tests. The following tasks were defined:

#### Task 1

Calculate the response of the headwall and door of the south igloo in the ESKIMO I test, using a finite element model with improved resolution.

#### Task 2

Calculate the response of the headwalls and doors of the east (C) and northeast (B) igloos in the ESKIMO II test.

#### Task 3

Predict response of the strengthened Stradley-type headwall and single-leaf sliding door of the northeast (B) igloo in the ESKIMO IV test.\*

---

\*Because of tight schedules, this task could not be completed before the test. Nevertheless, the analysis was performed before any results from the test became available.



## SECTION 2

## PRESSURE LOADING ON HEADWALLS

This section presents air-blast pressure histories used in the dynamic response calculations of headwall and door systems. Provisions for measuring air-blast overpressure data on headwalls were made in the plans for all shots in the ESKIMO test series. However, the measured data were generally meager and of low quality. Therefore, data from other tests and from theoretical considerations were used to design the pressure histories for the analytical calculations of the ESKIMO tests.

### 2.1 PRESSURE HISTORIES FOR ESKIMO 1 TEST

The pressure time histories for the south igloo in ESKIMO 1 used in the present study were the same as the corresponding histories calculated in the previous study (Ref. 2). These histories are shown in Figure 2-1. The three pressure histories represent loading for the three zones of the headwall, as shown in Figure 2-2, and differ only during the unloading phase of the pressure history. The differences reflect the influence of unloading signals propagating downward from the top of the headwall. The use of just three different zones was considered adequate for the finite element calculations. All the pressure histories incorporate a millisecond (msec) rise-time ramp front for compatibility with the integration time step.

Additional discussions on the calculation of the pressure histories for ESKIMO 1 may be found in Reference 2.



R-7556-1-4182

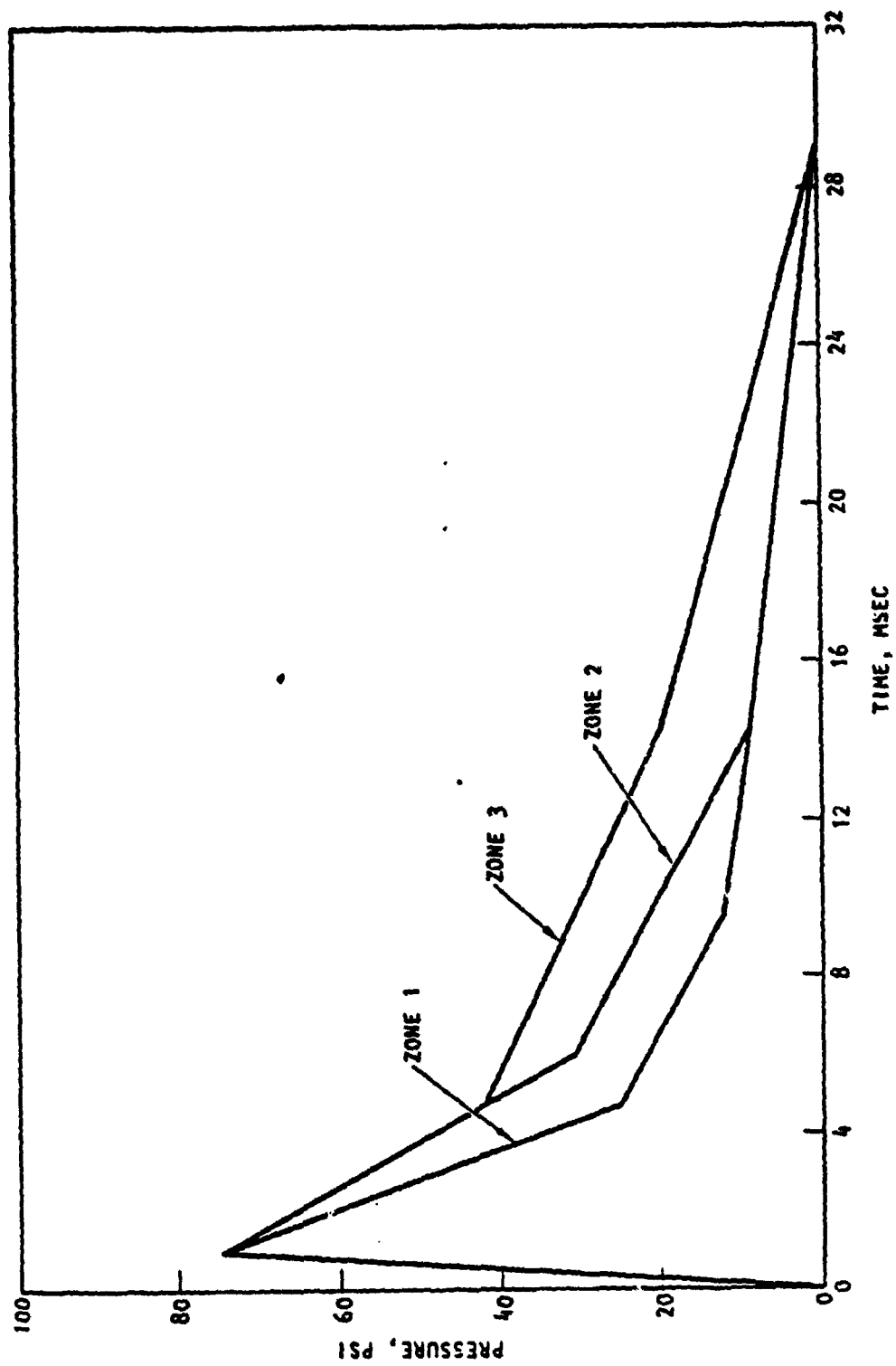


FIGURE 2-1. REFLECTED OVERPRESSURE ON SOUTH IGL00, ESKIMO 1



R-7556-1-4182

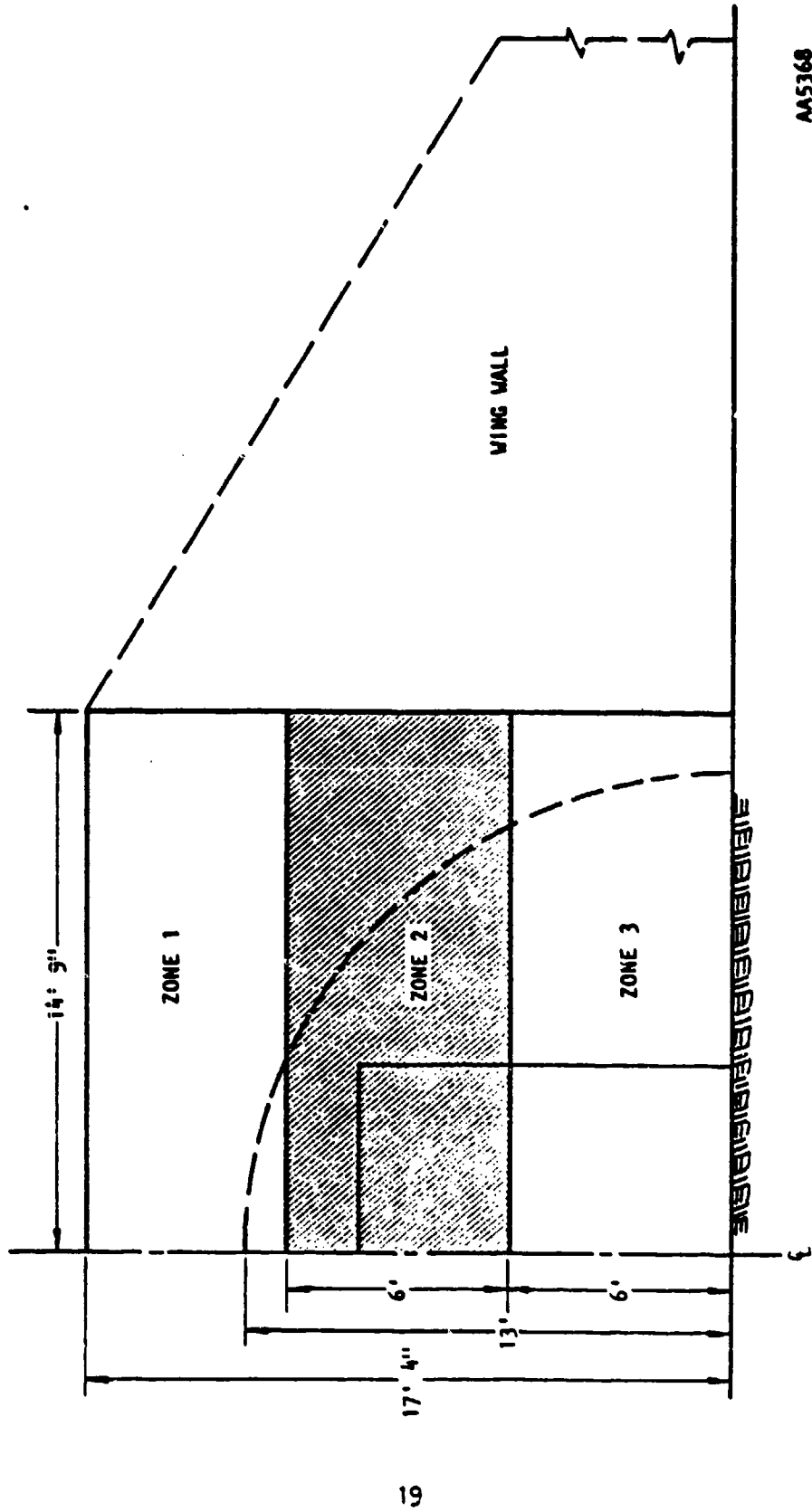


FIGURE 2-2. HEADWALL BLAST-PRESSURE LOADING ZONES, ESKIMO I



## 2.2 PRESSURE HISTORIES FOR ESKIMO II TEST

Although redundant air-blast instrumentation was provided at all five of the test igloos in ESKIMO II, obtaining reliable detailed descriptions of the blast loads applied to the magazine headwalls was difficult. Records from most of the gages were reported to be "difficult to read and considered unreliable." Peak-incident (side-on) and reflected overpressures measured at the east and northeast igloos were consistent with other experimental data and with the theory of gas dynamics for shock reflection. On the basis of the measured values and this consistency, a peak-loading pulse pressure of 260 psi was selected for the ESKIMO II calculations.

For the five test igloos the measured impulse varied by a factor of two from the lowest to the highest value. The nearly twofold variation in measured impulse may, in part, be due to the lack of rotational symmetry of the charge and surrounding revetment. The impulse for the east and west igloos is well below that for the other igloos. However, significant (20% to 30%) north-south and east-west variations in impulse are present. The impulse selected for the headwall loading pulse (1720 psi msec) is considered representative for the east and northeast igloos.

No positive-phase duration data were reported for the pressure histories measured at the headwalls. Pressure histories were not available for examination to establish durations. Scaling of previous magazine-safety test data, general high-explosives and nuclear-test data, and computational data suggested durations of 15 to 35 msec. Consideration of typical pressure history pulse shapes, the selected peak pressure, and the desired impulse led to the selection of a 30-msec duration. The resulting pulse developed for loading the east and northeast igloos of ESKIMO II is shown in Figure 2-3.

The three-zone description of the pressure loading of the headwall was retained for ESKIMO II. The pressure histories for Zones 1 and 2, which experience earlier unloading, are shown in Figure 2-3 superimposed on the pressure history for Zone 3 derived from measured peak pressure and impulse.

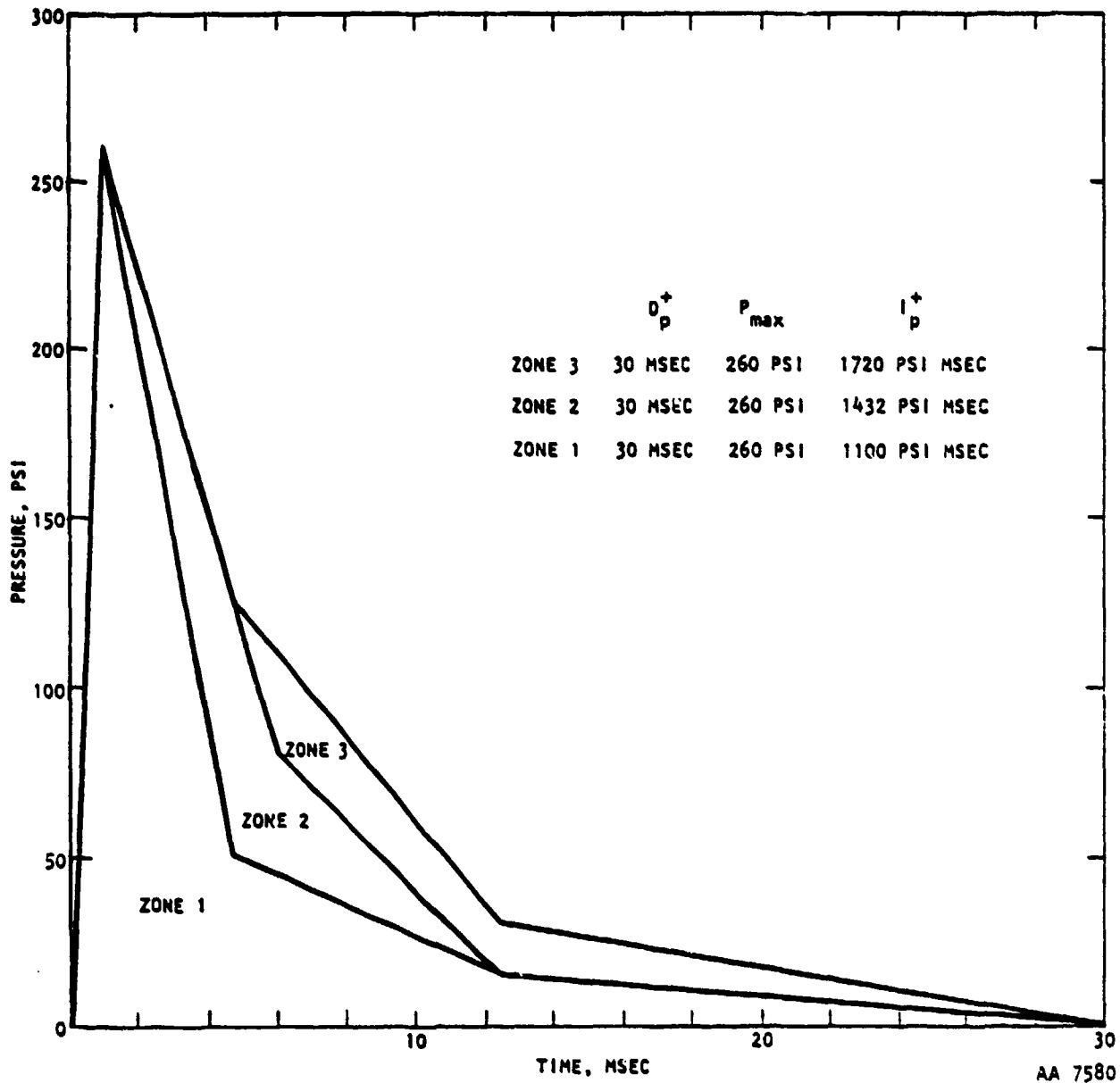


FIGURE 2-3. PROPOSED PRESSURE HISTORIES FOR NORTHEAST AND EAST IGLOOS, ESKIMO II



Adjustments in the pressure load history proposed for calculating response of the ESKIMO II east and northeast igloos may be made if more reliable estimates of positive-phase duration are obtained or if more accurate estimates of the impulse are obtained.

### 2.3 PRESSURE LOADING HISTORY FOR ESKIMO IV TEST

Eight pressure gages were placed, as shown in Figure 2-4, on the headwall of Igloo B (northeast igloo) in ESKIMO IV. This concentration of instrumentation was intended to measure the variation of pressure over the height of the headwall and to determine the uniformity of the pressure across the face. In addition, side-on pressure at ground level was measured at three ranges to establish the free-field blast pressure corresponding to the reflected overpressure loading on the headwall. Review of the "quick-look" data indicated that useful records were obtained from seven of the eight stations on the headwall and from all the free-field ground level stations.

At the 147-ft range, the free-field ground level station recorded a peak pressure of 62 psi. Empirical data for high-explosive detonations in air indicate that the peak reflected overpressure at the same range should be 290 psi (Ref. 7), whereas classical estimates of reflected shock strength for ideal gases indicate a peak reflected pressure of 265 psi. Raw reflected pressure peaks taken from the "quick-look" records range from 195 to 295 psi.

Pressure histories from Stations P1B, P4B, and P5B appeared to be influenced by movement or leakage of the door. The record from Station P4B suggests failure of the gage about 5 msec after blast arrival. The record from Station P7B shows a prominent oscillatory signal of about a 3-msec period, which distorts the early portion of the record. Development of pressure loading for the headwall of Igloo B (northeast) was therefore based primarily on the records from Stations P2B, P3B, P6B, and P8B, and on the classical treatment and empirical data for chemical explosions and shock waves in air.

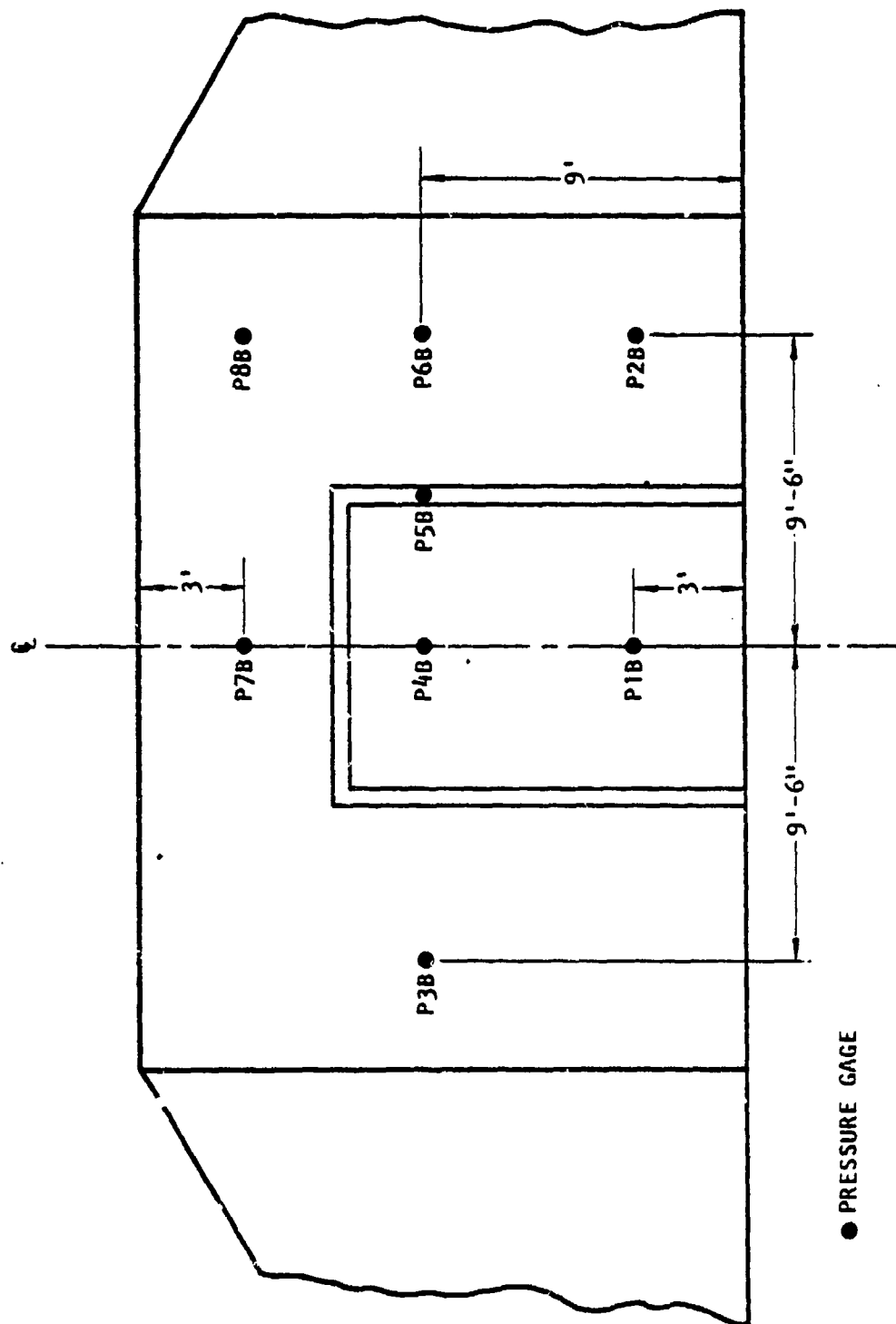


FIGURE 2-4. PLACEMENT OF PRESSURE GAGES, IGL00 B (NORTHEAST IGL00) OF ESKIMO IV



Comparison of traces from Stations P2B, P6B, and P8B, as shown in Figure 2-5, fails to support the assumption of systematic variation of the pressure history over the height of the headwall. Duration of the meaningful pressure loading on the headwall appears to be 14 msec. This is the duration adopted for pulses to be used in computing headwall response.

Precursors are apparent in all three pulses. The delay between earliest arrival and what is considered the main blast-pressure signal is approximately 1 msec. Comparison of signals from Stations P3B and P6B is shown in Figure 2-6. Although differences in peak pressure and precursor timing and amplitude are apparent, the signals show good agreement. Pressure differences during the decay phase are of the same order as the differences between signals from the lower, middle, and upper stations shown in Figure 2-5.

On the basis of the comparisons of "quick-look" data for Stations P2B, P3B, P6B, and P8B, and the analytical and empirical data for chemical explosions in air, a single pressure history was developed for the headwall response calculation. The pulse is shown in Figure 2-7 with a smoothed version of the free-field ground level (side-on) pressure history measured at the same range. The peak pressure, 280 psi, is consistent with the analytical, empirical, and experimental data. The duration, 14 msec, is consistent with the ESKIMO IV data, but is considerably shorter than that predicted from the analytical and empirical data. The impulse, 1180 psi msec, is consistent with both the ESKIMO IV data as shown in Figure 2-8 and with empirical data. The scaled empirical data (Ref. 7) indicate that the reflected pressure pulse corresponding to a 62-psi incident overpressure pulse from a 37,000-lb hemispherical TNT charge should have a peak pressure of 290 psi, a positive-phase duration of 34 msec, and an impulse of 1160 psi msec. Pulses closely resembling the representative reflected pulse shown in Figure 2-7 can be made to satisfy these requirements by adding a low amplitude tail. For example, the pulse shown in Figure 2-9 has a peak pressure of 290 psi, a duration of 31.7 msec, and an impulse of 1170 psi msec. Its close resemblance to the proposed short-duration pulse is obvious. The use of the short-duration pulse is considered satisfactory and may be preferred for reasons of economy in calculating headwall response.

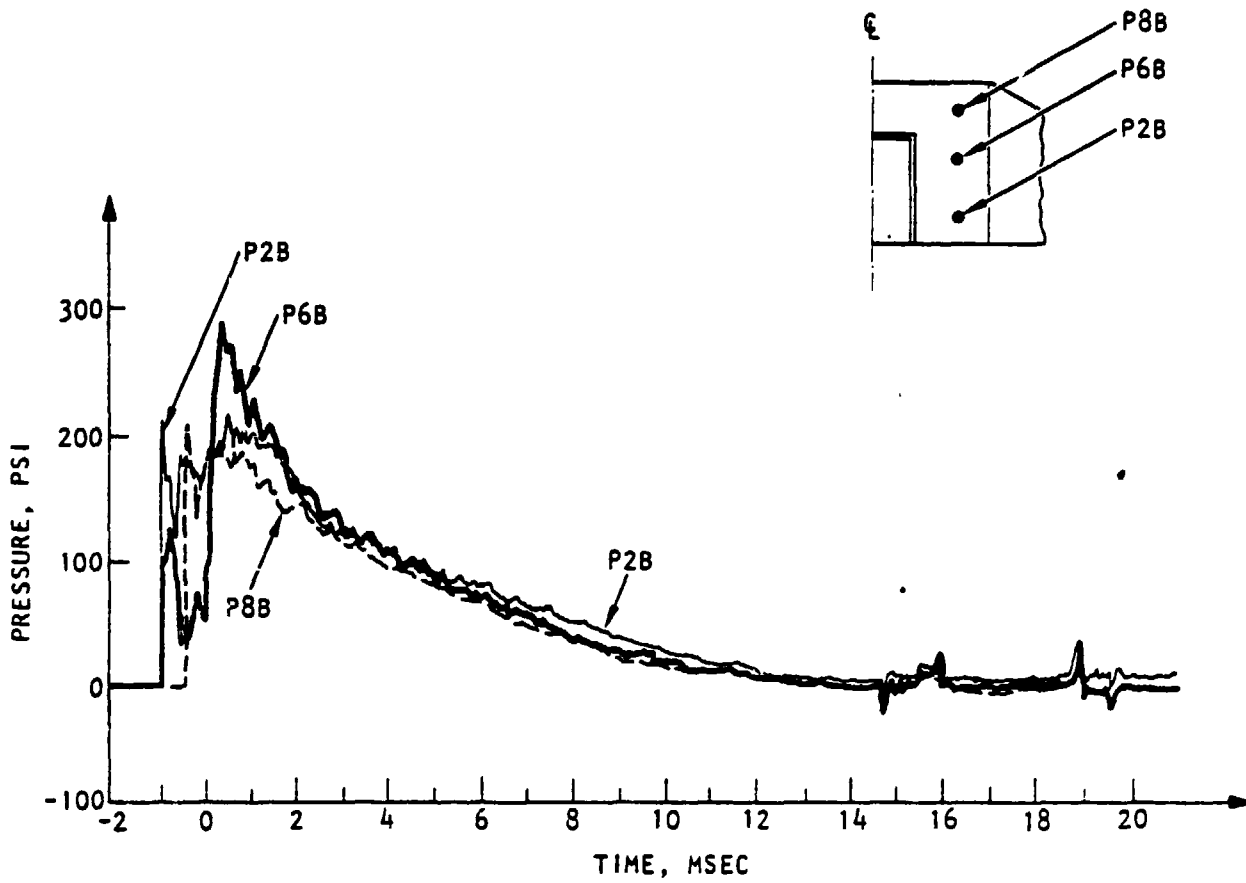


FIGURE 2-5. COMPARISON OF PRESSURE HISTORIES FOR A VERTICAL ARRAY OF GAGES, IGLOO B OF ESKIMO IV

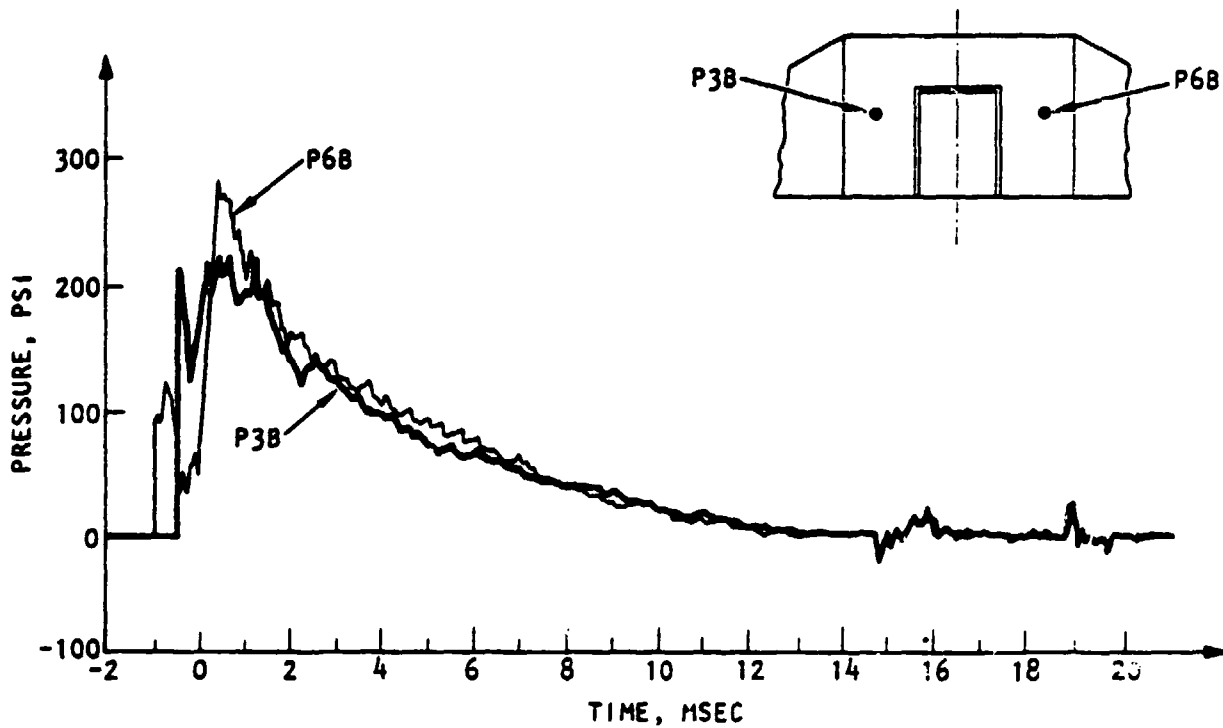


FIGURE 2-6. COMPARISON OF PRESSURE HISTORIES TO TEST UNIFORMITY OF PRESSURE LOADING ACROSS WIDTH OF HEADWALL, IGLOO B OF ESKIMO IV



R-7556-1-4182

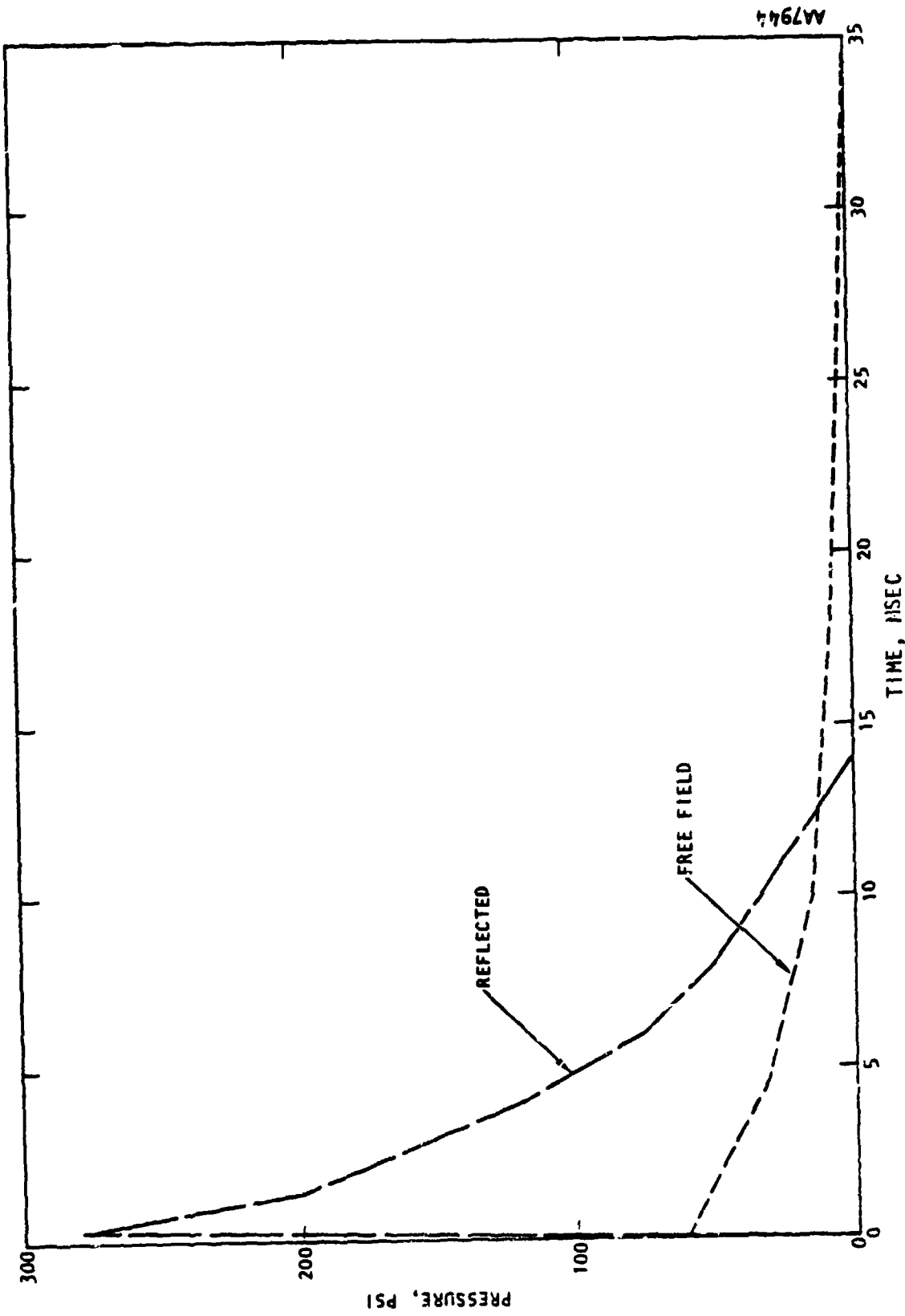


FIGURE 2-7. FREE-FIELD GROUND LEVEL AND REFLECTED HEADWALL PRESSURE PULSES FOR ANALYSIS OF IGL00 B, ESKIMO IV

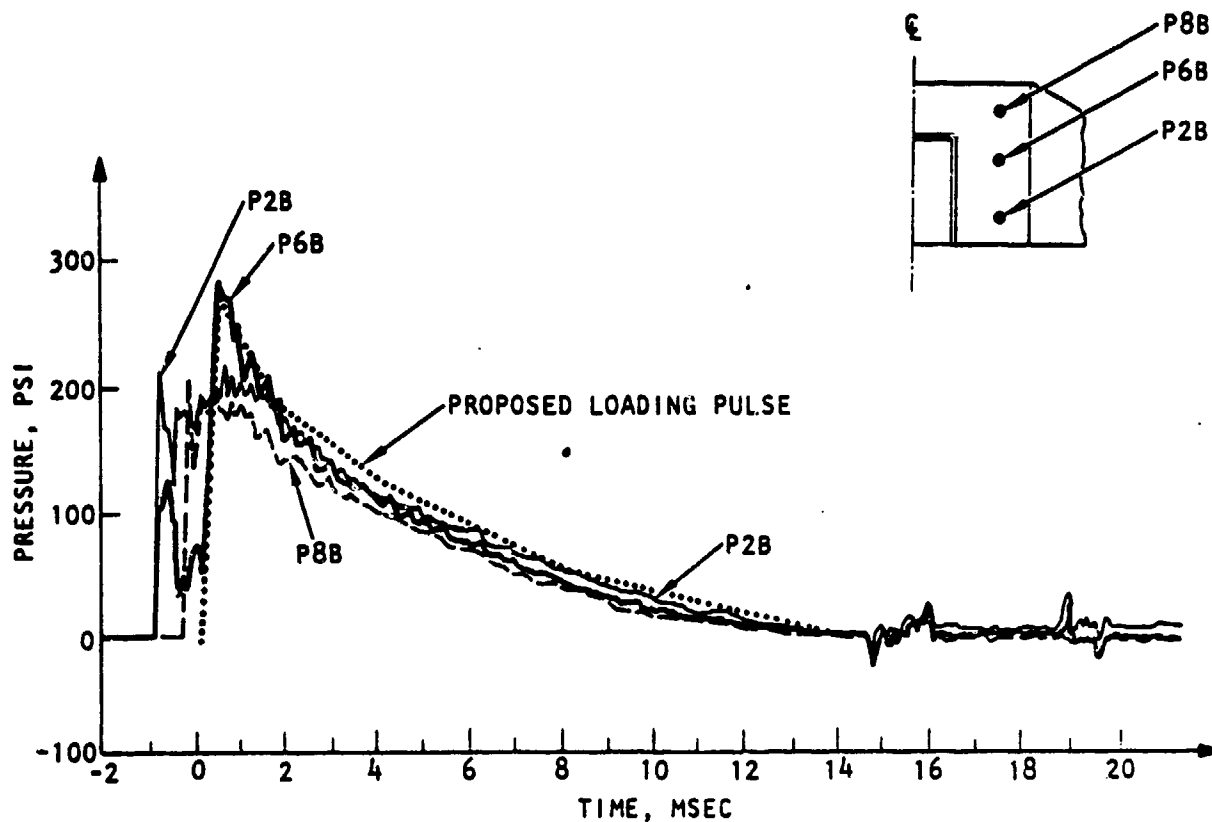


FIGURE 2-8. COMPARISON OF PRESSURE HISTORIES FOR A VERTICAL ARRAY OF GAGES WITH THE PROPOSED LOADING PULSE FOR RESPONSE ANALYSIS OF IGLOO B, ESKIMO IV



R-7556-1-4182

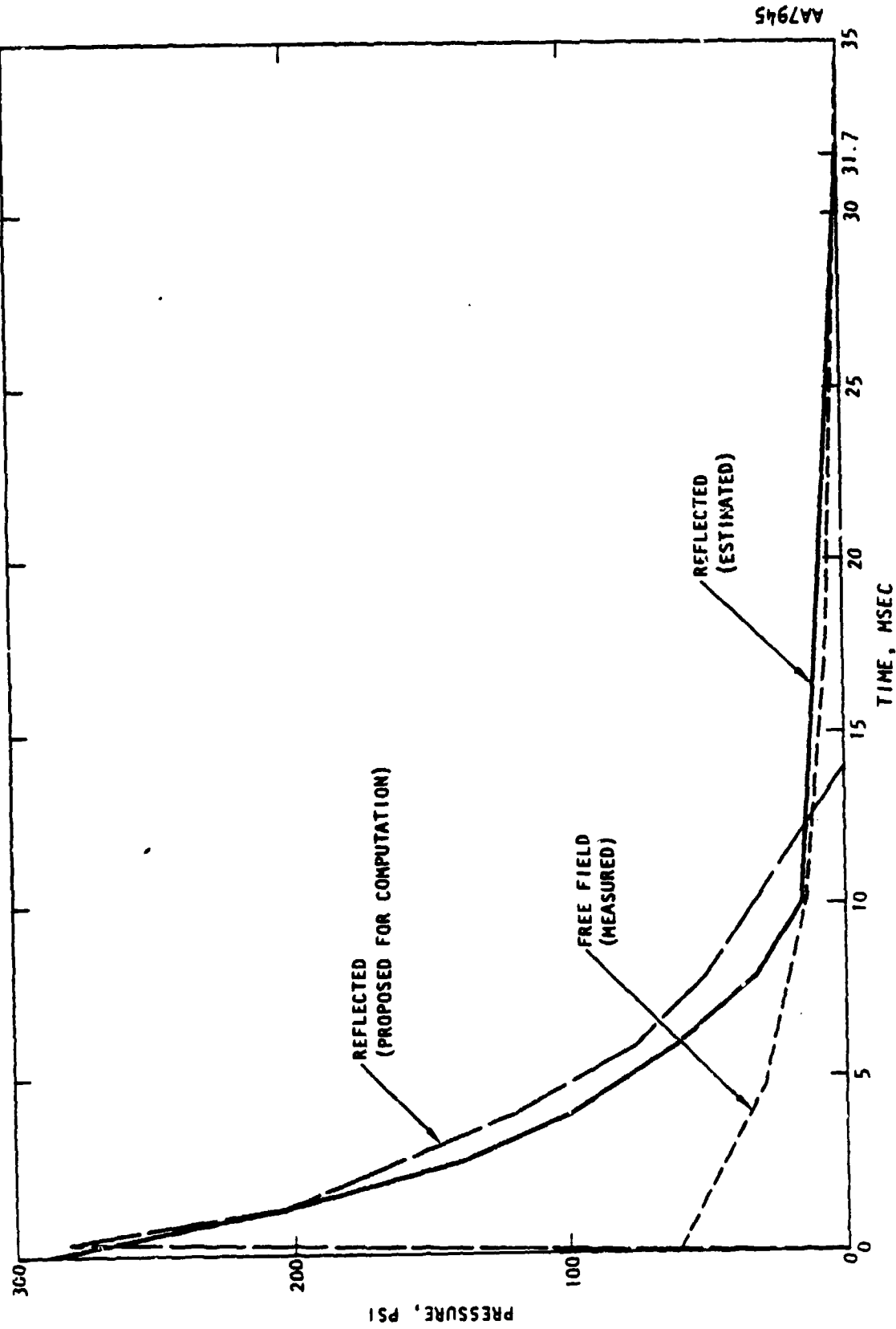


FIGURE 2-9. COMPARISON OF HEADWALL PRESSURE PULSE FOR ANALYSIS OF IGLOO 6 (ESKIMO IV) WITH ESTIMATED REFLECTED PULSE AND MEASURED FREE-FIELD GROUND LEVEL PULSE



## SECTION 3

STRUCTURAL MODEL OF HEADWALL  
AND DOOR SYSTEM

This section describes the finite element models of the headwalls in ESKIMO tests to be used in performing the dynamic analyses described in Section 5. The models are to be used in conjunction with the INSLAB computer program. Section 3.1 describes the finite element model of the south headwall in the ESKIMO I test. Also included in this section are the modeling techniques for considering the effects of soil supporting the headwall, concrete floor slab, and steel arch on the response of the headwall. Section 3.2 presents the finite element models for the east and northeast headwalls in the ESKIMO II test. Section 3.3 discusses the finite element of the northeast headwall in the ESKIMO IV test.

### 3.1 STRUCTURAL MODEL, ESKIMO I TEST

#### 3.1.1 FINITE ELEMENT MESH

Figure 3-1 shows a coarse finite element mesh of the south headwall in the ESKIMO I test which was used in the previous study to compute analytically the dynamic response of the headwall (Ref. 2). A refined finite element model of the same headwall used in the present study is shown in Figure 3-2. The previous model was necessarily coarse because the existing INSLAB code (Ref. 8) placed severe limits on the size of the model. To refine the model, the INSLAB code was modified to solve larger problems (Ref. 2). Table 3-1 presents a comparison of the coarse and refined finite element meshes of the south headwall in ESKIMO I.

The face of the magazine consists of a concrete headwall and two steel wingwalls. As discussed in Reference 2, the finite element model did not include the wingwalls, whose effect on the headwalls is considered negligible.

**Preceding page blank**

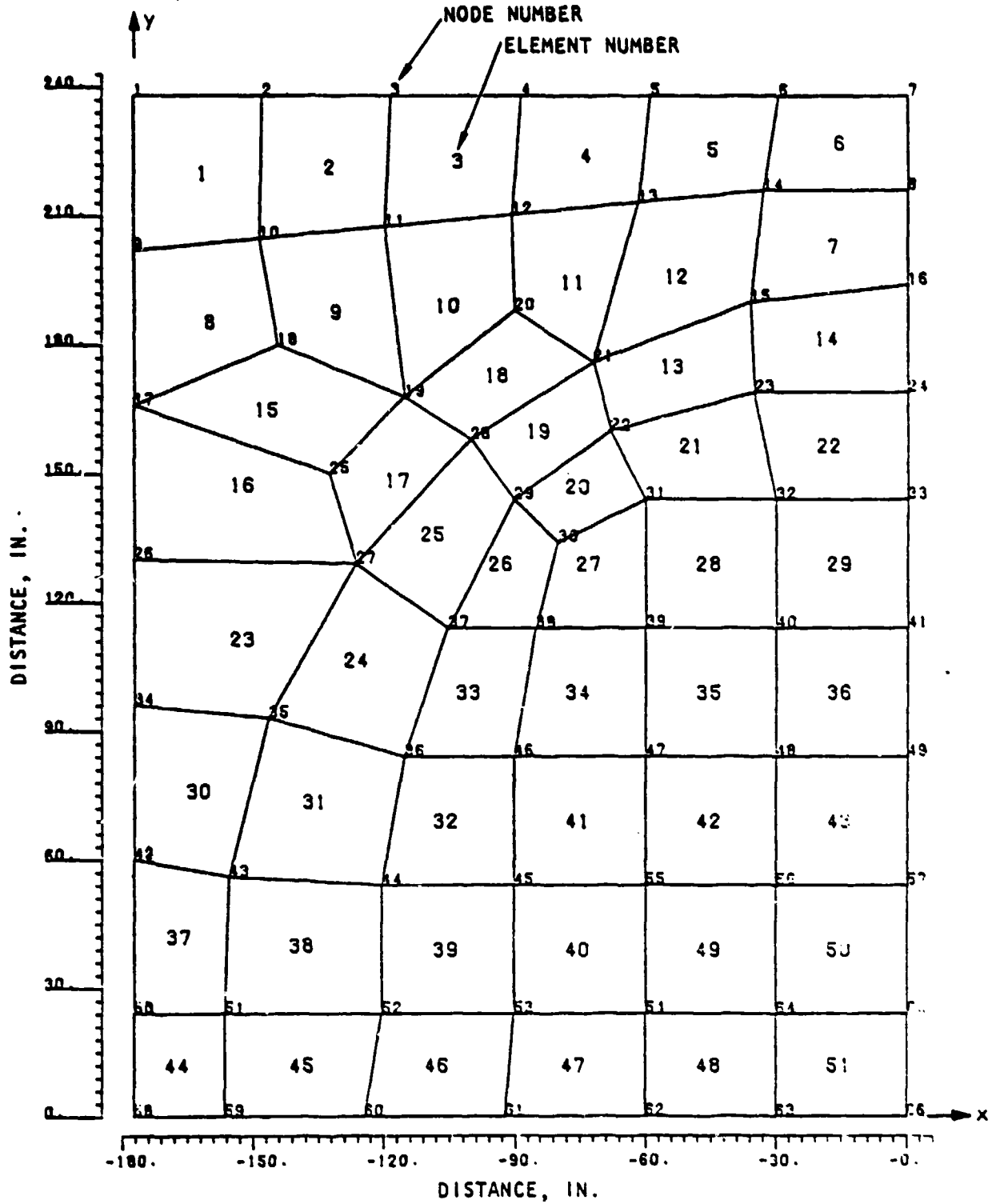


FIGURE 3-1. COARSE FINITE ELEMENT MODEL OF SOUTH HEADWALL, ESKIMO I



R-7556-1-4182

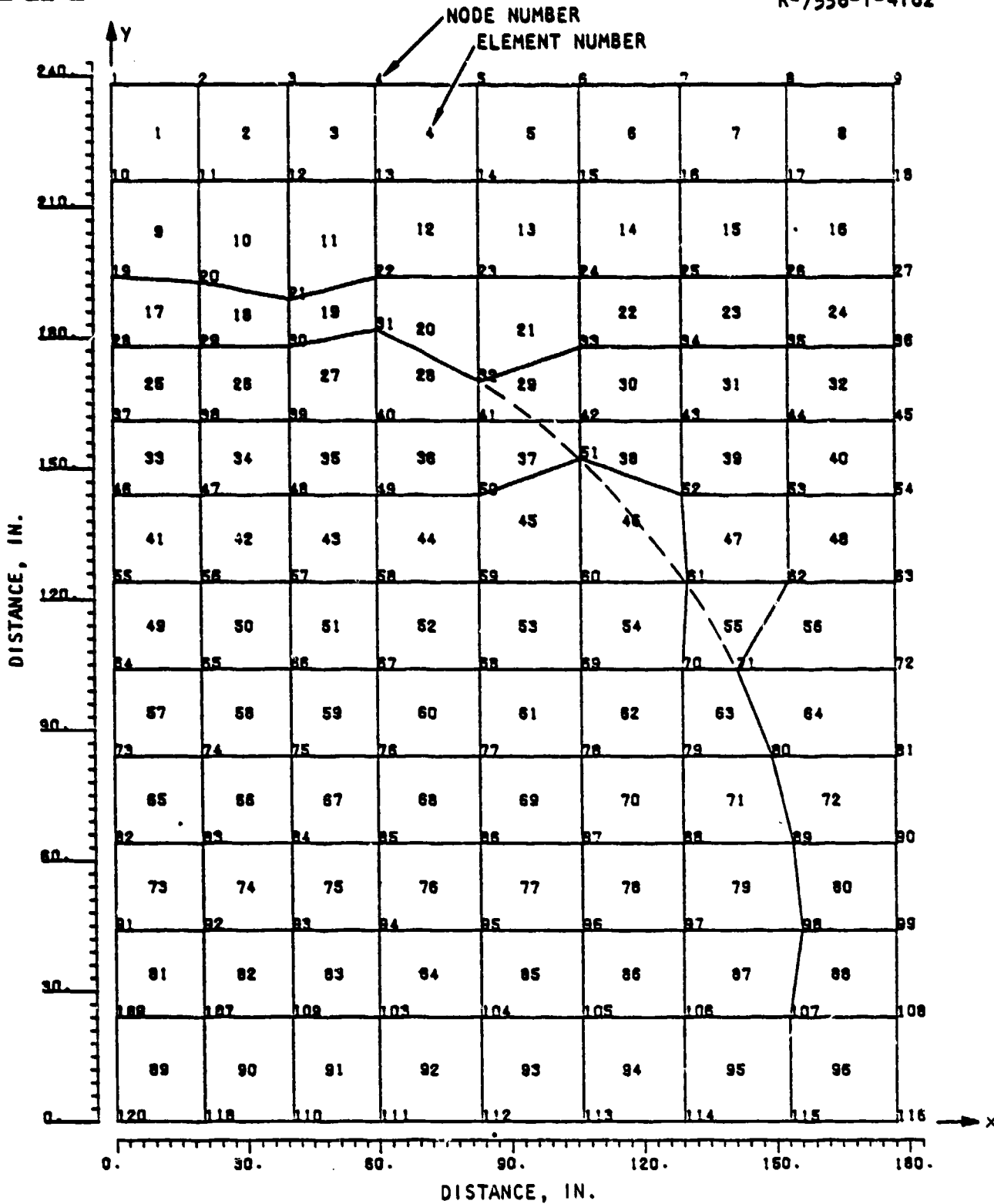


FIGURE 3-2. REFINED FINITE ELEMENT MODEL OF SOUTH HEADWALL, ESKIMO I

TABLE 3-1. COMPARISON OF COARSE AND REFINED  
FINITE ELEMENT MESHES

| Item to Be Compared   | Coarse Mesh Used<br>in Previous Study | Refined Model of<br>Present Study | Change,<br>% |
|---|---------------------------------------|-----------------------------------|--------------|
| 1. Total nodes  | 66                                    | 120                               | + 80         |
| 2. Total elements   | 51                                    | 96                                | + 90         |
| 3. Half bandwidth of<br>stiffness matrix                        | 33                                    | 33                                | 0            |
| 4. Total elements<br>representing<br>the door                   | 8                                     | 18                                | +125         |
| 5. Total discrete<br>elements representing<br>soil              | 43                                    | 71                                | + 65         |
| 6. Total discrete<br>elements representing<br>concrete floor    | 0                                     | 18                                | --           |
| 7. Nodes for which<br>response histories to<br>be obtained      | 10                                    | 19                                | + 90         |
| 8. Estimated fundamental<br>frequency of the<br>largest element | 1000 Hz                               | 2250 Hz                           | +125         |



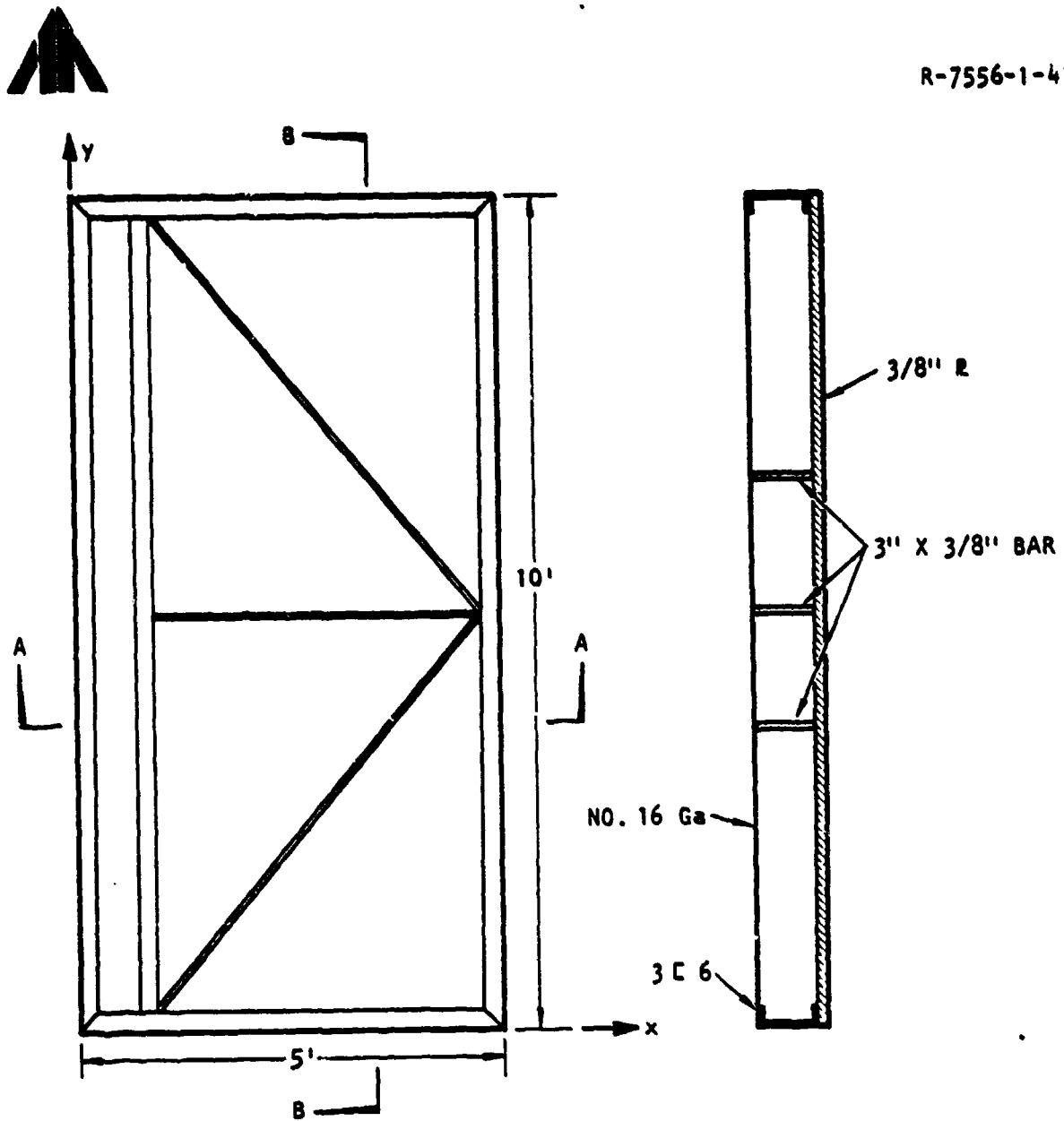
### 3.1.1.1 Properties of Door

The south-igloo headwall in ESKIMO I was fitted with double-leaf hinged steel doors. The door was constructed from a 3/8-in. plate supported by 3-in. channels and 3/8-in. plate stiffeners, as shown in Figure 3-3. A No. 16-gage steel plate was spot-welded on the inside of the door. The door is modeled as an orthotropic plate of uniform thickness possessing the characteristics of the real door. The equivalent properties of the steel door as computed in Reference 2 are summarized below:

| Property                   | Symbol   | Numerical Value            |
|----------------------------|----------|----------------------------|
| Equivalent plate thickness | $h$      | 2.04 in.                   |
| Modulus of elasticity      | $E_x$    | $32.4 \times 10^6$ psi     |
| Modulus of elasticity      | $E_y$    | $27.8 \times 10^6$ psi     |
| Equivalent density         | $\rho$   | 0.0812 lb/in. <sup>3</sup> |
| Yield moment               | $M_{xx}$ | 10.52 kip-in./in.          |
| Yield moment               | $M_{yy}$ | 12.83 kip-in./in.          |
| Plastic modulus            | $E_p$    | 0.1 of elastic modulus     |

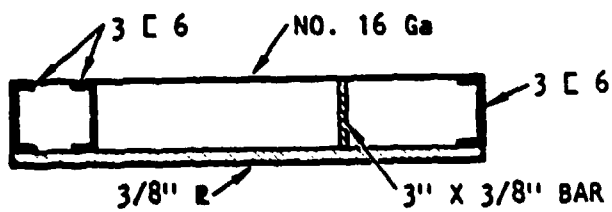
### 3.1.2.2 Properties of Headwall Section

A typical section of the headwall, showing the details of the reinforcement, is shown in Figure 3-4. To account for the rapid application of loading, the dynamic yield stress,  $f_y$ , for the reinforcing steel is taken as 52 ksi, as suggested in Reference 9. Similarly, the dynamic strength of concrete in compression,  $f'_c$ , is taken as 3900 psi, a 30% increase from the static strength of 3000 psi. Young's moduli for steel and concrete are assumed to be  $30 \times 10^6$  psi and  $3 \times 10^6$  psi, respectively.



(a) Elevation of the door

(c) Cross-section B-B along y-axis



(b) Cross-section A-A along x-axis

FIGURE 3-3. DOOR DETAILS FOR SOUTH IGLOO, ESKIMO I



R-7556-1-4182

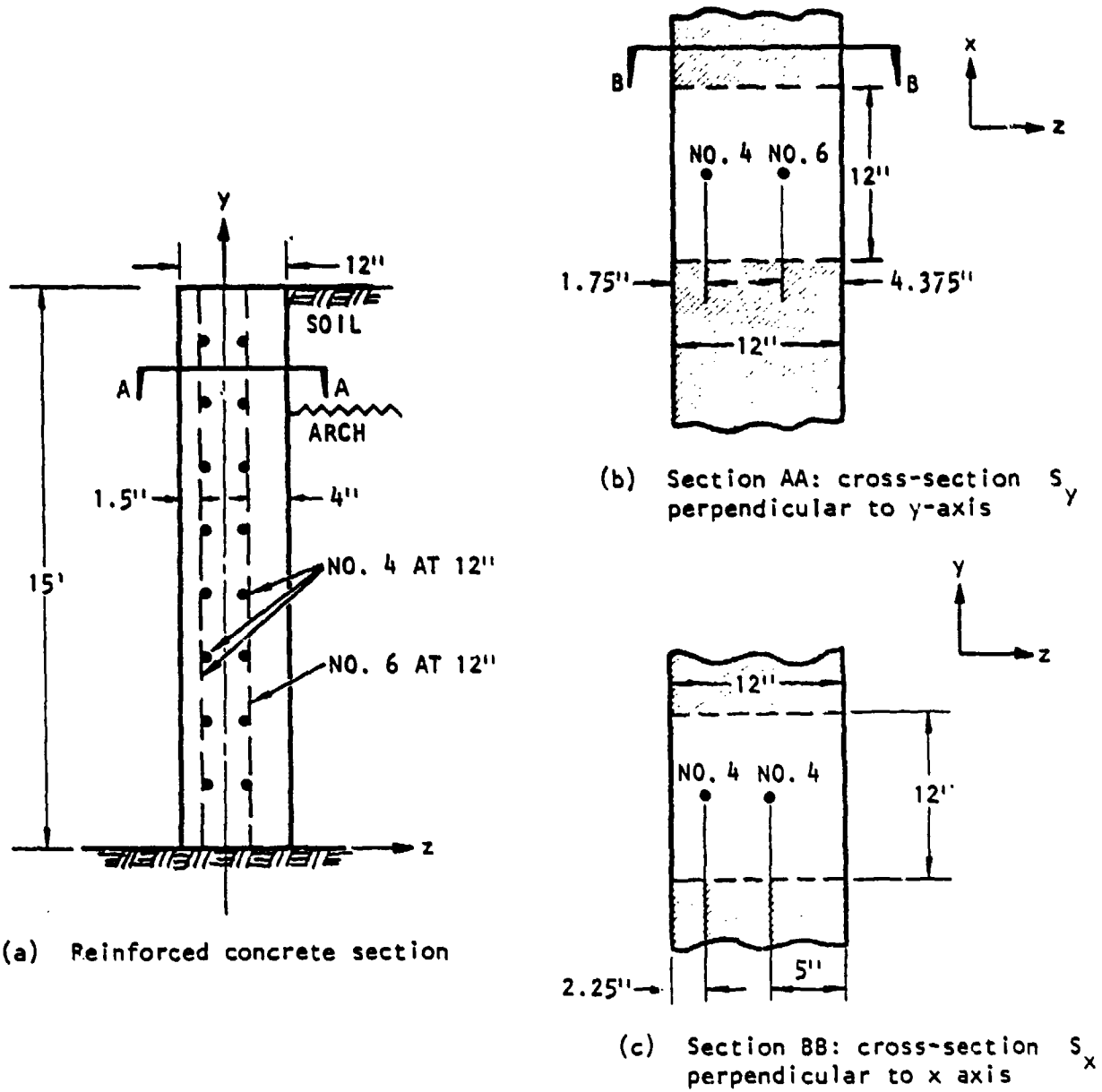


FIGURE 3-4. SKETCHES OF HEADVALL SECTIONS TO COMPUTE MATERIAL PROPERTIES (SOUTH IGLOO, ESKIMO 1)



Based on Figure 3-4 and the assumed material properties of reinforced concrete, the yield moments for both cross sections  $S_x$  and  $S_y$  are calculated. It is found that both cross sections are underreinforced; therefore, the yield moments are governed by the tensile strength of steel. The procedures for computing these moments are presented in Appendix B.

For Section  $S_x$

$$M_{yy}^+ = 121.2 \text{ kip-in./ft when the headwall is concave inward}$$

$$M_{yy}^- = 159.0 \text{ kip-in./ft when the headwall is concave outward}$$

For Section  $S_y$

$$M_{xx}^+ = 110.7 \text{ kip-in./ft when the headwall is concave inward}$$

$$M_{xx}^- = 69.2 \text{ kip-in./ft when the headwall is concave outward}$$

The headwall section is modeled as a homogeneous, orthotropic plate of uniform thickness possessing the same dynamic characteristics as the actual reinforced concrete headwall. The equivalent properties of the headwall section are given below:

| Property                   | Symbol | Numerical Value        |
|----------------------------|--------|------------------------|
| Equivalent plate thickness | $h$    | 12 in.                 |
| Modulus of elasticity      | $E_x$  | $3 \times 10^5$ psi    |
| Modulus of elasticity      | $E_y$  | $2 \times 10^5$ psi    |
| Equivalent density         | $\rho$ | 150 lb/ft <sup>3</sup> |

The values of  $E_x$  and  $E_y$  are obtained using the procedure described in Appendix C.



### 3.2 STIFFNESS OF SOIL

The ESKIMO tests (Refs. 1, 4, 5) showed that the compacted soils behind the headwall and covering the steel arch influence the behavior of the headwall significantly because of the interaction of soil and headwall. In the longitudinal direction, the earth cover merges smoothly with the ground behind the rear wall. Therefore, any support provided by the soil per unit area of the headwall is similar to an infinitely long compressible column. The response of the soil is expected to be highly nonlinear because the permanent displacements of the headwall are of the order of several inches (Refs. 1, 4, 5).

Actual test data regarding the strength of the compacted soil over the north igloo of the ESKIMO 1 test array are available (Ref. 10). In the test, two opposing rams were driven by a hydraulic jack horizontally outward against the earth fill through circular openings cut in the right and left sides of the corrugated steel arch. Load deflection curves were plotted for the soil over the igloo at the initial stage of the loading and the final stage (5 min after the application of loads). The spring constants of the soil based on these curves are shown in Table 3-2. It is noted that in the testing, the soil was allowed to settle for one minute before additional loading was applied. For the quantities of explosives normally stored in magazines, blast-pulse durations at distances of interest are of the order of tens of milliseconds. As a consequence, the corresponding stiffness is very high. To arrive at a reasonable dynamic stiffness of the soil, a column of soil subjected to step loading of magnitude  $P$  was investigated. The deflection  $\delta$  at time  $t$  is

$$\delta = \frac{PL}{AE}$$



TABLE 3-2. SOIL STIFFNESS FROM TEST IN NORTH IGL00

| Stage   | Location | K, lb/in. <sup>3</sup> |                   |             |
|---------|----------|------------------------|-------------------|-------------|
|         |          | P = 0 to 60 psi        | P = 60 to 270 psi | P > 270 psi |
| Initial | Right    | 700                    | 350               | 230         |
|         | Left     | 666                    | 245               | 133         |
| Final   | Right    | 600                    | 330               | 190         |
|         | Left     | 580                    | 235               | 133         |

The stiffness is defined as

$$K = \frac{P}{\delta} = \frac{AE}{L}$$

where

A = The cross-sectional area of the soil column

$$E = \rho c^2$$

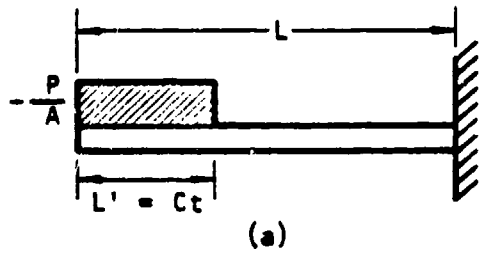
c = Wave velocity in the soil medium, 4000 ft/sec

$\rho$  = Mass density of the soil, 0.00018 lb-sec<sup>2</sup>/in.<sup>4</sup>

$$L = Ct$$

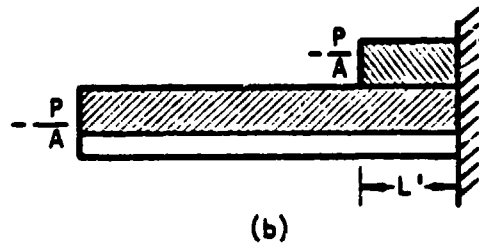
Because of the reflections of the pressure wave at the ends of the soil column, different expressions for the deflections were derived and are illustrated in Figures 3-5a to 3-5c. The resulting stiffness with respect to time is shown in Figure 3-5d.

The dynamic stiffness calculations are based on a one-dimensional wave propagation model. Neither soil friction nor wave dispersion was considered; therefore, the true values should be a little higher than the test data. In addition, there was ample time during the test for soil to settle; whereas in the dynamic stiffness calculation, there is very little time for soil to



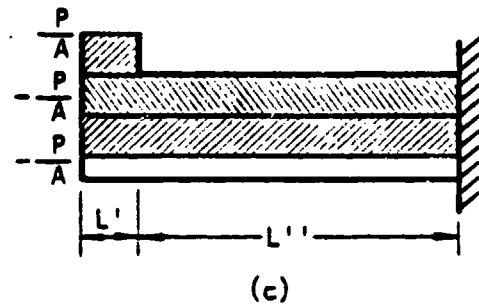
$$t < \frac{L}{C}$$

$$\delta = \frac{PL'}{AE} = \frac{Pct}{AE}$$



$$\frac{L}{C} < t < \frac{2L}{C}$$

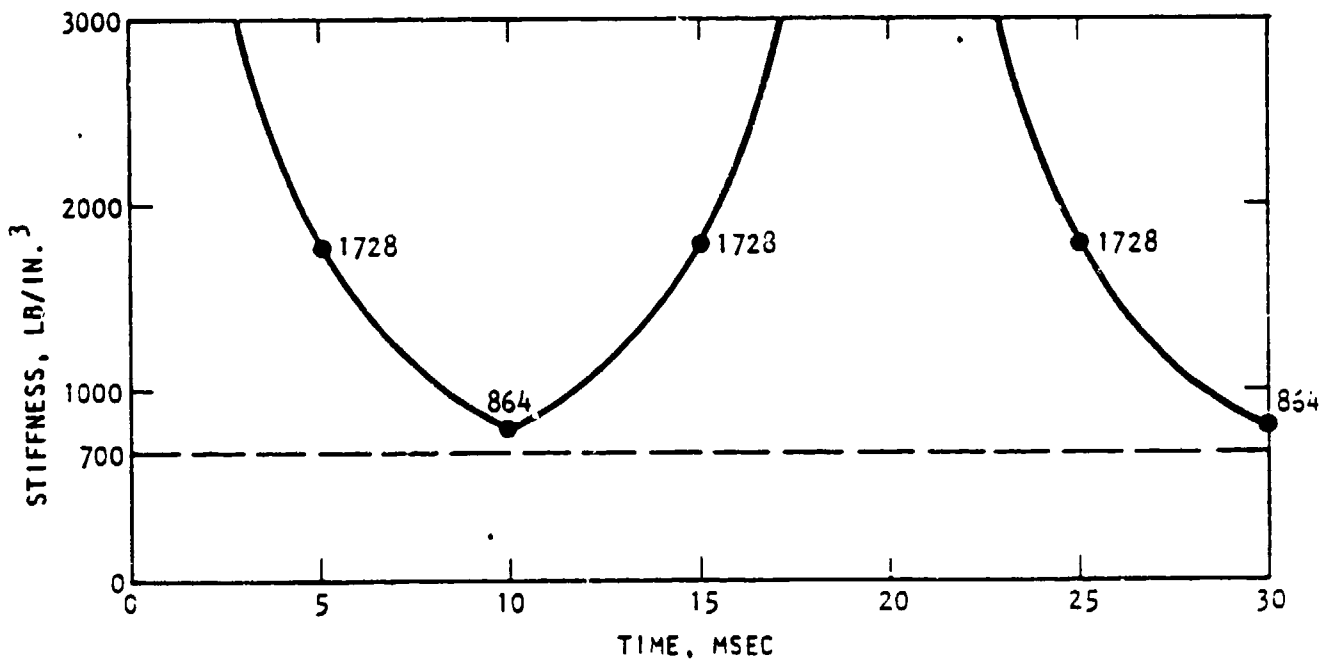
$$\delta = \frac{PL}{AE} + \frac{PL'}{AE}$$



$$\frac{2L}{C} < t < \frac{3L}{C}$$

$$\delta = \frac{PL}{AE} + \frac{PL}{AE} - \frac{PL'}{AE}$$

$$= \frac{P(L + L'')}{AE}$$



(d)

FIGURE 3-5. DYNAMIC STIFFNESS OF SOIL



settle. The modulus of elasticity for soil under high pressure conditions is much smaller than that under low pressure conditions, as can be seen in Table 3-2, which shows lower static stiffnesses at high pressure levels. It is doubtful that the effect of loading magnitude is important, especially when the peak pressure occurs for only a 3-msec duration.

The lowest dynamic stiffness, occurring at 10 msec, 30 msec, 50 msec, etc., is 864 lb/in.<sup>3</sup> (Fig. 3-5d), which is slightly higher than the static stiffness shown in Table 3-2 (700 and 666 lb/in.<sup>3</sup> for right and left locations, respectively) in the initial stage. Since the major explosive loadings used in this study were applied to the headwall within the first few milliseconds, the stiffness is subject to rapid change during this period. A value of 1300 lb/in.<sup>3</sup> is considered to be the best estimate on the soil stiffness.

### 3.1.3 MODEL REPRESENTATION FOR SOIL AND HEADWALL INTERACTION

In most analyses involving structures supported on soil, a common practice is to represent the soil by spring-mass or spring-dashpot systems (Ref. 11). This approach is valid if the motions are small so that the soil response is linearly elastic. Since the soil behind the headwall behaves in a highly nonlinear fashion, the conventional approach of representing soil by spring-mass or spring-dashpot systems may not be useful. In addition, the presence of springs would not allow the headwall to undergo permanent deflection. For this reason, viscous damping elements, or dashpots, were used in the previous study (Ref. 2). Massless dashpots with damping coefficient equal to  $\rho C$  per unit area of headwall were used, where  $\rho$  is the mass density and  $C$  is the wave velocity of the soil. The computed displacements from the study generally exceeded the measured values from the test. The use of dashpots alone was considered to be a factor in producing excessive displacements.



In order to determine the best possible model to represent the soil, the three test cases shown in Figure 3-6 were considered. A section of the headwall was sliced along the vertical plane. The base of the headwall was embedded in the ground. The top of the arch line varies from 13 ft at the center to zero at the ends of the headwall. A value of 5 ft was arbitrarily selected. The rear of the wall, from the top of the steel arch to the top of the headwall, was supported by earth fill.

In Case A, the earth fill was represented by a series of elastic springs attached to the nodes on the headwall, as shown in Figure 3-6. A certain percentage of the mass of soil was concentrated at each of these nodes, as discussed in Reference 2. The stiffness of the springs was equal to 1300 lb/in. per unit area of the headwall section. In Case B, the earth fill was modeled by a series of linear dampers attached to the nodes on the headwall section. The coefficient of the dampers was taken equal to  $\rho C$ .

In Case C, the soil medium behind the headwall was modeled by linear dampers and nonlinear springs in series attached to the nodes on the headwall section. The coefficients of the linear dampers were equal to  $\rho C$ . The nonlinear springs were one-way springs that can resist motion only in one direction, i.e., in compression. The stiffness of the springs in compression was equal to 1300 lb/in. per unit area of the headwall section.

All three models were subjected to the same blast-pressure loading experienced by the south igloo in ESKIMO I. Dynamic responses of the models in three cases were obtained using TRI/SAC code (Ref. 12), a general finite-element computer program capable of solving linear and nonlinear problems. Cases A and B were solved with the linear step-by-step option of TRI/SAC (Ref. 12), whereas Case C was solved with the nonlinear step-by-step option.

The response time histories at selected locations are shown in Figures 3-7 through 3-11. In Case A, displacement responses oscillate at high frequencies and eventually attenuate to zero (Fig. 3-7). This type of behavior of the headwall is in contrast to the observed behavior in the ESKIMO I test,

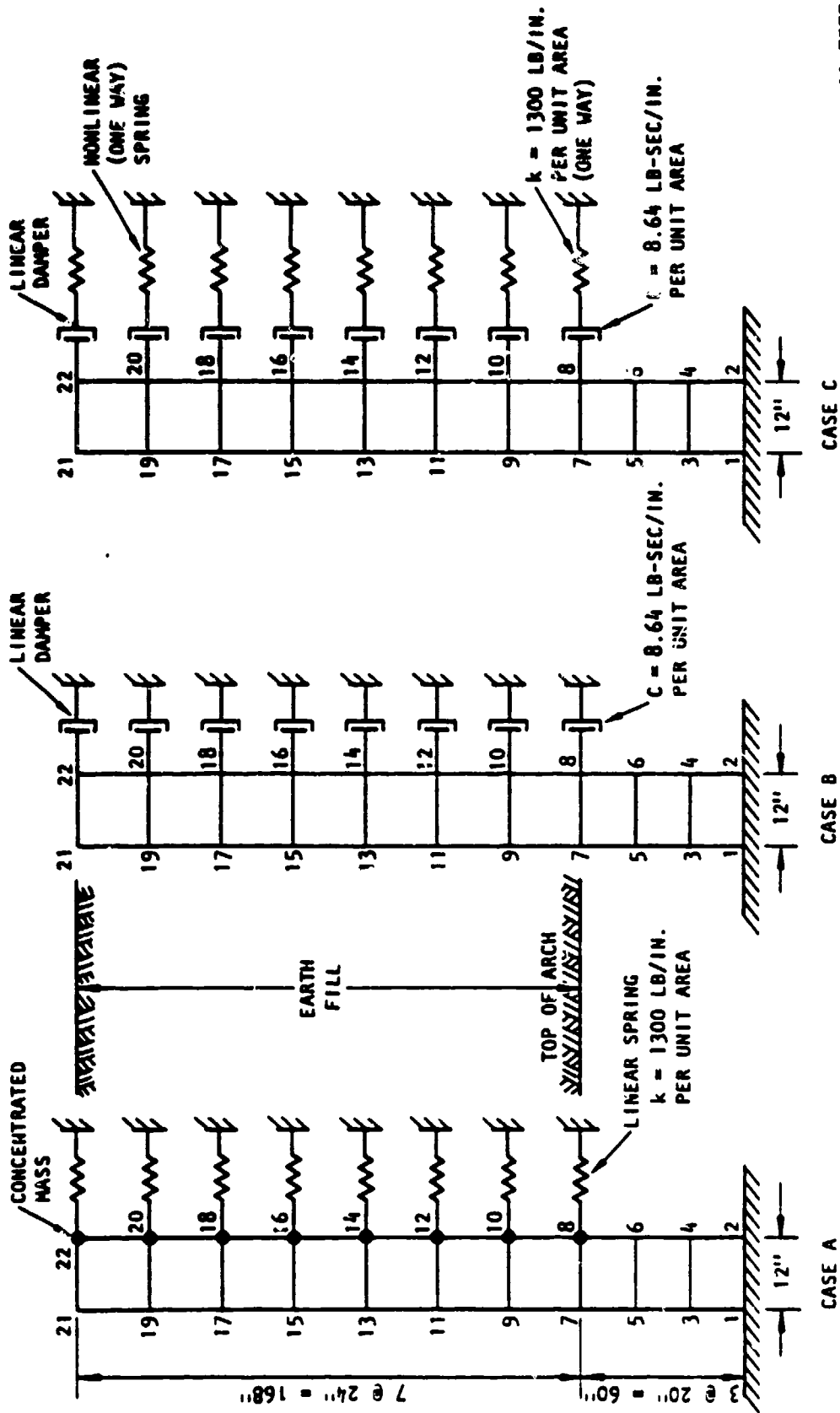
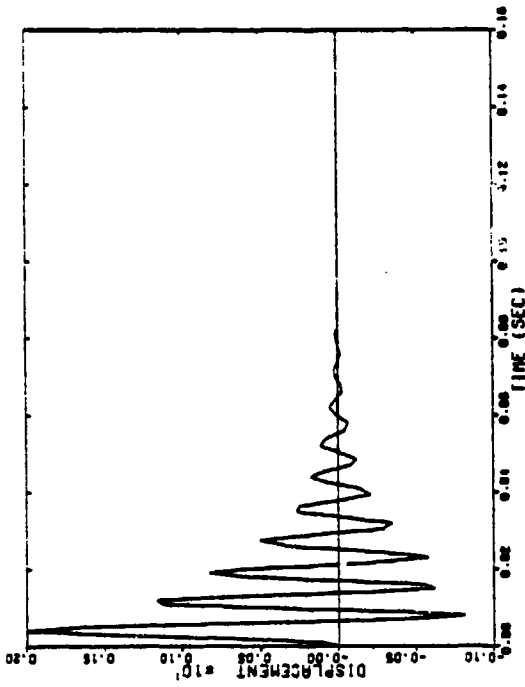
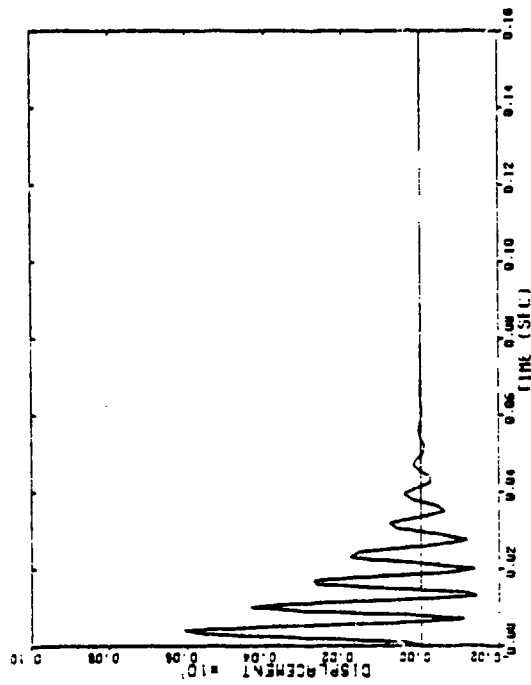


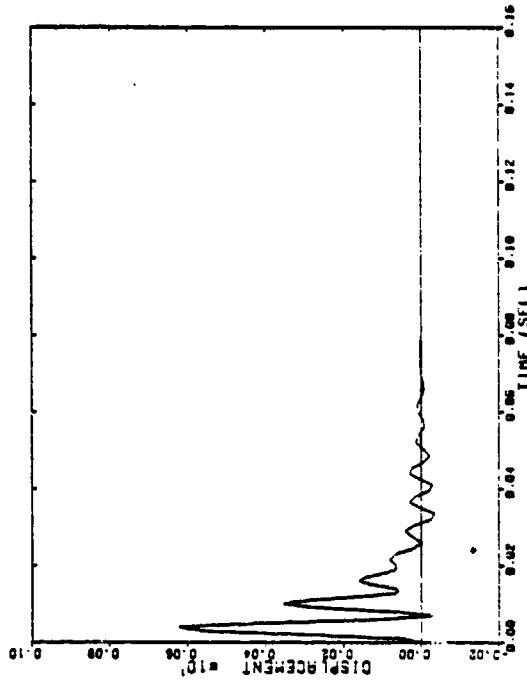
FIGURE 3-6. TEST PROBLEMS TO DETERMINE A SUITABLE MODEL TO REPRESENT SOIL



(a) Node 8

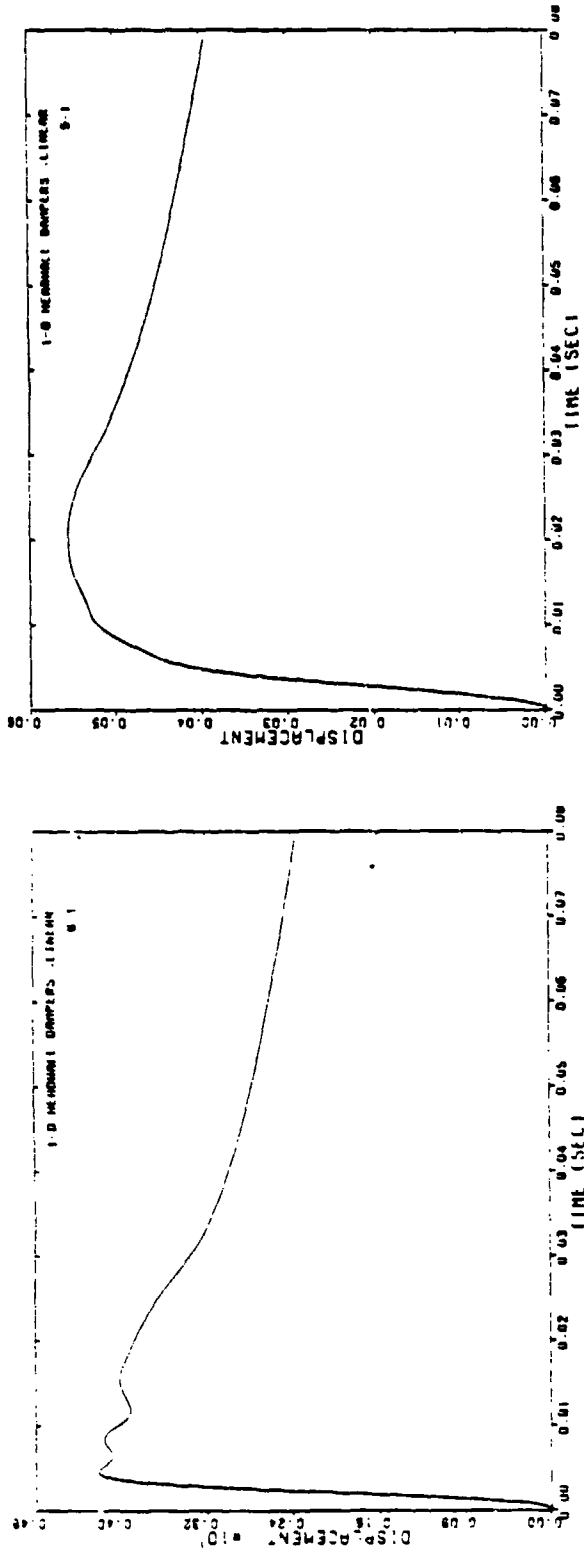


(b) Node 9

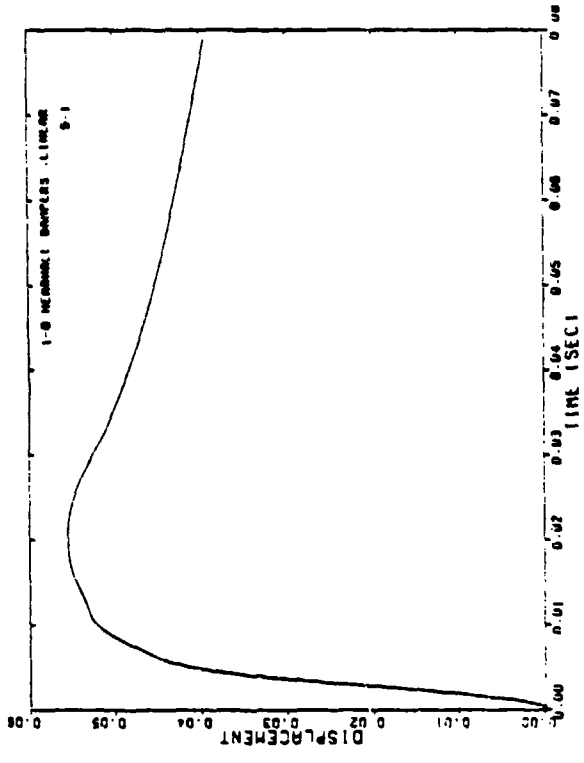


(c) Node 22

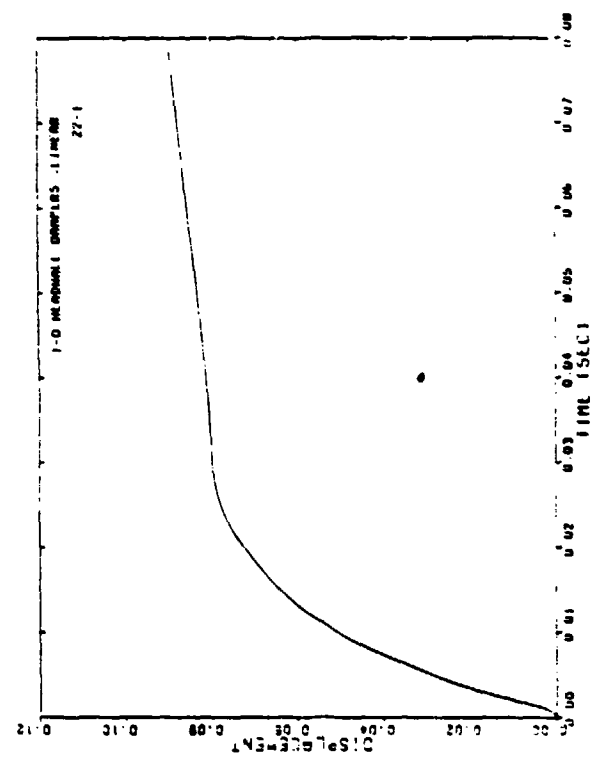
FIGURE 3-7. CASE A: DISPLACEMENT-TIME HISTORIES OF THE HEADWALL  
(Displacements are in inches.)



(a) Node 8

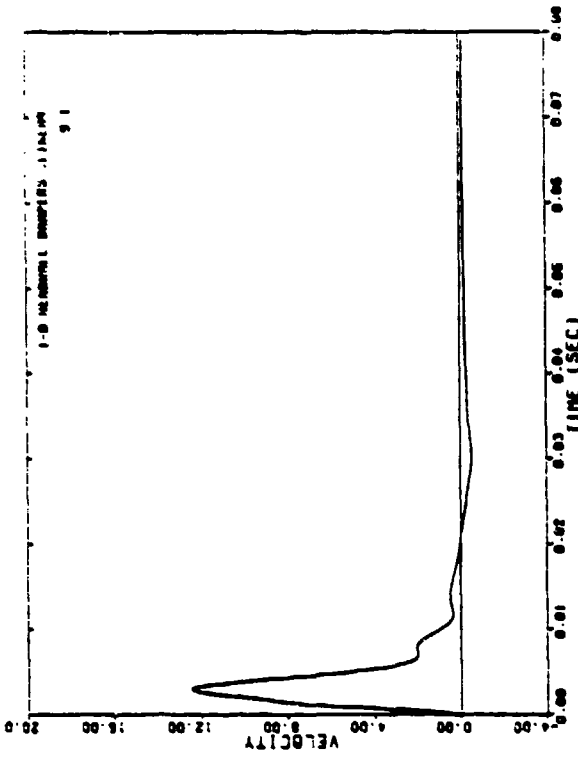


(b) Node 9

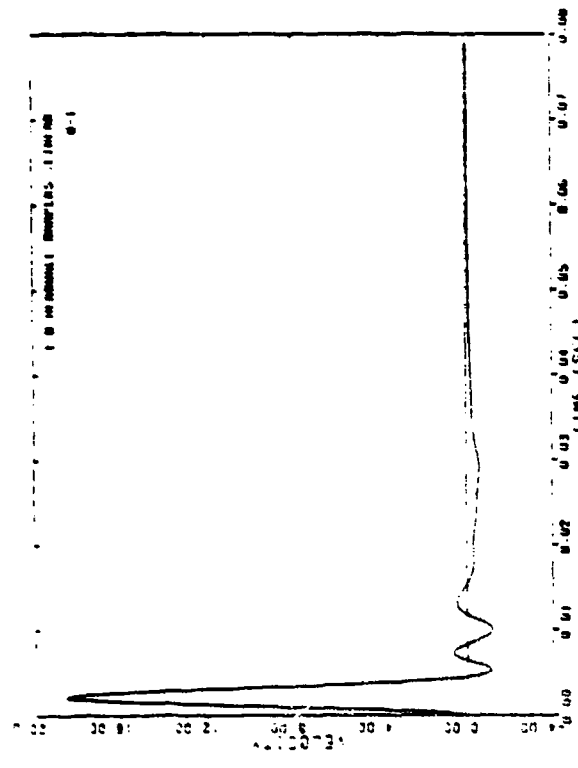


(c) Node 22

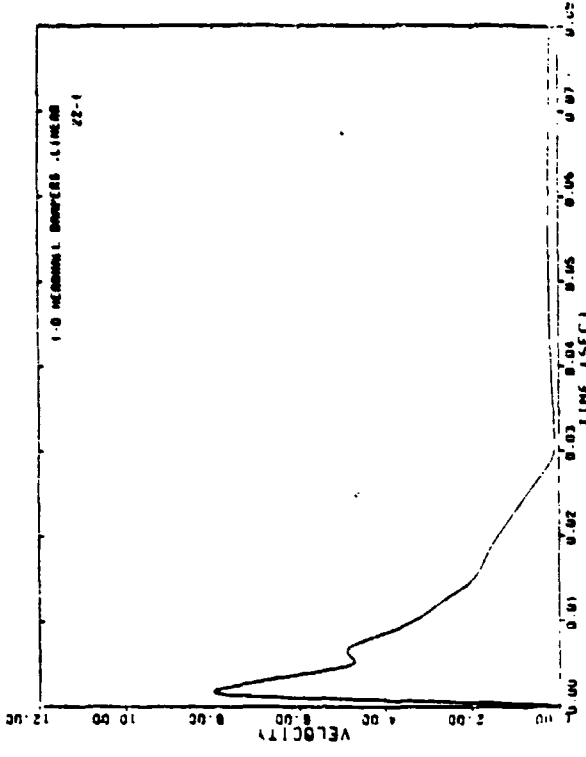
FIGURE 3-8. CASE B: DISPLACEMENT-TIME HISTORIES OF THE HEADWALL (Displacements are in inches.)



(a) Node 8

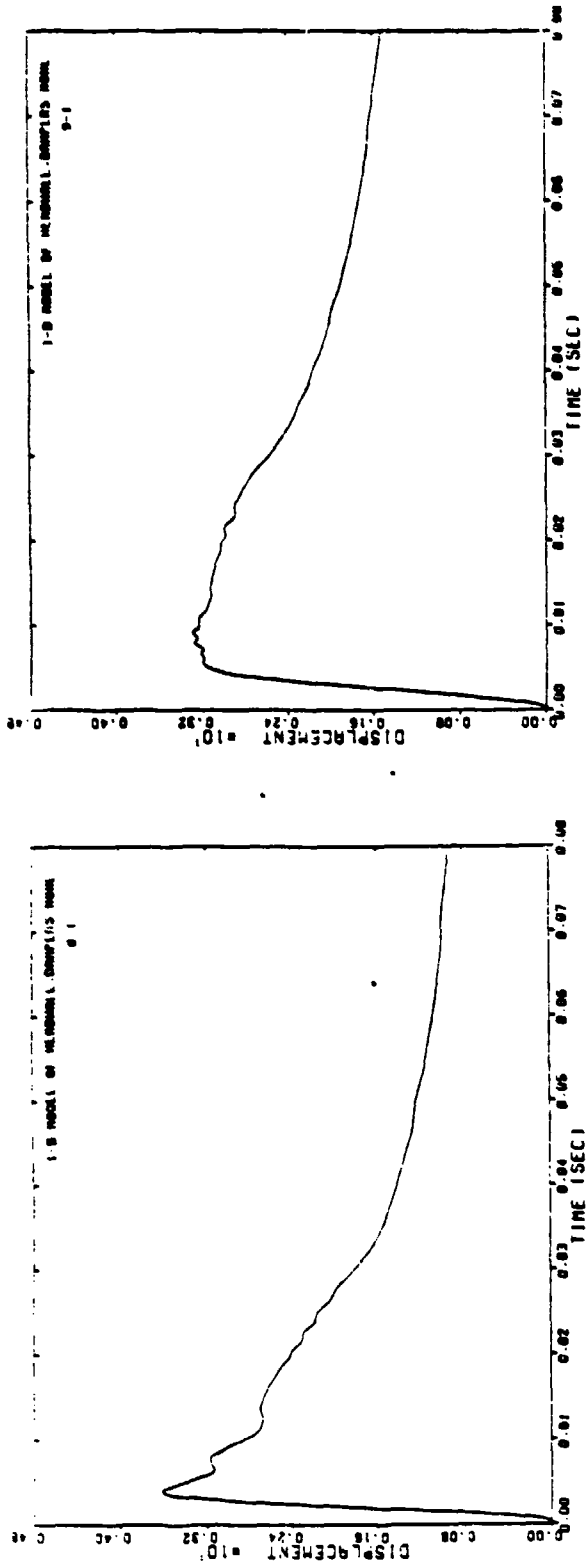


(b) Node 9

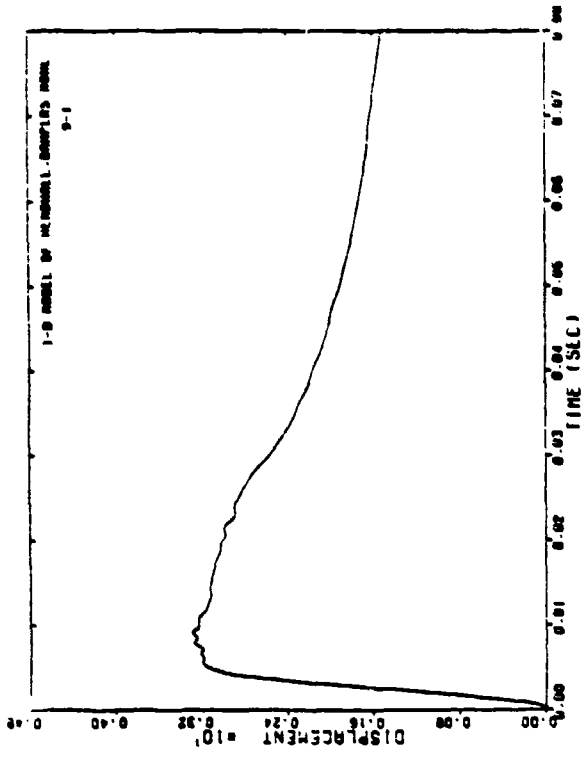


(c) Node 22

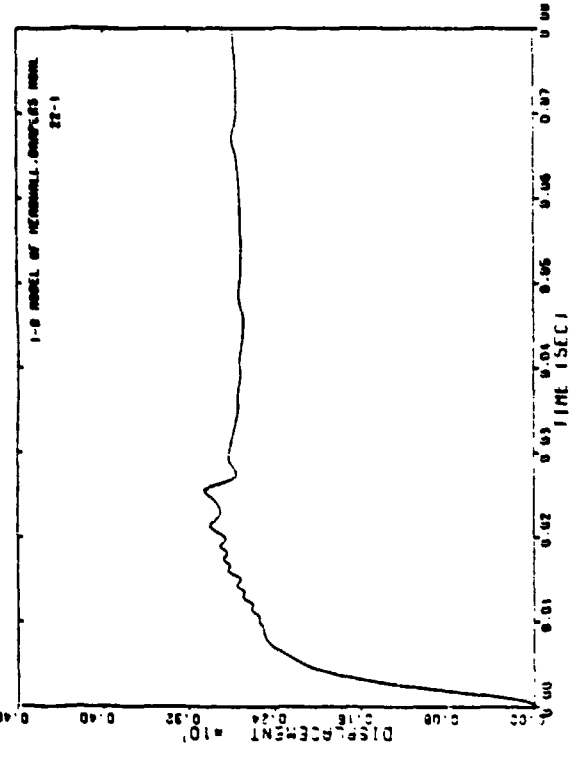
FIGURE 3-9. CASE B: VELOCITY-TIME HISTORIES OF THE HEADWALL  
(Velocities are in in./sec units.)



(a) Node 8

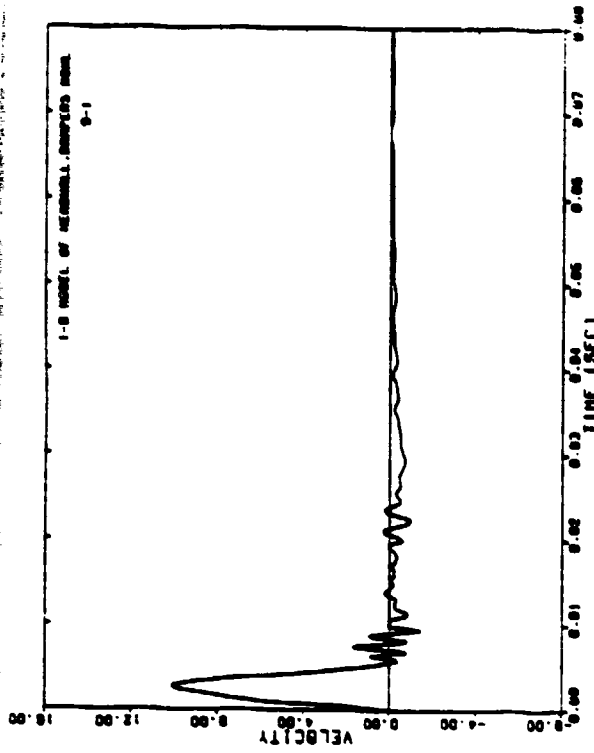


(b) Node 9

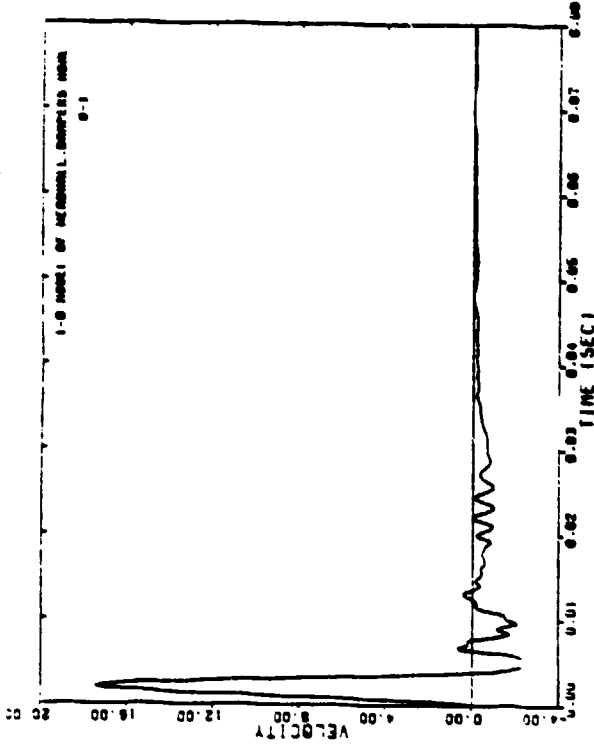


(c) Node 22

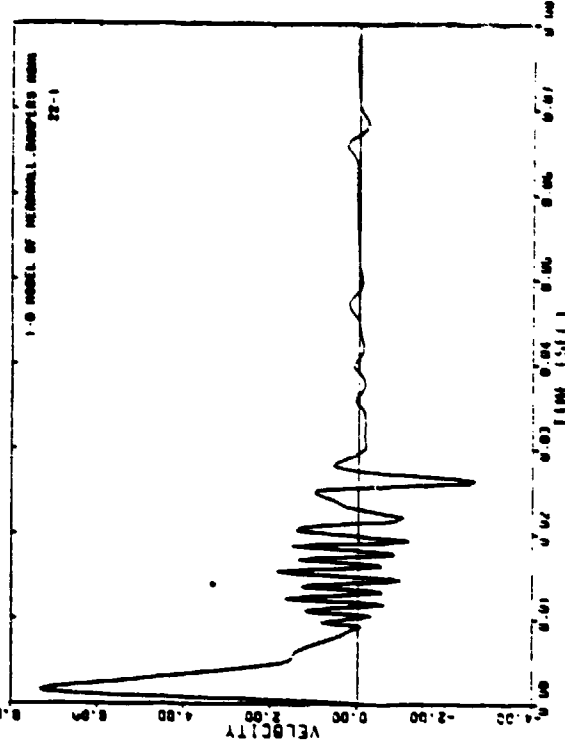
FIGURE 3-10. CASE C: DISPLACEMENT-TIME HISTORIES OF THE HEADWALL (Displacements are inches.)



(a) Node 8



(b) Node 9



(c) Node 22

FIGURE 3-11. CASE C: VELOCITY-TIME HISTORIES OF THE HEADWALL  
(Velocities are in in./sec units.)



where large permanent displacements of headwalls were noted. The headwall in Case B (Fig. 3-8) does not exhibit any oscillations initially and then stabilizes at a displacement level slightly smaller than the maximum value. The displacement and velocity time histories for Case C are shown in Figures 3-10 and 3-11, respectively. The behavior of the headwall in Case C is similar to Case B except that the final displacements in Case C are well below the maximum values.

In the ESKIMO I test, a gap of several inches between the headwall and the earth fill was noted (Ref. 1). This indicated that the permanent displacements of the headwalls were significantly smaller than the maximum values reached during the test. The soil model of Case C (Fig. 3-6) appears to best represent the qualitative behavior of the earth fill in the ESKIMO tests. However, the magnitude of the displacements obtained in Case C indicates that reduced numerical values of coefficients for the springs and dampers must be used. In the absence of any relevant measurements, the only guidelines for choosing these coefficients is their performance in small test problems. It was found that, in such a test problem, a spring constant of 40 lb/in. per unit area and a damping coefficient of 0.75 lb-sec/in. per unit area produced headwall displacements that were of the order of magnitude observed in ESKIMO I.

This combination of linear damper and nonlinear one-way spring was used to represent the interaction of soil with the finite element mesh of the south headwall (Fig. 3-2). The constants for the spring and dashpot at a node were based on the total tributary area of soil to be concentrated at that node. The existing INSLAB code did not provide for nonlinear springs. Therefore, the program was modified to accept nonlinear one-way springs. Theoretical details on the incorporation of these springs, along with some test cases, are presented in Appendix A.



### 3.1.4 EFFECTS OF CONCRETE FLOOR SLAB

The floor of the south igloo in ESKIMO 1 is a concrete slab 6-in. thick, which thickens to 12 in. near the headwall. The reinforcement consists of No. 4 bars spaced 12 in. apart, 3 in. below the top surface of the slab. Linear spring elements and concentrated masses are used to model the effects of the floor. The spring constant per unit area of the floor slab, determined in response to a static-compressive stress, is

$$k_L = 12,500 \text{ lb/in.}^3$$

This value was obtained assuming Young's modulus of concrete to be

$$E_c = 3 \times 10^6 \text{ lb/in.}^2$$

and the length of the igloo to be 20 ft. The stiffness of the floor in response to a dynamic load would be larger than the value given above. However, the fact that the rear wall of the igloo is not anchored perfectly would result in a slightly lower stiffness value. Assuming that the various unknowns compensate for each other, the static stiffness was used in modeling the effect of the floor.

The value of the mass of the floor slab participating in the mass/spring representation was chosen to preserve the fundamental frequency of longitudinal vibration of the floor. The resulting value is equal to the mass of a strip of floor slab 3.2-ft wide.



### 3.1.5 EFFECTS OF STEEL ARCH

The main function of the steel arch in a magazine is to protect the contents of the magazine from the weather and from the earth fill over the magazine. The only structural requirement for the arch is to support the earth fill around the arch. The material used in the arch for the south igloo headwall (ESKIMO 1) is No. 1-gage corrugated steel. The corrugation increases the bending and circumferential stiffness of the arch, but reduces its longitudinal, or axial, stiffness.

To study the longitudinal stiffness of the arch, one corrugation of the arch is considered. Since this is symmetrical at the centerline of the fold, only one half of the fold is necessary. The curved fold is approximated by a straight segment AB, as shown in Figure 3-12. Under the action of a horizontal load P at end A of the segment, the horizontal displacement of A results due to bending and axial compression of the member AB. The component of deflection due to bending can be calculated as

$$\delta_b = \frac{PL^3 \sin^2 \theta}{12EI \cos^3 \theta}$$

and the component due to axial compression is given by

$$\delta_a = \frac{PL \cos \theta}{AE}$$

where EI and AE are, respectively, the bending and axial stiffnesses of the arch. Therefore the total horizontal displacement of A is

$$\delta = \frac{PL^3 \sin^2 \theta}{12EI \cos^3 \theta} + \frac{PL \cos \theta}{AE}$$

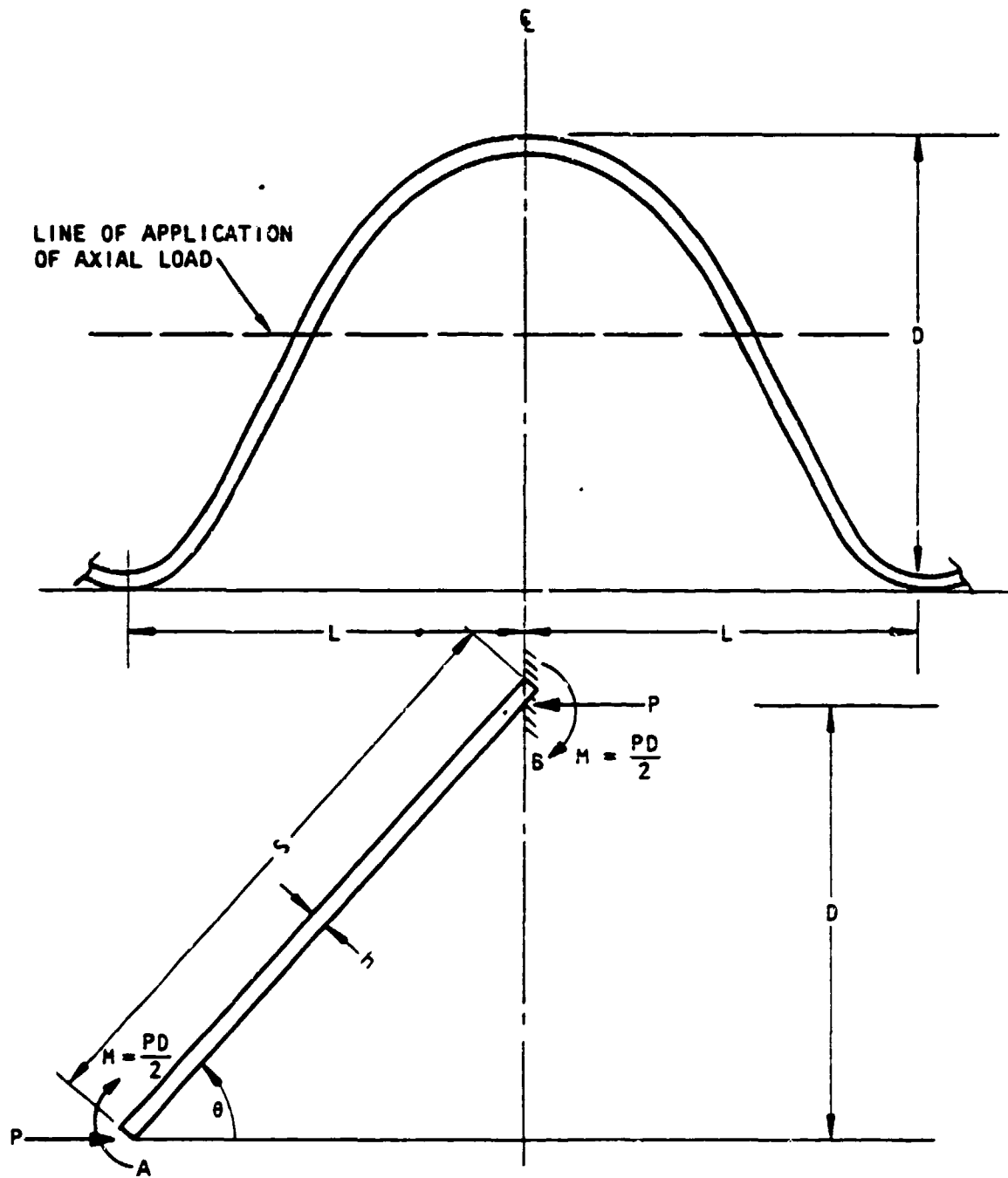


FIGURE 3-12. AXIAL STIFFNESS OF STEEL ARCH



For a unit width of the arch, the following values are used to compute  $\delta$ :

$$A = 0.2758 \text{ in.}^2$$

$$E = 30 \times 10^6 \text{ psi}$$

$$I = 0.001748 \text{ in.}^4$$

$$L = 3 \text{ in.}$$

$$h = 0.2758 \text{ in.}$$

$$\theta = 33.7^\circ$$

The horizontal displacement  $\delta$  is computed as

$$\delta = (2.32 \times 10^{-5} \text{ in./lb}) P$$

If the corrugated arch were to be treated as if it were constructed of an equivalent uncorrugated material, the relation between load and deflection would be

$$\delta = \frac{PL}{AE_e}$$

where  $E_e$  is the equivalent elastic modulus of the uncorrugated material. This relation can be used to determine the equivalent modulus, making use of the above relation between load and deflection. The result is

$$E_e = 4.68 \times 10^5 \text{ psi}$$

The buckling stress of the equivalent uncorrugated arch is computed from the relation

$$\sigma = \frac{E_e h}{a \sqrt{3(1 - \nu^2)}}$$



where  $a$  is the radius of the arch ( $a = 156$  in.),  $h$  is the thickness of the arch, and  $\nu$  is Poisson's ratio of the arch material (assumed  $\nu = 0.25$ ). The buckling stress is computed to be 495 psi. Although this is the theoretical buckling stress for the equivalent uncorrugated arch, buckling experiments on cylindrical shells show that the stress at which the shells buckle is seldom better than 30% of the theoretical value (Ref. 13). Thus, the buckling stress of the arch is estimated to be 150 psi.

Nodal point 31 of the finite element grid of Figure 3-2 is a typical nodal point located on the arch. The length of the arch that is attributed to this node is about 24 in. Therefore, the force acting on this node due to buckling of the arch is 990 lb. At no time can the force of the arch on Node 31 exceed this value. This node is also influenced by an area of about 143 in.<sup>2</sup> of soil backfill. Using Node 28 (see Fig. 3-1) of the previous calculation of ESKIMO 1, south igloo, as a guide, the expected peak displacement and velocity of Node 31 are 5 in. and 150 in./sec, respectively. The soil is represented with springs having a stiffness of 40 lb/in. per unit area, and dampers having a viscosity of 0.75 lb-sec/in. per unit area. These values result in a peak force of 28,600 lb due to elasticity of the soil, and an additional peak force of 16,100 lb due to damping. By comparison, the contribution of the arch is expected to be negligible.

A study of the permanent deformations and damage patterns of headwalls in the ESKIMO tests indicate that the steel arch appears to strongly influence the behavior of the headwalls during the tests. As an example, Figure 3-13 is a contour diagram of the deformation of a headwall after the ESKIMO 1 test. The deformation contours generally approximate the shape of the steel arch, which was semicircular. Figure 3-14 shows a front photographic view of the same headwall after the test. The crack pattern experienced by the headwall again approximates the shape of the steel arch. It is believed that this phenomenon occurs because the arch separates the supported and unsupported areas of the headwall. In particular, the unsupported area of

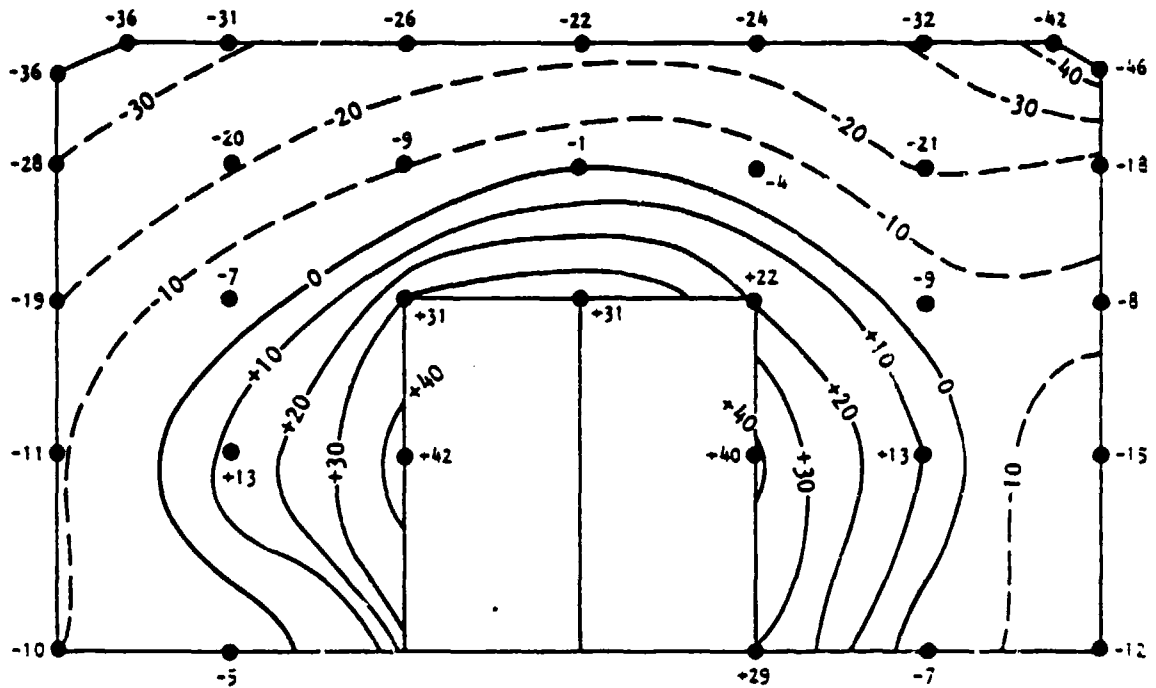


FIGURE 3-13. MOVEMENT OF HEADWALL OF NORTH ACCEPTOR IGLOO, ESKIMO I. A plus value shows movement away from the donor magazine; a minus value shows movement toward. The units are in hundredths of feet.



R-7556-1-4162

Copy available to DDC does not  
permit fully legible reproduction

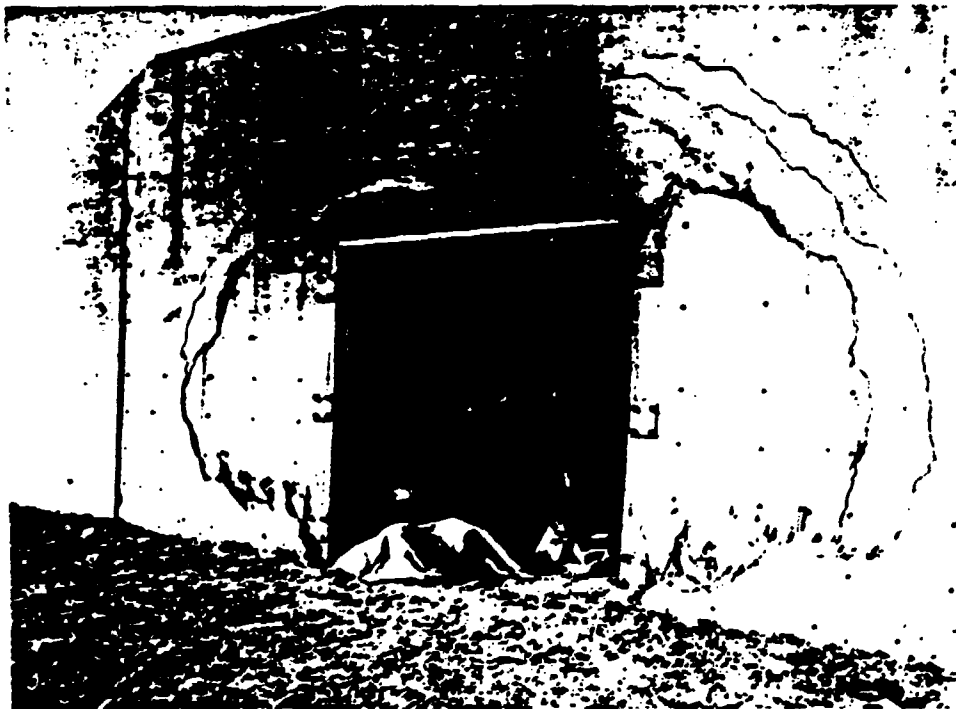


FIGURE 3-14. HEADWALL OF NORTH IGLOO, ESKIMO I. Note crack  
pattern approximating shape of steel arch.

Copy available to DDC does not  
permit fully legible reproduction



the headwall is semicircular, and hence it is not surprising that the permanent deformation and damage patterns of the headwall resemble the shape of the arch. In addition, the sharpness of the steel arch causes high stresses in the headwall, causing local failure along the arch line.

### 3.2 STRUCTURAL MODELS OF HEADWALLS IN ESKIMO II

Two different headwalls in the ESKIMO II test have been analyzed. These are the Igloo C (east) and Igloo B (northeast) headwalls. The structural models of these headwalls are described in the following subsections.

#### 3.2.1 IGLOO C (EAST) HEADWALL

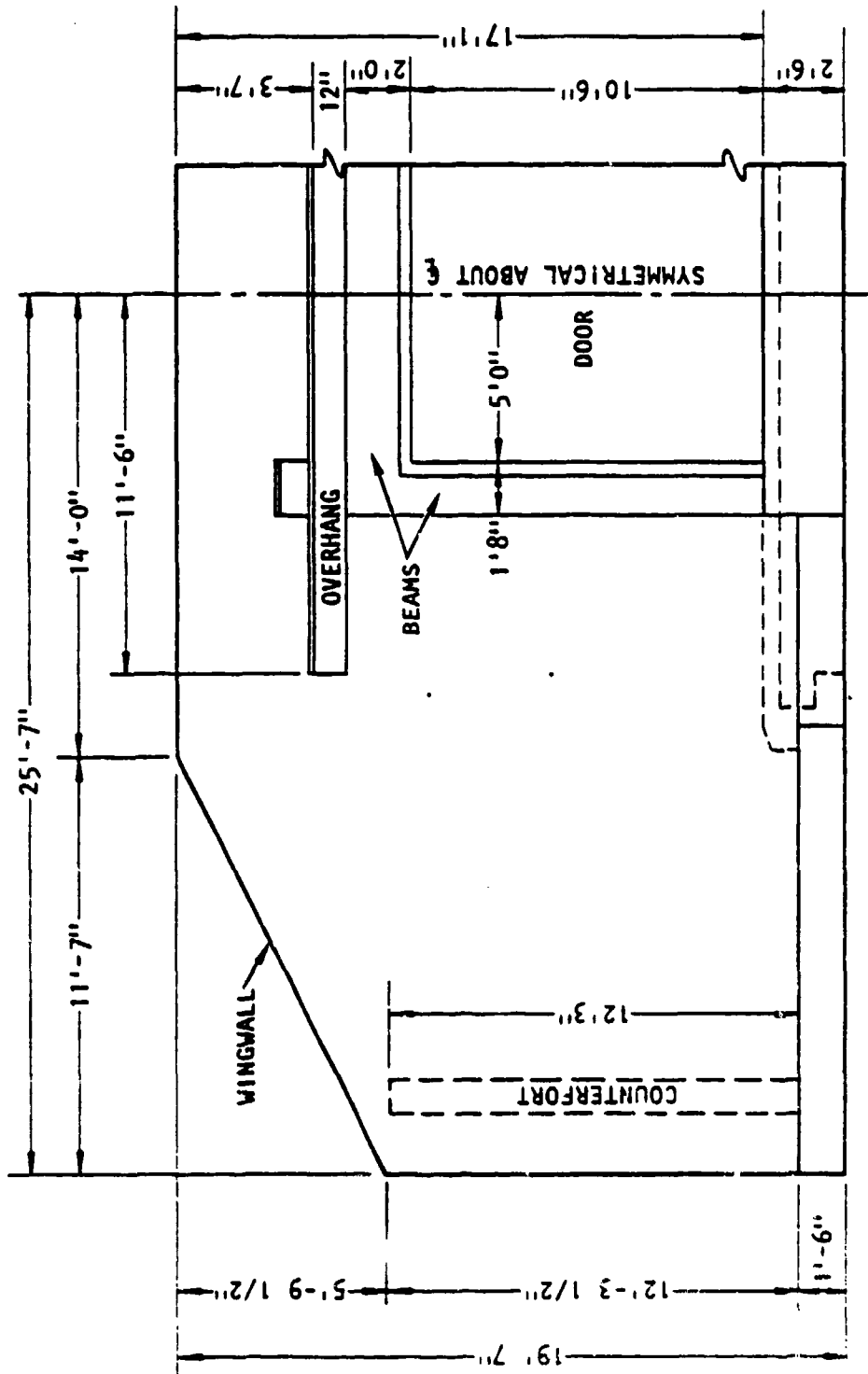
As described in Section 1.2, the east headwall in the ESKIMO II test is identical in every respect to the igloos used in ESKIMO I. Therefore, the finite element model of the east headwall in ESKIMO II is identical to the model of the south headwall in ESKIMO I (Fig. 3-2) described in Section 3.1.

#### 3.2.2 IGLOO B (NORTHEAST) HEADWALL

Figure 3-15 shows a plan and an elevation of the Igloo B (northeast) headwall in the ESKIMO II test. The wingwalls are of reinforced concrete construction and are monolithic with the headwall. Therefore, the finite element model of the headwall shown in Figure 3-16 includes the portion of the wingwall up to the counterfort in order to consider the effect of the wingwall on the response of the headwall. As described before, an oval-shaped steel arch is used behind the headwall to support the soil. The opening in the headwall for the door is strengthened with concrete beams, as shown in Figure 3-15. On top of the horizontal beam, there is an overhang that extends 3 ft from the headwall. Since there is very little reinforcement provided along the vertical direction, the overhang is not considered to function as a structural member. Therefore, although the mass of the overhang is included in the finite element model, the stiffness is not. In designing the finite element mesh shown in Figure 3-16, the beams are represented by separate



R-7556-1-4182



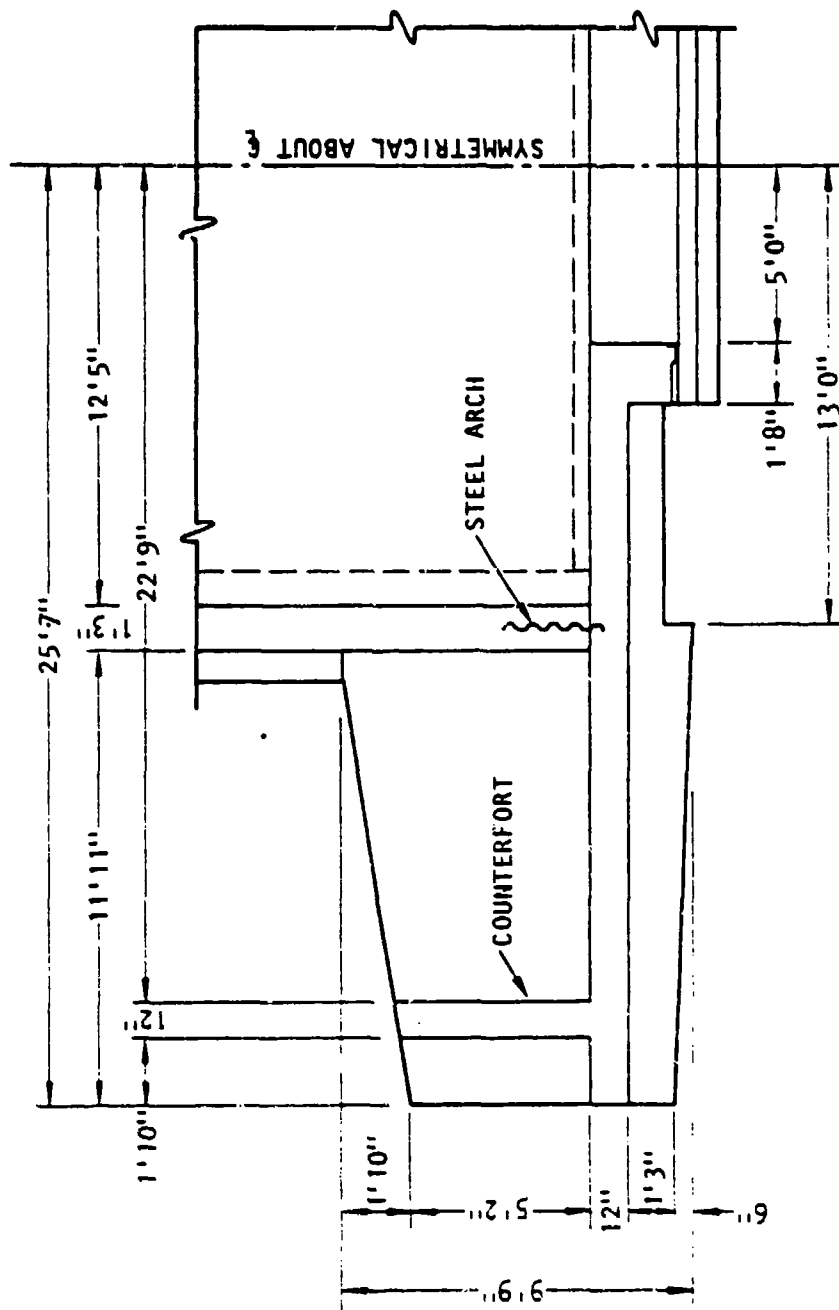
SCALE: 3/16" = 1'0"

(a) Partial elevation

FIGURE 3-15. IGLOO C (NORTHEAST) HEADMALL, ESKIMO II



R-7556-1-4182



(b) Partial plan

FIGURE 3-15. (CONCLUDED)

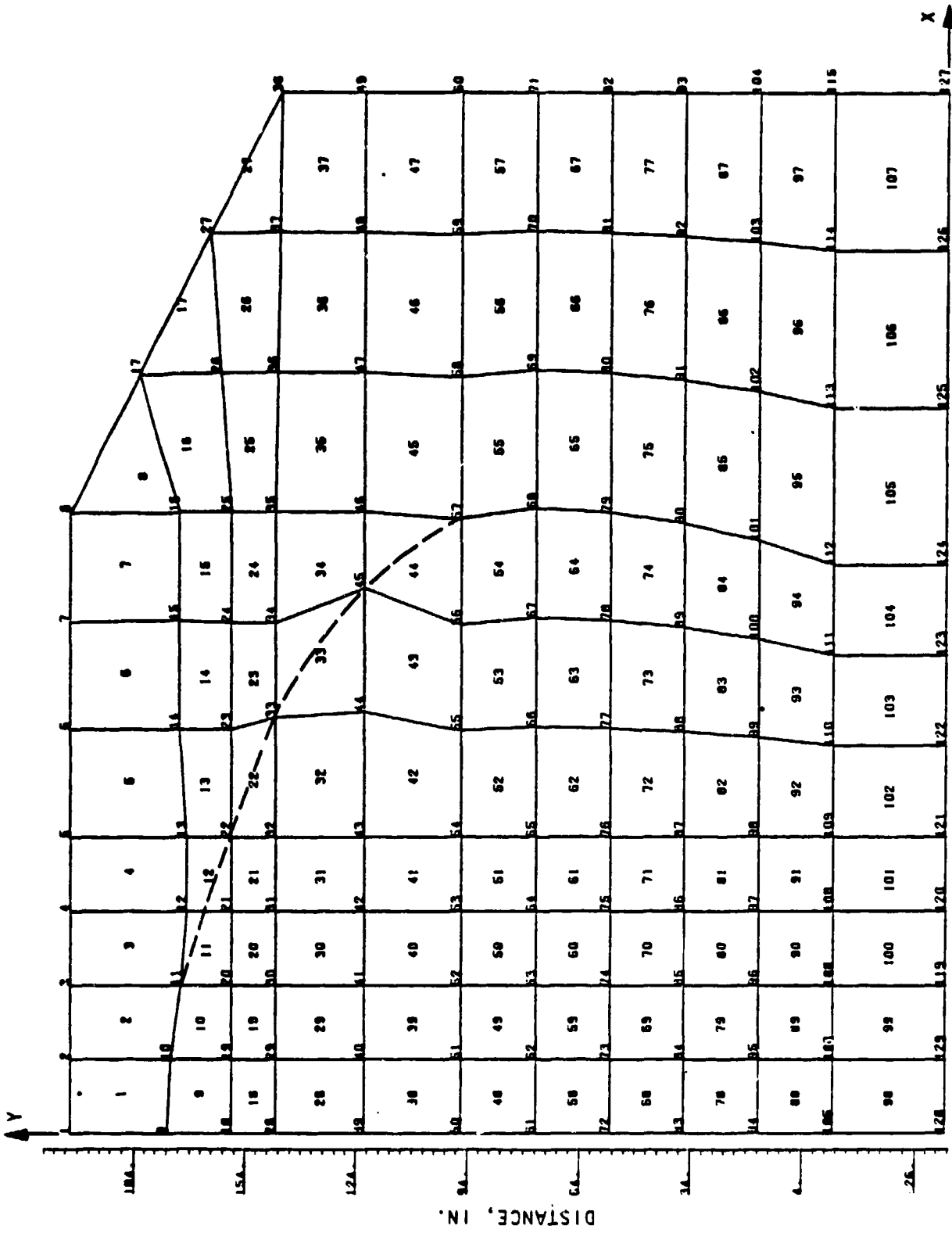


FIGURE 3-16. FINITE ELEMENT MESH OF IGLOO B (NORTHEAST) HEADWALL, ESKIMO 11



elements so that the actual beam properties can be assigned to only the elements representing the beams. This avoids the averaging of properties that becomes necessary when the same element represents the beam and a portion of headwall. The arch line is placed as closely as possible on the edges of the finite elements. In order to minimize the use of triangular elements, the arch line is permitted to run across the Elements 11, 12, 22, 33, and 44, as shown in Figure 3-16. The finite element shown in Figure 3-16 consists of a total of 107 plate elements and 127 nodes.

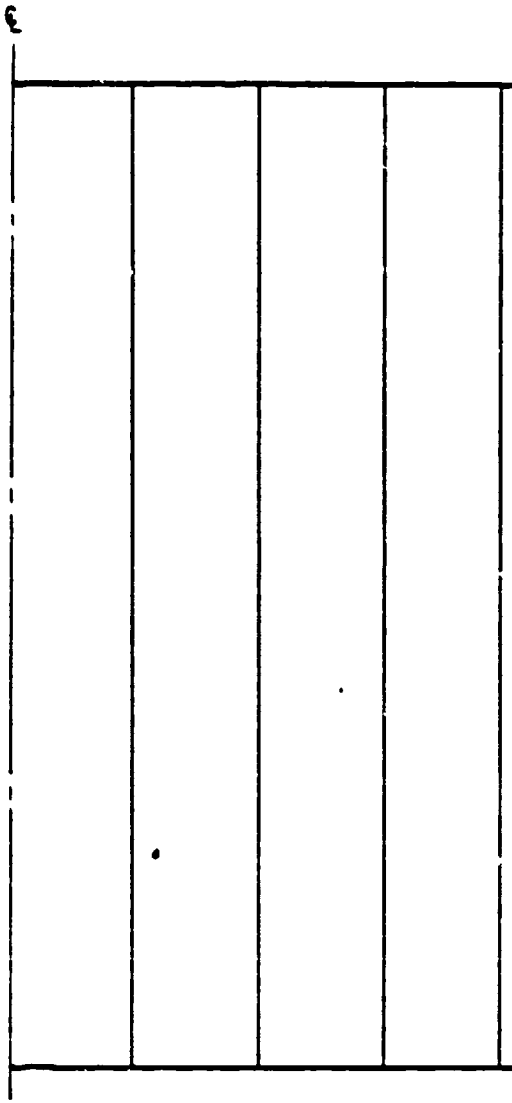
The biparting and sliding steel door of the northeast igloo consists of a 5/8-in. plate and a 1/4-in. plate sandwiching five 5110 steel sections arranged vertically as shown in Figure 3-17. Following the procedures described in Reference 2, the material properties of the elements representing the steel door are computed. These values are summarized below:

| Property                   | Symbol   | Numerical Value              |
|----------------------------|----------|------------------------------|
| Equivalent plate thickness | $h$      | 4.14 in.                     |
| Modulus of elasticity      | $E$      | $30 \times 10^3$ ksi         |
| Equivalent density         | $\rho$   | $0.0773$ lb/in. <sup>3</sup> |
| Yield moment               | $M_{xx}$ | 68.6 kip-in./in.             |
| Yield moment               | $M_{yy}$ | 92.9 kip-in./in.             |
| Plastic modulus            | $E_p$    | 0.1 of elastic modulus       |
| Poisson's ratio            | $\nu$    | 0.25                         |

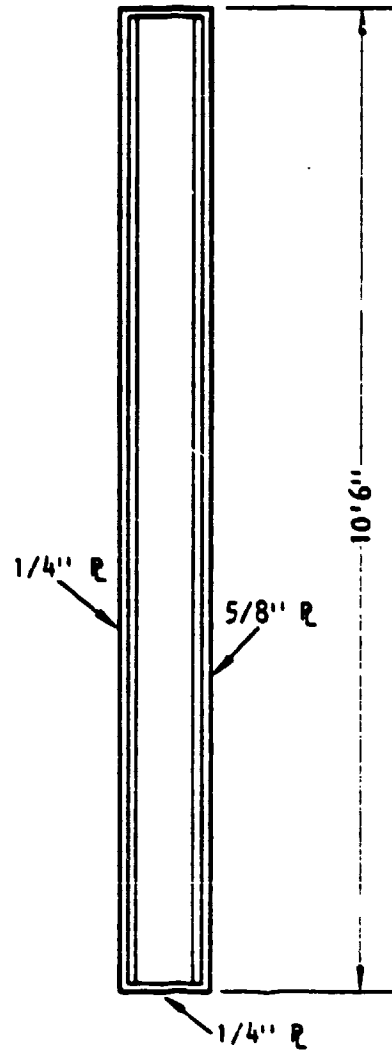
The headwall and wingwall are modeled as homogeneous plates of uniform thickness possessing the same dynamic characteristics as the actual reinforced-concrete sections. The yield moments for these plates are computed using the procedures described in Appendix B. The yield moments and equivalent properties of the headwall and wingwall sections are shown in Table 3-3.



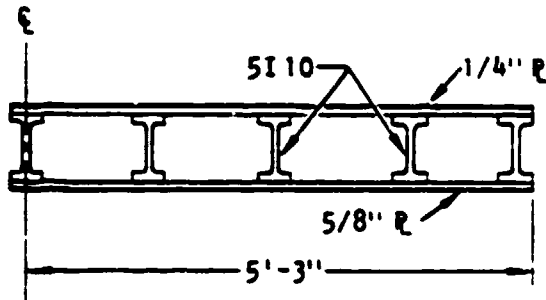
R-7556-1-4182



(a) Elevation



(b) Longitudinal section



(c) Cross section

FIGURE 3-17. CONFIGURATION OF STEEL DOOR FOR IGLOO B (NORTHEAST), ESKIMO II



TABLE 3-3. PROPERTIES OF HEADWALL AND WINGWALL SECTIONS OF IGLOO B (NORTHEAST), ESKIMO II

| Property                      | Value for Headwall Section | Value for Wingwall Section |
|-------------------------------|----------------------------|----------------------------|
| Equivalent plate thickness, h | 12 in.                     | 12 in.                     |
| Modulus of elasticity, E      | $4.6 \times 10^5$ psi      | $2.67 \times 10^5$ psi     |
| Equivalent density, $\rho$    | 150 lb/ft <sup>3</sup>     | 150 lb/ft <sup>3</sup>     |
| Yield moment, $M_{xx}^+$      | 290 kip-in./ft             | 101 kip-in./ft             |
| Yield moment, $M_{xx}^-$      | -231 kip-in./ft            | -79 kip-in./ft             |
| Yield moment, $M_{yy}^+$      | 196 kip-in./ft             | 192 kip-in./ft             |
| Yield moment, $M_{yy}^-$      | -160 kip-in./ft            | -83 kip-in./ft             |

AA8012

The supporting system of the headwall consists of the backfill on top of the steel arch, the concrete floor slab, and the soil below the floor slab. These supports are represented in the form of springs and dampers as described in Sections 3.1.3 and 3.1.4.

### 3.3 STRUCTURAL MODEL OF IGLOO B (NORTHEAST) HEADWALL, ESKIMO IV

Figure 3-18 shows the finite element model of the headwall of the northeast igloo in the ESKIMO IV test. An oval-shaped steel arch supports the soil for this igloo. The door opening in the headwall is strengthened with concrete beams. The vertical beam extends to the top of the headwall. As in the case of the northeast headwall in the ESKIMO II test, the model of this headwall represented the beams by separate elements. An effort was made, as far as possible, to place the arch line on the edges of the finite elements. However, in order to minimize the use of triangular elements, the arch line was permitted to run across Elements 22, 33, 43, and 53, as shown in Figure 3-18. The finite element mesh for this headwall is designed so that

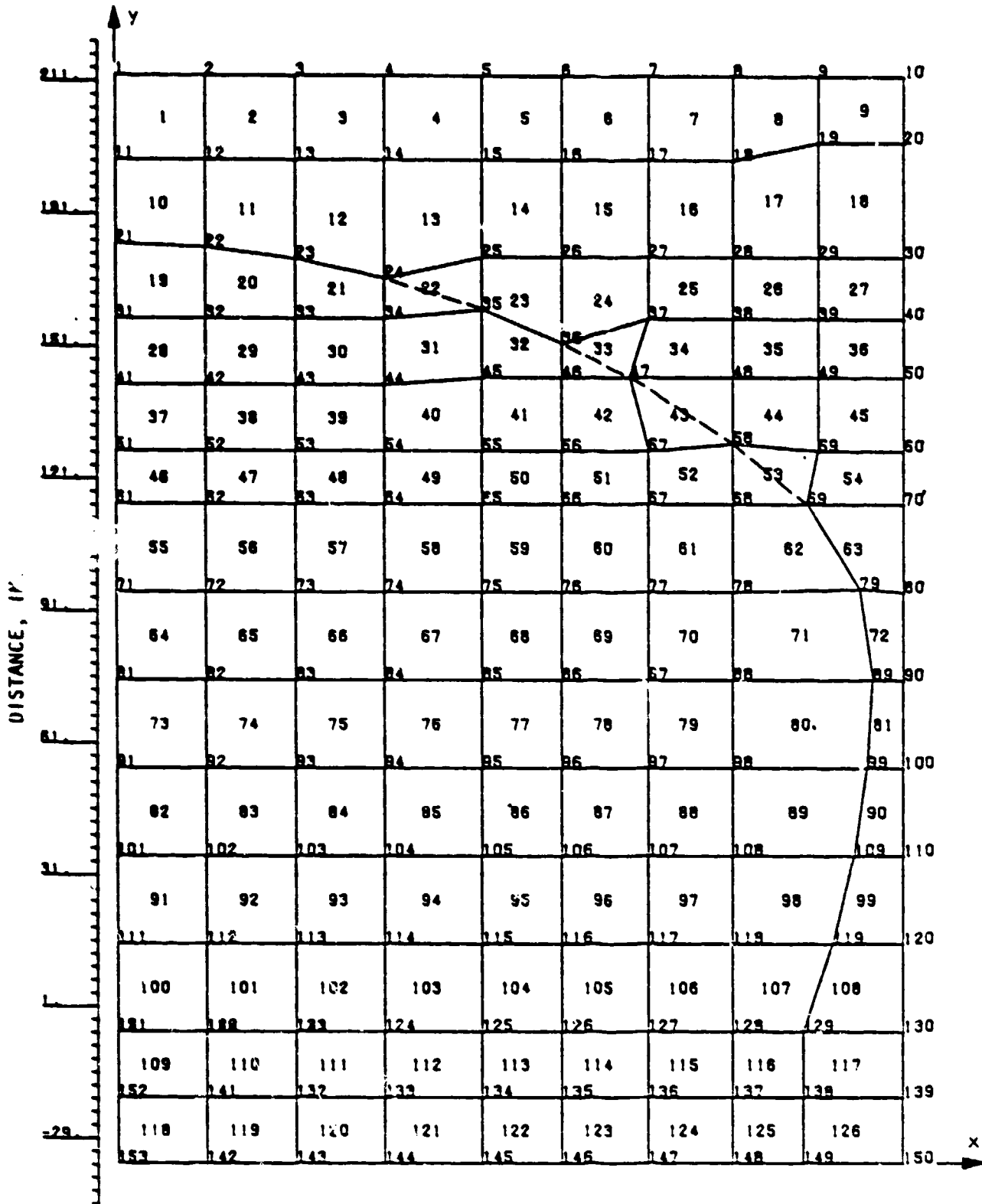


FIGURE 3-19. FINITE ELEMENT MODEL OF NORTHEAST HEADWALL, ESKIMO IV



the locations of the accelerometers and the LVDT transducers (see Sec. 4) generally correspond to some nodes in the mesh. This facilitates a direct comparison of the test and calculated results. The finite element mesh of the headwall shown in Figure 3-18 consists of a total of 126 elements and 150 nodes.

The single-leaf sliding steel door of this headwall consists of a 3/8-in. plate and a 1/4-in. plate, strengthened by four 6WF25 wide flange sections and two 6 [13 channels, all running horizontally. Two 6 [13 channels also run vertically along the two ends. This arrangement is shown in Figure 3-19. Following the procedures described in Reference 2, the material properties of the elements representing the steel door were computed. These values are summarized below:

| Property                   | Symbol   | Numerical Value           |
|----------------------------|----------|---------------------------|
| Equivalent plate thickness | $h$      | 4.49 in.                  |
| Modulus of elasticity      | $E$      | $30 \times 10^3$ ksi      |
| Equivalent density         | $\rho$   | 0.059 lb/in. <sup>3</sup> |
| Yield moment               | $M_{xx}$ | 107.0 kip-in./in.         |
| Yield moment               | $M_{yy}$ | 94.5 kip-in./in.          |
| Plastic modulus            | $E_p$    | 0.1 of elastic modulus    |
| Poisson's ratio            | $\nu$    | 0.25                      |

To account for the variation of section properties, a total of nine different materials is used to describe the model, as shown in Figure 3-20. Material No. 1 refers to the properties of the steel door, as discussed above. Due to the different arrangement of the reinforcing steel, the headwall section is assigned four different materials with Nos. 2, 3, 8, and 9, as shown in Figure 3-20. Material Nos. 5, 6, and 7 are used to represent the beams. Material 4 is assigned to the footing of the headwall. The material properties assigned to each material number is shown in Table 3-4. The yield moments of all concrete sections are computed using the procedures described in Appendix B.

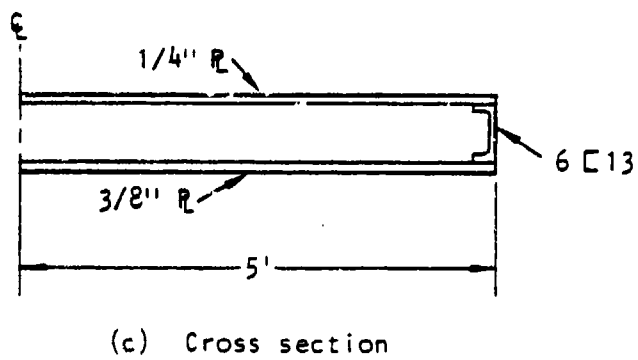
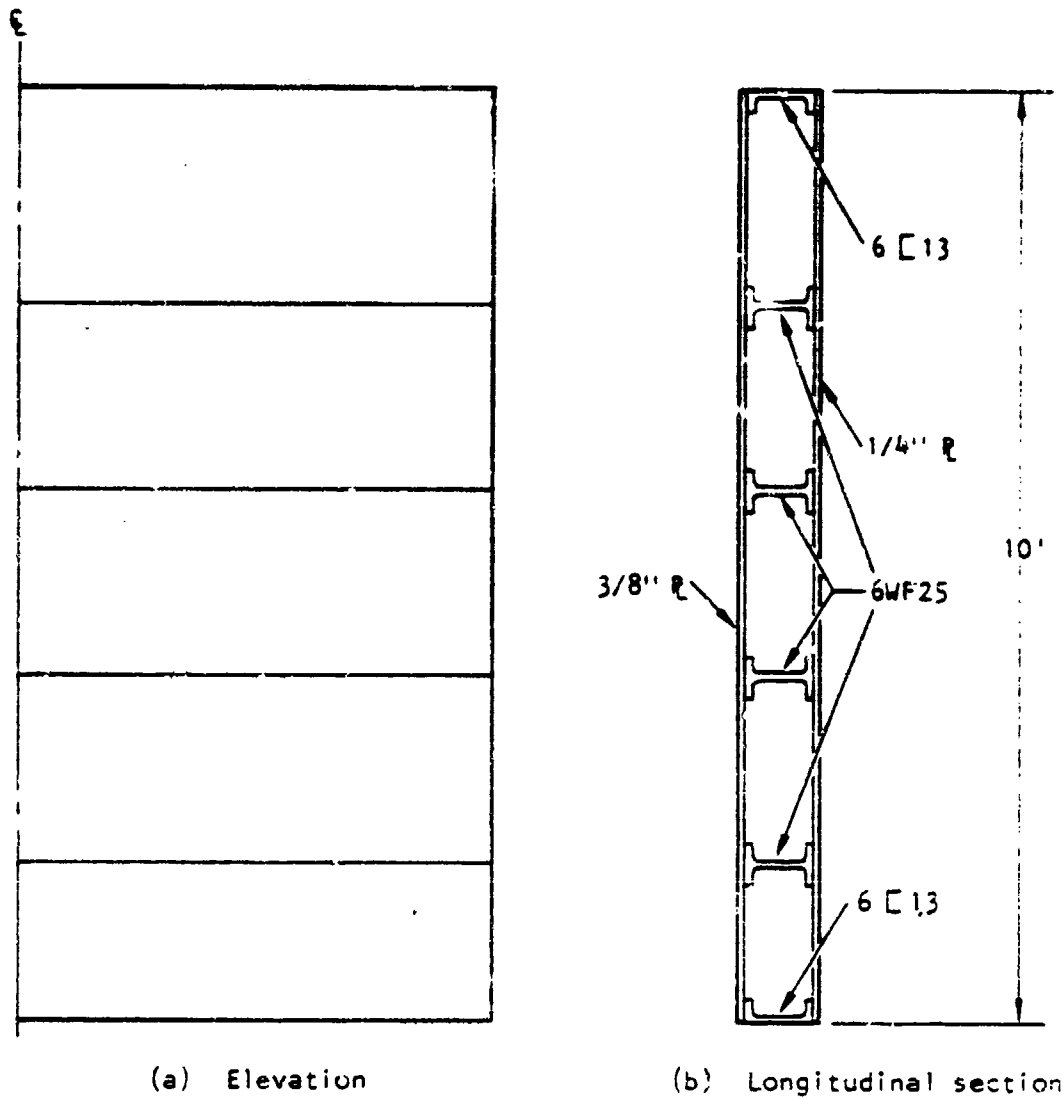


FIGURE 3-19. CONFIGURATION OF STEEL DOOR FOR IGLOO B (NORTHEAST) HEADWALL, ESKIMO IV



R-7556-1-4182

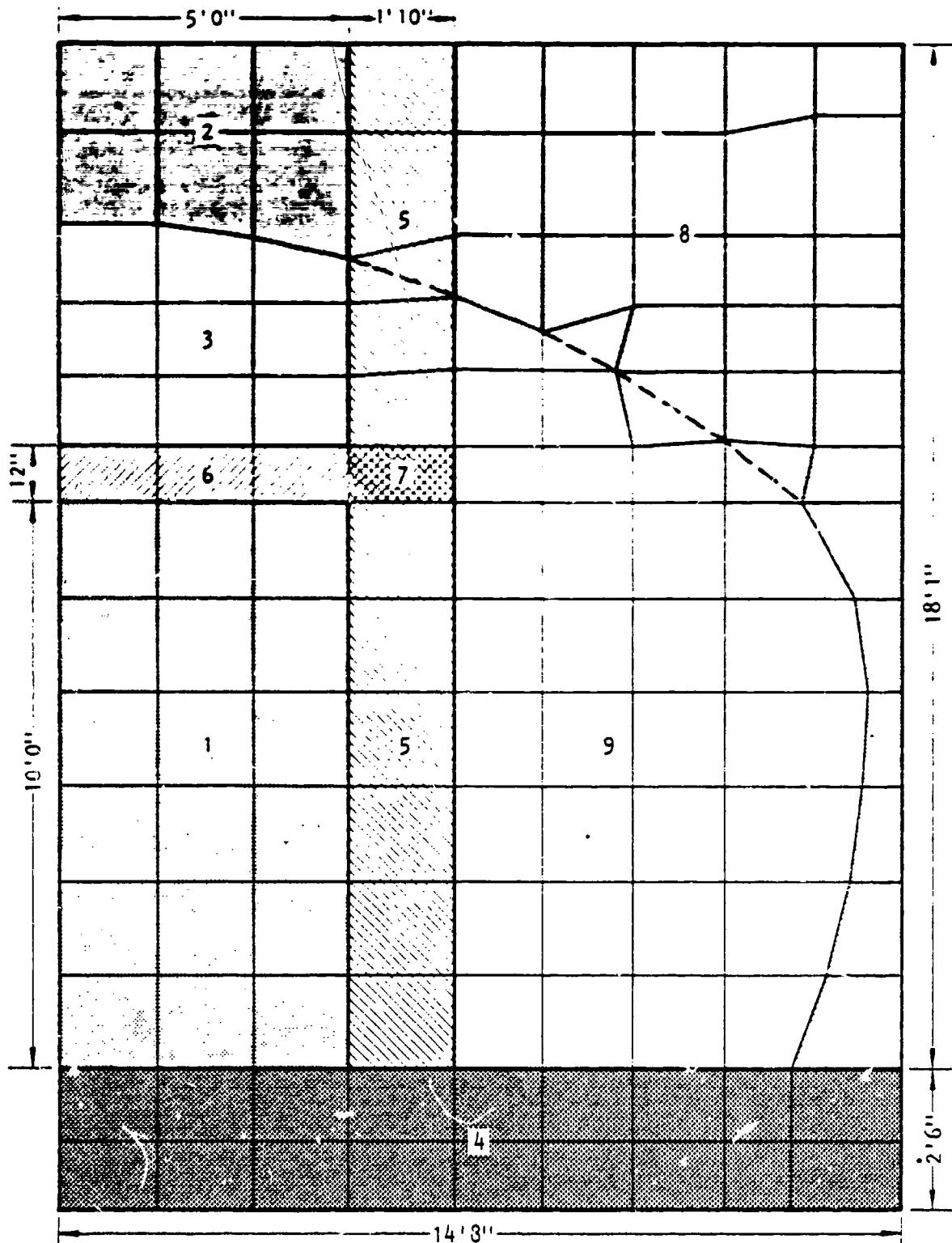


FIGURE 3-20. REGIONS OF DIFFERENT MATERIAL PROPERTIES FOR IGLOO B (NORTHEAST) HEADWALL, ESKIMO IV



TABLE 3-4. MATERIAL PROPERTIES FOR IGLOO B (NORTHEAST) HEADWALL, ESKIMO IV

| Material No. | Young's Modulus, psi | Poisson Ratio, $\nu$ | Thickness h, in. | Unit Yield Moments, lb-in./in. <sup>3</sup> |                       |               |               | Mass Density $\rho$ , lb-sec <sup>2</sup> /in. <sup>4</sup> |
|--------------|----------------------|----------------------|------------------|---|-----------------------|---------------|---------------|---|
|              |                      |                      |                  | $\uparrow M_{xx}/h^2$                       | $\uparrow M_{yy}/h^2$ | $-M_{xx}/h^2$ | $-M_{yy}/h^2$ |   |
| 1            | $3 \times 10^7$      | 0.25                 | 4.49             | 4690.00                                     | 5300.00               | -4690.00      | -5300.00      | 0.0592  |
| 2            | $2.95 \times 10^5$   | 0.20                 | 12.00            | 60.45                                       | 138.52                | -45.05        | -41.66        | 0.087   |
| 3            | $4.26 \times 10^5$   | 0.20                 | 12.00            | 57.70                                       | 133.37                | -119.65       | -82.29        | 0.087   |
| 4            | $1.2 \times 10^5$    | 0.20                 | 42.00            | 22.72                                       | 0.01                  | -22.72        | -41.43        | 0.087   |
| 5            | $1.19 \times 10^6$   | 0.70                 | 30.00            | 0.01  | 411.03                | -88.69        | -654.30       | 0.087   |
| 6            | $8.22 \times 10^5$   | 0.20                 | 30.00            | 304.90                                      | 0.01                  | -304.90       | -87.29        | 0.087   |
| 7            | $1.78 \times 10^6$   | 0.20                 | 30.00            | 304.90                                      | 44.03                 | -304.90       | -654.30       | 0.087   |
| 8            | $3.6 \times 10^5$    | 0.20                 | 12.00            | 136.82                                      | 130.89                | -44.43        | -43.42        | 0.087   |
| 9            | $7.01 \times 10^5$   | 0.20                 | 12.00            | 195.70                                      | 185.01                | -186.78       | -115.42       | 0.087   |

AA8051



R-7556-1-4182

The supporting system of the headwall consists of the backfill on top of the steel arch, the concrete floor slab, and the soil below the floor slab. The representation of these supports in the form of springs and dampers is described in Sections 3.1.3 and 3.1.4.



## SECTION 4

### INSTRUMENTATION FOR ESKIMO IV

This section describes Agbabian Associates' recommendations on the instrumentation of the igloos in the ESKIMO IV test: types of transducers that were to be used, their locations on the headwalls and doors, and the ranges of variables over which the transducers were to be calibrated. The recommendations reflected a desire to obtain sufficient measurements of the northeast headwall, since this is the only headwall of ESKIMO IV that was analyzed using the INSLAB code.

#### 4.1 PRESSURE GAGES

The Kistler gages were used to measure pressure-time histories on headwalls in the ESKIMO IV test. These quartz crystal piezoelectric transducers were selected because of their excellent past performance in similar events. Table 4-1 shows estimated peak pressures and the ratings of pressure gages that were scheduled to be used in ESKIMO IV. Table 4-1 also shows similar information for the Ballistic Research Laboratory (BRL) self-recording mechanical gages, placed in pairs, to measure far-field pressures along radial lines in the northwest, west, and south directions.

Figure 4-1 shows the recommended arrangement of pressure gages on the northeast igloo (Igloo B). The primary objective of this recommendation was to determine the variation of pressure loading on the wall in vertical and horizontal directions. Because of the symmetry of the loading with respect to the centerline of the headwall, all gages except one were placed on the right half of the headwall. The gage on the left half of the headwall was intended to detect any significant deviations in the symmetry of the loading. The arrangement shown in the figure commits 8 pressure gages for the northeast igloo. Figure 4-2 shows the recommended arrangement of the pressure gages on the remaining two igloos.

TABLE 4-1. SCHEDULE OF GAGES FOR MEASUREMENT OF AIR BLAST, ESKIHO IV

| Kistler Gages                    |  |                                  |                                 |
|----------------------------------|--|----------------------------------|---------------------------------|
| Gage Position                    | Radial Distance from Explosive Donor, ft | Estimated Peak Overpressure, psi | Calibrated to Overpressure, psi |
| Gages Mounted in Igloo Headwalls | 147                                      | 215 <sup>†</sup>                 | 400                             |
| Ground-Level Gages Northwest     | 134                                      | 65 <sup>†</sup>                  | 120                             |
|                                  | 147                                      | 52                               | 100                             |
|                                  | 167                                      | 41                               | 80                              |

| BRL Self-Recording Gages         |                    |                      |                     |                     |                             |                     |
|----------------------------------|--------------------|----------------------|---------------------|---------------------|-----------------------------|---------------------|
| Radial Distance R from Donor, ft | R/W <sup>1/3</sup> | No. of Gages, NW Leg | No. of Gages, W Leg | No. of Gages, S Leg | Est. P <sub>max</sub> , psi | Capsule Rating, psi |
| 250                              | 7.5                | 2                    | 2                   | 2 <sup>5</sup>      | 17.0                        | 25                  |
| 334                              | 10.0               | 2                    | 2                   | 2                   | 10.0                        | 15                  |
| 440                              | 13.5               | 2                    | 2                   | 2                   | 5.5                         | 15                  |
| 600                              | 18.0               | 2                    | 2                   | 2                   | 3.6                         | 5                   |
| 835                              | 25.0               | 2                    | 2                   | 2                   | 2.3                         | 5                   |
| 1100                             | 33.0               | 2                    | 2                   | 2                   | 1.5                         | 5                   |
| 1500                             | 45.0               | 2                    | 2                   | 2                   | 1.0                         | 1                   |

\*Reflected

†Side-on

‡250-ft position is on SW Leg instead of S Leg



R-7556-1-4182

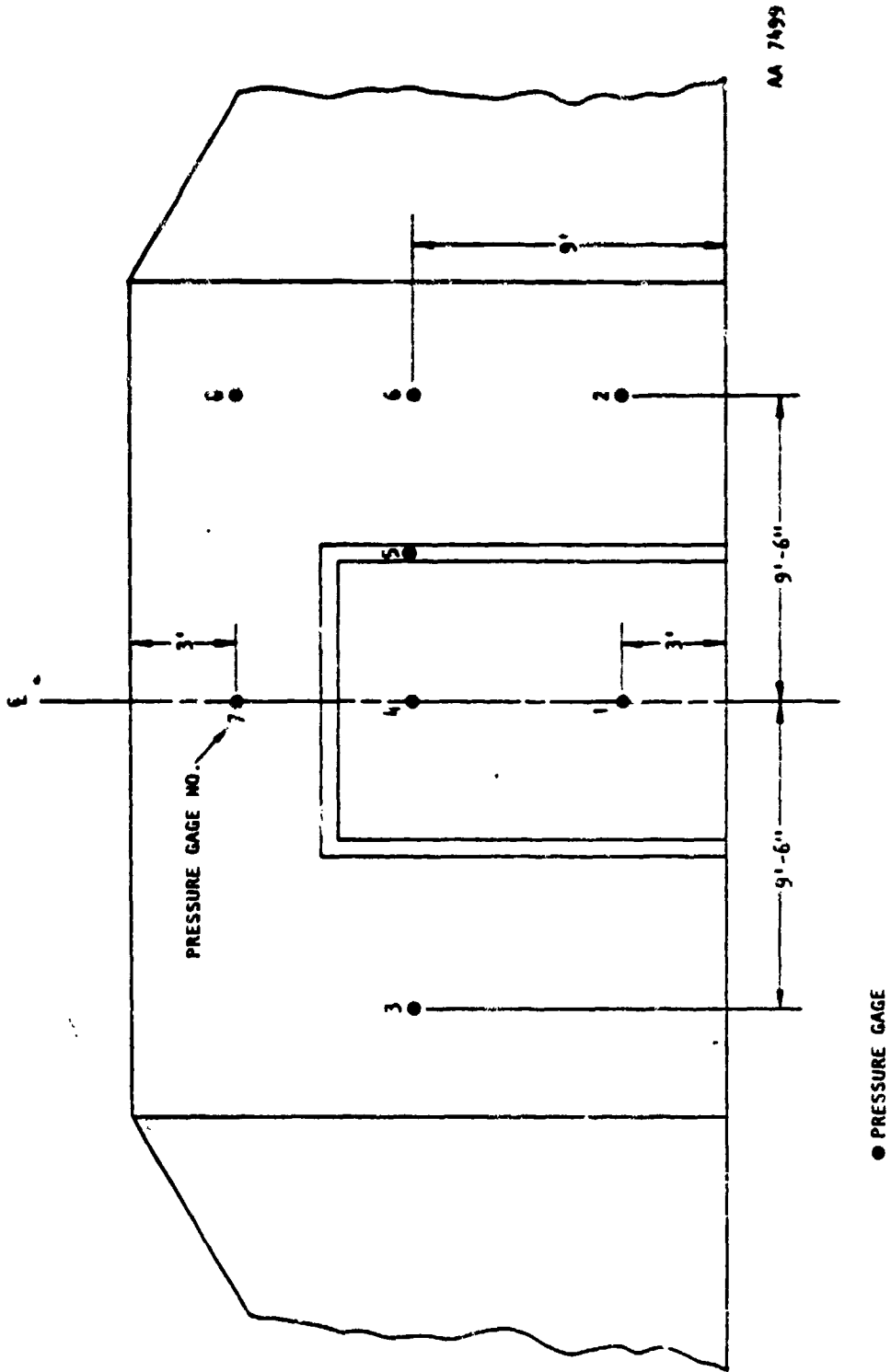
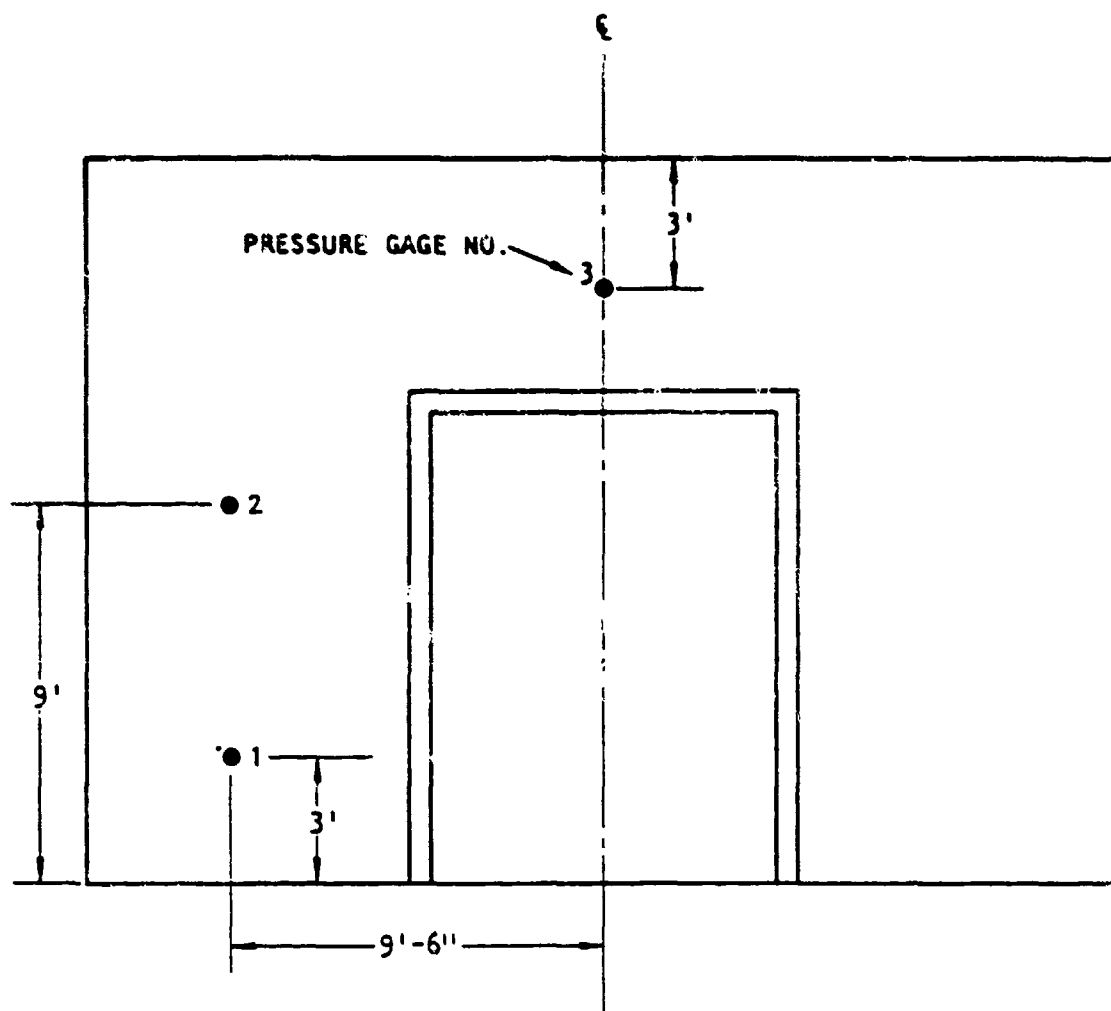


FIGURE 1-1. PLACEMENT OF PRESSURE GAGES ON NORTHEAST (B) 1G100, ESKIMO IV



● PRESSURE GAGE

FIGURE 4-2. PLACEMENT OF PRESSURE GAGES ON EAST (D) AND WEST (E) IGLOOS, ESKIMO IV



#### 4.2 ACCELEROMETERS

Accelerometers (Model 114 by Setra Systems Inc.) were used to measure acceleration-time histories at various locations on headwalls in the ESKIMO IV test. These gages yield good response from zero hertz to several hundred hertz, and the damping of the seismic element is essentially independent of the changes in ambient temperature. Table 4-2 shows estimated peak accelerations and ratings of the accelerometers used in ESKIMO IV.

Recommended placement of the accelerometers on the headwall of the northeast (B) igloo is shown in Figure 4-3. Because of the assumed symmetry of the loading and the structure, the transducers were placed only on one side of the centerline of the igloo. The recommended locations for the gages generally coincided with the nodes of the finite element mesh that was used to analyze the headwall. As shown in the figure, a total of 12 accelerometers was placed on this headwall and no accelerometers were placed on the headwalls of the east (D) and west (E) igloos.

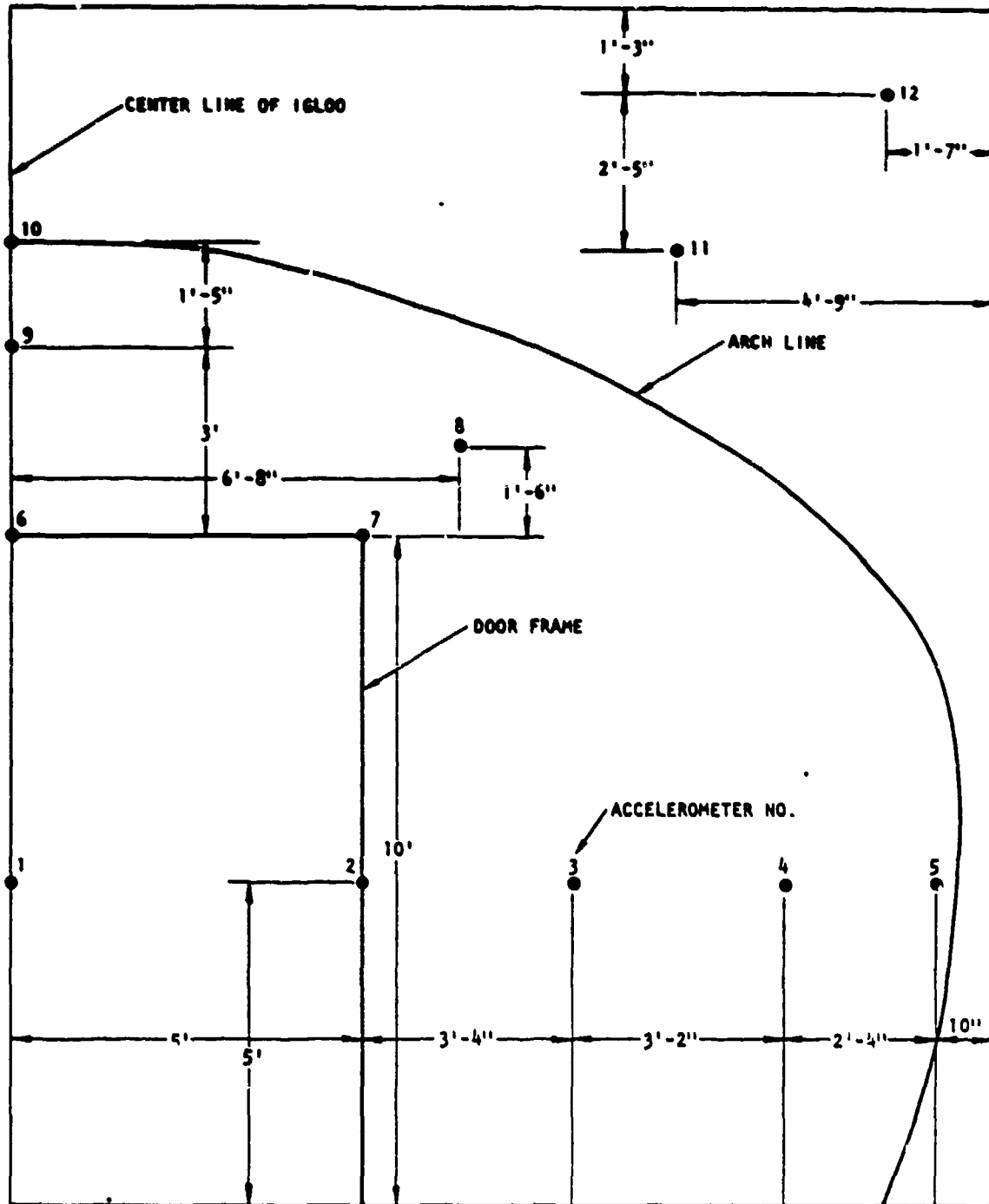
The impulse response of the accelerometers was checked out prior to the test with a drop-table calibration device. This portable device was carried to the site for one-the-spot checkout of the accelerometers.

#### 4.3 LINEAR MOTION TRANSDUCERS

Long-stroke displacement transducers of the LVDT type were used in ESKIMO IV to measure movement of the concrete headwall. The female part of the transducer was attached to a universal joint mounted on a rail section (mass) that was suspended from the corrugated metal roof of the igloo by chains. The male or rod portion was supported by universal joints, with one universal joint securely attached to the headwall at the desired point of measurement. An effort was made to reference as many transducers as practical to the same mass.



R-7556-1-4182



AA 7501

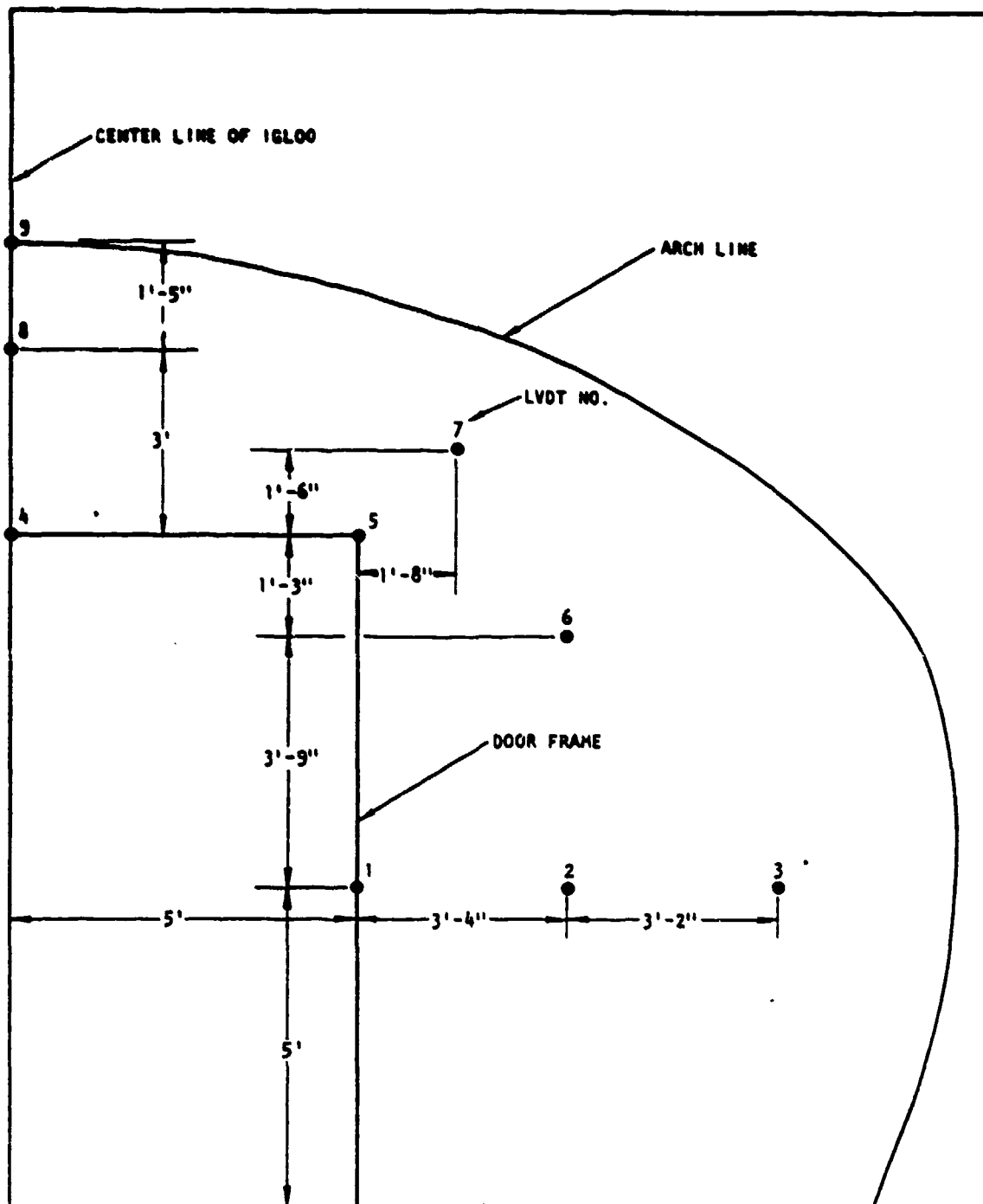
● ACCELEROMETER

FIGURE 4-3. PLACEMENT OF ACCELEROMETERS ON HEADWALL OF NORTHEAST IGLOO, ESKIMO IV

TABLE 4-2. SCHEDULE OF ACCELEROMETERS FOR  
NORTHEAST IGLOO, ESKIMO IV

| Position                   | Estimated<br>Maximum<br>Acceleration,<br>g | Desired<br>Accelerometer<br>Rating,<br>g |
|----------------------------|--|--|
| Door                       | 630  | 1000                                     |
| Headwall -- away from door | 150  | 300                                      |
| Headwall -- near door      | 200  | 300                                      |

Figure 4-4 shows recommended placement of the displacement transducers (LVDT) on the headwall of the northeast igloo. Again, the locations shown for LVDTs generally coincided with the nodes of the finite element mesh. Nine LVDTs were placed on the northeast igloo, as shown in the figure, and 6 LVDTs were placed on the remaining two igloos.



AA 7500

● LVDT

FIGURE 4-4. PLACEMENT OF LVDT TRANSDUCERS ON HEADWALL OF NORTHEAST IGLOO, ESKIMO IV



## SECTION 5

## DYNAMIC RESPONSE OF HEADWALLS IN ESKIMO TESTS

5.1 INTRODUCTION

This section describes the results of dynamic analyses of four different headwalls in the ESKIMO tests. The four headwalls considered are the south (and west) headwall in the ESKIMO I test, the east and northeast headwalls in the ESKIMO II test, and the northeast headwall in the ESKIMO IV test. The analyses were performed subjecting the finite element model of the headwall and door systems to blast loads. The finite element models are discussed in Section 3 and the pressure loadings applicable to each model are given in Section 2. The dynamic response of the models was obtained with the modified INSLAB code (Ref. 3), a nonlinear, dynamic finite element program. The results of these analyses are compared with the available test results from the ESKIMO tests.

Because Section 5 requires some 70 figures to present the analysis results, they have been grouped at the end of the section text. Figure 5-1 et seq. begins on page 106.

5.2 RESPONSE OF SOUTH HEADWALL, ESKIMO I

The results of the ESKIMO I calculation using the refined finite element model of the south headwall (Fig. 3-2, Sec. 3) are presented in this section. The finite element model of the headwall was subjected to the pressure loadings shown in Figure 2-1 (Sec. 2). The results of the calculation are also applicable to the west headwall, since the south and west headwalls have identical geometries and were exposed to the same loading. These results are shown as time-history plots of the headwall motion and contour plots of the displacement of the headwall. Comparisons are made between these results and the results of the prior calculation of Reference 2. In addition, where experimental measurements are available, comparisons are made between the calculation and the actual response of the south and west igloos of ESKIMO I.



### 5.2.1 TIME-HISTORY DATA

Figures 5-1 through 5-9 show displacement, velocity, and acceleration histories computed at several locations on the south and west headwalls and doors of the ESKIMO 1 event. In addition, Figures 5-10 through 5-12 show displacement histories at several other locations. Typically, these response histories exhibit a steady climb to peak displacement, followed by a recovery of displacement such that the magnitude of the final displacement is less than half the magnitude of the peak displacement. Furthermore, the frequency content of the displacement histories is extremely low compared to the input pressure histories. The rise times of the displacement histories are often 30 or 40 msec, whereas the rise time of the input pressure history is 1 msec. This is because the fundamental frequency of the headwall is very low compared to the predominant frequencies in the input loading.

The tendency for final displacements to be smaller than the peak displacements is due primarily to the use of nonlinear spring elements in modeling the soil backfill behind the headwall. A second factor is the use of linear springs to model the concrete floor slab. In contrast, the calculations of Reference 2 used only damping elements to model both the backfill and the foundation. This latter formulation resulted in final displacements that were nearly equal to the peak displacements.

Figure 5-1 shows the motion of Node 1, which corresponds to the top center of the headwalls of the south and west igloos of ESKIMO 1. The peak positive displacement\* is 0.3 in., whereas the final displacement is negative and is equal to 0.7 in. This indicates the presence of a gap about

---

\*In this report the positive displacement of a headwall represents movement away from the source, or into the igloo; and the negative displacement represents movement towards the source, or out of the igloo.



1-in. wide between the headwall and the compressed backfill after the shock. Figure 5-13 (from Ref. 2), which shows the motion of the corresponding point of the prior calculation, predicts no such gap. However, gaps between the headwall and the soil have been observed during posttest inspection of the acceptor magazines. This indicates that the present method of modeling the soil is a step in the right direction. The displacement histories of other nodes on the backfill portions of the headwalls are shown in Figure 5-10.

Figure 5-2 shows the response history of Node 19, located on the top of the arch line of the south and west headwalls. The response of the corresponding point of the prior calculation is shown in Figure 5-14 (from Ref. 2). The displacement histories begin in very similar fashion, reaching displacements of several inches after 40 msec. At that time the present calculation begins to recover displacement, whereas the prior calculation continues to show increased displacement. A gap of about 2.75 in. develops in the current calculation. A large difference in final position of the headwall is shown in the two calculations. The current calculation shows a final displacement of about 0.3 in., whereas the prior calculation shows a 6-in. final displacement. A similar situation exists with Figure 5-1. Figure 5-11 shows the displacement histories of several other locations along the arch line.

Figures 5-5 and 5-8 show the responses of points located within the arch line on the south and west headwalls. While less strongly influenced by the soil backfill than points located on or outside the arch line, these points also show considerable recovery from peak displacement. However, the ratios of final displacement to peak displacement are greater in these cases than in those more directly dependent on soil behavior. Figure 5-15 (from Ref. 2) shows the response for the prior calculation of the point corresponding to that of Figure 5-8. The displacement histories between the two cases disagree in the ratio of final displacement to peak displacement, and in the magnitude of the peak displacement. The two cases are in good agreement on the peak velocity and the peak acceleration, although the durations are different.



Figures 5-3, 5-4, and 5-7 show the responses of points on the boundary between the headwall and the steel door. In the present calculation, the door is connected to the headwall only along its top and side edges. It is free along its bottom and center edges. As a result, the door exerts a great deal of influence on the headwall along the contact boundary. Since the connection along this boundary is accomplished by hinges, all of this influence is transmitted to the headwall in the form of shear force. The resulting displacements are considerably larger, therefore, than displacements of the headwall not along the boundary. For example, the displacement of Node 49 (Fig. 5-4) exceeds that of the adjacent point, Node 50 (Fig. 5-5). Similarly, the displacement of Node 76 (Fig. 5-7) exceeds that of Node 77 (Fig. 5-8). Figures 5-16, 5-17, and 5-18 (from Ref. 2) show points of the prior calculation that correspond, respectively, to Figures 5-3, 5-4, and 5-7 of the current calculation. In the previous calculation, the door was modeled as having shear support along the bottom boundary as well as along the top and side. As a result, the door played a slightly less important role in the displacements of the prior calculation. The peak displacements of the present calculation are comparable to those of the prior calculation; and, in the case of Node 46 (Fig. 5-3), the peak displacement greatly exceeds that of the corresponding point in the prior calculation. However, the final displacements are below those of the prior calculation.

Experimental data from the south igloo, for a location corresponding to Node 46, is available. A comparison between the measured data and the computed response is given in Table 5-1. Although the average acceleration is in good agreement, the duration and the velocities are not. The trend of the comparison suggests that, locally, the door may have broken free of its support during loading. Had this been able to occur in the finite element model, the unloading of Node 46 would have been initiated much earlier, resulting in lower velocities. This would have been accomplished without significantly altering the average acceleration. It would be desirable in future calculations to possess the capability of modeling breakable hinges.

TABLE 5-1. MOTION OF SOUTH HEADWALL (ESKIMO 1)  
ABOVE CENTER OF DOOR

| Item   | Measured Value<br>for South Igloo | Present Calc.<br>(Node 46) | Prior Calc.<br>(Node 33) |
|--|-----------------------------------|----------------------------|--------------------------|
| Maximum Velocity, fps  | 27.9                              | 44.2                       | 20                       |
| Average Velocity from<br>Initial Motion to Peak<br>Displacement, fps | 13.3                              | 29.0                       | 11.7                     |
| Time Interval from<br>Initial Motion to<br>Peak Velocity, msec       | 14.4                              | 25.6                       | 11.2                     |
| Average Acceleration<br>from Initial Motion<br>to Peak Velocity, g   | 60                                | 53.6                       | 64.8                     |

In addition to the gage data for the south headwall above the center of the door, experimental data exist also in the form of motion picture film. From these films it was possible to estimate, although not with great precision, the velocity of the upper corners of the doorways of the south and west igloos. Although it was also possible to measure displacements, flying debris in the igloos obscured the view of the door prior to maximum displacement. The peak velocities of the corner points are presented in Table 5-2.

TABLE 5-2. PEAK VELOCITIES OF UPPER CORNER OF DOOR

| Source                        | Peak Velocity, fps |
|-------------------------------|--------------------|
| South Igloo (Measured)        | 33                 |
| West Igloo (Measured)         | 19                 |
| Current Calculation (Node 49) | 19.2               |
| Prior Calculation (Node 31)   | 16.6               |



Figures 5-6 and 5-9 show the motion of points on the interior of the steel door. The displacements are very large. However, the displacement values shown in the figures are probably typical of the order of magnitude of the actual door displacements. Figure 5-19 (from Ref. 2) shows the motion of the point in the prior calculation corresponding to that of Figure 5-6. Actual measurements from the motion picture film of the west igloo are available, although visibility was obscured prior to maximum displacement. The maximum deflections of the center of the door, as determined by the three independent means, are listed in Table 5-3.

TABLE 5-3. PEAK DEFLECTION OF CENTER OF DOORWAY

| Source                        | Displacement, in. |
|-------------------------------|-------------------|
| West Igloo (Measured)         | 30*               |
| Present Calculation (Node 73) | 20.6              |
| Prior Calculation (Node 49)   | 10.4              |

\*The motion picture record terminated prior to maximum displacement. The value shown is the largest observed displacement prior to termination of the record.

Figure 5-12 shows the displacement histories of several points at ground level on the headwall. Figure 5-20 (from Ref. 2) is comparable to Figure 5-12a. From this comparison it is evident that there is a great difference between the two calculations in modeling the foundation. The foundation of the present calculation is much more rigid than the foundation of the prior calculation. Accelerometers located on the floors of both the south and the west igloos provide experimental base motion data. The results are presented in Table 5-4.



TABLE 5-4. PEAK ACCELERATION OF BASE OF HEADWALL

| Source                         | Peak Acceleration, g |
|--------------------------------|----------------------|
| South Igloo (Measured)         | 6.3                  |
| West Igloo (Measured)          | 5.5                  |
| Present Calculation (Node 104) | 19.8                 |
| Present Calculation (Node 108) | 12.9                 |
| Prior Calculation (Node 52)    | 66.2                 |

### 5.2.2 STATIC HEADWALL MEASUREMENT

The static headwall measurements involved setting up survey monuments 3 ft in front of the igloo headwalls. The distances from the monuments to the headwalls were measured at selected points before the test. These distances were again measured after the test. The net changes in position represented the permanent displacement of the headwalls. A gap of approximately 0.2 ft was found between the back of the south headwall and the earth cover at the top left corner, and a similar space 0.1-ft wide was found at the top right corner. This demonstrates that the static measurements are not the maximum displacements but are the permanent movements of the headwall. These permanent displacements of the headwalls are shown in Figures 5-21 and 5-22 (Ref. 1). All the measurements are subject to  $\pm 0.05$  ft of error because pretest measurements showed that the walls deviated from a true vertical plane by that amount. The measured displacement patterns indicate that the headwalls appear to have responded in different ways. More pronounced yielding on the steel arch was found in the south igloo. In the west igloo, there was clear indication that the steel arch acted as a reaction line resisting headwall movement. The difference in the observed data, therefore, implies that material properties in the two igloos are not the same. As was mentioned before, the finite element models used to predict the responses of the south and west igloos are identical. The assumed material properties of the model would therefore seem to represent characteristics that are a compromise between the actual properties of the south igloo and those of the west igloo.



Figure 5-23 shows a contour plot of the computed displacements at 0.22 sec of the current ESKIMO I calculation. As can be seen from the response curves (Figs. 5-1 through 5-12), motion of the headwall has essentially stopped by that time. This figure can be interpreted, therefore, as a plot of the computed permanent displacements. The deformed shape of the headwall appears to be very similar to that of the west igloo, although the magnitudes of the displacements differ considerably. It appears as if the west igloo experienced a rigid body displacement not experienced in the calculation. The backfill and the foundation of the finite element model were too stiff to permit substantial deformation. If a rigid body displacement of 0.15 ft is added to every point of Figure 5-23, the contour plot of Figure 5-24 results. This plot is in much better agreement with Figure 5-22 than is Figure 5-23. The rigid body displacement does not change the stress field in the headwall. The largest discrepancy between Figures 5-24 and 5-22 is the magnitude of the displacements above the door. The calculation shows them to be substantially higher than the measured values. This may be due to the inability of hinges to fail in the finite element model.

There seems to be no means of adjusting Figure 5-23 such that it compares well with the deformation of the south headwall, shown in Figure 5-21. It is surprising that the south and the west igloos, being of essentially the same construction and subject to similar load conditions, should exhibit such dissimilar deformation. Figure 5-21 indicates that the most pronounced feature of the deformation of the south headwall seems to be the folding about a vertical axis. In the case of the west headwall, there seems to have been a tendency toward folding about a horizontal axis. The difference between the computed deformations of the finite element analysis and those of the west headwall appears to be smaller than the difference between the deformations of the south and west headwalls. This implies that the stiffness properties of the igloos, particularly of the soil backfill, are variable. Furthermore, these variable properties exert considerable influence on the deformation of the headwalls.



The final displacements of the current calculation are considerably smaller than the peak displacements. It has already been noted that strong evidence exists to indicate that the same is true of the actual head walls. For the sake of comparison with the final deformations, Figure 5-25 shows the displacement contours of the headwall of the finite element model at 0.042 sec, a time at which much of the headwall was in the vicinity of peak displacement. The comparison indicates that the final displacement contours do not provide an accurate measure of the severity of loading that occurred during the blast. Time-dependent measurements are essential for determining peak stresses during such an experiment.

### 5.2.3 CONCLUSIONS

The finite element calculation discussed in this section is a modification of a previous calculation of the response of the south and west headwalls of the ESKIMO I event. The modifications included increasing the number of elements, representing the soil backfill and the foundation by different models, changing the boundary condition along the bottom edge of the door, and increasing the flexibility of the concrete. Several differences between the present calculation and the earlier calculation have been pointed out. The most notable difference is the tendency, in the present calculation, for final displacements to be significantly smaller than peak displacements. The differences between the calculations appear to result primarily from the changes in the type of model (for example, using nonlinear springs for the backfill) rather than from the increase in the number of elements. It appears that the finite element grids are fine enough, and that further improvements in correlation between calculation and experiment are to be obtained through improving the means of modeling the influence of the various components.



Comparison of the calculated results with the experimental results indicates that improved correlation might be obtainable by modeling breakable hinges along the top and side boundaries of the door. This would limit the influence of the door on the headwall, and perhaps lower the headwall displacements adjacent to the doorway. In order to incorporate such a hinge element into future calculations, it will be necessary to know the ultimate strength of the door/headwall connection.

A second area of modification of the finite element model is the stiffness of the soil backfill and the foundation. The permanent displacements of the headwalls indicate that these components should be modeled as softer. As pointed out in Section 4, assigning values to the soil parameters was largely a matter of intuition, plus trial and error. Experimental measurements establishing the nature of participation of the soil in the response of the headwall are needed. This participation is evidently quite complex, thus rendering static laboratory tests of soil properties inadequate. In fact, the only experimental means of determining the participation of the backfill seems to be the ESKIMO series itself. It must be noted that further reduction of the stiffness of the backfill will result in the steel arch applying a significant influence on the headwall. Thus future calculations may have to include the effects of the arch.

The comparison of final displacements of the south and west headwalls indicated a variability in the stiffness of various components of the igloos. This variability increases the confusion over the role of the backfill, the arch, and the foundation in the headwall response. It suggests that there may always be a significant degree of uncertainty concerning the parameters used in modeling a headwall test.



### 5.3 RESPONSE OF EAST HEADWALL, ESKIMO II

The finite element model for the east headwall of ESKIMO II is the same as that used for the south headwall of ESKIMO I, since the two headwalls are of identical construction. Therefore, the model shown in Figure 3-2 (Sec. 3) was subjected to the pressure loading applicable to the ESKIMO II test. The pressure loading histories are shown in Figure 2-3 (Sec. 2). The results from the dynamic response calculation are presented as time-history plots of the headwall motion and contour plots of the displacement of the headwall. Comparisons are made between the calculation and the available experimental measurements on the east headwall in ESKIMO II.

#### 5.3.1 RESPONSE TIME HISTORIES

Since the model used in this study is the same as the one used for the south headwall of ESKIMO I except for the pressure loading, the response time histories are shown at the same nodes as in Section 5.2 in order to compare the results due to different loading environments. These responses are plotted in Figures 5-26 through 5-36.

The general shapes of these time histories are similar to the corresponding ones for the south headwall in ESKIMO I except that the magnitudes of the present time histories are, in most cases, greater. It is seen from Figure 5-26, for example, that the displacement of Node 1 rises initially to a positive peak of 0.8 in., then reverses the motion to reach a negative peak of 2.5 in. The positive peak is 25% greater than the corresponding peak at the same node for the south headwall in ESKIMO I, whereas the negative peak is 40% greater.

The motions at nodes located outside the steel arch, where the headwall is supported by soil, are only slightly greater than those in ESKIMO I. However, the peak pressure in ESKIMO II is roughly three times greater than that in ESKIMO I. Within the arch, the headwall motions in the present case are much greater. For example, at Node 50 the maximum displacement is about two and a half times greater than the corresponding value



in ESKIMO I; and at the center of the door (Node 73), the maximum displacement is about three times greater. This phenomenon may be due to the fact that the headwall and the door within the arch are unsupported and yield sooner than the region outside the arch. After yielding, additional loading causes disproportionately large displacements.

Figure 5-33a shows that the maximum displacement of the center of the door is about 86 in., which is greater than the width of the door (60 in.). Since the INSLAB computer program is based on the theory of small displacements, the above displacement value may be subjected to significant error. However, the large displacements predicted by the program simply reinforce the fact that the door would be bent out of shape under the loading experienced by the headwall.

As noted above, the response calculation of the east headwall showed that the steel door would be blown open under the pressure loading assumed for the ESKIMO II test. After the door is blown open, a redistribution of the pressure on the headwall will take place, resulting in a net reduction of the total load on the headwall. However, the calculation assumed that the pressure was acting uniformly on the headwall and the door throughout the calculation. Therefore, the calculation considered higher loading than was the actual case and the computed headwall motions would be significantly different after the door is blown open. The computation for the response of the east headwall, ESKIMO II, was terminated at about 165 msec; whereas for the ESKIMO I calculation this point was at about 240 msec. Because of this, the permanent displacements of the headwall are not clearly identified for most nodes in Figures 5-26 through 5-36. In any event, for the reason mentioned above, the computed permanent displacements are expected to be in significant error.



### 5.3.2 COMPARISON OF COMPUTED RESULTS WITH TEST DATA

In the ESKIMO II test, linear motion transducers were positioned above the center of the doorways of the five igloos. For the east igloo, this location corresponds to Node 46 of the finite element model (Fig. 3-2). A comparison between the test data and the computed motions for this location is shown in Table 5-5. The computed duration and velocities are much higher than the measured values. However, as in the case of the south igloo in ESKIMO I, the average acceleration is in good agreement. As suggested in Reference 4, the measured data at this location are very sensitive to the type of doorstop devices used for inhibiting the movement of the door top, relative to the headwall. Also, as discussed before, the computed motions may be greater because the separation of the door from the headwall was not considered in the analysis.

Two accelerometers, one on each door leaf, were mounted on the east igloo (ESKIMO II). However, these gages failed to perform properly and therefore no useful data were obtained, as observed in Reference 4.

The static measurements intended to record the permanent headwall deformations were performed as described in Reference 4. Figure 5-37 shows these deformations on one half of the headwall and door system for the east igloo, ESKIMO II.

Since the measurements are made on the whole headwall but only one half of the headwall is used in the finite element model, there are two measured values for each node of the model except those at the centerline of the headwall. The contours in Figure 5-37 are based on the average of the two measured values where applicable. All the values are in hundredths of a foot, and the positive value indicates deformation into the igloo.

TABLE 5-5. MOTION OF EAST HEADWALL (ESKIMO II)  
ABOVE CENTER OF DOORWAY

| Item  | Measured Value | Computed Value (Node 46) |
|---|----------------|--------------------------|
| Maximum velocity, ft/sec  | 33.3           | 102                      |
| Average velocity from initial motion to peak, ft/sec            | 31.5           | 72                       |
| Time from initiation of motion to maximum velocity, msec        | 6.75           | 20                       |
| Average acceleration from initial motion to maximum velocity, g | 153            | 155                      |



As was discussed in Section 5.3, the east headwall, ESKIMO II, had not reached steady state at the end of the calculation. Therefore, it is difficult to compare quantitatively the calculated results with measured results. However, all the nodes indicate that the accelerations and velocities become small near the end of the computation. The displacement contours at two instants of time late in the calculation ( $t = 145$  msec and  $t = 157.5$  msec) are shown in Figures 5-38 and 5-39. In both figures the maximum displacements are at the top center of the door, with an order of magnitude of 1.3 ft. Although this is much higher than the measured value, the general deformed patterns are quite similar to the measurements (Fig. 5-37). In addition, the contours in Figure 5-37 do not extend to the doorway, because the door was blown off during the test. The computed displacement contours, however, extend routinely into the doorway.

#### 5.4 RESPONSE OF NORTHEAST HEADWALL, ESKIMO II

This section presents the results from the dynamic analysis of the northeast headwall in ESKIMO II. The results from the dynamic response calculation are presented as time-history plots of the headwall motion and contour plots of the displacement of the headwall. Also presented are comparisons of experimental data with the results from the calculation. The finite element model of the headwall is shown in Figure 3-16 (Sec. 3). This model is subjected to the blast pressure loadings shown in Figure 2-3 (Sec. 2). These same loadings are applicable to the east headwall, since the two headwalls were at the same distance from the source.

##### 5.4.1 RESPONSE TIME HISTORIES

Figures 5-40 through 5-55 show displacement, velocity, and acceleration time histories computed at several nodes in the finite element model of the northeast headwall and door system of ESKIMO II. As in the case of the south headwall, ESKIMO I, the displacement histories for this case exhibit lower frequencies compared to the input loading. The rise times of



the displacement histories are longer than 20 msec, whereas the rise time of the input pressure history is 1 msec. As observed in Section 5.2.1, this phenomenon is attributed to the low fundamental frequency of the headwall and door system.

Table 5-6 shows the computed maximum and permanent displacements at several nodes. It is clear from this table that the maximum displacements of the nodes inside the arch line are much greater than the corresponding values of the nodes outside the archline. However, no such correlation exists for the permanent displacements. The observation implies that the soil behind the headwall is very effective in resisting the dynamic forces on the wall, but does not greatly influence the residual displacements of the wall.

Although the east headwall is subjected to the same loading as the northeast headwall, the geometries of these two headwalls are different. Therefore, the relative responses of the headwalls will be compared in order to get an insight into their relative strengths and their performances in the test. Because of the differences in the finite element models of the headwalls, a node in one model may not correspond exactly to a node in the other. Each comparison is therefore made between two nodes located in the same general area.

For the northeast headwall, Node 9 is located at the crown of the steel arch. The maximum displacement at this node is 4.7 in. The corresponding node for the east headwall, Node 19, has the maximum displacement of 8.2 in. Similar comparison is seen in Table 5-7 for other locations on or inside the arch. Although the area of the northeast headwall supported by the backfill soil is much smaller than that of the east headwall, the additional stiffness due to the presence of the concrete beams around the doorway of the northeast headwall appears to have reduced the maximum displacements of the headwall significantly.



TABLE 5-6. COMPUTED MAXIMUM AND PERMANENT DISPLACEMENT OF NORTHEAST HEADWALL, ESKIMO II

| Node No. | Maximum Displacement, in. | Permanent Displacement, in. | Location                           |
|----------|---------------------------|-----------------------------|------------------------------------|
| 9        | 4.7                       | 0.3                         | On the arch line                   |
| 16       | 1.9                       | -0.4                        | Outside the arch                   |
| 22       | 4.1                       | 0.2                         | On the arch line                   |
| 39       | 7.3                       | 1.5                         | Inside the arch, on door frame     |
| 42       | 6.0                       | 1.1                         | Inside the arch, on door frame     |
| 45       | 2.6                       | 0.7                         | On the arch line                   |
| 60       | 1.4                       | 0.8                         | Outside the arch                   |
| 72       | 17.0                      | 7.5                         | Inside the arch, on center of door |
| 75       | 4.7                       | 1.3                         | Inside the arch, on door frame     |
| 77       | 4.0                       | 1.1                         | Inside the arch                    |
| 79       | 2.8                       | 1.1                         | On the arch line                   |
| 81       | 1.3                       | 0.8                         | Outside the arch                   |
| 101      | 0.9                       | 0.3                         | On the arch line                   |
| 105      | 16.5                      | 8.0                         | Inside the arch, on door frame     |
| 108      | 0.4                       | 0.1                         | Inside the arch, on door frame     |
| 115      | 0.1                       | 0.0                         | Outside the arch                   |



TABLE 5-7. COMPARISON OF COMPUTED MAXIMUM DISPLACEMENTS FOR ESKIMO II

| East Headwall |                           | Northeast Headwall |                           | General Location                                 |
|---------------|---------------------------|--------------------|---------------------------|--|
| Node          | Maximum Displacement, in. | Node               | Maximum Displacement, in. |  |
| 19            | 8.2                       | 9                  | 4.7                       | Crown of the arch                                |
| 46            | 45.0                      | 39                 | 7.3                       | Top center of door                               |
| 49            | 20.0                      | 42                 | 6.0                       | Top corner of door                               |
| 73            | 86.0                      | 72                 | 17.0                      | Center of door                                   |
| 76            | 21.0                      | 75                 | 4.7                       | Center edge of door                              |
| 77            | 15.0                      | 77                 | 4.0                       | Inside arch, along horizontal centerline of door |
| 103           | 0.3                       | 108                | 0.4                       | Bottom corner of door                            |



Perhaps the most obvious difference between the two headwall responses is seen in the steel door area. The maximum displacements in the door area for the northeast headwall are much smaller than those for the east headwall (Table 5-7). At the center of the door, for example, the maximum displacement for the northeast igloo is 17 in. as against 86 in. for the east headwall. As described in Section 1, the door system for the northeast igloo is of the biparting and sliding type, whereas the door system for the east igloo is of the double leaf and hinged type. The results of the calculations, therefore, suggest that the biparting and sliding type is superior to the double leaf and hinged type for resisting the blast loads.

#### 5.4.2 COMPARISON OF COMPUTED RESULTS WITH TEST DATA

As explained in Section 5.3.2, linear motion transducers were placed above the center of the doorways of all the igloos in the ESKIMO II test. For the northeast igloo this position corresponds to Node 39 of the finite element model (Fig. 3-16, Sec. 3). A comparison between the test data and the computed motions for this location is shown in Table 5-8. Among the four items compared, the times from initiation of motion to maximum velocity are in good agreement between the computed and measured values. The remaining items show that the computed values are about two times greater. As mentioned before, the motion of this point is very sensitive to the type of door-stop device used for inhibiting the movement of the door relative to the headwall. Also, the computed motions may be greater because the separation of the door from the headwall was not considered in the analysis.

Two accelerometers were mounted, one on each door leaf. The gage on the left door leaf failed to perform, while the gage on the right door leaf recorded a peak acceleration value of 1200g. The computed value at the corresponding location (Node 72) is seen from Figure 5-47 to be 1300g.

TABLE 5-8. MOTION OF NORTHEAST HEADWALL, ESKIMO II,  
ABOVE CENTER OF DOORWAY

| Item  | Measured Value | Computed Value (Node 39) |
|---|----------------|--------------------------|
| Maximum velocity, ft/sec  | 14.3           | 32                       |
| Average velocity from initial motion to peak, ft/sec            | 10.4           | 21                       |
| Time from initiation of motion to maximum velocity, msec        | 17             | 19                       |
| Average acceleration from initial motion to maximum velocity, g | 26             | 52                       |



The permanent deformations of the northeast headwall are given in Reference 4, and are shown plotted in Figure 5-56. The contours in the figure are based on the average of the two measurements at symmetrical points on the headwall. Figure 5-57 shows the computed displacement contours of the headwall at 109 msec. Since the motions become essentially steady state at this time, the displacements of the headwall at this instant are equal to the permanent displacements of the headwall.

Figures 5-56 and 5-57 show that the maximum deformations occur around the doorway. The contours seem to follow the patterns of the steel arch and the floor slab. In general, the measured values are slightly higher than the computed values. In both figures, the movements tend to be smaller toward the top and the bottom of the headwall. At the top of the headwall, the computed displacements are negative, whereas the measurements show small positive values. In general, the wingwall experiences smaller displacements. At the far end of the wingwall, some displacements are negative. This may be due to the fact that the headwall is supported by the soil outside the arch and is subject to rotation about the support.

#### 5.5 RESPONSE OF NORTHEAST HEADWALL, ESKIMO IV

The response calculation of the northeast headwall, ESKIMO IV, was to have been performed before the test was conducted on 10 September 1975, so that the analytical results could be used to predict the behavior of the headwall and door system in the test. Because of tight schedules, the above calculation could not be completed before the test; but the calculation was performed before any results from the test were available. This assured that the calculation was performed independently of the test and was not subject to any bias that could have resulted from reviewing the test results before performing the calculation.



As of the writing of this report, the data from the ESKIMO IV test are available only in preliminary form. Therefore, the test results reflect raw data that may be subject to future corrections. This fact should be kept in mind when comparing the analytical results with the test data.

### 5.5.1 RESPONSE TIME HISTORIES

Figures 5-58 through 5-69 show displacement, velocity, and acceleration time histories computed at several locations on the northeast headwall of the ESKIMO IV event. These locations generally correspond to those of the northeast headwall of the ESKIMO II event, for which the motion time histories are shown in Figures 5-40 through 5-55. Since the structural configuration of the northeast headwall, ESKIMO IV, closely resembles the northeast headwall of the ESKIMO II test, a comparison of the responses of both northeast headwalls will be made.

The motion time histories shown in Figures 5-58 through 5-69 reflect calculations with a duration of 186 msec. The displacement time histories at most locations show a single peak at about 25 msec and become steady state after about 100 msec. These time histories are quite similar to those for the northeast headwall of ESKIMO II, both in magnitudes and general behavior. The input blast pressure for ESKIMO IV is slightly higher than that for ESKIMO II, but the resulting peak displacements of the headwall are slightly lower in ESKIMO IV, as shown in Table 5-9. Therefore, it can be concluded that the northeast headwall structure in ESKIMO IV is stronger than that in ESKIMO II for resisting blast loadings.

The response time histories corresponding to the steel door at Nodes 61, 64, 91, 94, 121, and 124 are shown respectively in Figures 5-60, 5-61, 5-63, 5-64, 5-68, and 5-69. For the northeast igloo of ESKIMO II, the peak displacements along the edges of the door are only slightly higher; but those at the center of the door are significantly higher than the values shown in Table 5-9 for ESKIMO IV. The primary reason for these differences



TABLE 5-9. COMPARISON OF MAXIMUM DISPLACEMENTS OF NORTHEAST HEADWALLS OF ESKIMO II AND ESKIMO IV IGLOOS

| ESKIMO II |                           | ESKIMO IV |                           | General Location                                  |
|-----------|---------------------------|-----------|---------------------------|---|
| Node      | Maximum Displacement, in. | Node      | Maximum Displacement, in. |   |
| 9         | 4.7                       | 21        | 3.1                       | Crown of the arch                                 |
| 22        | 4.1                       | 24        | 3.6                       | On the arch line near the crown                   |
| 39        | 7.3                       | 61        | 6.0                       | Top center of the door                            |
| 42        | 6.0                       | 64        | 5.4                       | Top corner of the door                            |
| 45        | 2.7                       | 69        | 2.7                       | On the arch line, at the level of the door top    |
| 72        | 17.0                      | 91        | 5.2                       | Center of the door                                |
| 75        | 4.7                       | 94        | 3.7                       | Right center edge of the door                     |
| 77        | 4.0                       | 97        | 3.3                       | Inside the arch, at the level of the door center  |
| 79        | 2.8                       | 93        | 2.6                       | On the arch line, at the level of the door center |
| 105       | 16.5                      | 121       | 5.3                       | Bottom center of the door                         |
| 108       | 0.4                       | 124       | 0.3                       | Bottom corner of the door                         |



is the door configurations. In ESKIMO IV, the door is of a single-leaf sliding type, whereas the door in ESKIMO II is of a biparting sliding type. The single-leaf type has a much greater stiffness to resist deflection at the center of the door than does the double-leaf type. Therefore, other things being equal, the double-leaf door experiences higher deflection than the single-leaf one.

### 5.5.2 COMPARISON OF COMPUTED RESULTS WITH TEST DATA

As in the case of the other Eskimo tests, posttest measurements were made on the headwalls of the ESKIMO IV test (Ref. 6), in order to obtain permanent displacements of the headwalls. Figure 5-70 shows the permanent displacement contour lines of the northeast headwall based on the average of two measured values due to the symmetry of the headwall at the vertical centerline. The computed displacement contours at time  $t = 158$  msec are shown in Figure 5-71. As noted before, the computed displacements become steady state after about 100 msec and therefore the displacements of the headwall at 158 msec represent the permanent displacements. A comparison of the computed and measured contours shows that the computed displacements generally are smaller than those measured. However, the differences are not great and are not significant because the magnitudes of the permanent displacements are small. The contours do not indicate any strong influence of the arch on the headwall response.

Figures 4-3 and 4-4 (Sec. 4) show the locations of the accelerometers and the linear motion transducers mounted on the northeast headwall and door for ESKIMO IV. The measured acceleration and displacement time histories for the northeast headwall are shown respectively in Figures 5-72 and 5-73. These records are reproduced from the preliminary report (Ref. 6) on the ESKIMO IV test. As such, these records have not been corrected for drifts and other random errors. This fact should be kept in mind in the following discussion involving the measured time histories.



The measured displacement time histories at several locations on the headwall and door are shown in Figure 5-73. The displacements shown are in inch units and are plotted as functions of time expressed in msec units. Next to each time history the node in the finite element mesh of the headwall (Fig. 3-18, Sec. 3) to which the time history corresponds, is shown. Of the eight measured displacement time histories, direct comparison with the calculated histories is possible at only four locations. These are at Nodes 21, 64, 94, and 97 and the corresponding time histories are shown respectively in Figures 5-58, 5-61, 5-64, and 5-65. A comparison of the calculated and measured displacement at the four locations shows that shapes of the pulses are in good agreement. Table 5-10 shows a comparison of the maximum displacements and permanent displacements. The agreement between the computed and measured permanent displacements is very good. The computed maximum displacements are somewhat higher than those measured. Nevertheless, the differences between the computed and measured values are small in comparison with those found for the headwalls in the ESKIMO I and II tests.

The measured acceleration time histories at several locations on the headwall and door are shown in Figure 5-72. The accelerations are given in the units of  $g$  (gravity constant) and the time is expressed in msec units. Next to each record the corresponding node in the finite element mesh (Fig. 3-18, Sec. 3) is shown. Out of a total of eleven records, the computed pulses are available only at seven locations. These are at Nodes 21, 61, 64, 91, 94, 97, and 99 and the corresponding acceleration pulses are given respectively in Figures 5-58, 5-60, 5-61, and 5-63 through 5-66. The measured pulses are shown up to a maximum of 50 msec, while the duration of the computed time histories is 186 msec. The general shapes of the computed pulses are different from those measured. The measured records show small motions after about 25 msec. In contrast, the computed acceleration records show strong motions even after 150 msec. This is attributed to the fact that in the actual test, cracking and crushing of concrete dissipates large amounts of energy. Although the INSLAB code accounts for



TABLE 5-10. COMPARISON OF MAXIMUM AND PERMANENT DISPLACEMENTS OF NORTHEAST IGLOO, ESKIMO IV

| Location |           | Maximum Displacements, in. |          | Permanent Displacements, in. |          |
|----------|-----------|----------------------------|----------|------------------------------|----------|
| Node     | Gage I.D. | Measured                   | Computed | Measured                     | Computed |
| 94       | L-1-B     | 3.0                        | 3.7      | 0.8                          | 0.9      |
| 97       | L-2-B     | 3.2                        | 3.3      | 1.0                          | 1.0      |
| 64       | L-5-B     | 3.6                        | 5.3      | 1.0                          | 0.8      |
| 21       | L-9-B     | 1.9                        | 3.1      | *                            | 0.3      |

\*The transducer seemed to have failed after recording about 50 msec of motion.



the energy dissipation through the yielding of concrete, it is not intended to consider the crushing of concrete. Therefore, the energy dissipation model in the calculation may underestimate the actual energy loss. A comparison of the computed and measured maximum accelerations at various locations on the headwall and door is shown in Table 5-11. The agreement between the measured and computed values is good and the differences are small in comparison with similar differences in the ESKIMO I and II tests.

In ESKIMO IV, unlike in the previous ESKIMO tests, the headwalls were heavily instrumented to measure pressure, acceleration, and displacement time histories on the headwall and door systems. As described in Section 4, the northeast headwall was instrumented with seven pressure gages, twelve accelerometers, and nine linear motion transducers. This provided for the first time an opportunity to compare the computed and measured time histories of accelerations and displacements at several locations on the headwall. The information contained in the measured records can be used to adjust the parameters of soil models in any future calculations to improve the analytical prediction capabilities.

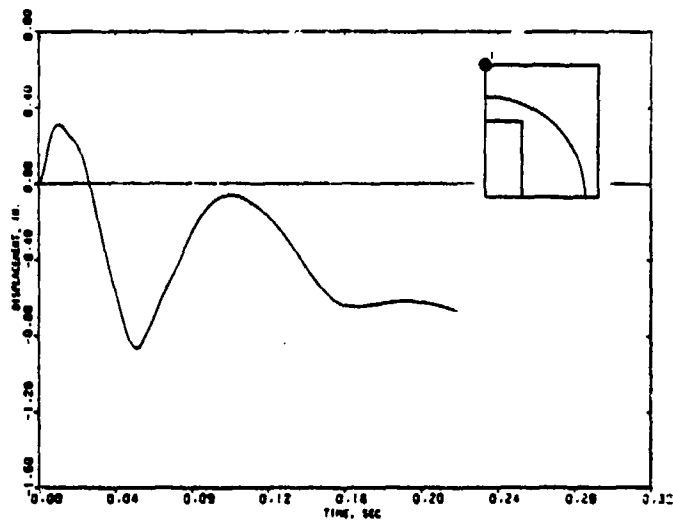
TABLE 5-11. COMPARISON OF MAXIMUM ACCELERATION OF  
NORTHEAST IGL00, ESKIMO IV

| Location |           | Maximum Accelerations, g |          |
|----------|-----------|--------------------------|----------|
| Node     | Gage I.D. | Computed                 | Measured |
| 21       | A-10-B    | 258                      | 225      |
| 61       | A-6-B     | 280                      | 208      |
| 64       | A-7-B     | 196                      | 238      |
| 91       | A-1-B     | 1550                     | 1250*    |
| 94       | A-2-B     | 236                      | 395      |
| 97       | A-3-B     | 272                      | 151      |
| 99       | A-5-B     | 264                      | 241      |

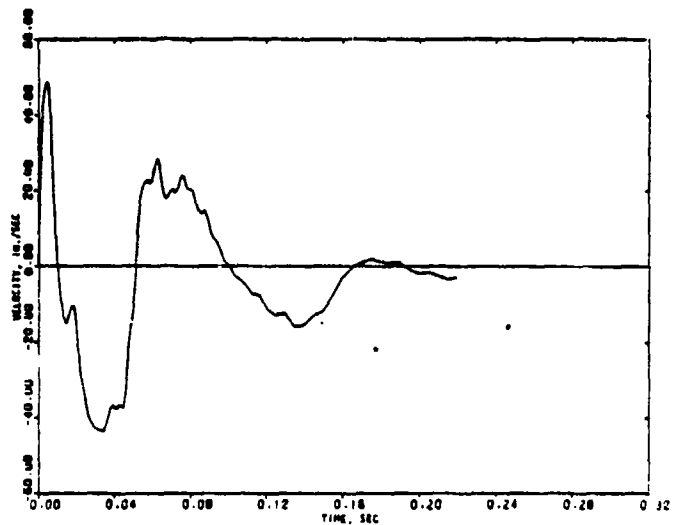
\*Estimated value, since the gage exceeded the rating limit



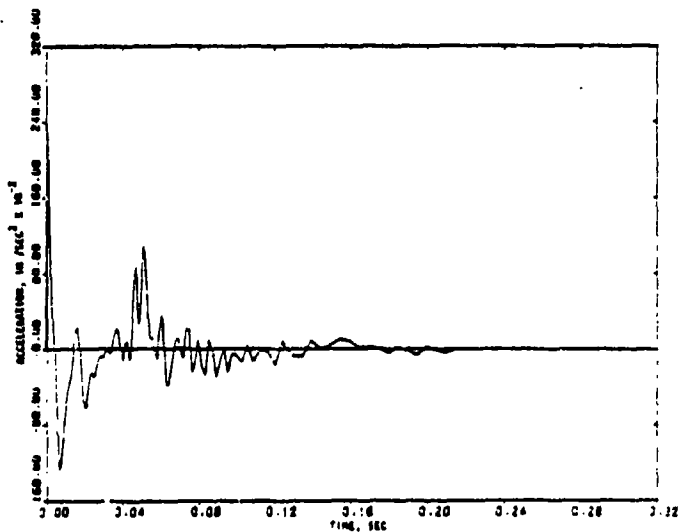
R-7556-1-4182



(a) Displacement



(b) Velocity

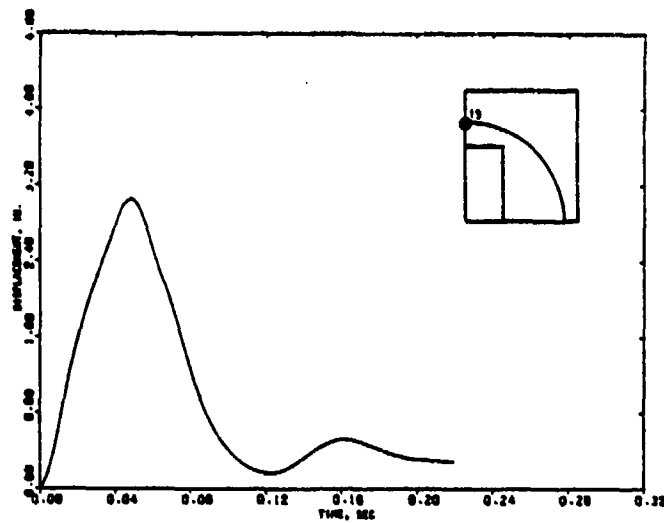


(c) Acceleration

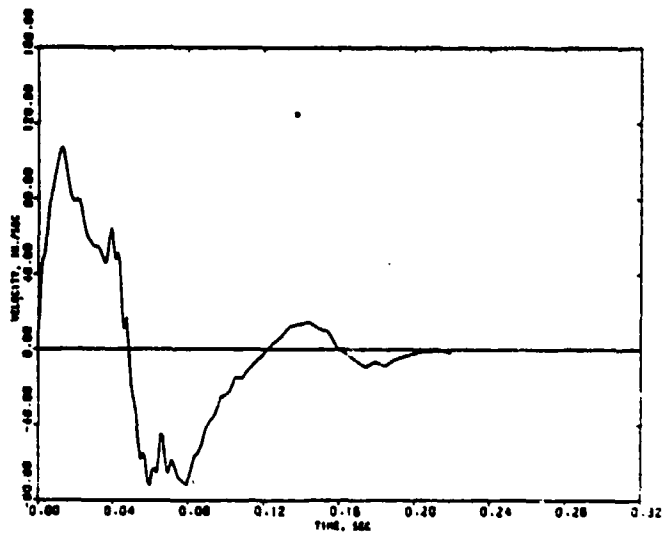
FIGURE 5-1. COMPUTED MOTION OF SOUTH AND WEST IGLOOS AT NODE 1  
(Refined ESKIMO-1 calculation)



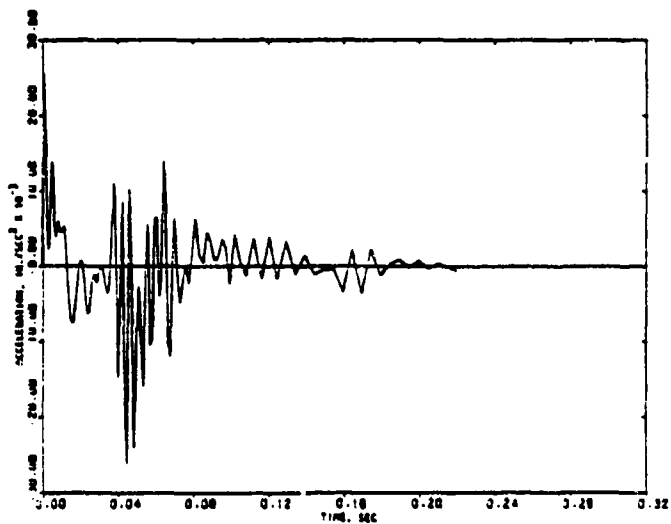
R-7556-1-4182



(a) Displacement



(b) Velocity

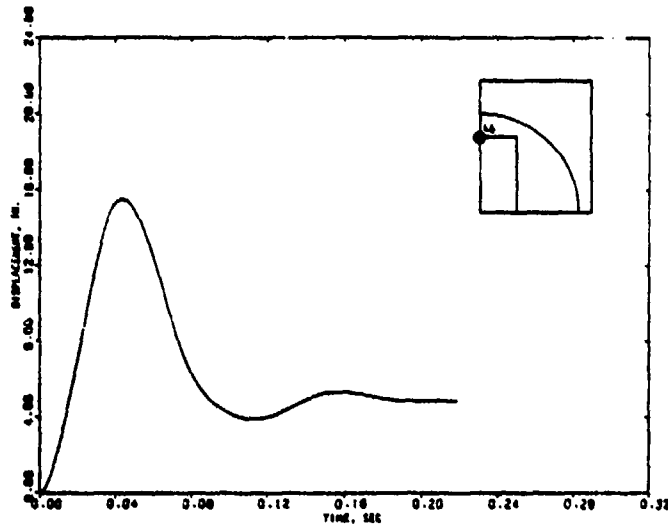


(c) Acceleration

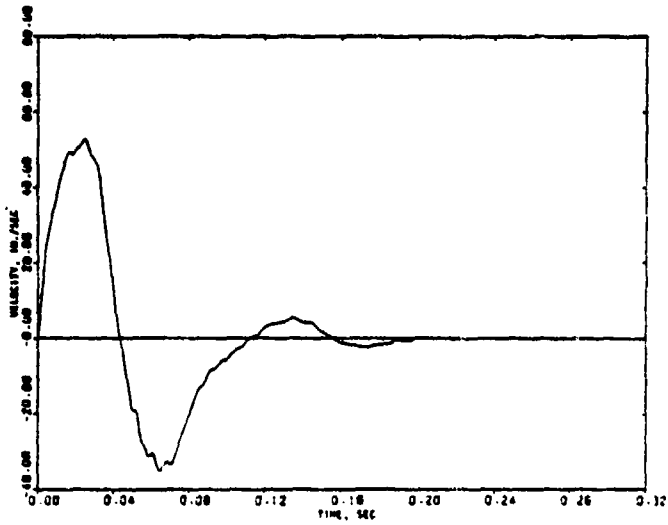
FIGURE 5-2. COMPUTED MOTION OF SOUTH AND WEST IGLOOS AT NODE 19  
(Refined ESKIMO-1 calculation)



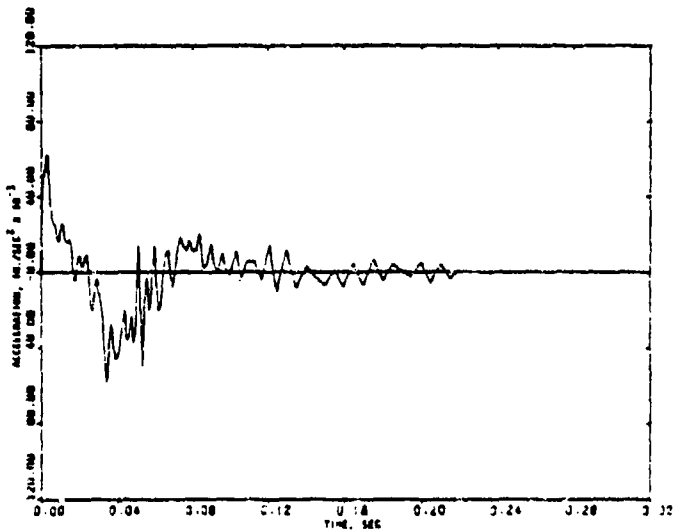
R-7556-1-4182



(a) Displacement



(b) Velocity

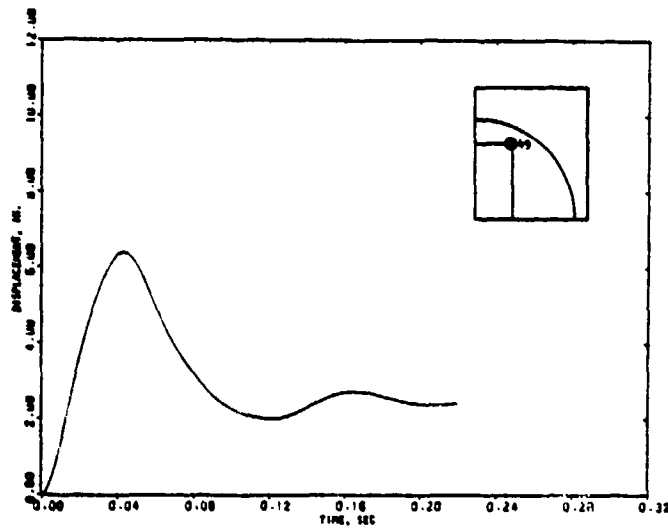


(c) Acceleration

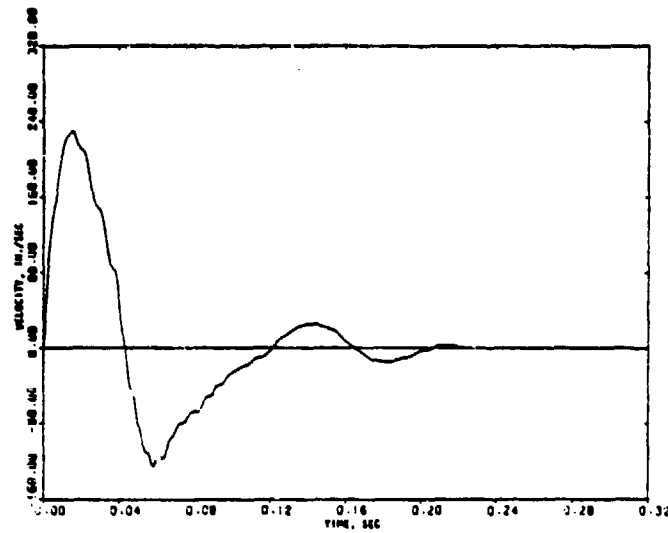
FIGURE 5-3. COMPUTED MOTION OF SOUTH AND WEST IGLOOS AT NODE 46  
(Refined ESKIMO-1 calculation)



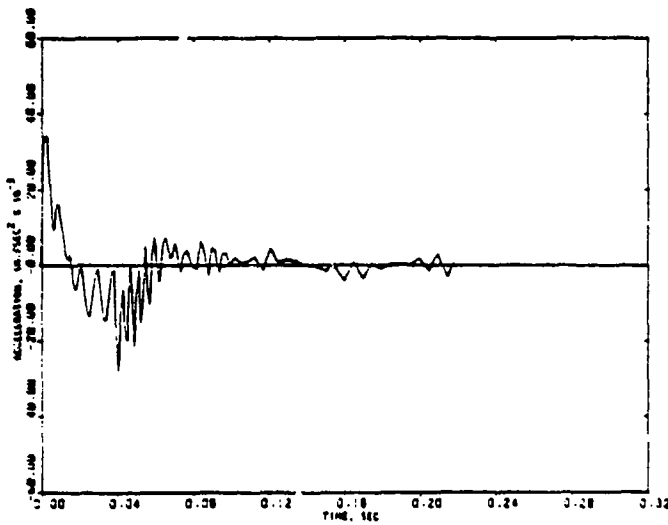
R-7556-1-4182



(a) Displacement

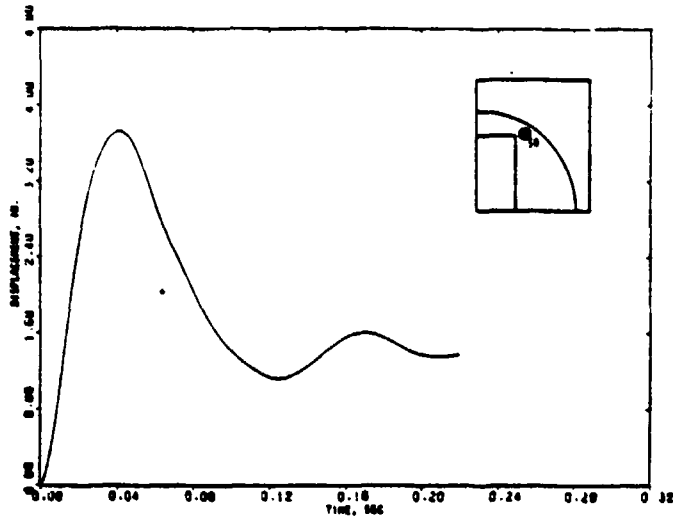


(b) Velocity

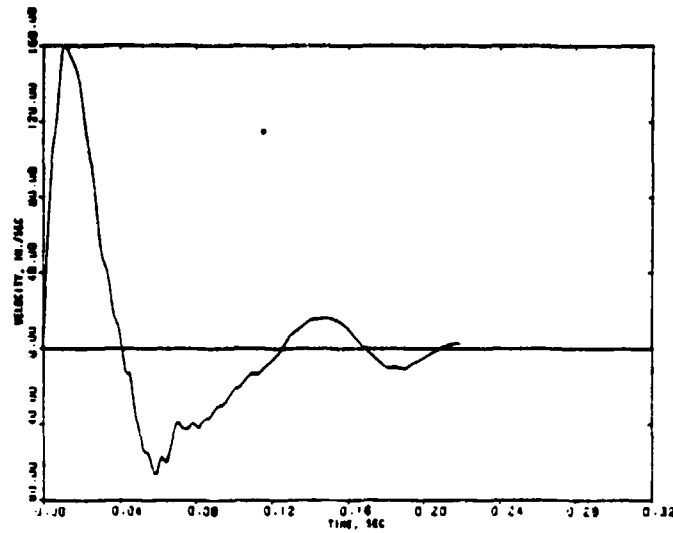


(c) Acceleration

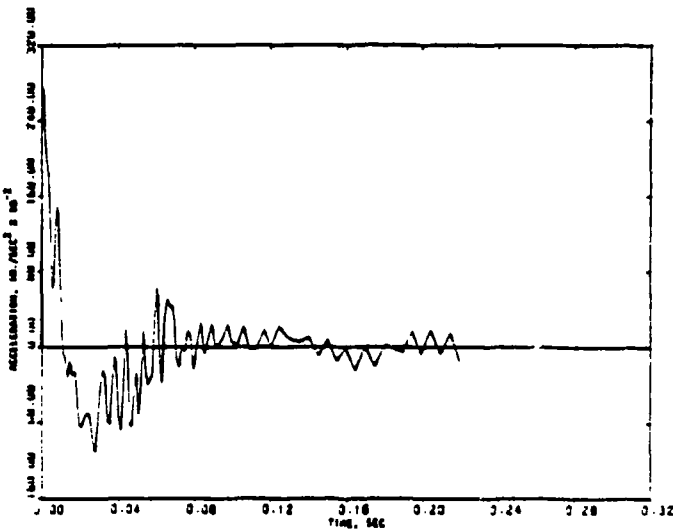
FIGURE 5-4. COMPUTED MOTION OF SOUTH AND WEST IGLOOS AT NODE 49  
(Refined ESKIMO-1 calculation)



(a) Displacement

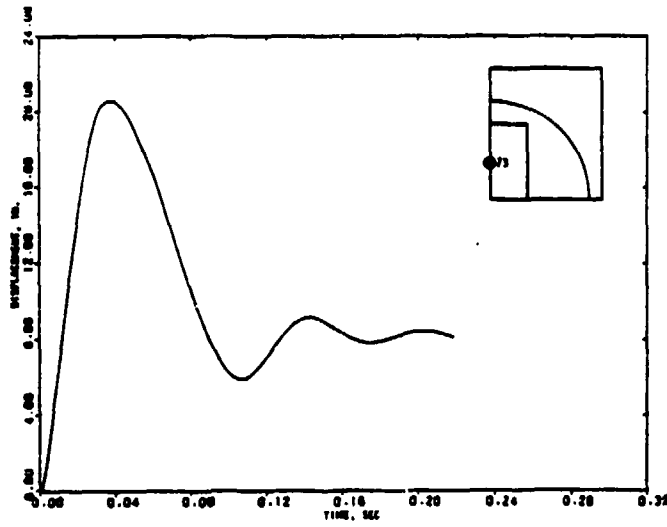


(b) Velocity

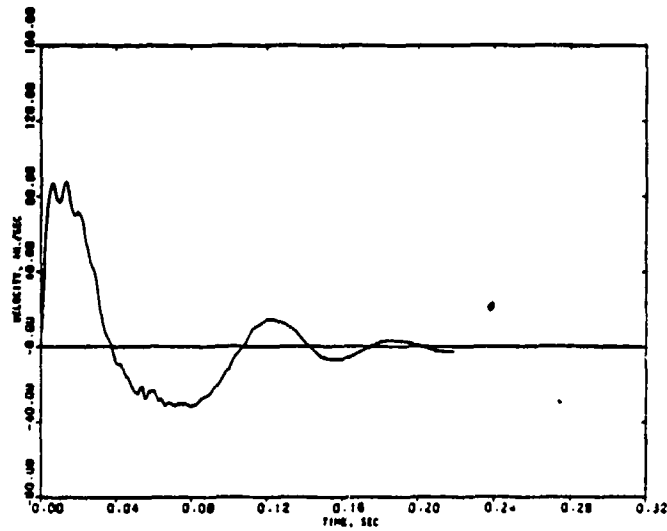


(c) Acceleration

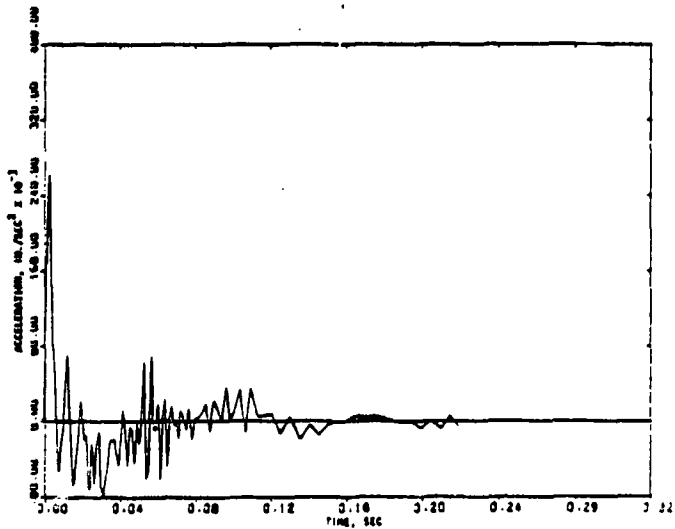
FIGURE 5-5. COMPUTED MOTION OF SOUTH AND WEST IGLOOS AT NODE 50  
(Refined ESKIMO-1 calculation)



(a) Displacement



(b) Velocity

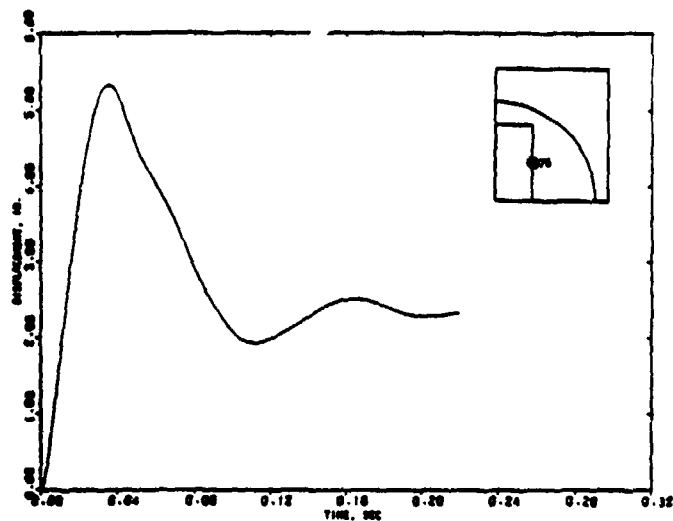


(c) Acceleration

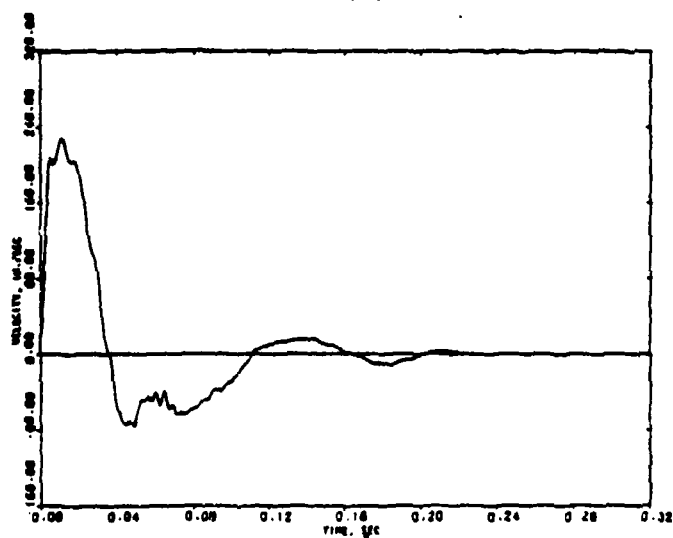
FIGURE 5-6. COMPUTED MOTION OF SOUTH AND WEST IGLOOS AT NODE 73  
(Refined ESKIMO-1 calculation)



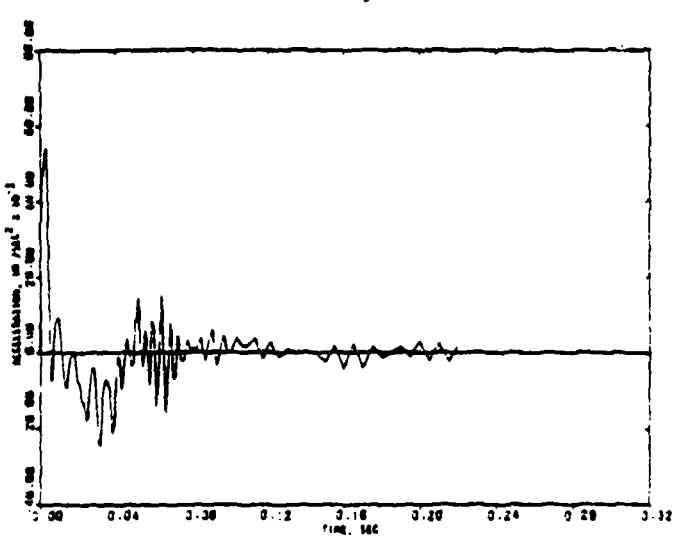
R-7556-1-4182



(a) Displacement

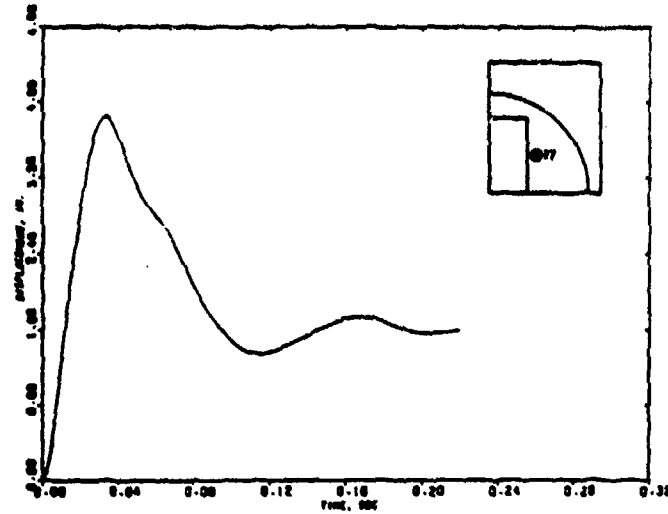


(b) Velocity

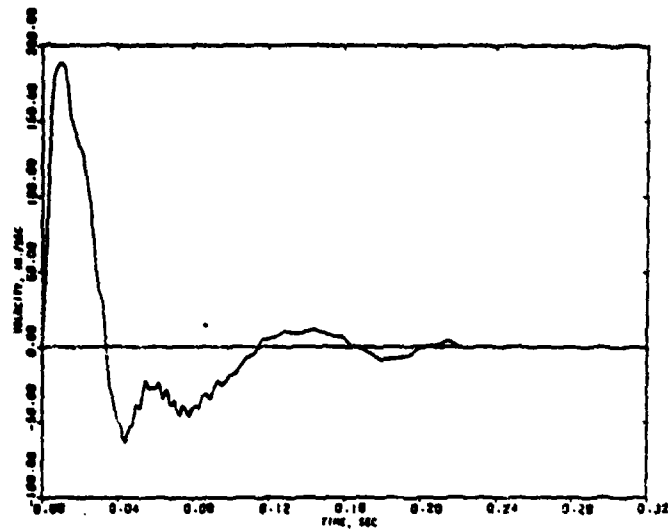


(c) Acceleration

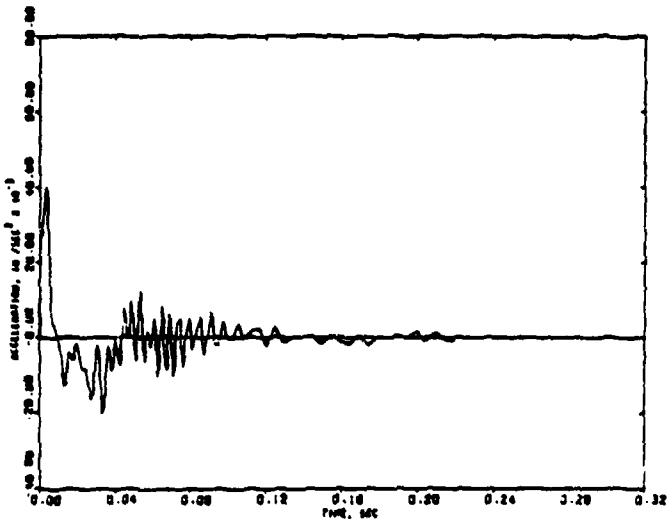
FIGURE 5-7. COMPUTED MOTION OF SOUTH AND WEST IGLOOS AT NODE 76  
(Refined ESKIMO-1 calculation)



(a) Displacement

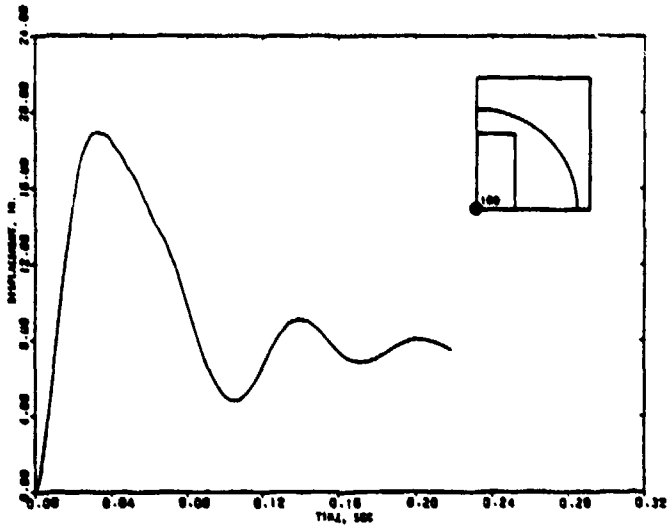


(b) Velocity

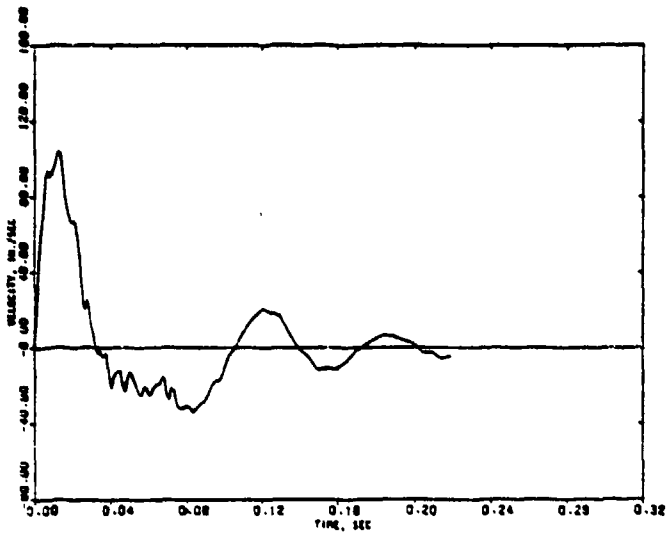


(c) Acceleration

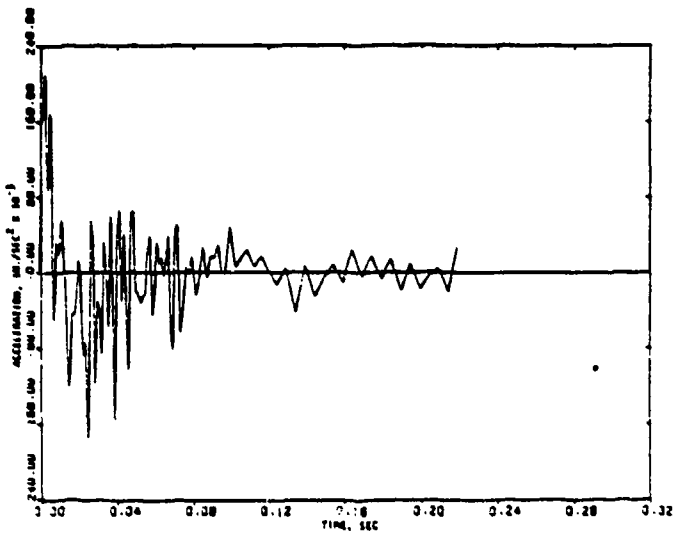
FIGURE 5-8. COMPUTED MOTION OF SOUTH AND WEST IGLOOS AT NODE 77  
(Refined ESKIMO-1 calculation)



(a) Displacement

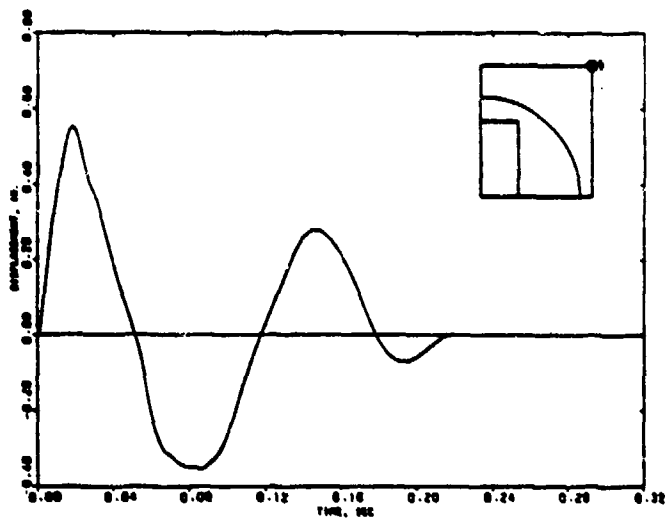


(b) Velocity

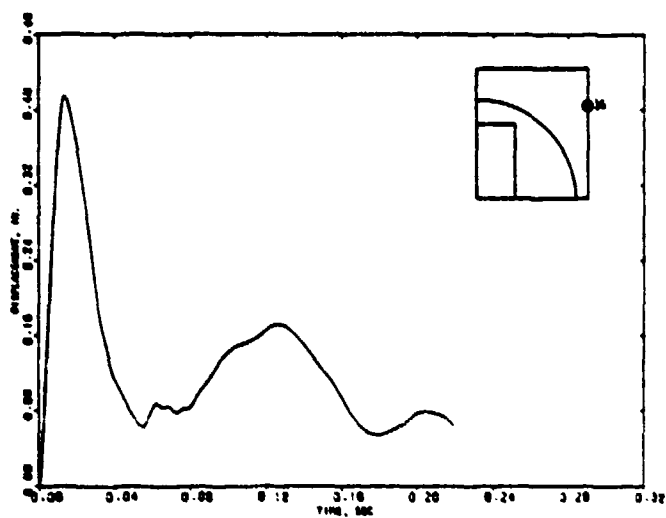


(c) Acceleration

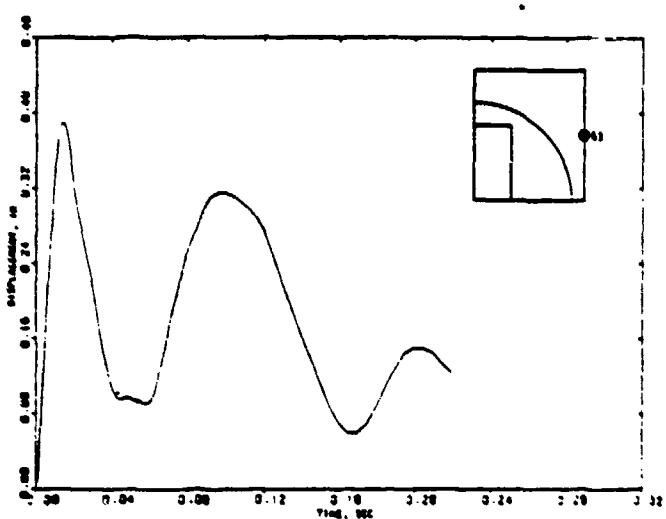
FIGURE 5-9. COMPUTED MOTION OF SOUTH AND WEST IGLOOS AT NODE 100 (Refined ESKIMO-1 calculation)



(a) Node 9

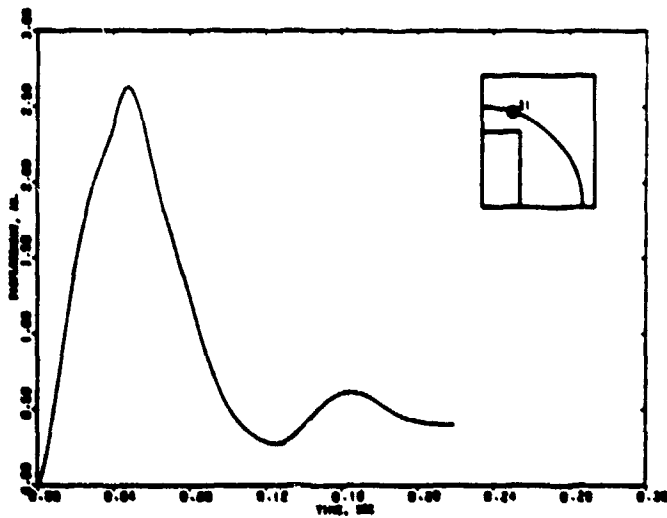


(b) Node 36

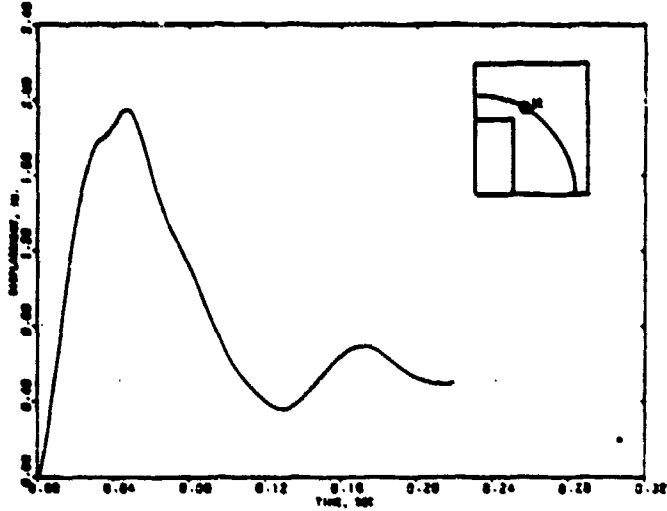


(c) Node 63

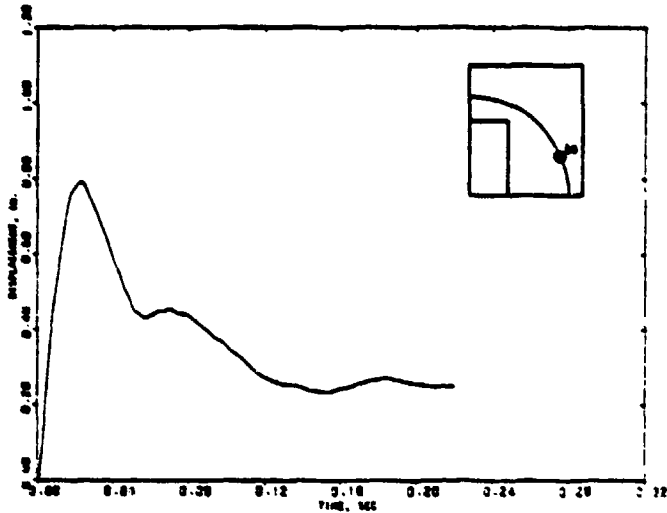
FIGURE 5-10. COMPUTED DISPLACEMENTS ALONG EDGES OF HEADWALLS OF SOUTH AND WEST IGLOOS (Refined ESKIMO-1 calculation)



(a) Node 21

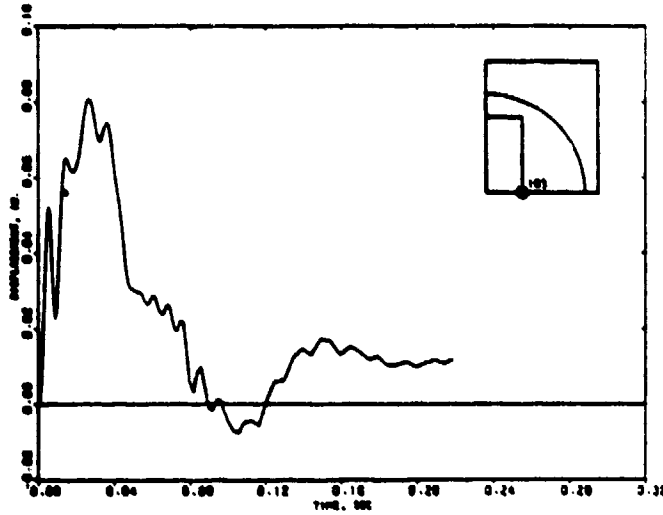


(b) Node 32

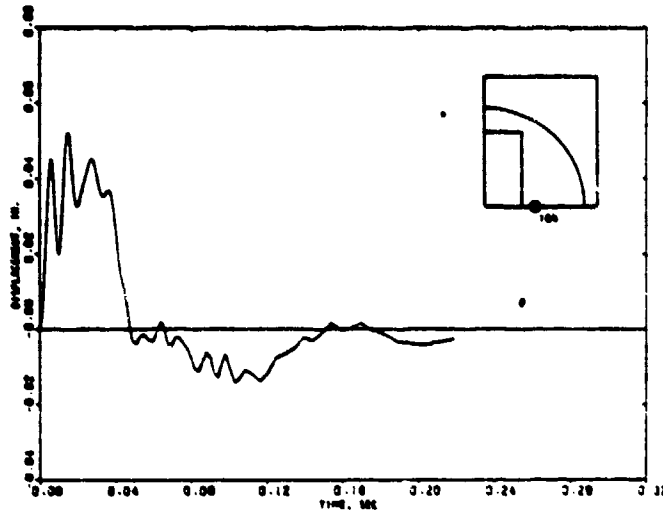


(c) Node 80

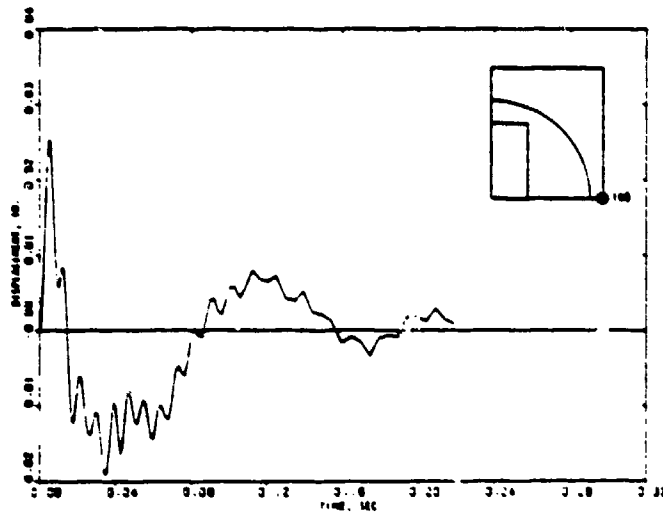
FIGURE 5-11. COMPUTED DISPLACEMENTS ALONG ARC LINE OF HEADWALLS OF SOUTH AND WEST IGLOOS (Refined ESKIMO-1 calculation)



(a) Node 103

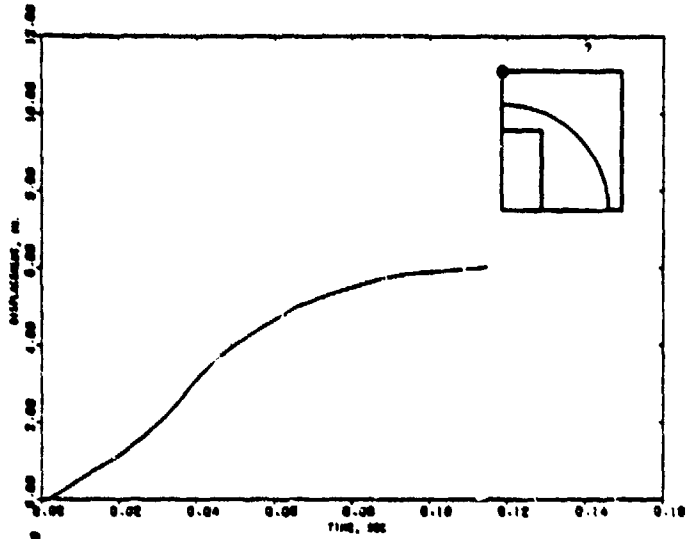


(b) Node 104

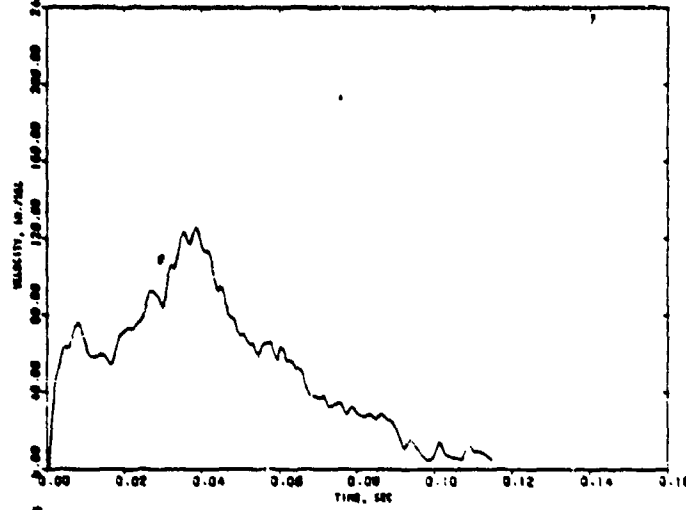


(c) Node 108

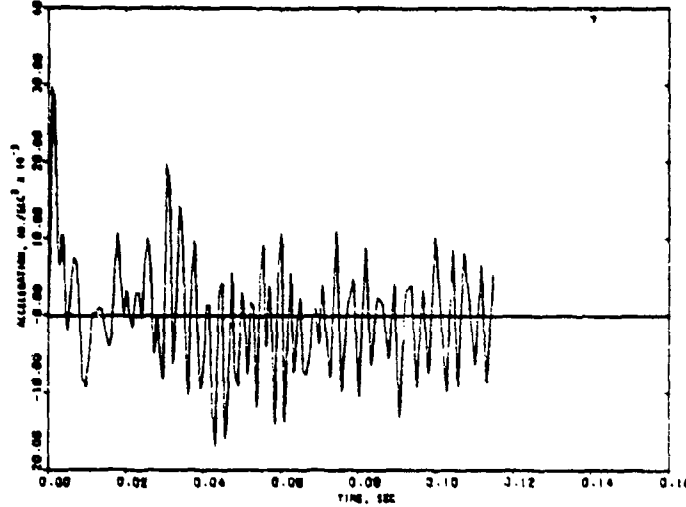
FIGURE 5-12. COMPUTED DISPLACEMENT AT GROUND LEVEL OF SEVERAL LOCATIONS ON SOUTH AND WEST IGLOOS (Refined ESKIMO-1 calculation)



(a) Displacement

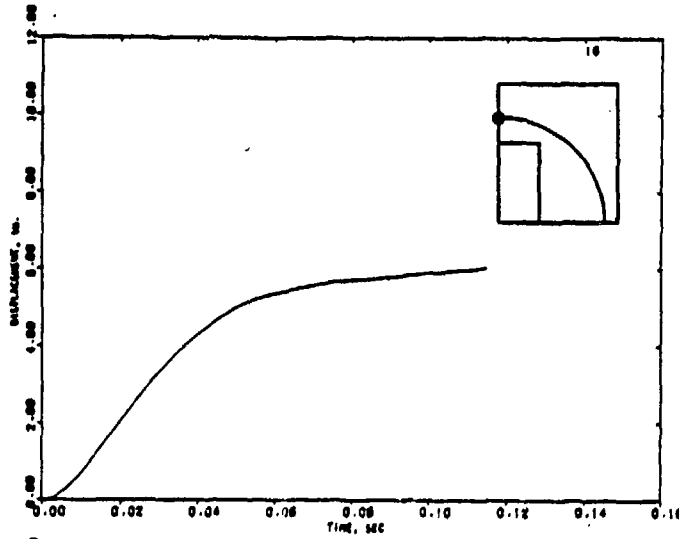


(b) Velocity

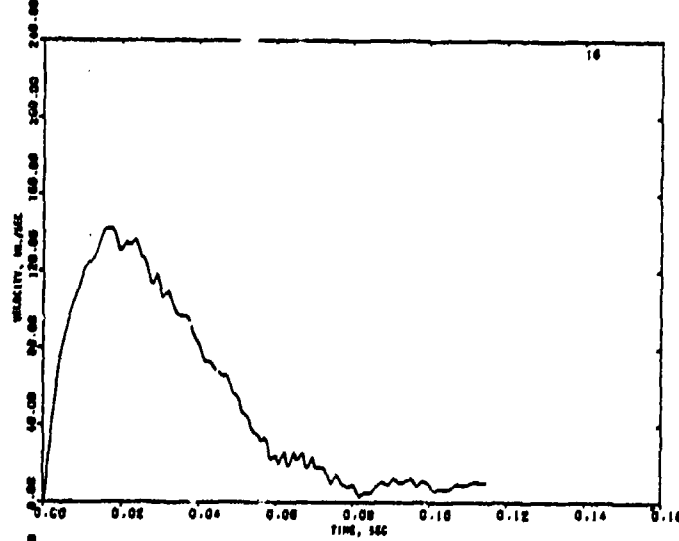


(c) Acceleration

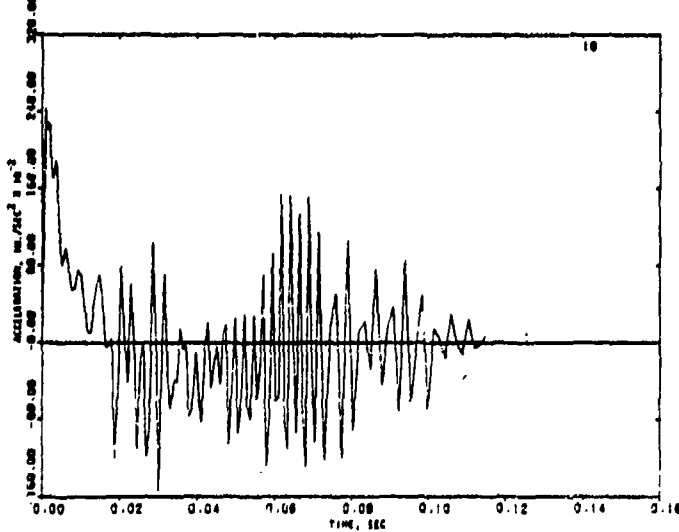
FIGURE 5-13. COMPUTED MOTION FROM PRIOR CALCULATION CORRESPONDING TO NODE 1



(a) Displacement

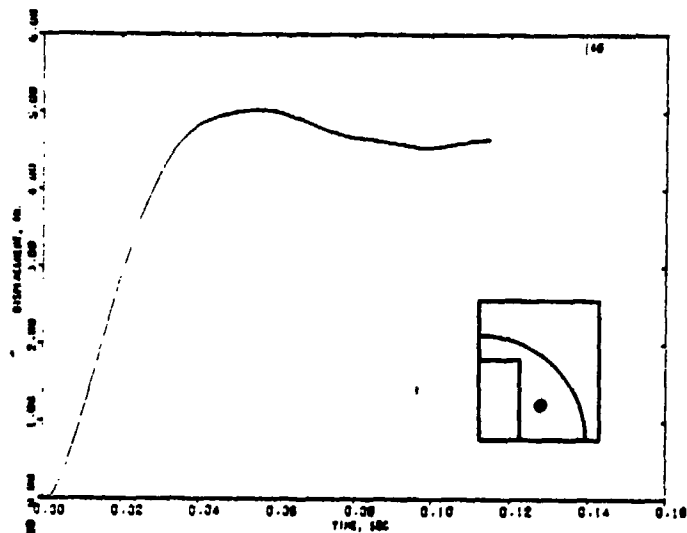


(b) Velocity

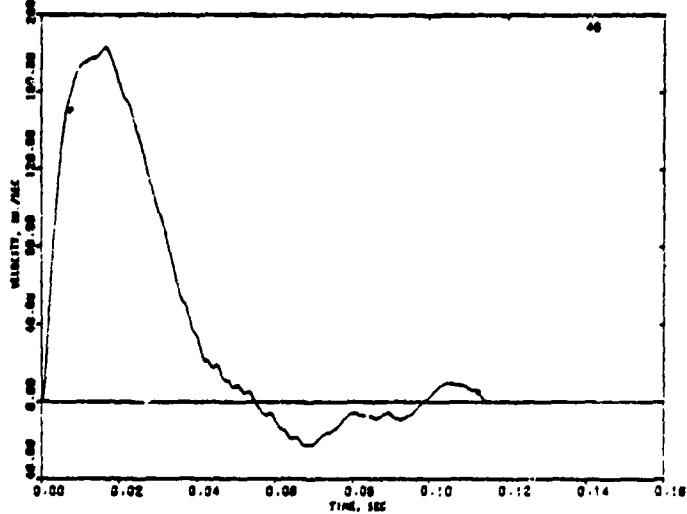


(c) Acceleration

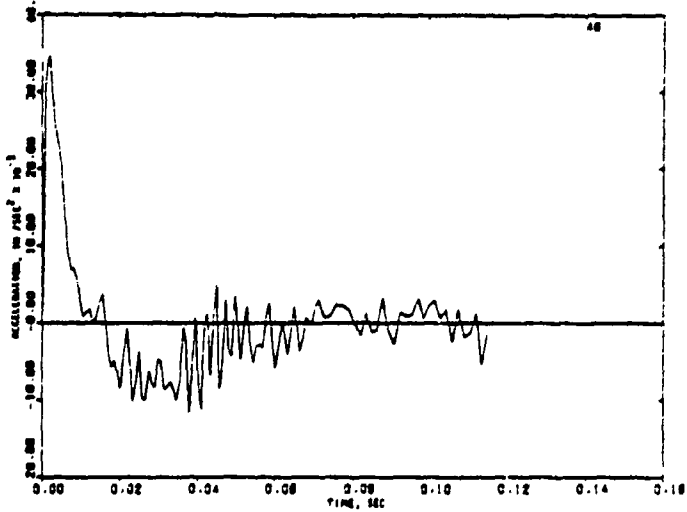
FIGURE 5-14. COMPUTED MOTION FROM PRIOR CALCULATION CORRESPONDING TO NODE 19



(a) Displacement



(b) Velocity

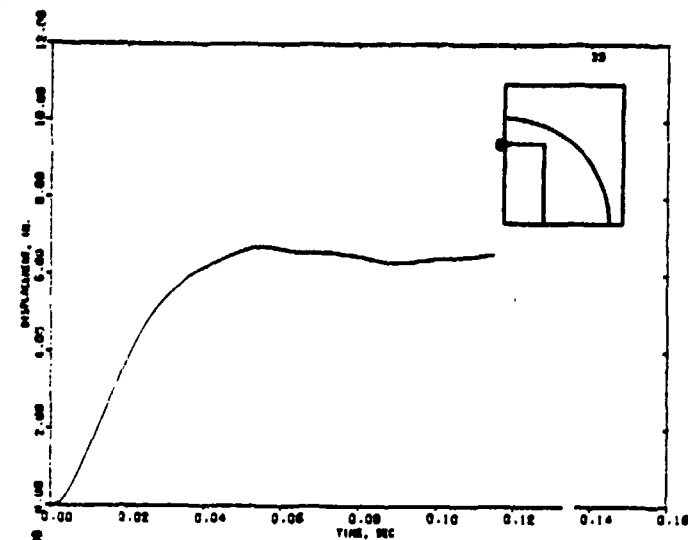


(c) Acceleration

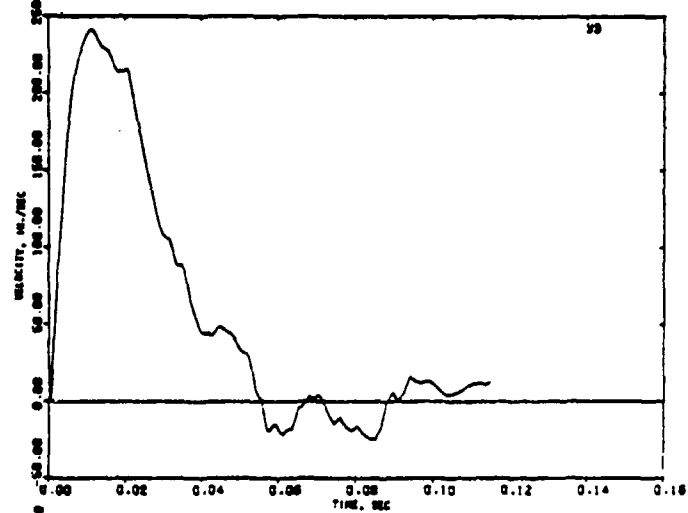
FIGURE 5-15. COMPUTED MOTION FROM PRIOR CALCULATION CORRESPONDING TO NODE 77



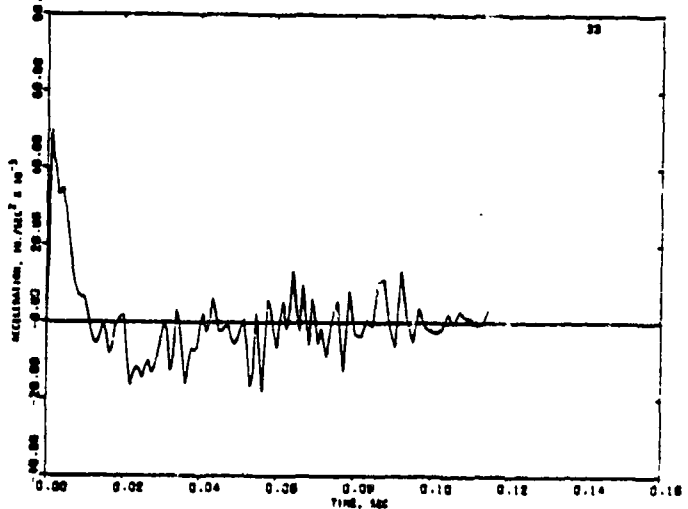
R-7556-1-4182



(a) Displacement



(b) Velocity

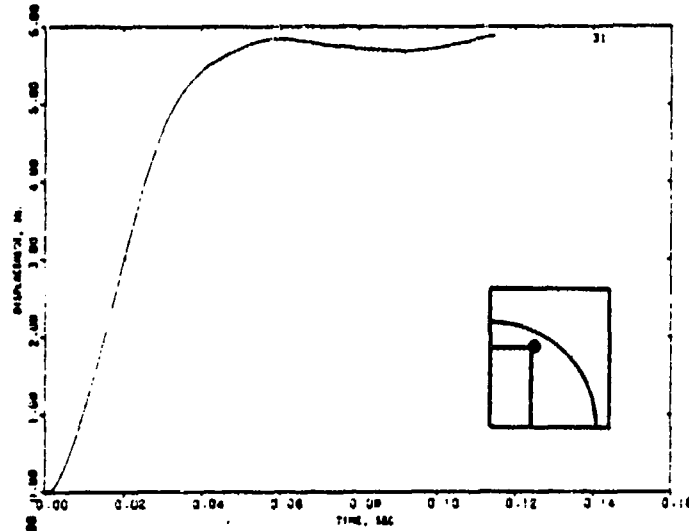


(c) Acceleration

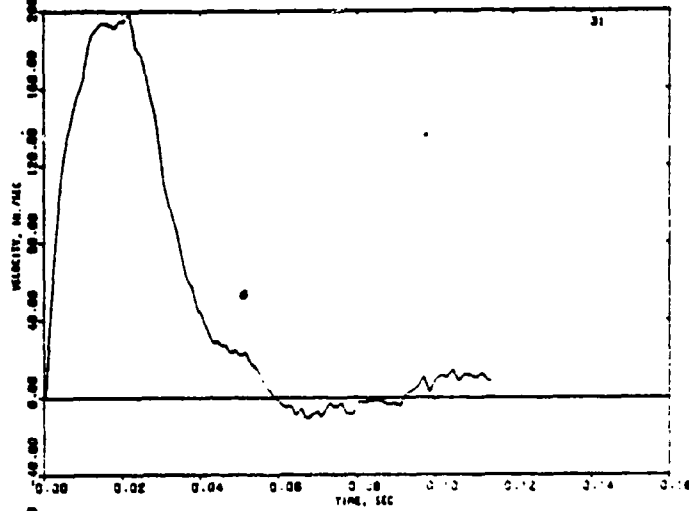
FIGURE 5-16. COMPUTED MOTION FROM PRIOR CALCULATION CORRESPONDING TO NODE 46



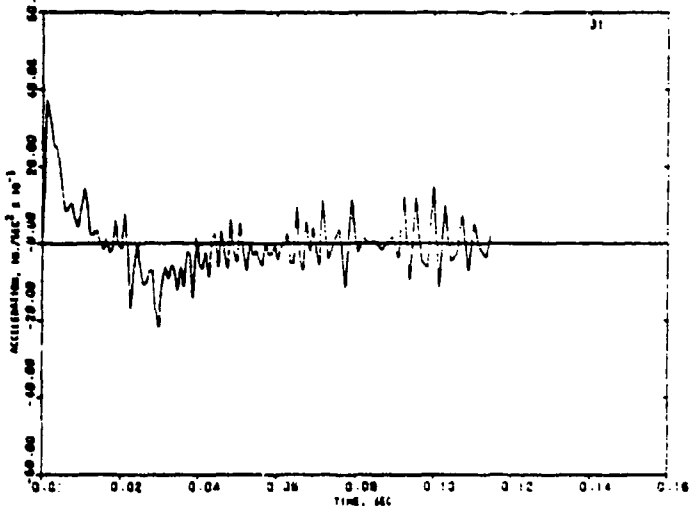
R-7556-1-4182



(a) Displacement



(b) Velocity

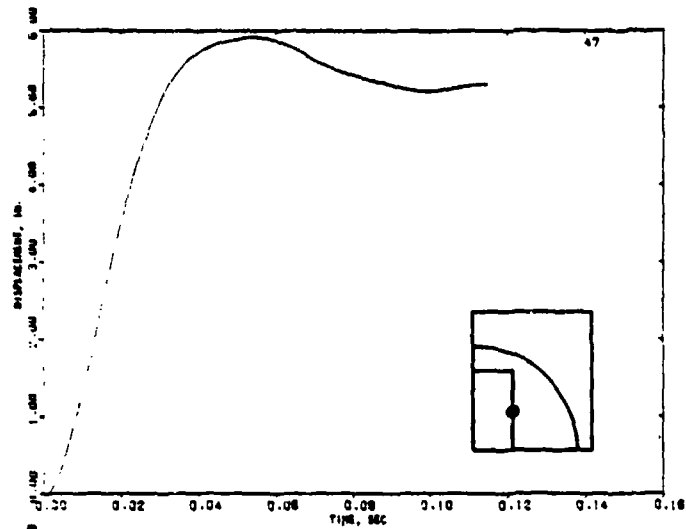


(c) Acceleration

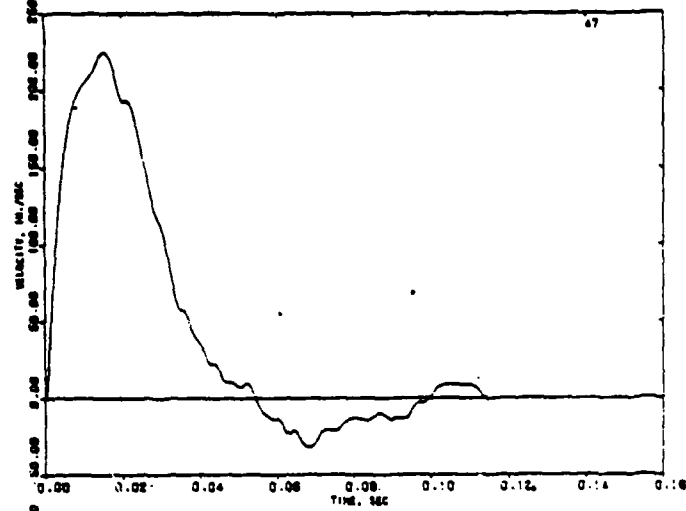
FIGURE 5-17. COMPUTED MOTION FROM PRIOR CALCULATION CORRESPONDING TO NODE 49



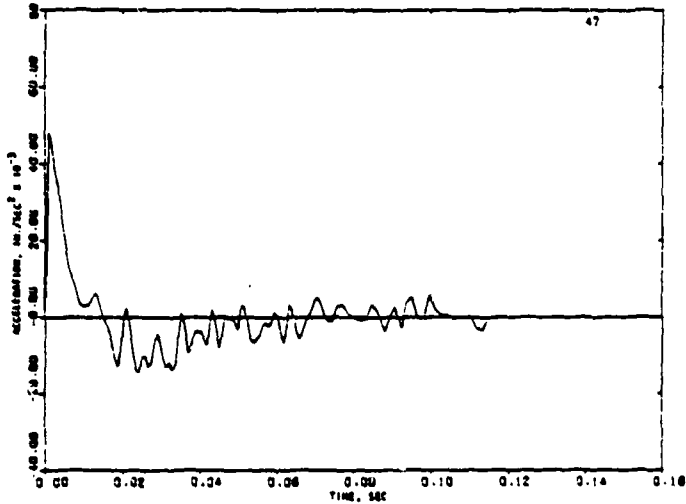
R-7556-1-4182



(a) Displacement

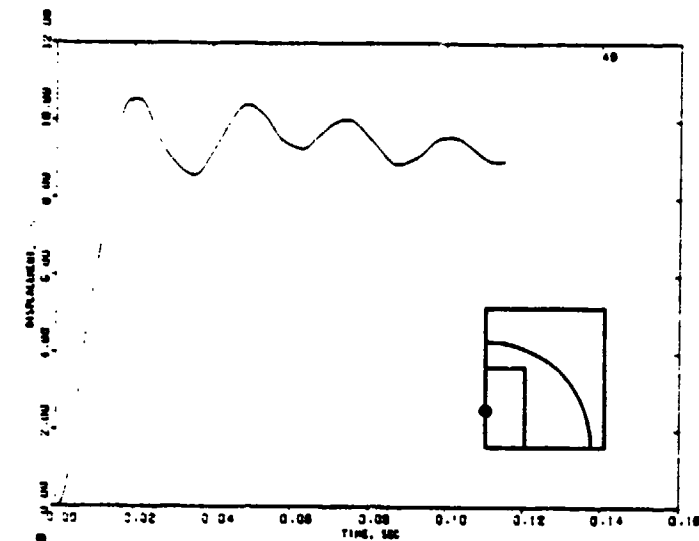


(b) Velocity

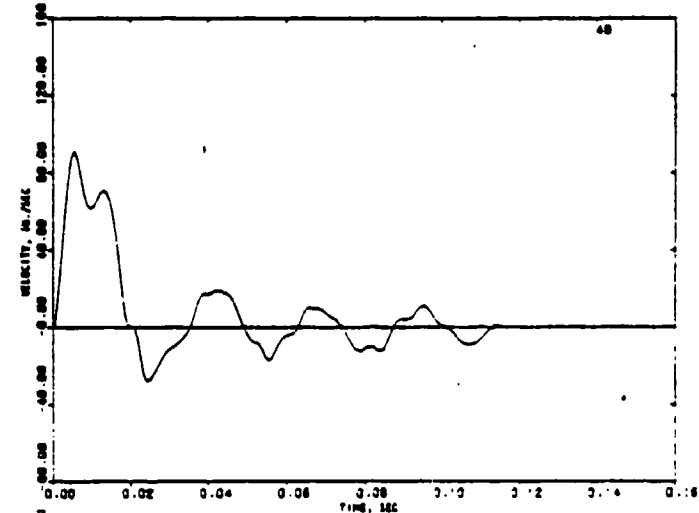


(c) Acceleration

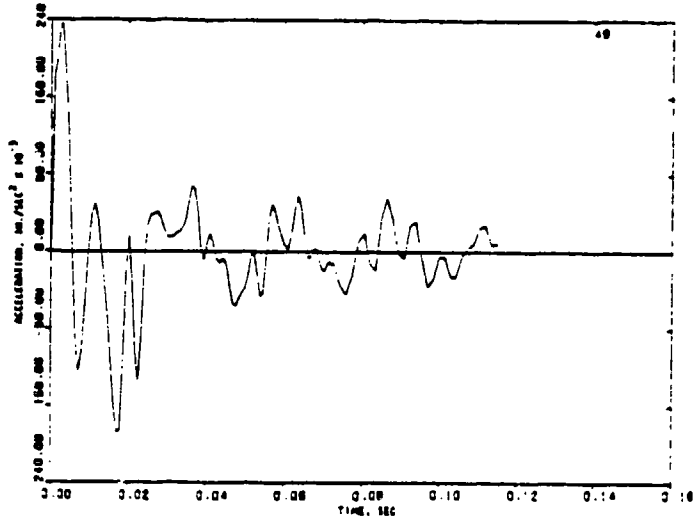
FIGURE 5-18. COMPUTED MOTION FROM PRIOR CALCULATION CORRESPONDING TO NODE 76



(a) Displacement

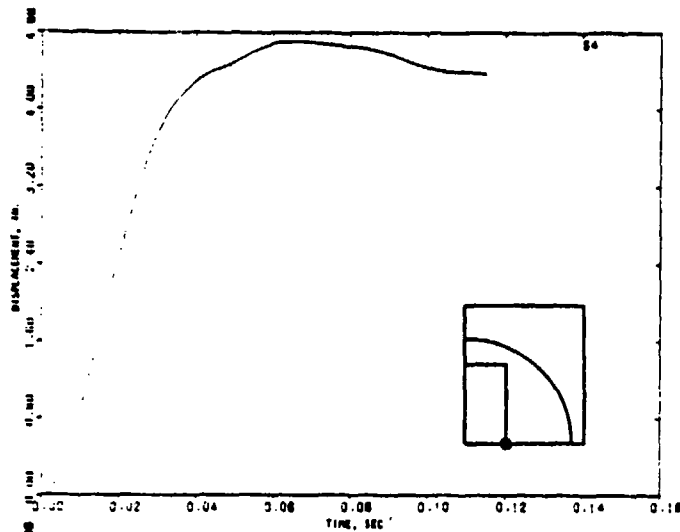


(b) Velocity

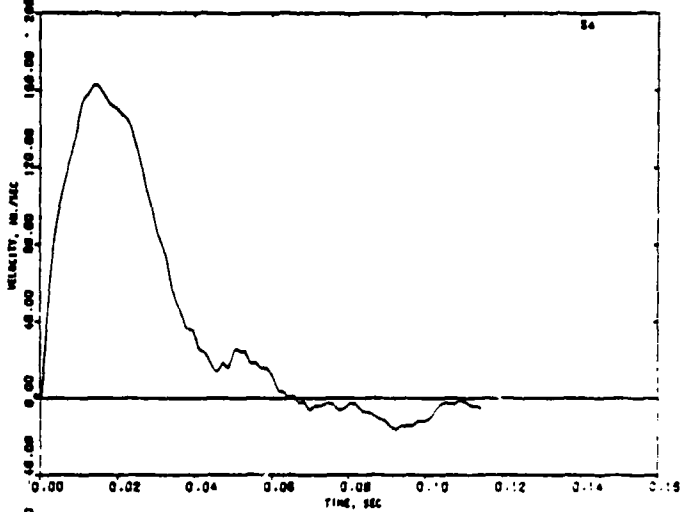


(c) Acceleration

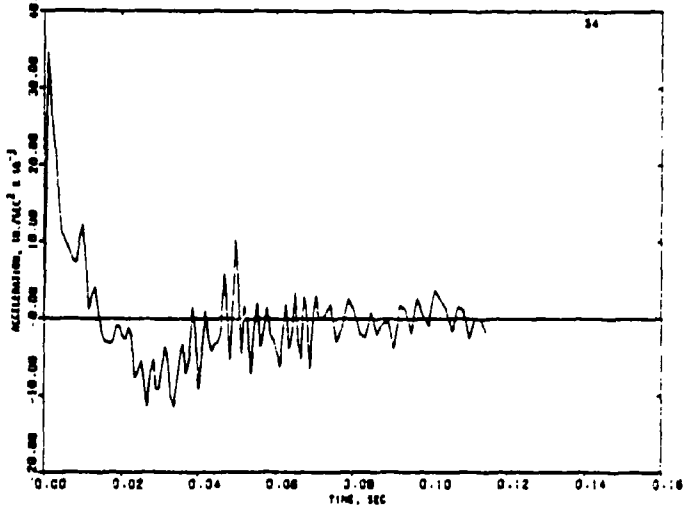
FIGURE 5-19. COMPUTED MOTION FROM PRIOR CALCULATION CORRESPONDING TO NODE 73



(a) Displacement



(b) Velocity



(c) Acceleration

FIGURE 5-20. COMPUTED MOTION FROM PRIOR CALCULATION CORRESPONDING TO NODE 103



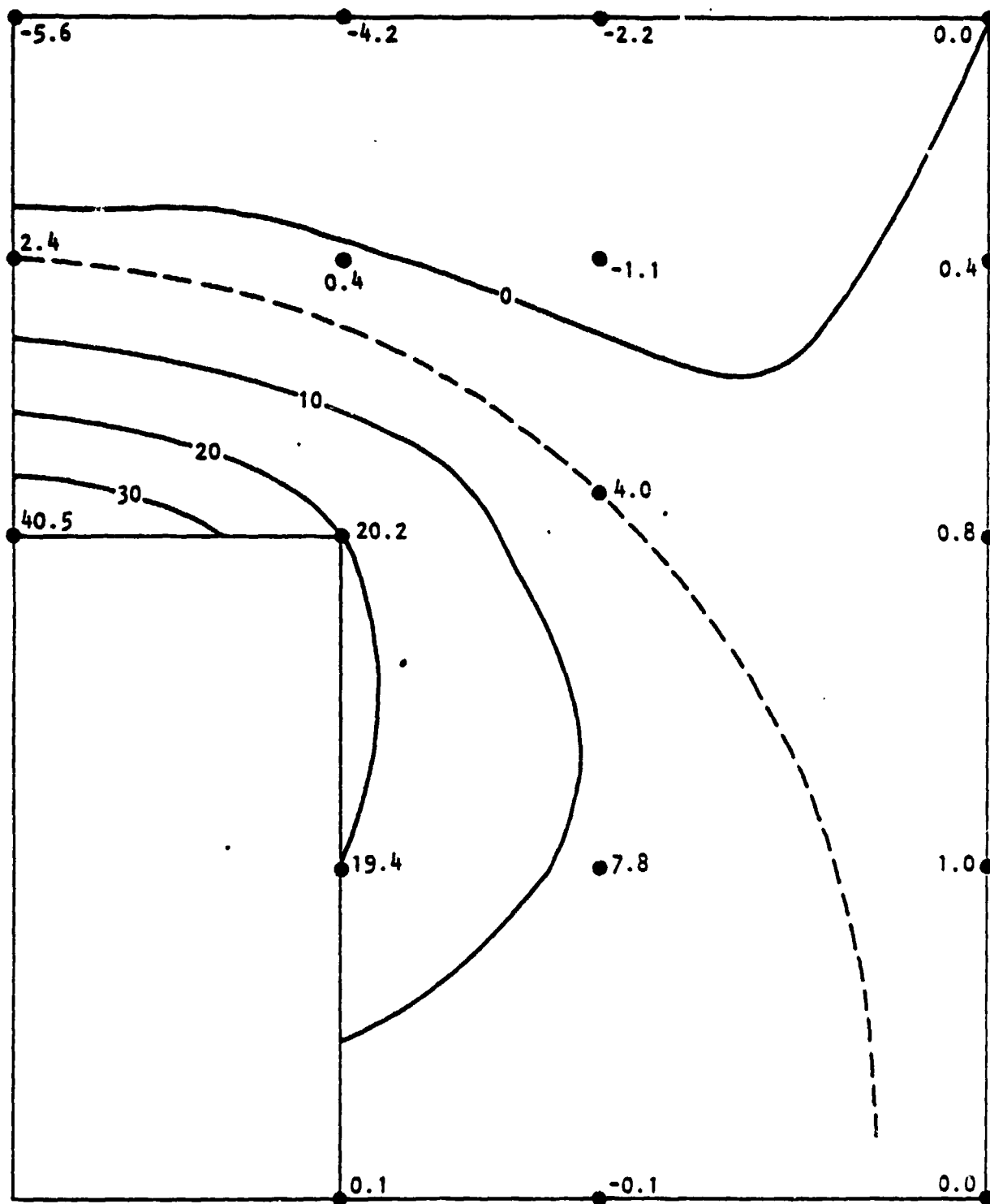


FIGURE 5-23. COMPUTED DISPLACEMENTS (IN HUNDREDTHS OF A FOOT) OF THE HEADWALLS OF THE SOUTH AND WEST IGLOOS, ESKIMO I, 0.22 SEC AFTER ARRIVAL OF THE BLAST WAVE

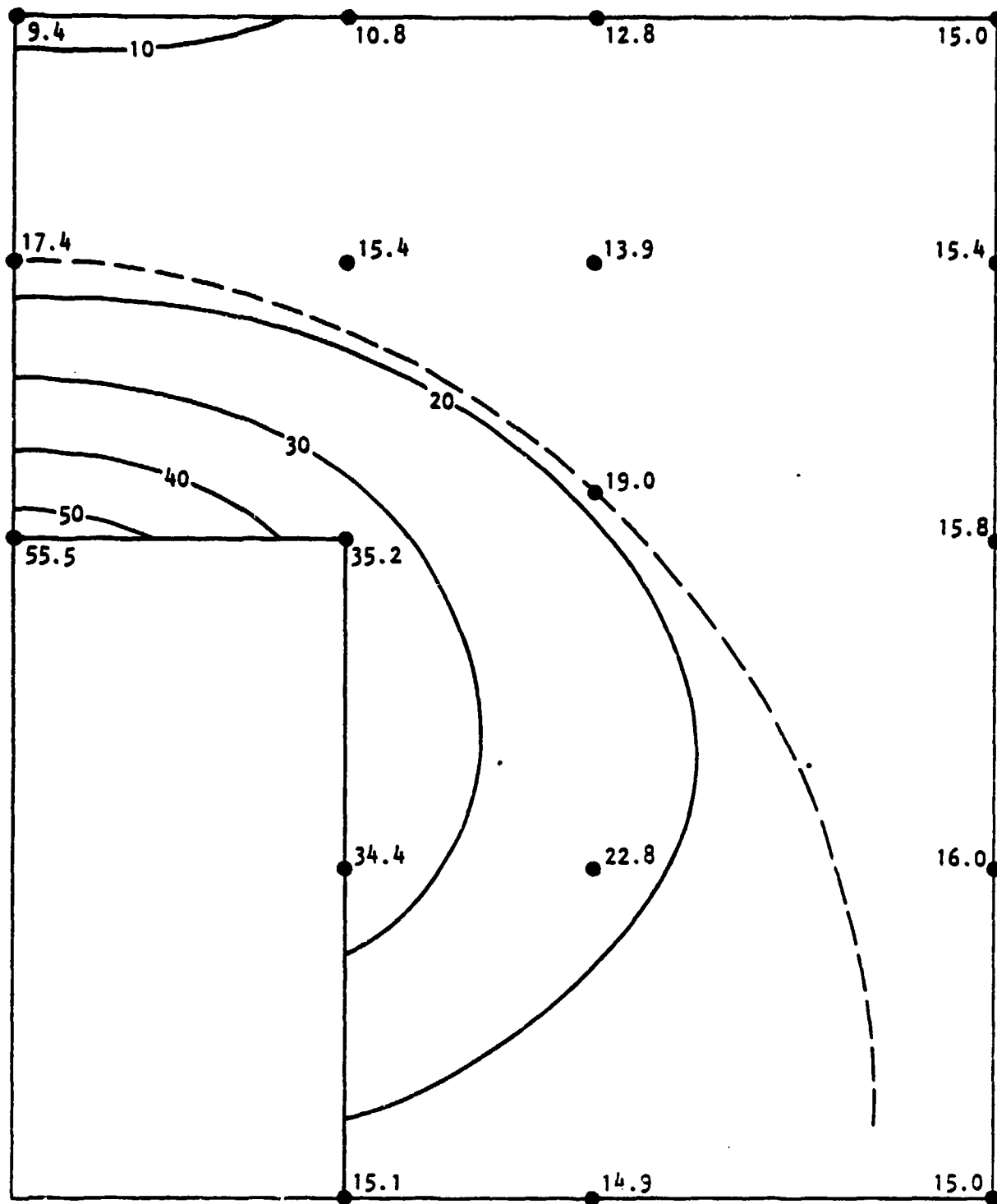


FIGURE 5-24. COMPUTED DISPLACEMENTS (IN HUNDREDTHS OF A FOOT) WITH A RIGID BODY DISPLACEMENT OF 0.15 FT ADDED IN FOR THE SAKE OF COMPARISON WITH THE WEST IGLOO, ESKIMO I

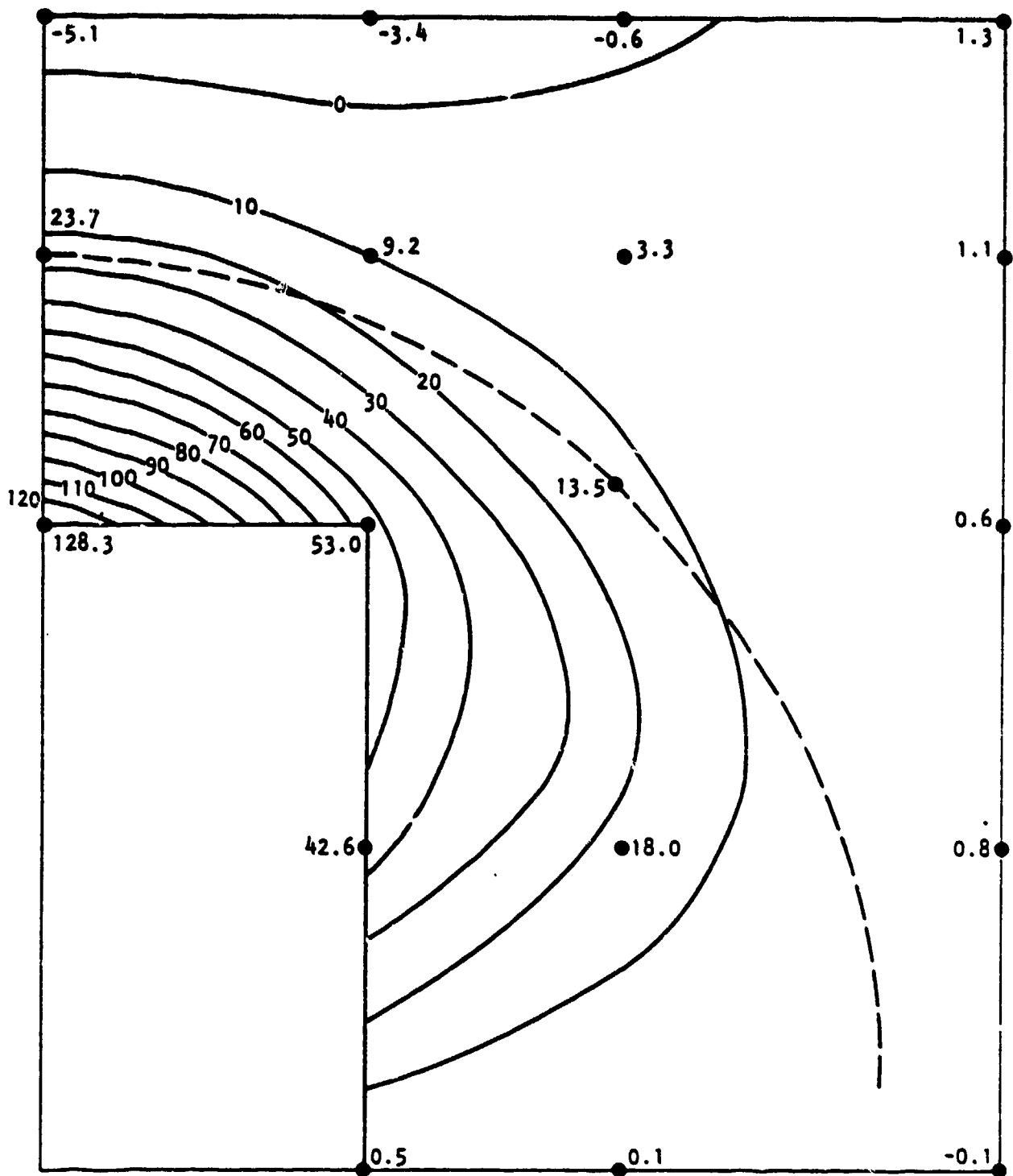
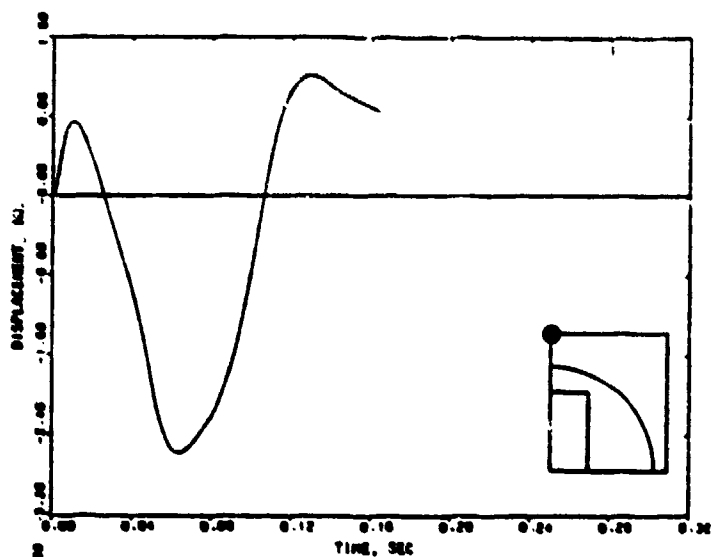
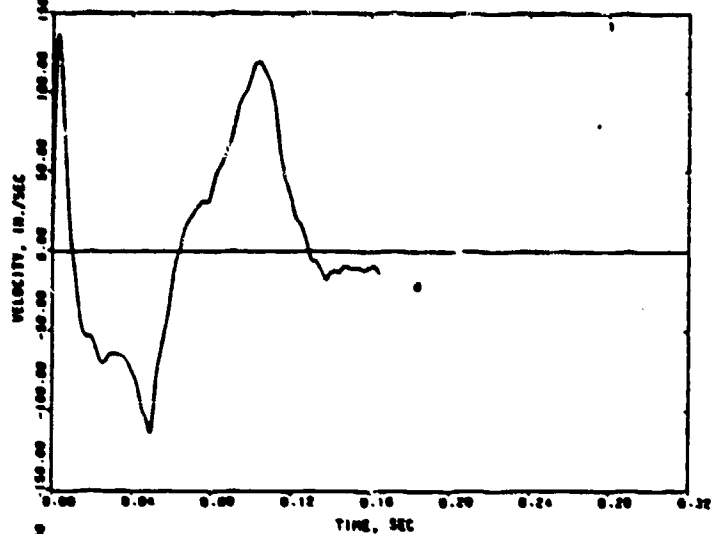


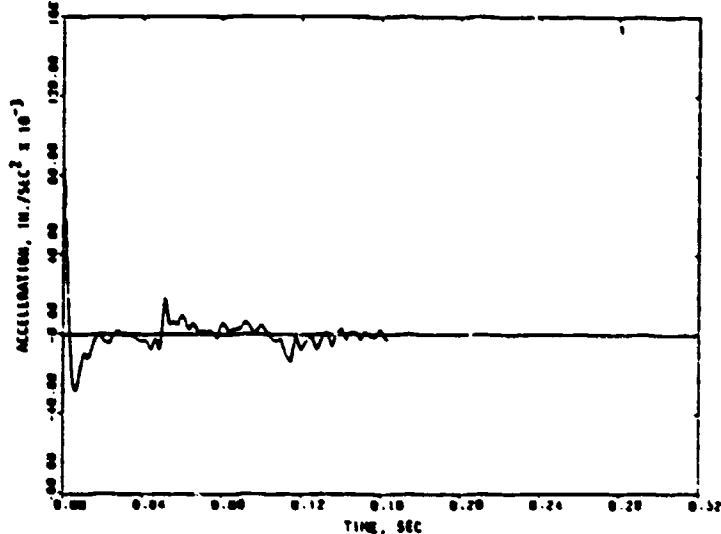
FIGURE 5-25. COMPUTED DISPLACEMENTS (IN HUNDREDTHS OF A FOOT) OF THE HEADWALLS OF THE SOUTH AND WEST IGLOOS, ESKIMO 1, 0.042 SEC AFTER ARRIVAL OF THE BLAST



(a) Displacement



(b) Velocity

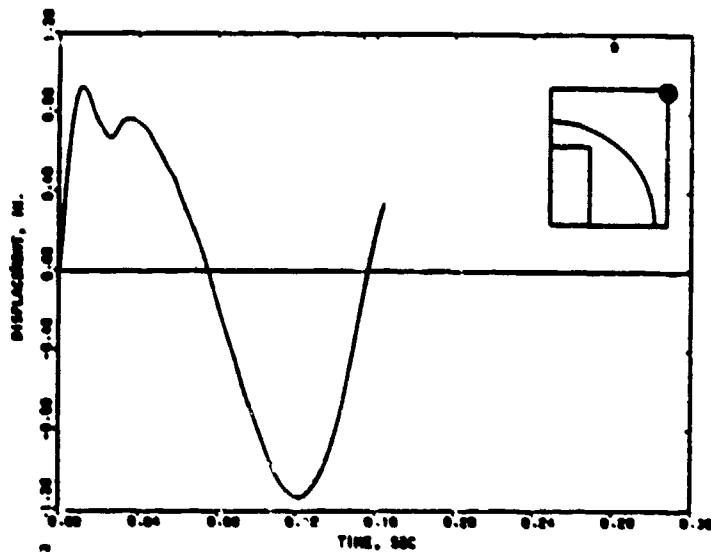


(c) Acceleration

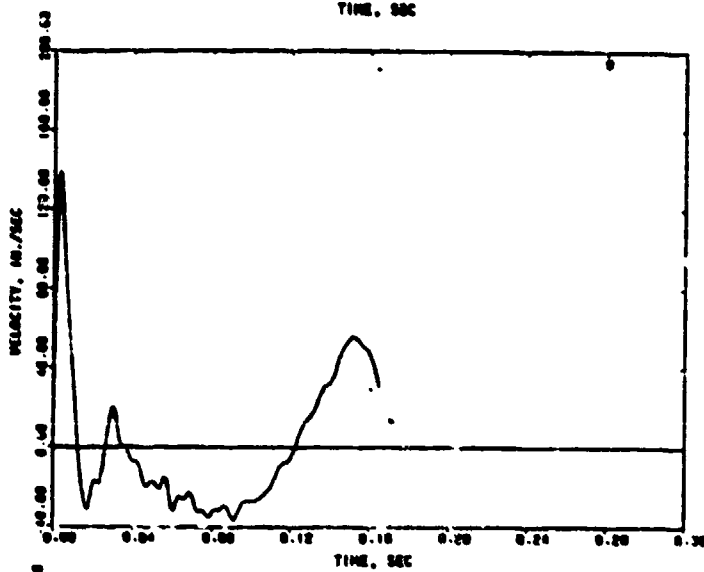
FIGURE 5-26. COMPUTED MOTION OF EAST HEADWALL (ESKIMO II) AT NODE 1



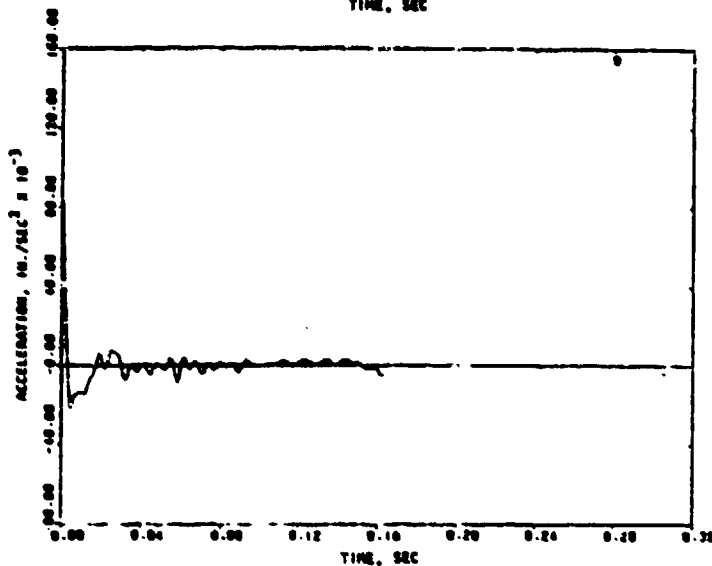
R-7556-1-4182



(a) Displacement

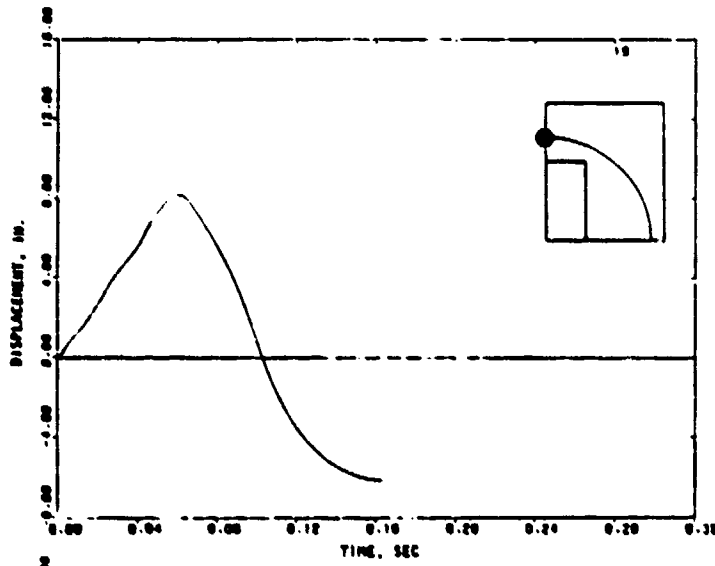


(b) Velocity

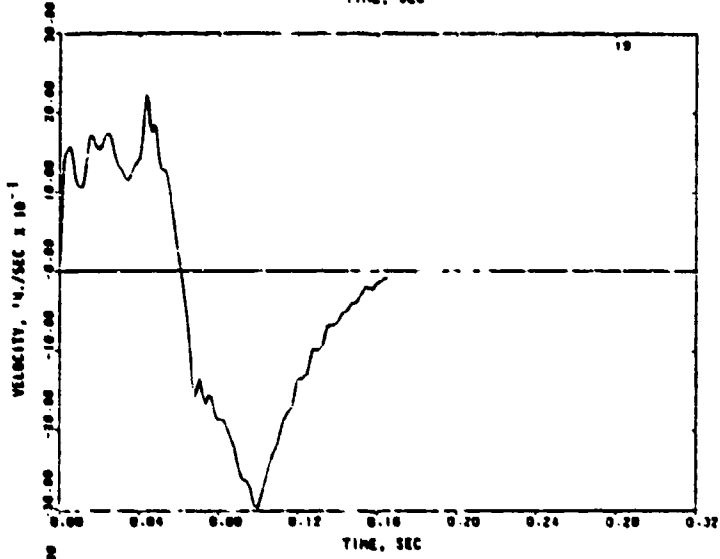


(c) Acceleration

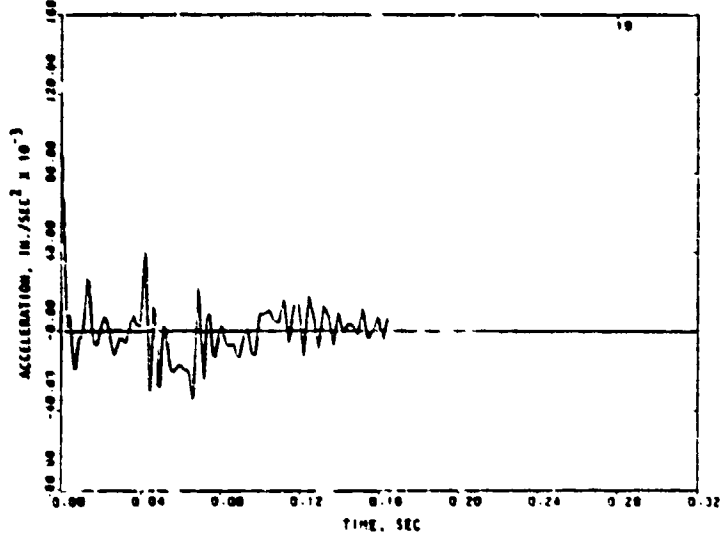
FIGURE 5-27. COMPUTED MOTION OF EAST HEADWALL (ESKIMO II) AT NODE 9



(a) Displacement

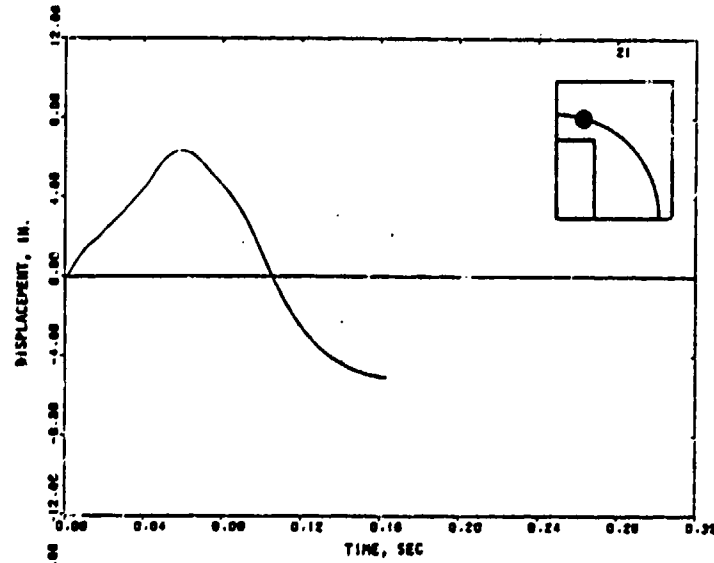


(b) Velocity

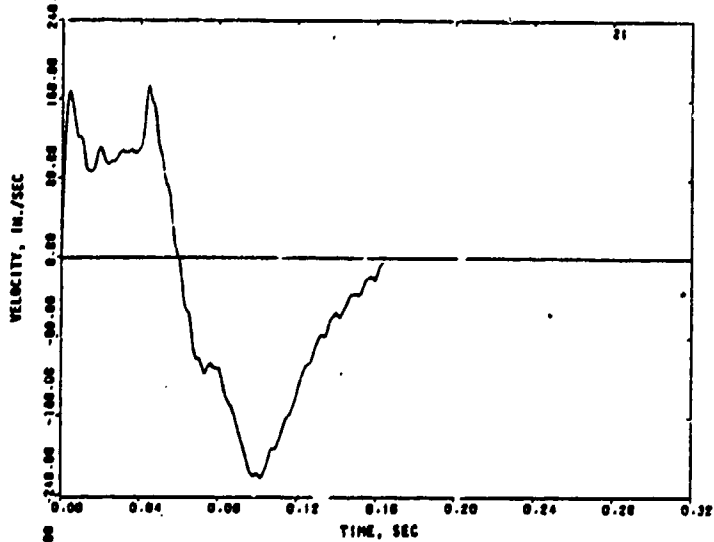


(c) Acceleration

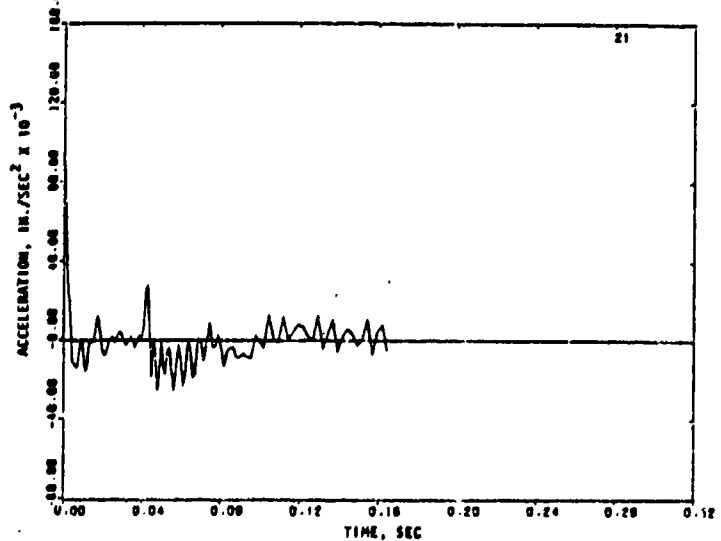
FIGURE 5-28. COMPUTED MOTION OF EAST HEADWALL (ESKIMO II) AT NODE 19



(a) Displacement



(b) Velocity

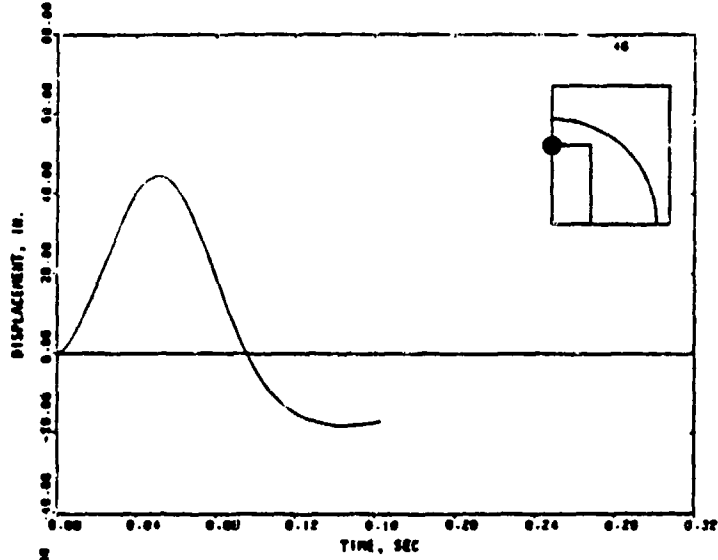


(c) Acceleration

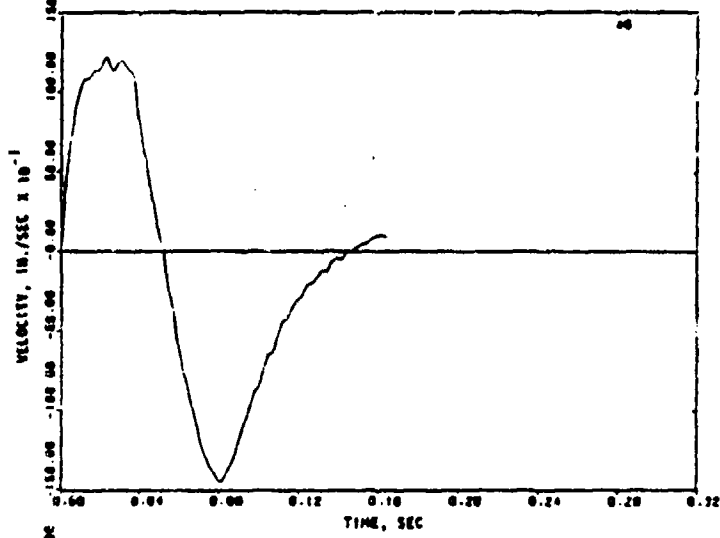
FIGURE 5-29. COMPUTED MOTION OF EAST HEADWALL (ESKIMO II) AT NODE 21



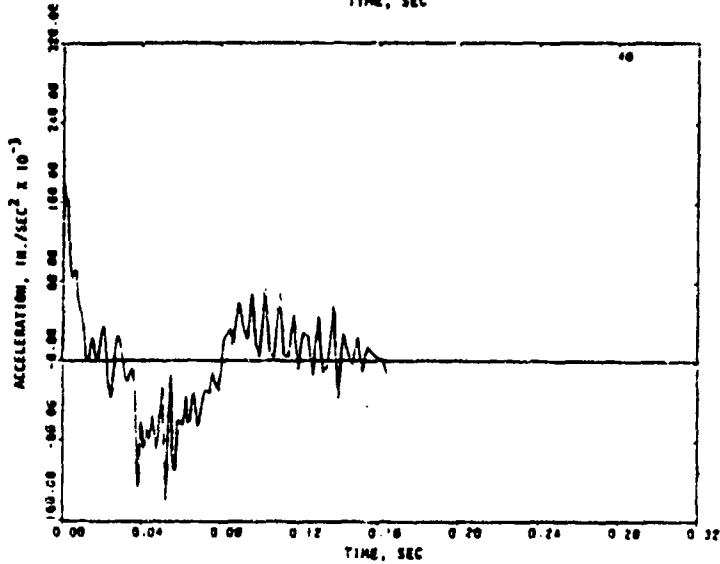
R-7556-1-4182



(a) Displacement



(b) Velocity



(c) Acceleration

FIGURE 5-30. COMPUTED MOTION OF EAST HEADWALL (ESKIMO II) AT NODE 46



P-7556-1-4182

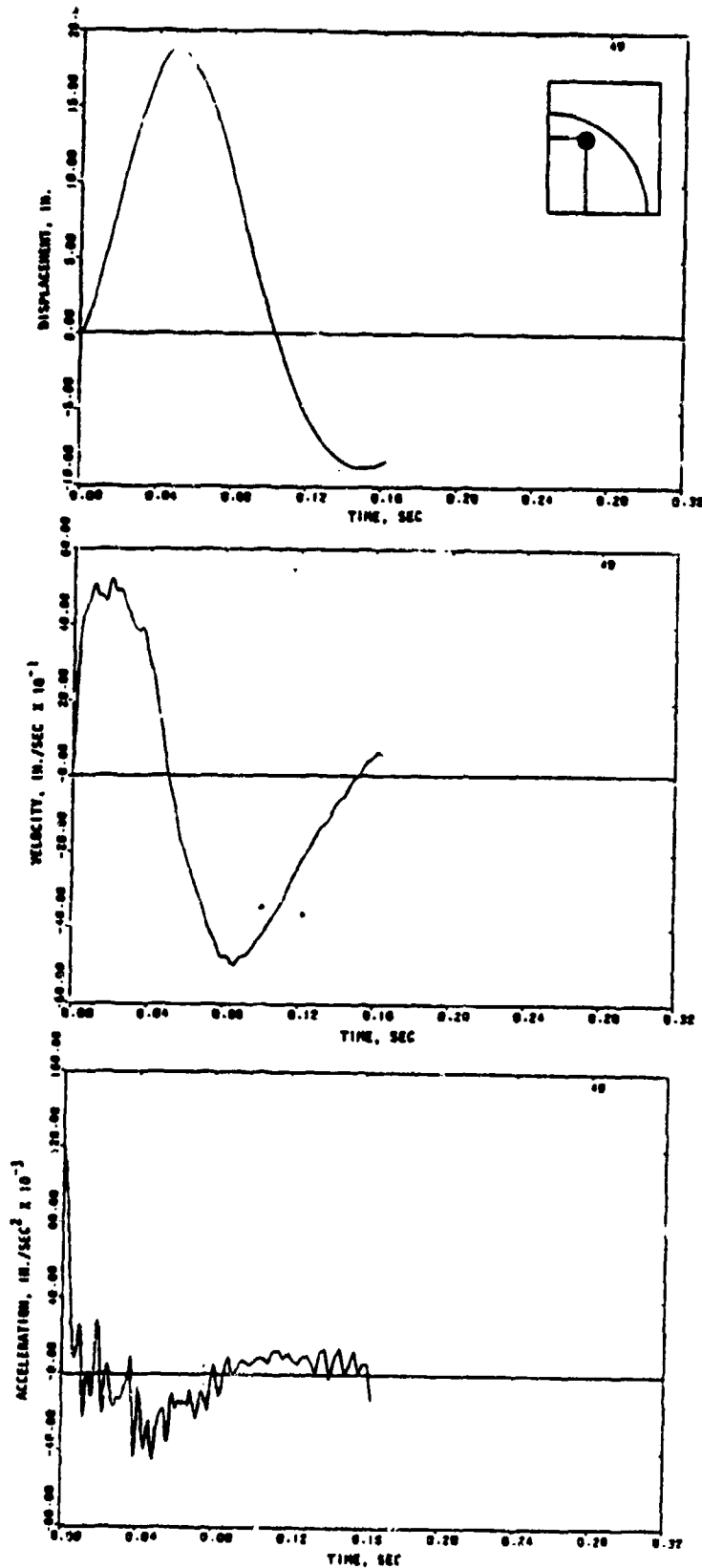
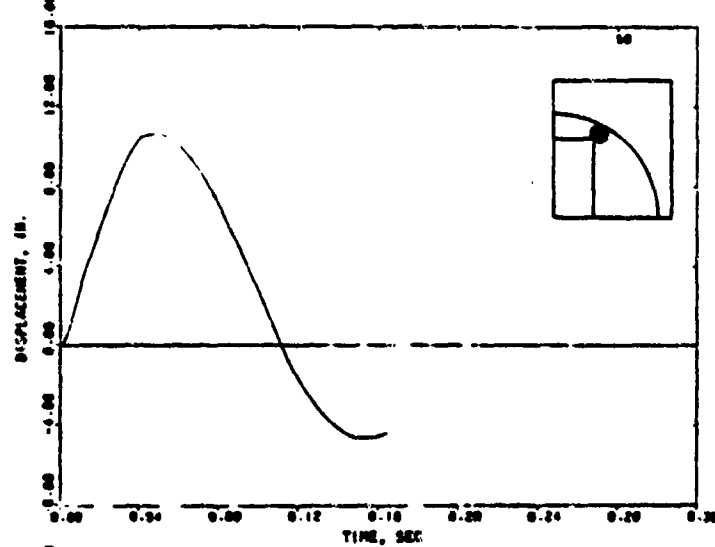
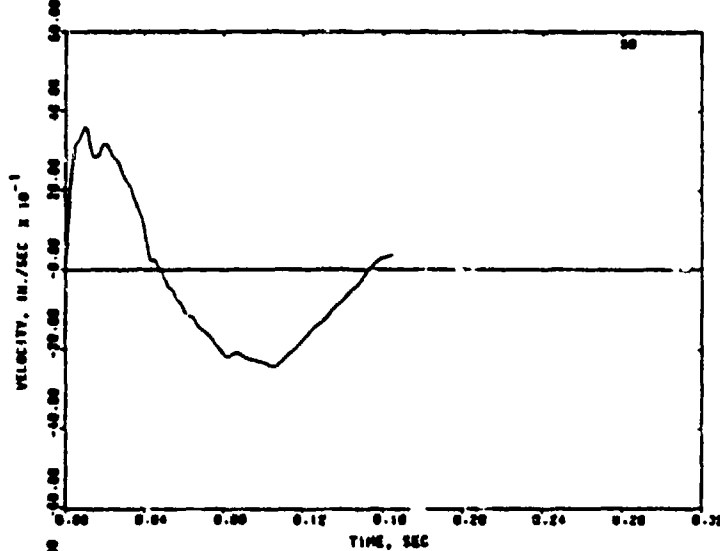


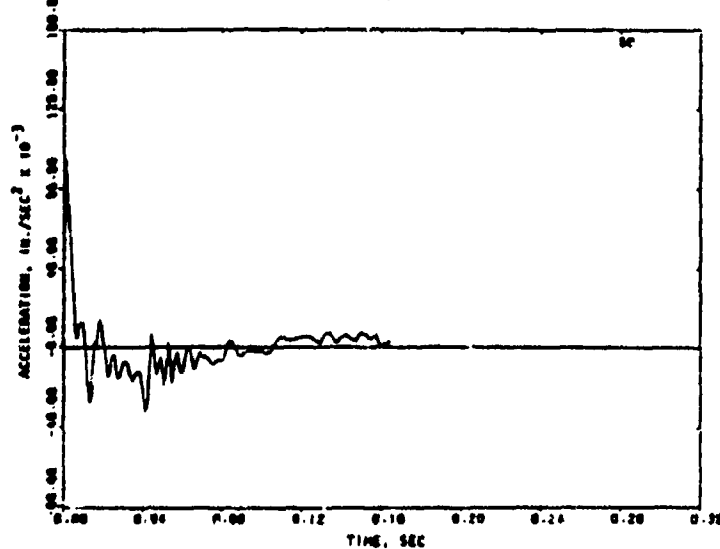
FIGURE 5-31. COMPUTED MOTION OF EAST HEADWALL (ESKIMO II) AT NODE 49



(a) Displacement



(b) Velocity

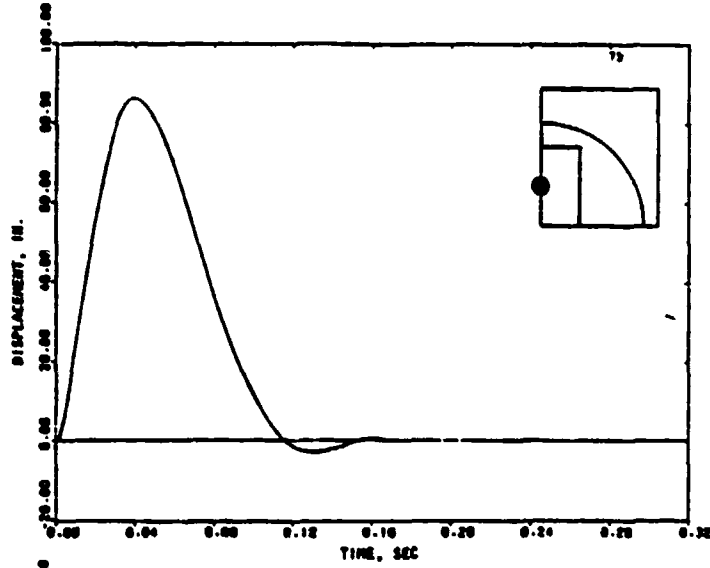


(c) Acceleration

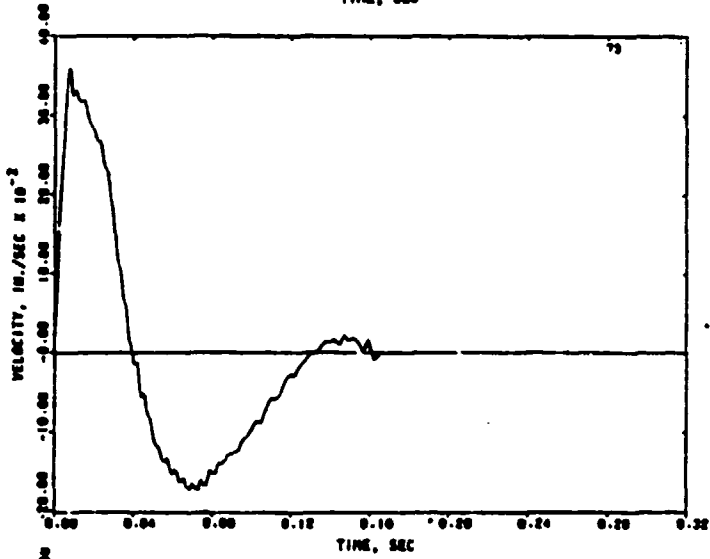
FIGURE 5-32. COMPUTED MOTION OF EAST HEADWALL (ESKIMO II) AT NODE 50



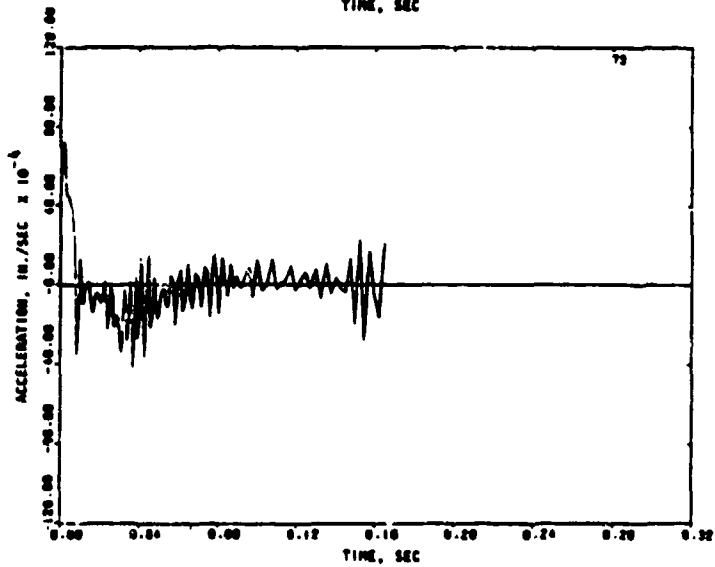
R-7556-1-4182



(a) Displacement



(b) Velocity

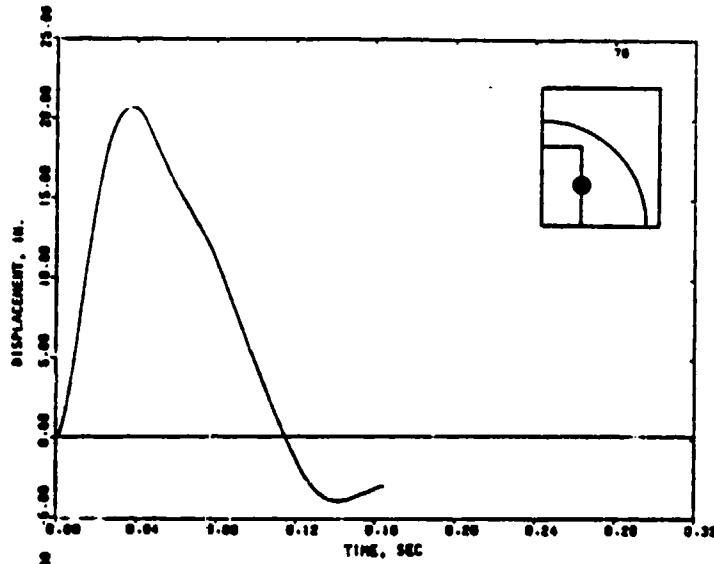


(c) Acceleration

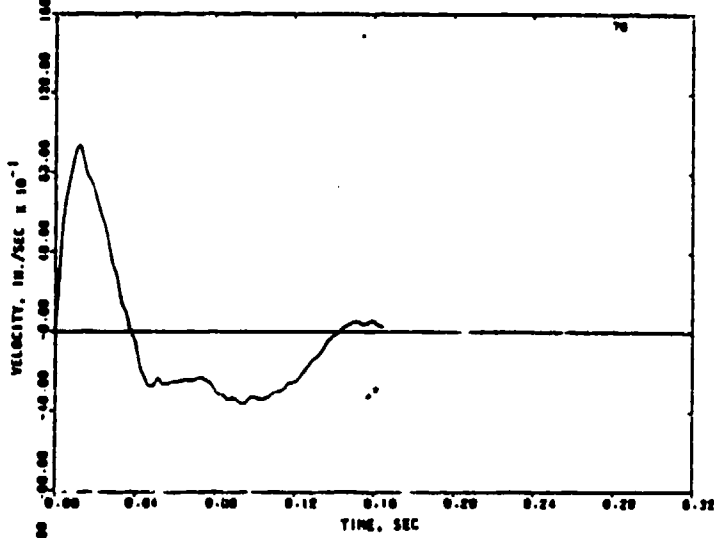
FIGURE 5-33. COMPUTED MOTION OF EAST HEADWALL (ESKIMO II) AT NODE 73



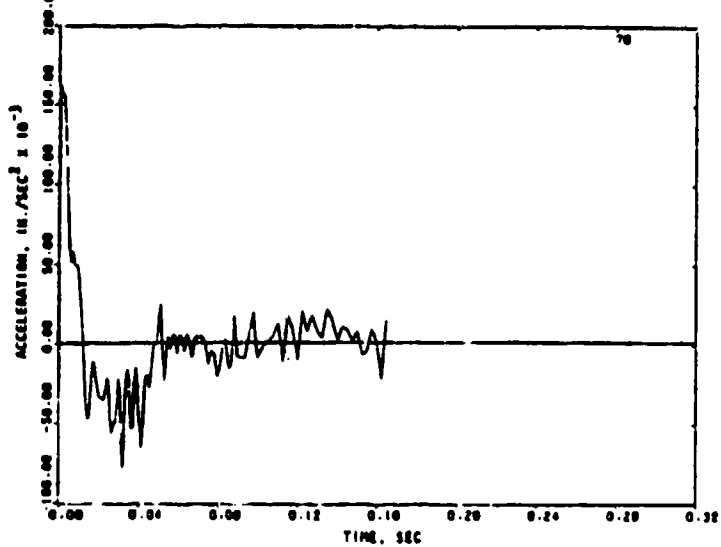
R-7356-1-4182



(a) Displacement



(b) Velocity

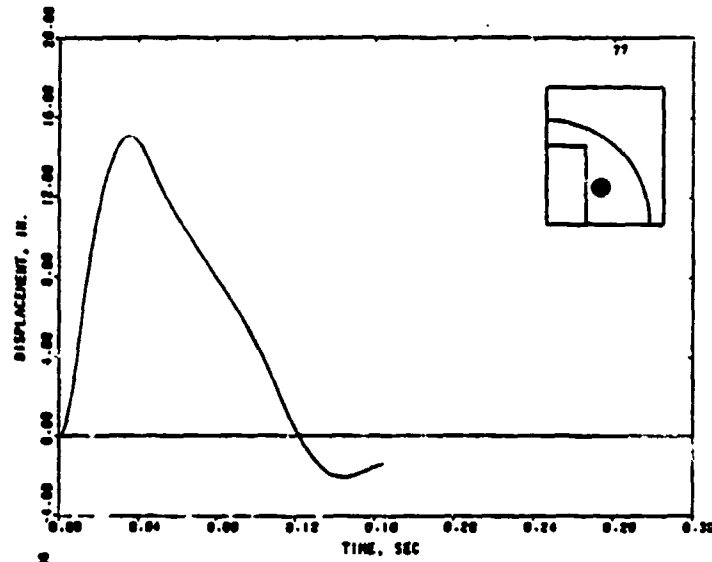


(c) Acceleration

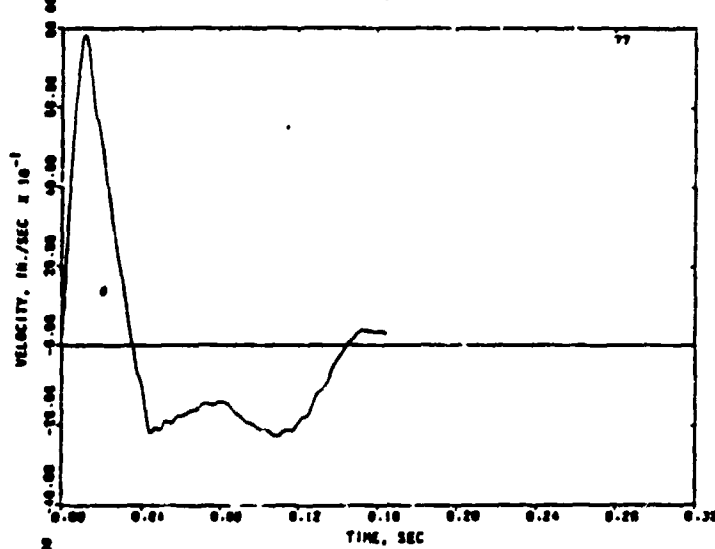
FIGURE 5-34. COMPUTED MOTION OF EAST HEADWALL (ESKIMO 11) AT NODE 76



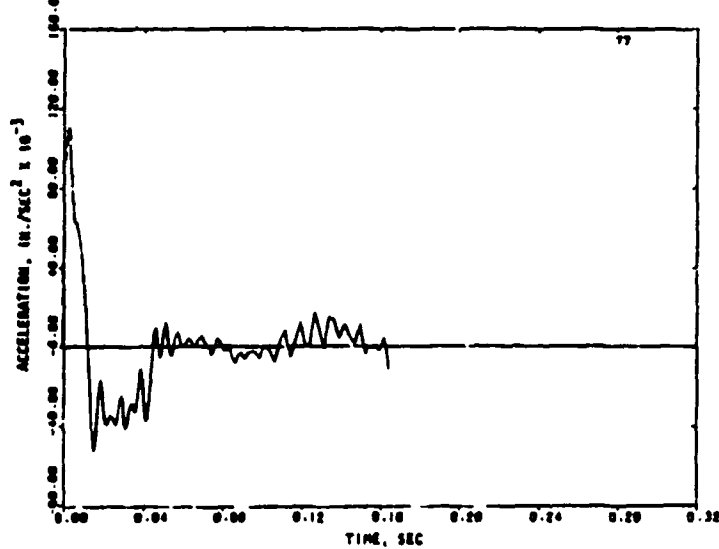
R-7556-1-4182



(a) Displacement



(b) Velocity

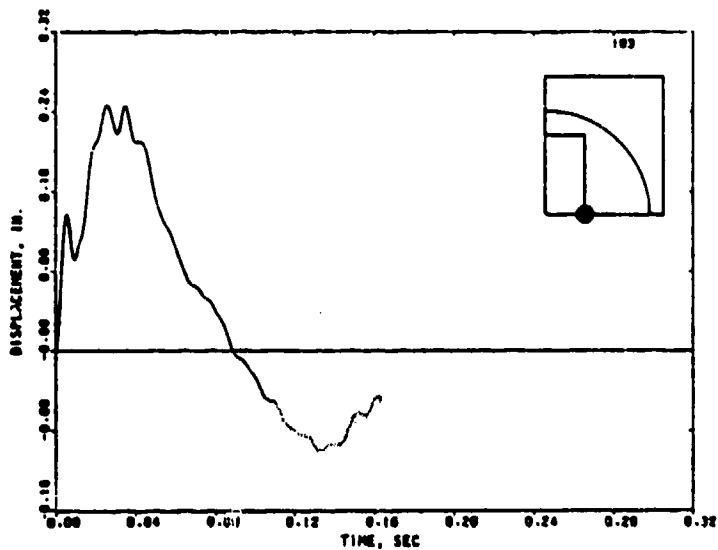


(c) Acceleration

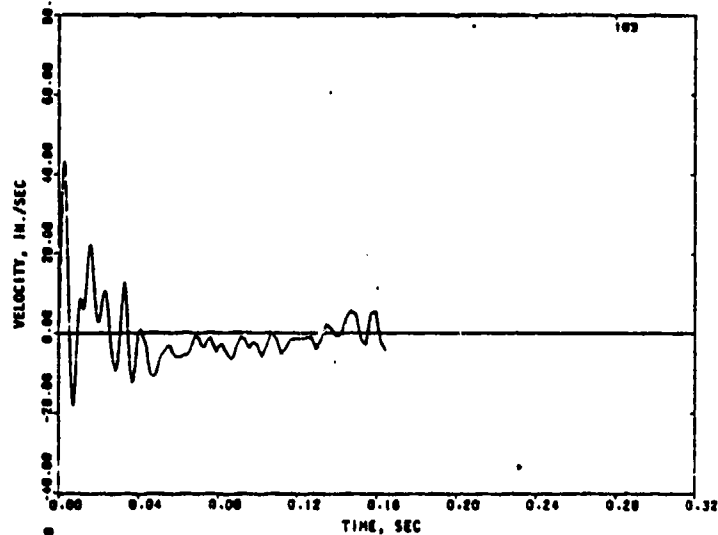
FIGURE 5-35. COMPUTED MOTION OF EAST HEADWALL (ESKIMO II) AT NODE 77



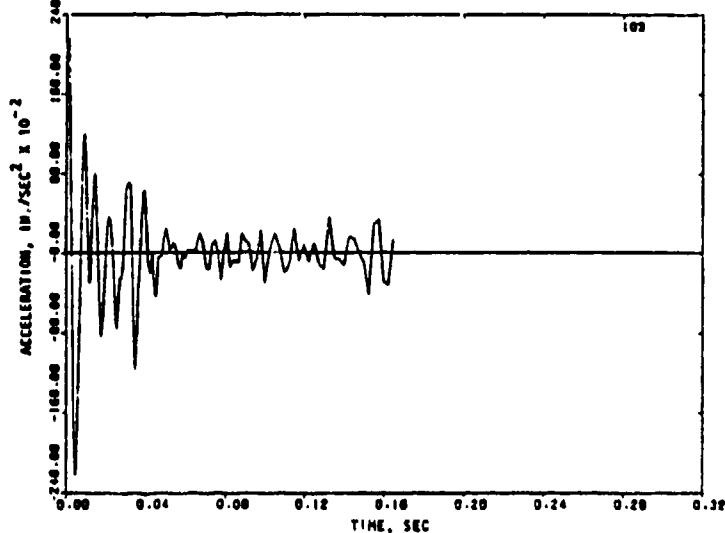
R-7556-1-4182



(a) Displacement



(b) Velocity



(c) Acceleration

FIGURE 5-36. COMPUTED MOTION OF EAST HEADWALL (ESKIMO II) AT NODE 103

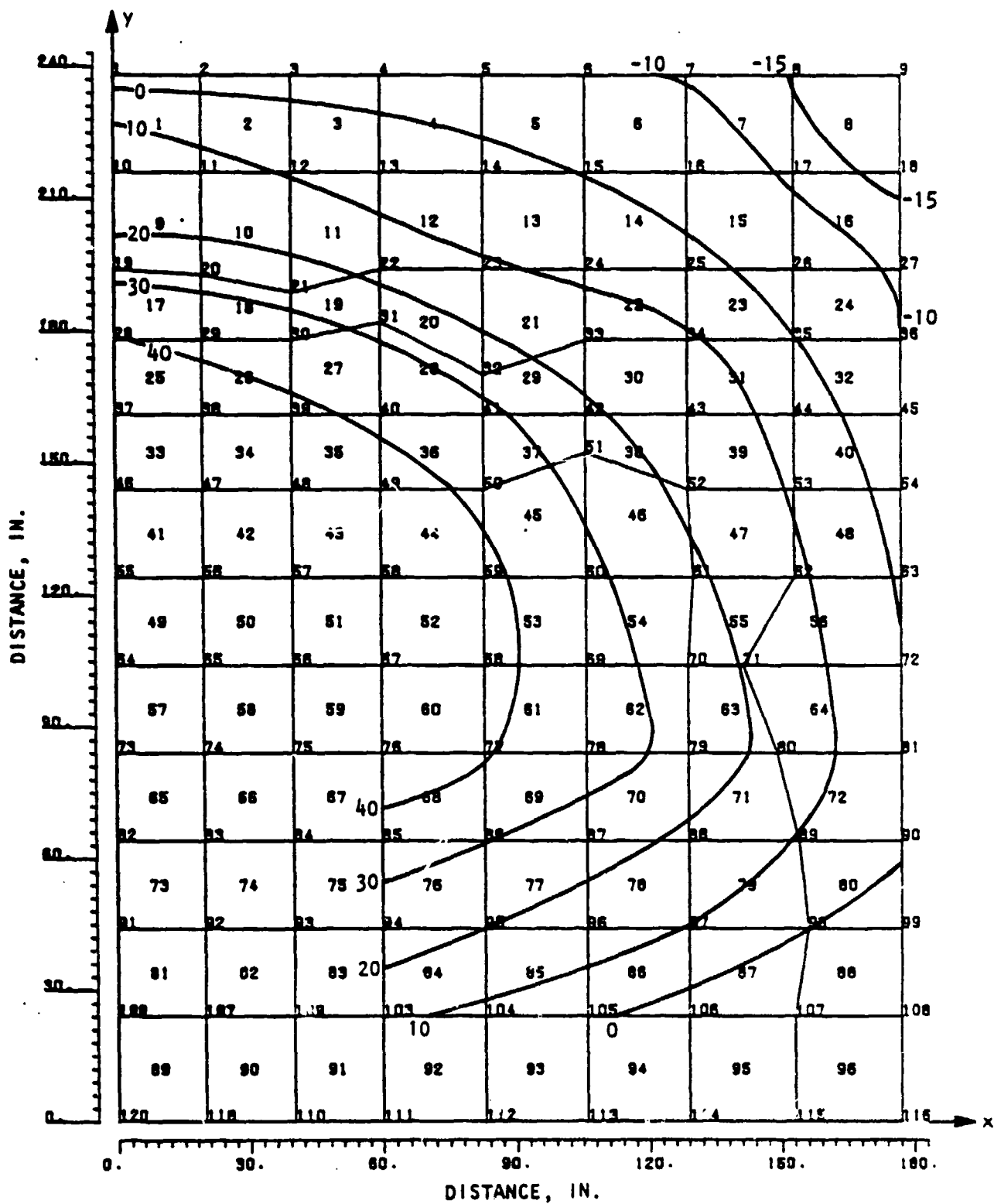


FIGURE 5-37. PERMANENT DISPLACEMENT CONTOURS OF EAST HEADWALL, ESKIMO II

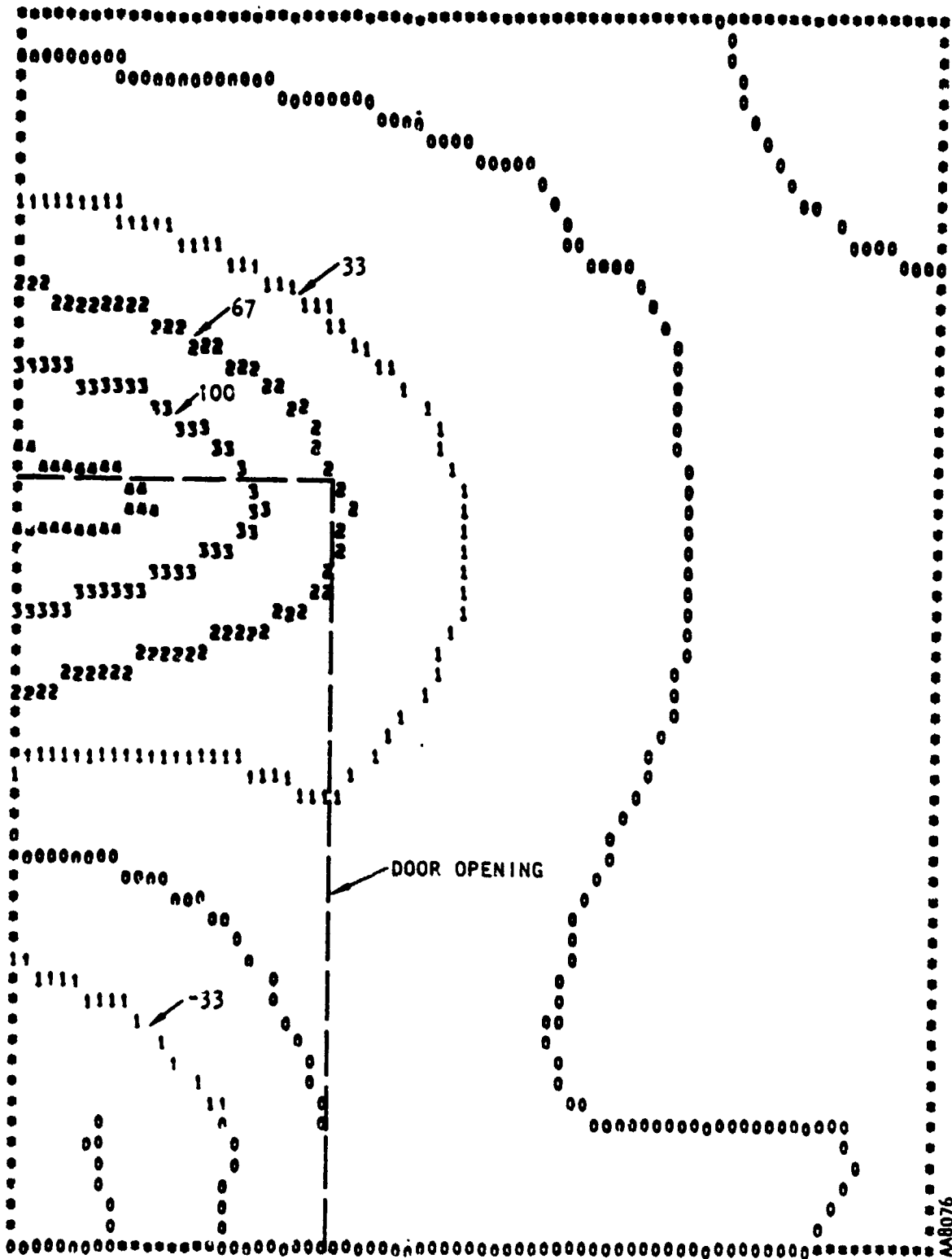


FIGURE 5-38. COMPUTED DISPLACEMENT CONTOURS OF EAST HEADWALL AT  $t = 145$  MSEC

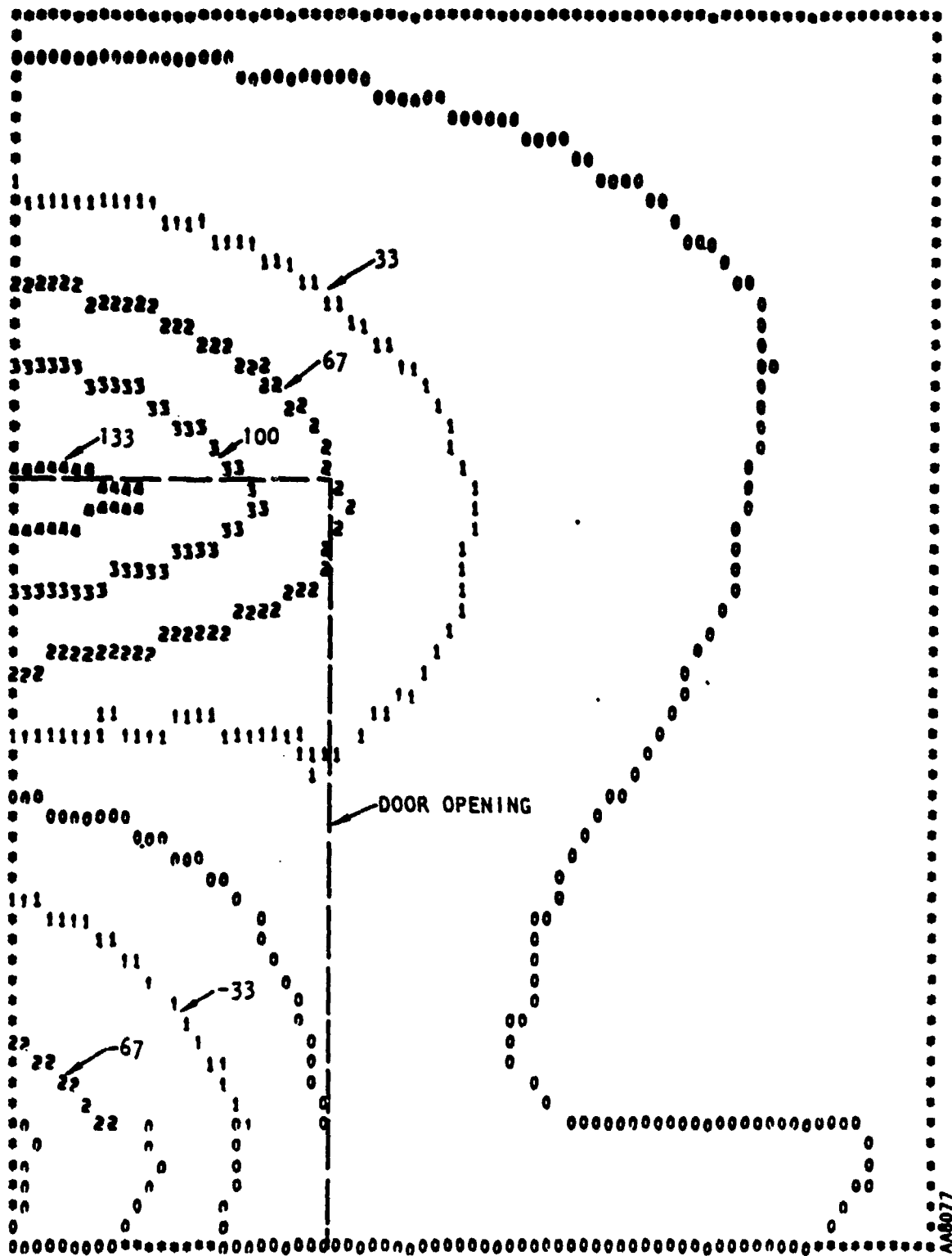
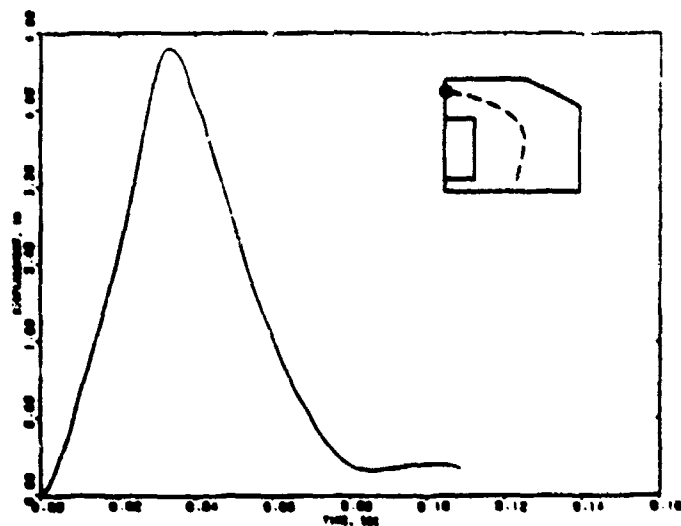


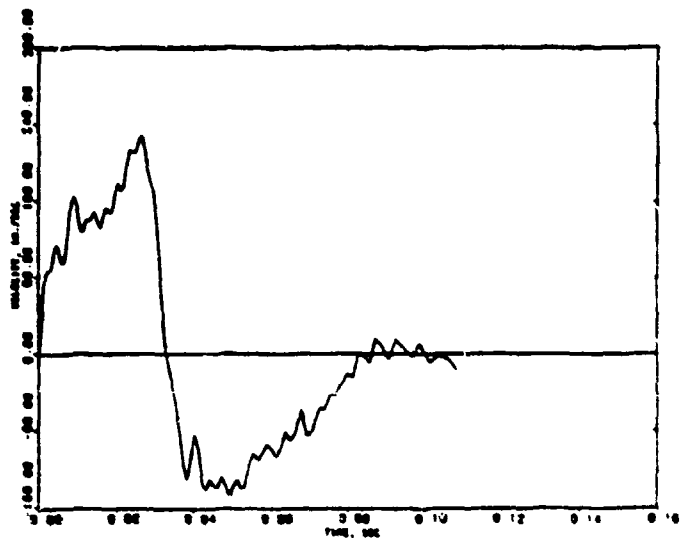
FIGURE 5-39. COMPUTED DISPLACEMENT CONTOURS OF EAST HEADWALL AT  $t = 157$  MSEC



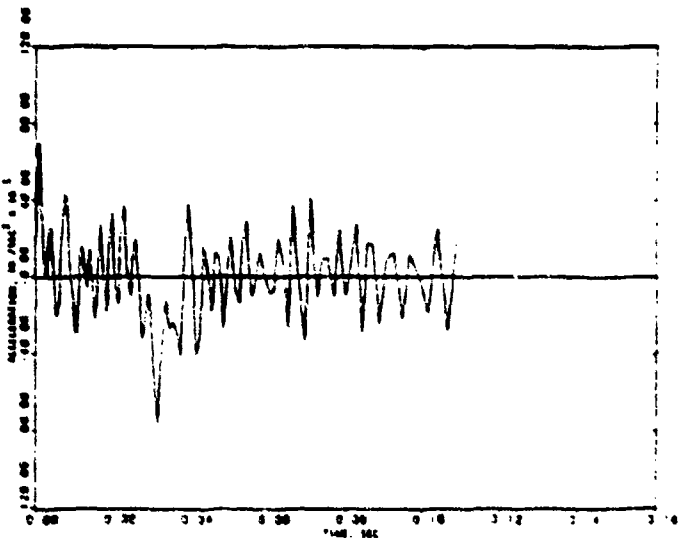
R-7556-1-4182



(a) Displacement



(b) Velocity

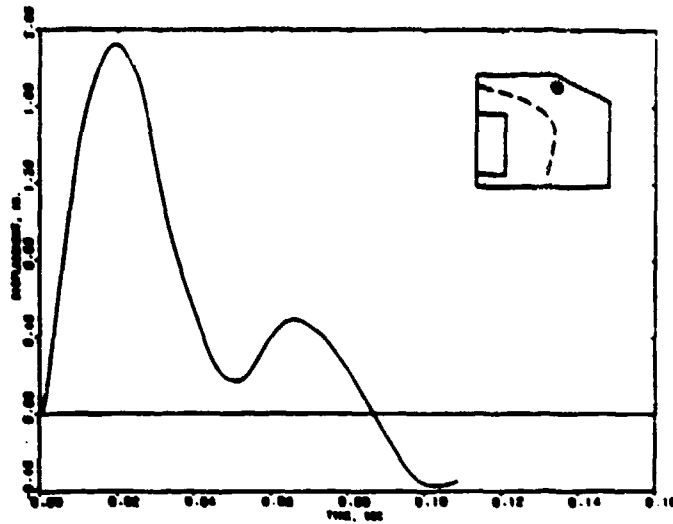


(c) Acceleration

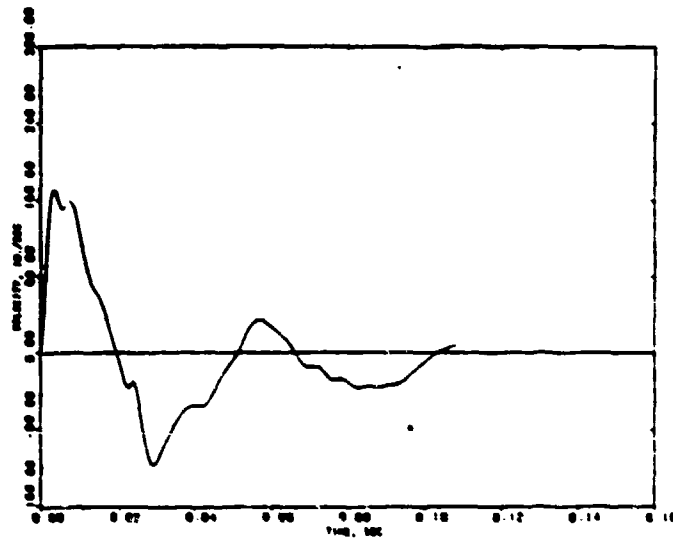
FIGURE 5-40. COMPUTED MOTION OF NORTHEAST IGLOO (ESKIMO II) AT NODE 9



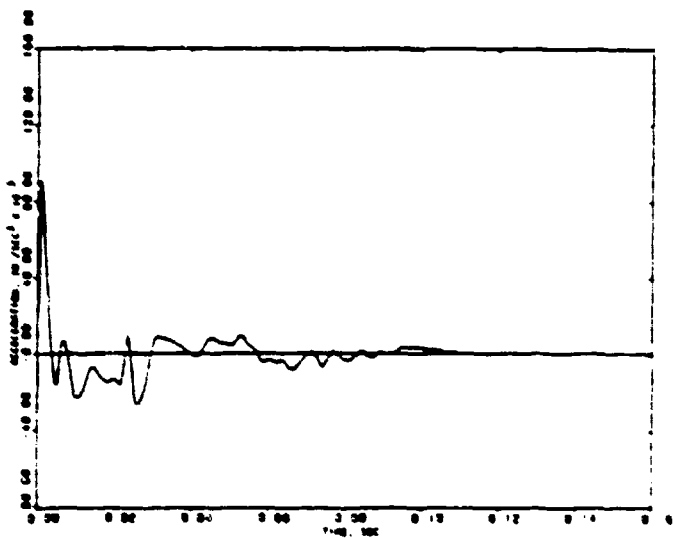
R-7556-1-4182



(a) Displacement



(b) Velocity

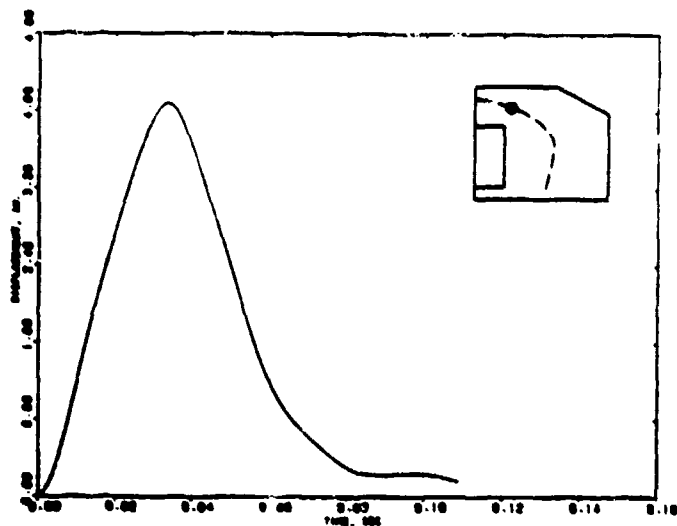


(c) Acceleration

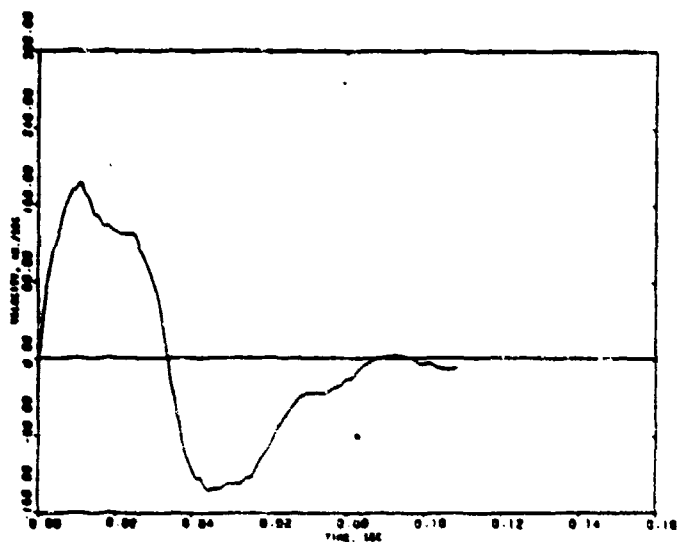
FIGURE 5-41. COMPUTED MOTION OF NORTHEAST IGLOO (ESKIMO 11) AT NODE 16



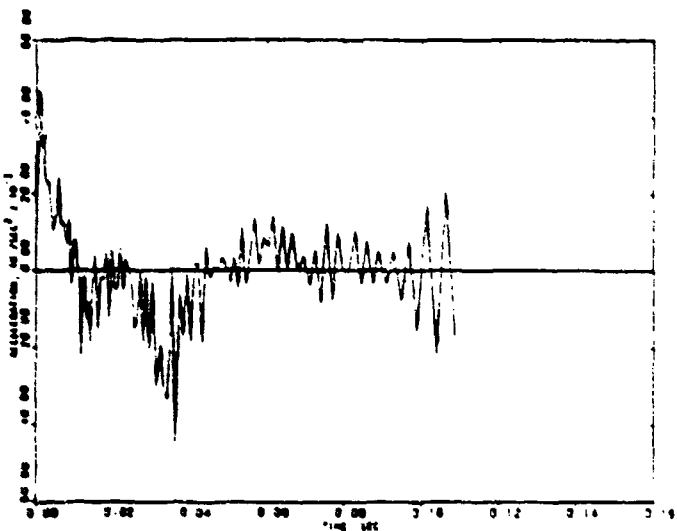
R-7556-1-4182



(a) Displacement



(b) Velocity

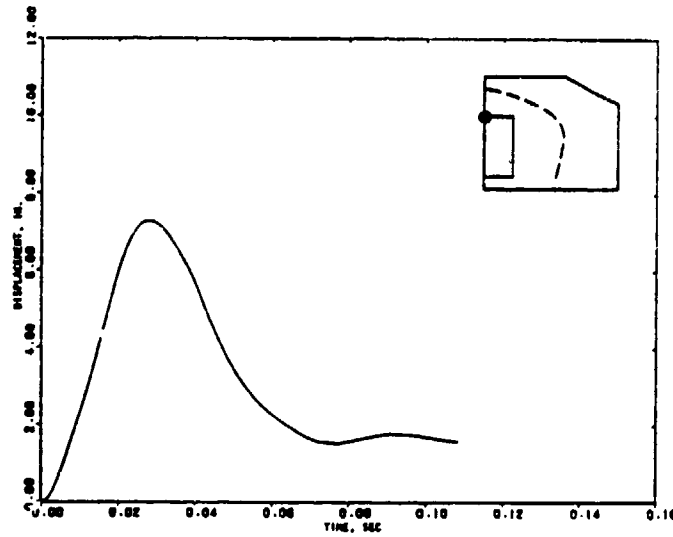


(c) Acceleration

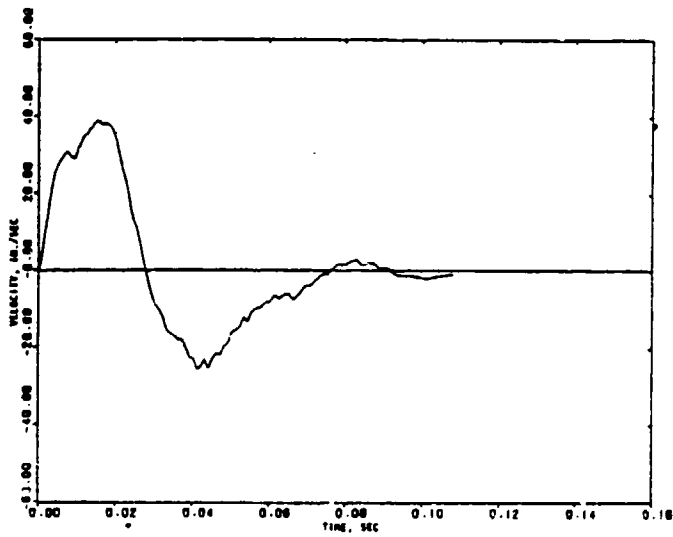
FIGURE 5-42. COMPUTED MOTION OF NORTHEAST IGLOO (ESKIMO 11) AT NODE 22



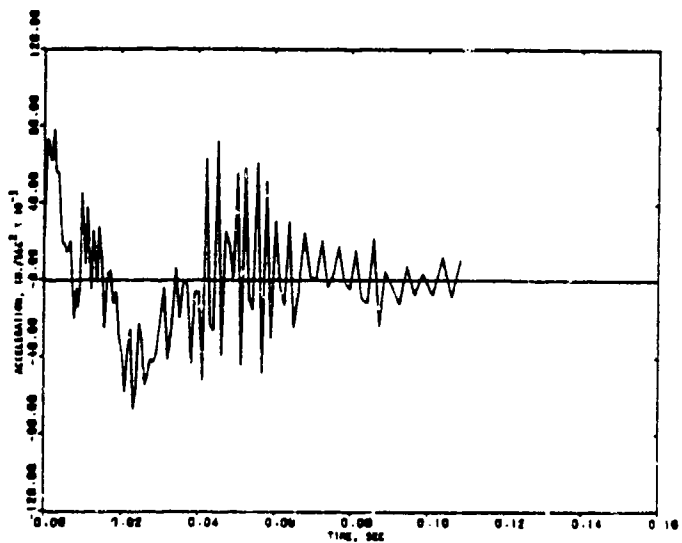
R-7556-1-4182



(a) Displacement



(b) Velocity

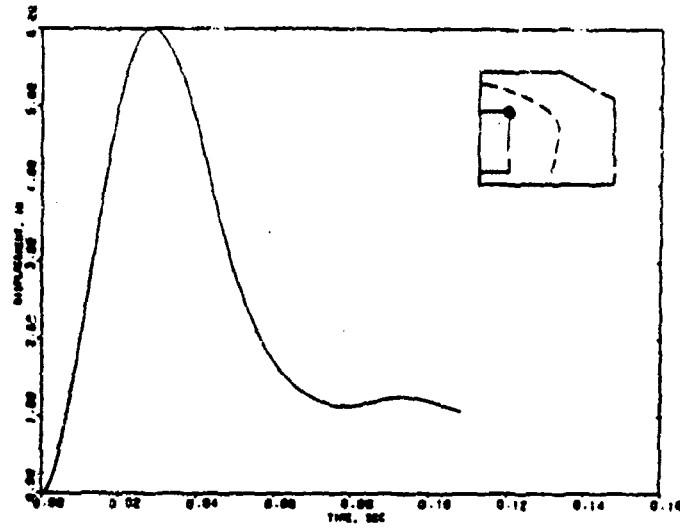


(c) Acceleration

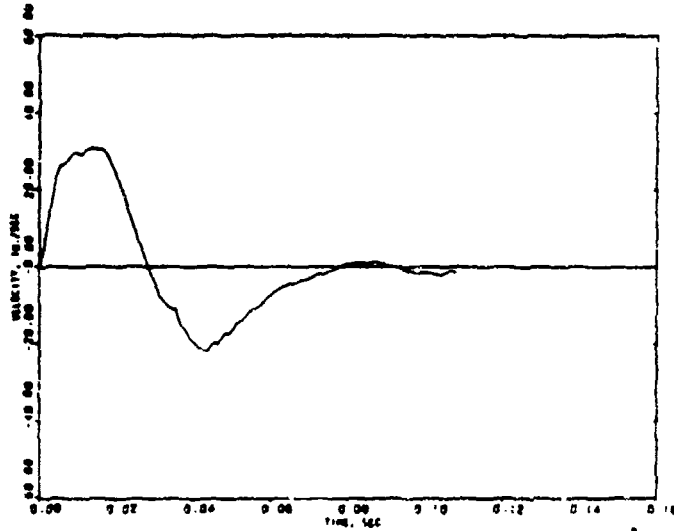
FIGURE 5-43. COMPUTED MOTION OF NORTHEAST IGL00 (ESKIMO 11) AT NODE 39



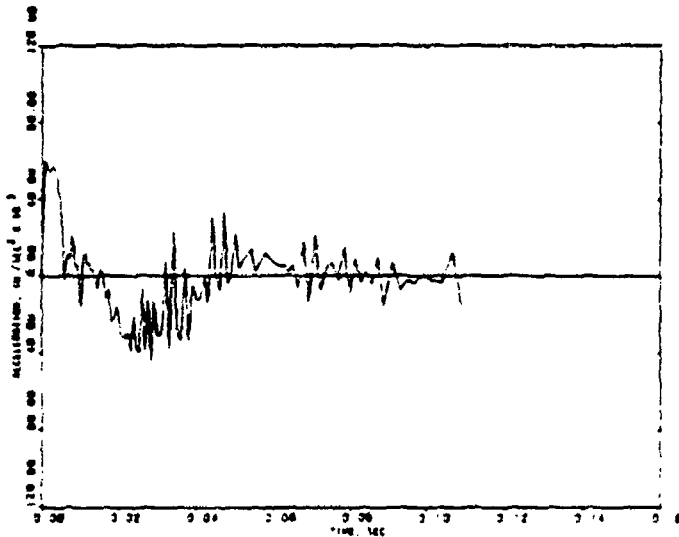
R-7556-1-4182



(a) Displacement



(b) Velocity

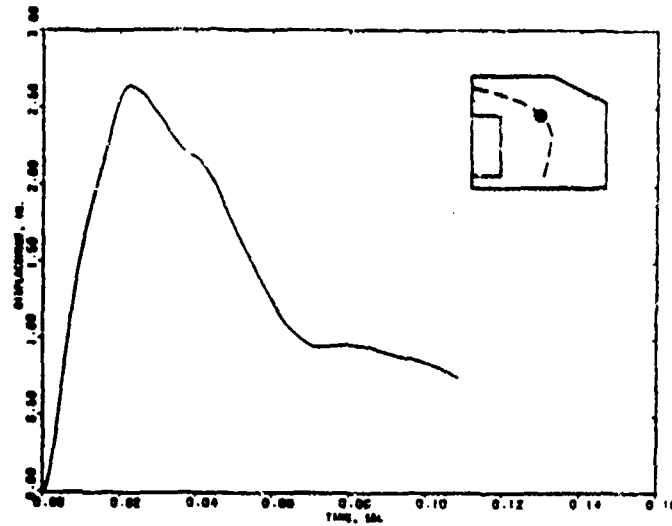


(c) Acceleration

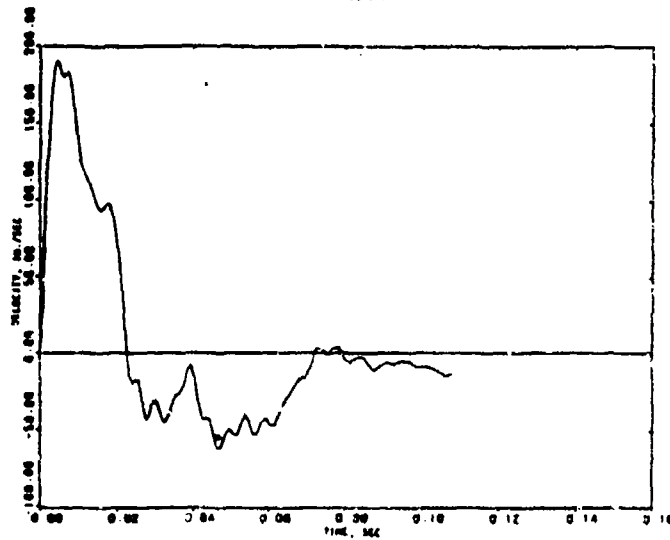
FIGURE 5-44. COMPUTED MOTION OF NORTHEAST IGLOO (ESKIMO 11) AT NODE 42



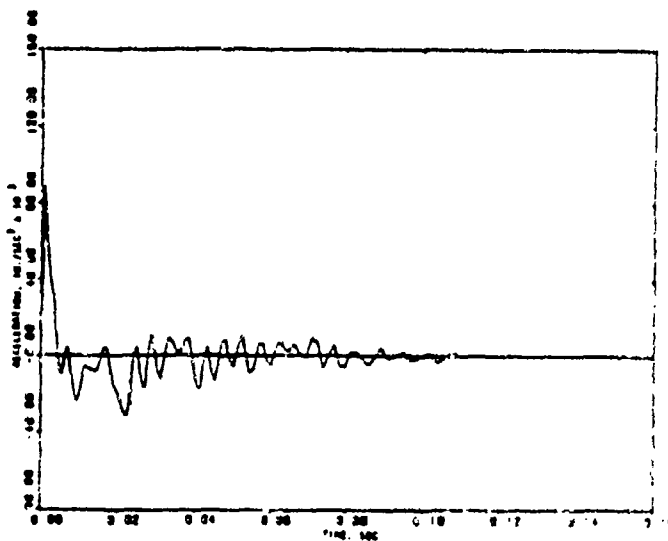
R-7556-1-4182



(a) Displacement



(b) Velocity

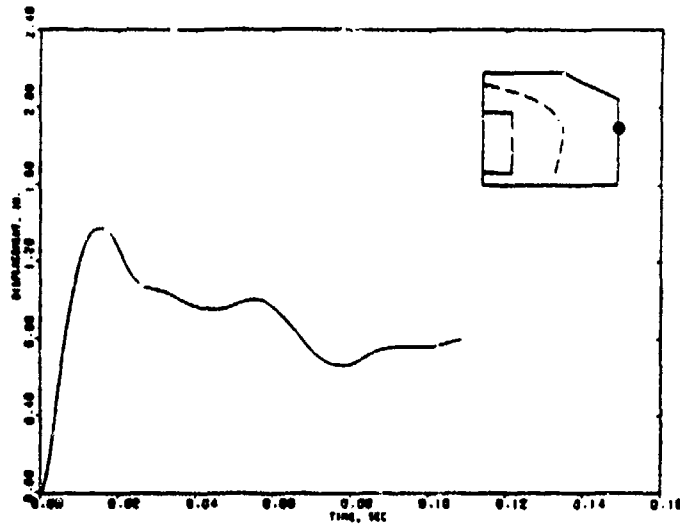


(c) Acceleration

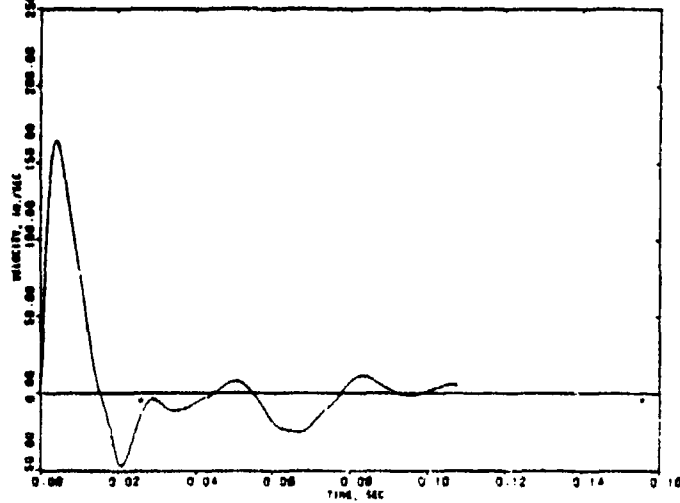
FIGURE 5-45. COMPUTED MOTION OF NORTHEAST IGLCO (ESKIMO II) AT NODE 45



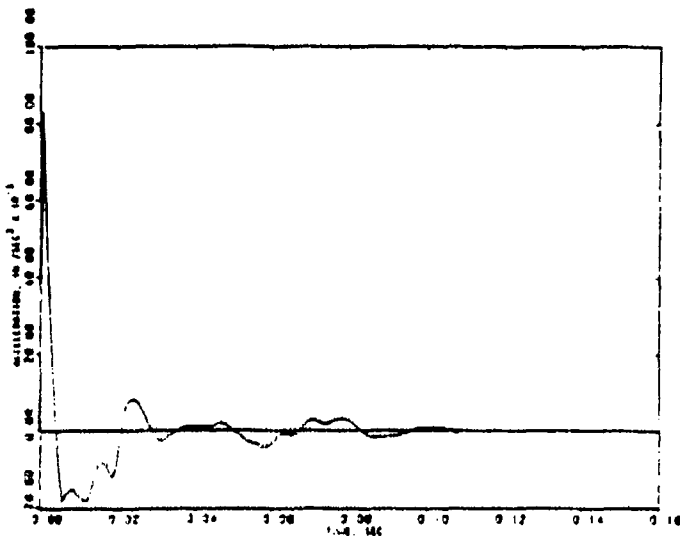
R-7556-1-4182



(a) Displacement



(b) Velocity

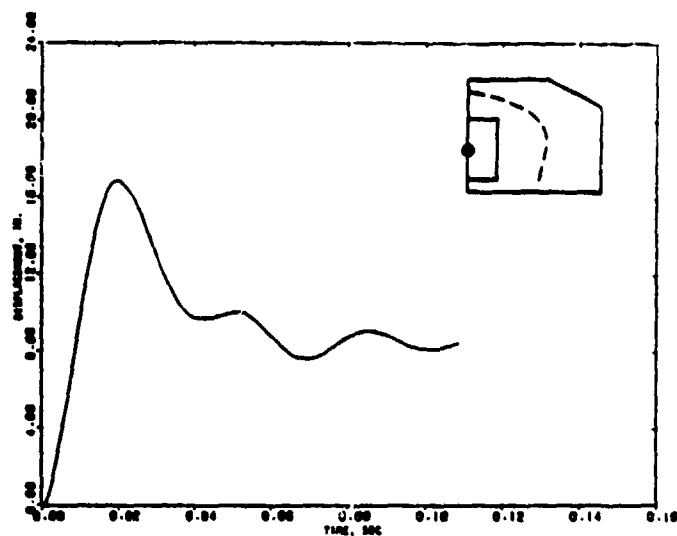


(c) Acceleration

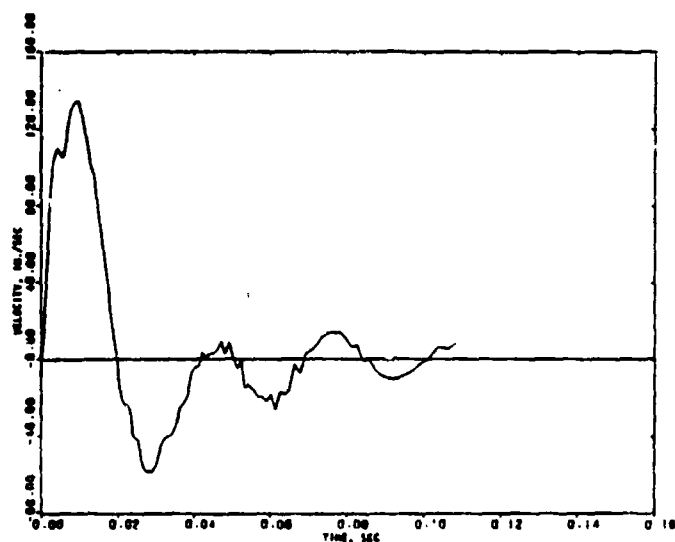
FIGURE 5-46. COMPUTED MOTION OF NORTHEAST IGLOO (ESKIMO 11) AT NODE 60



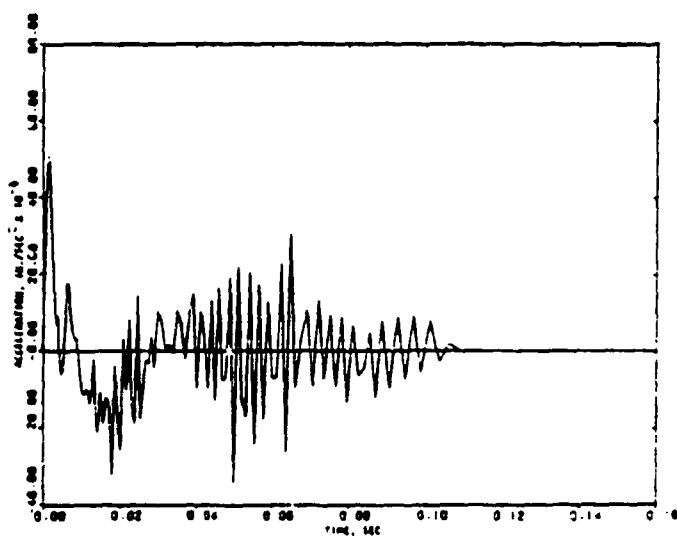
R-7556-1-4182



(a) Displacement



(b) Velocity

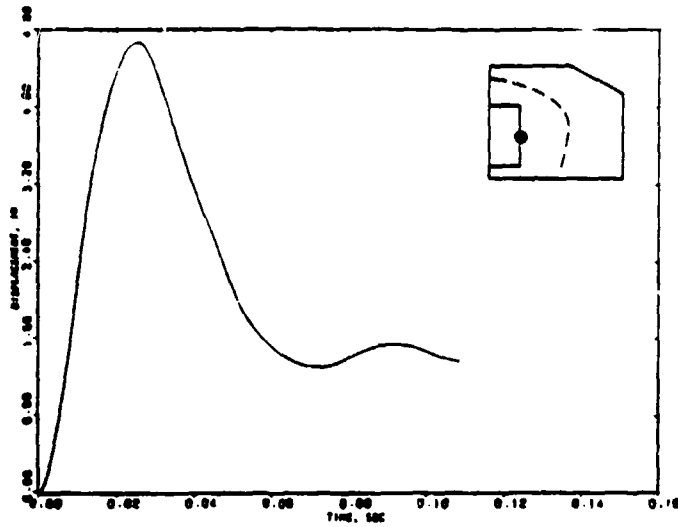


(c) Acceleration

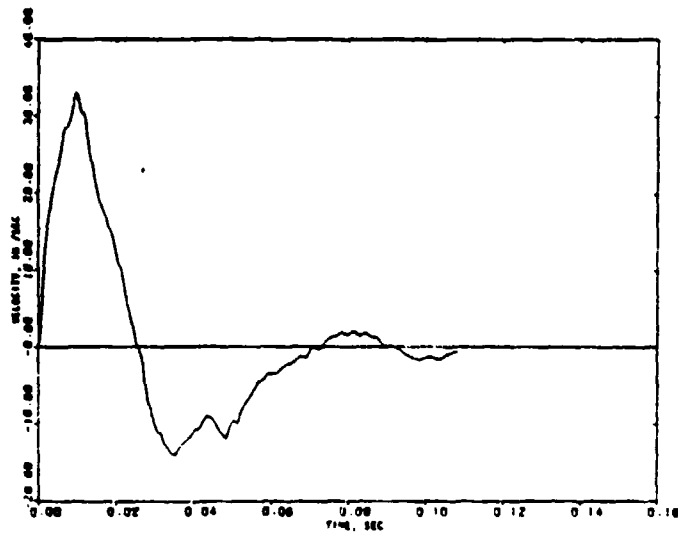
FIGURE 5-47. COMPUTED MOTION OF NORTHEAST IGL00 (ESKIMO 11) AT NODE 72



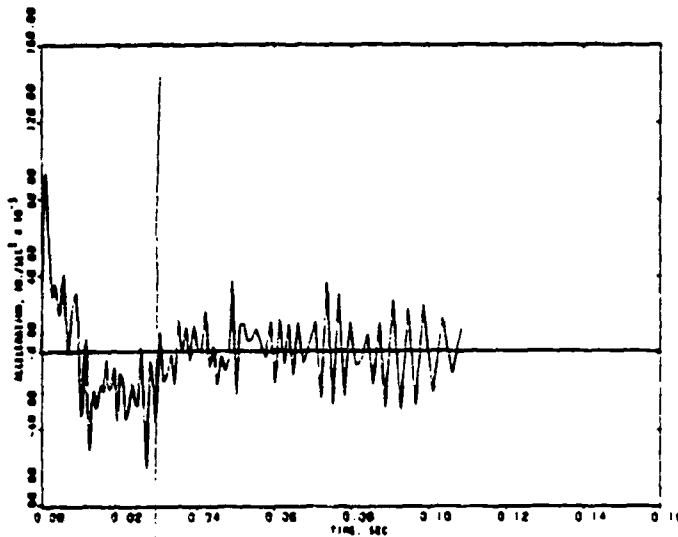
R-7556-1-4182



(a) Displacement

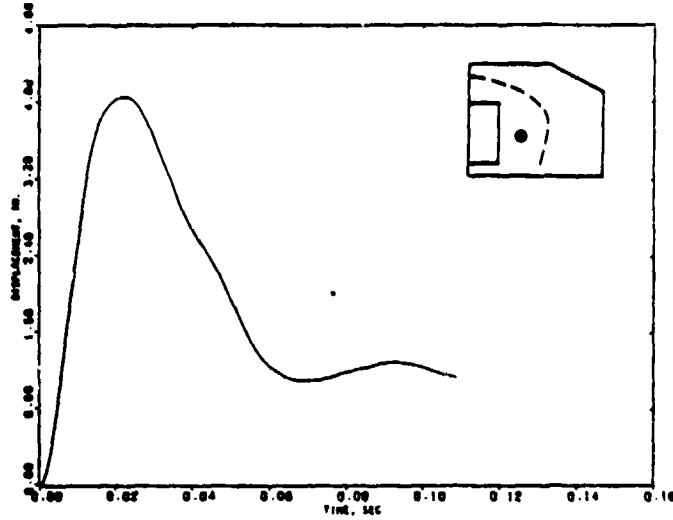


(b) Velocity

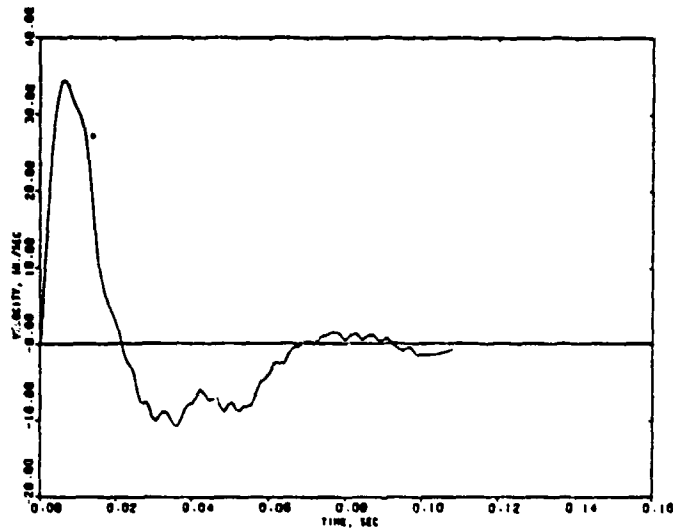


(c) Acceleration

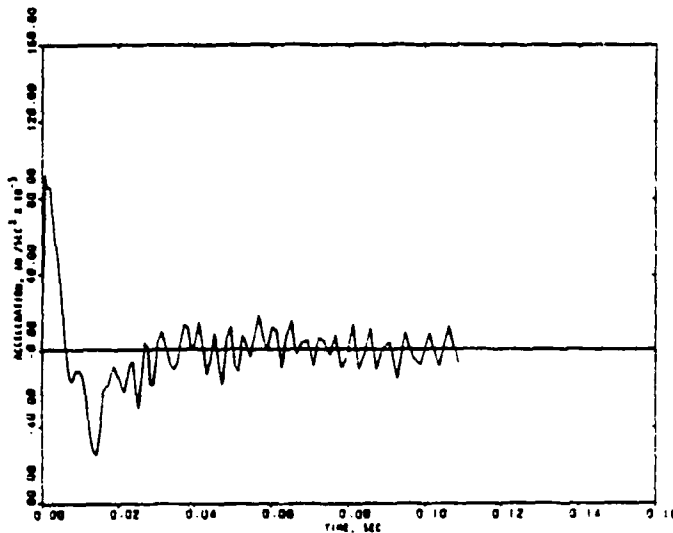
FIGURE 5-48. COMPUTED MOTION OF NORTHEAST IGLOO (ESKIMO II) AT NODE 75



(a) Displacement



(b) Velocity

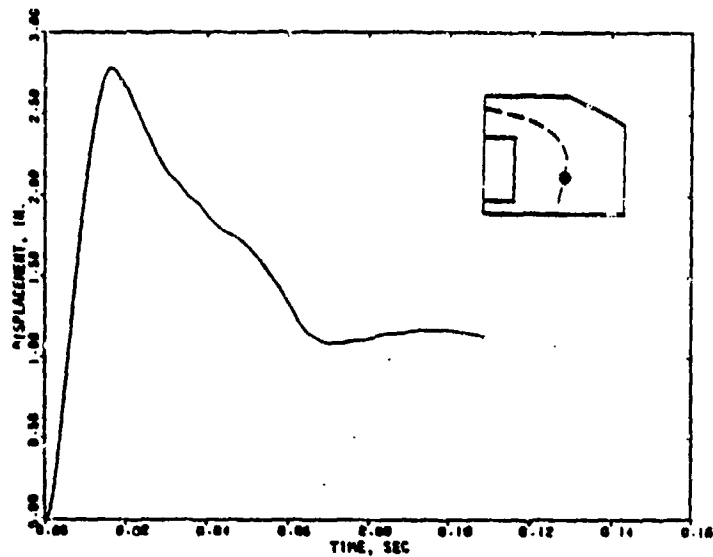


(c) Acceleration

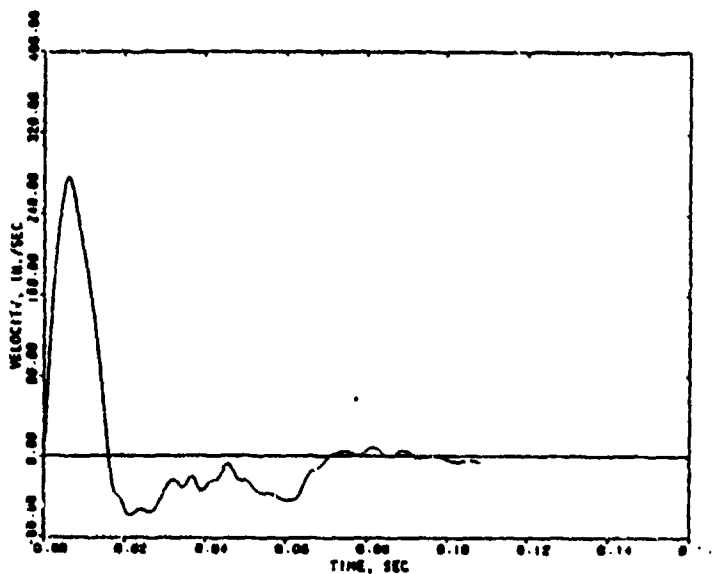
FIGURE 5-49. COMPUTED MOTION OF NORTHEAST IGLOO (ESKIMO 11) AT NODE 77



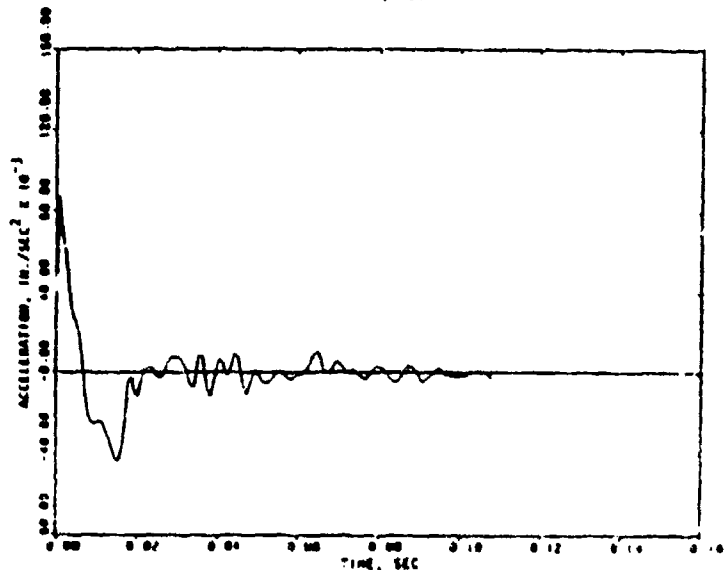
R-7556-1-4182



(a) Displacement

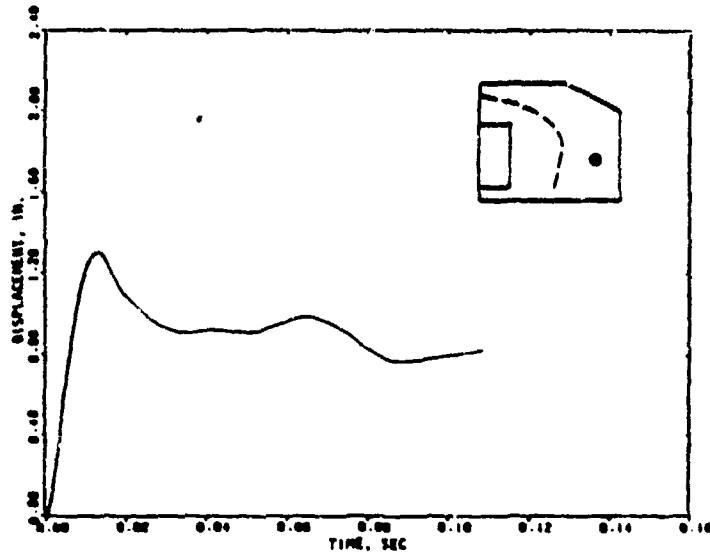


(b) Velocity

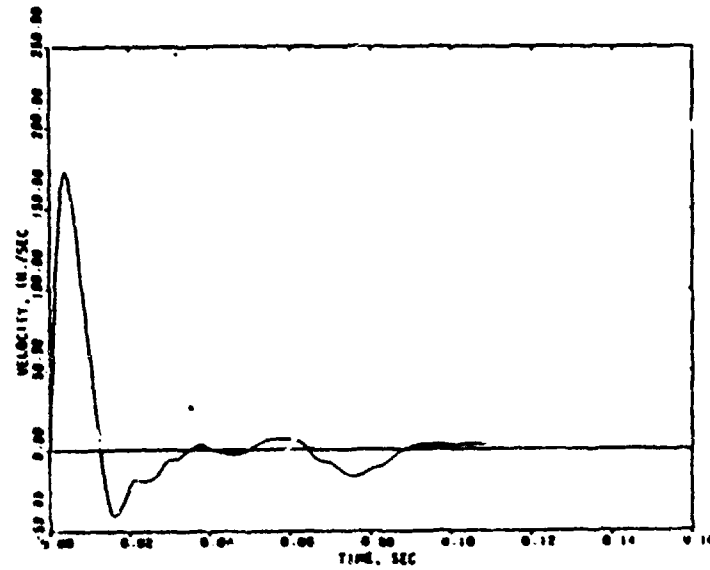


(c) Acceleration

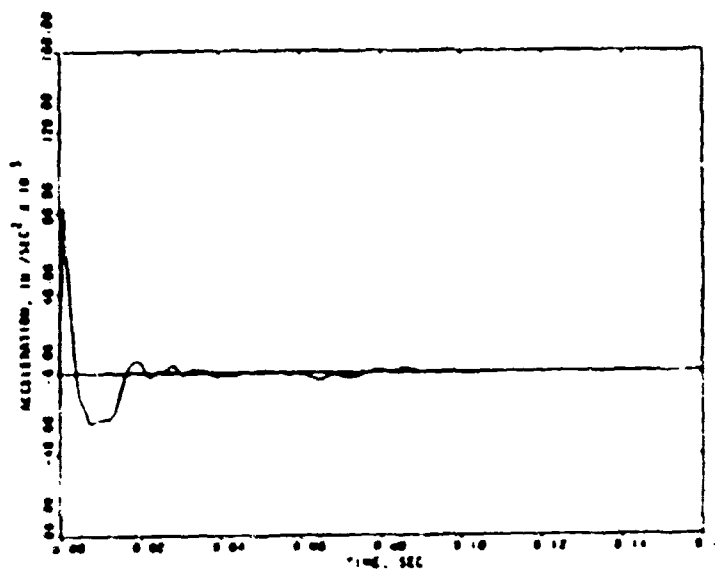
FIGURE 5-50. COMPUTED MOTION OF NORTHEAST IGLOO (ESKIMO 11) AT NODE 79



(a) Displacement



(b) Velocity



(c) Acceleration

FIGURE 5-51. COMPUTED MOTION OF NORTHEAST IGLOO (ESKIMO II) AT NODE 3'

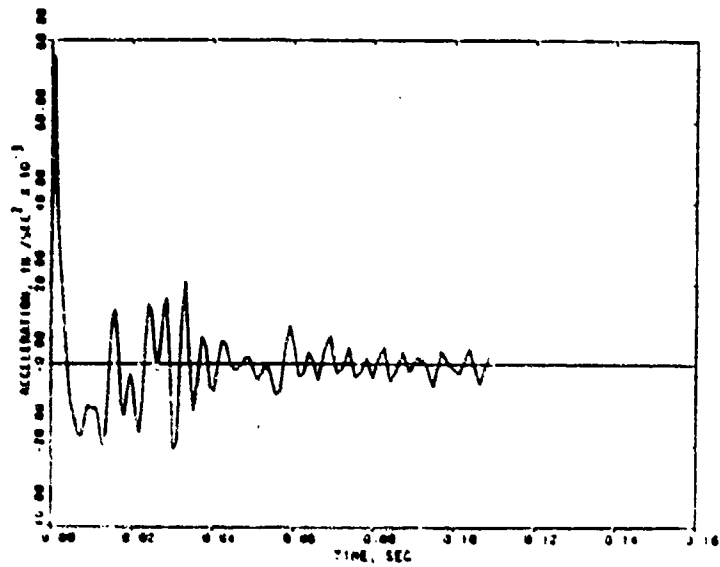
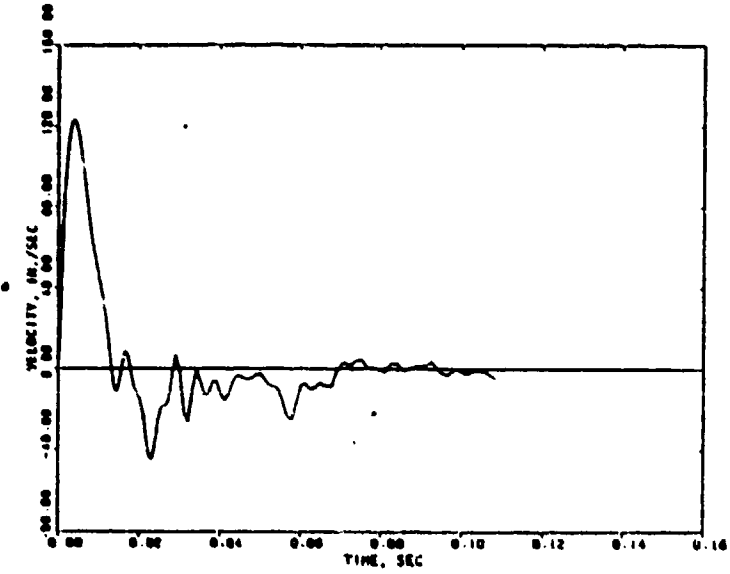
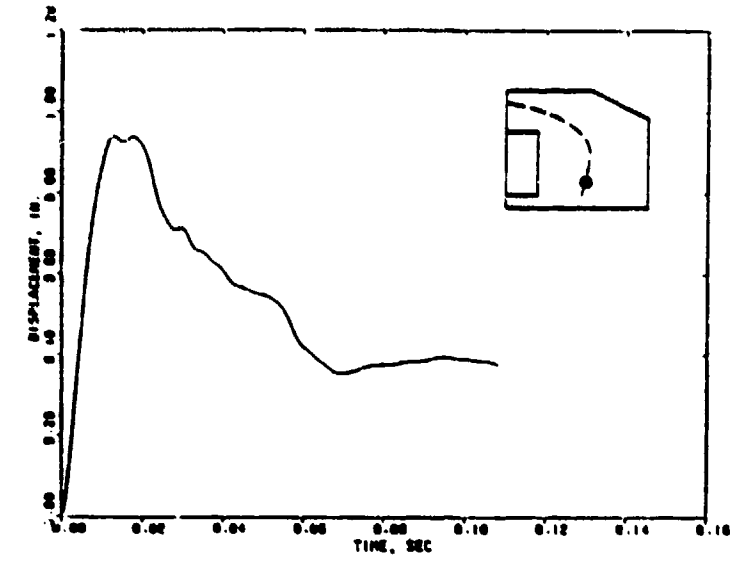
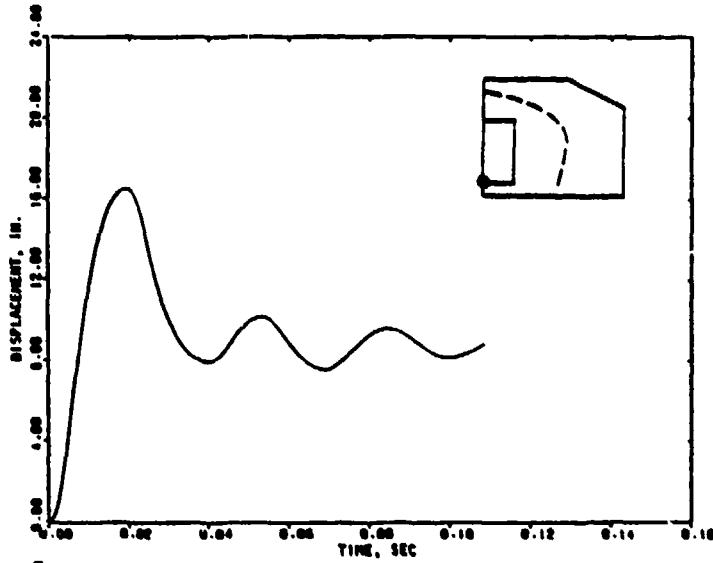
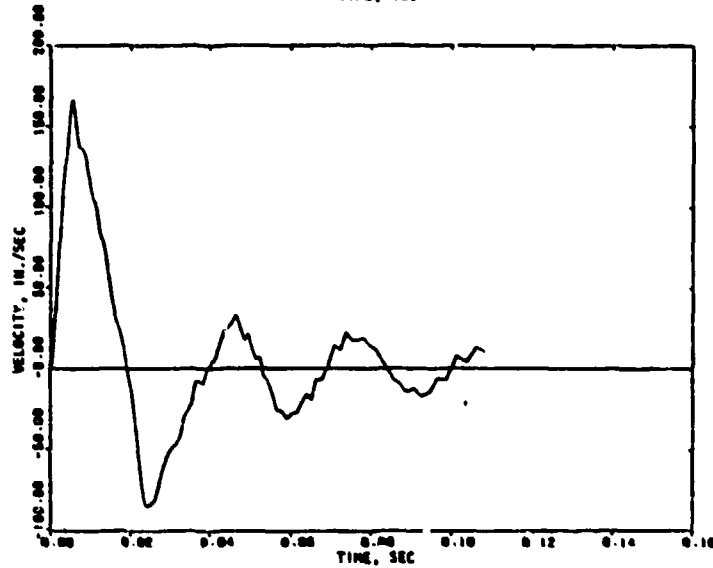


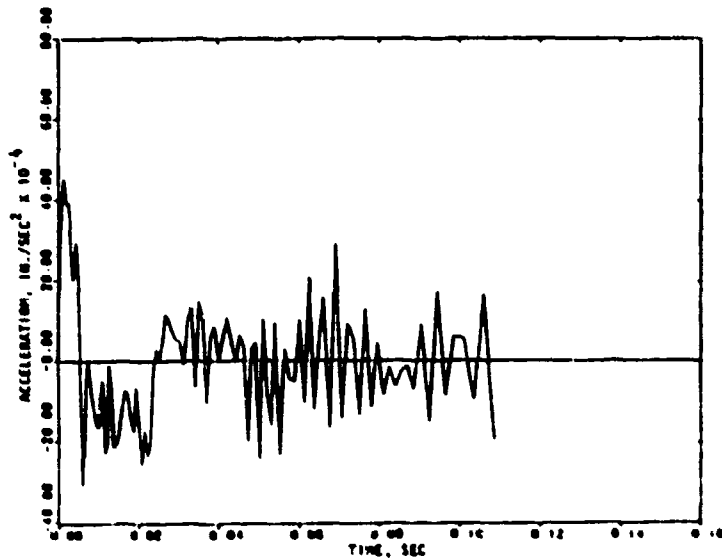
FIGURE 5-52. COMPUTED MOTION OF NORTHEAST IGLOO (ESKIMO II) AT NODE 101



(a) Displacement



(b) Velocity

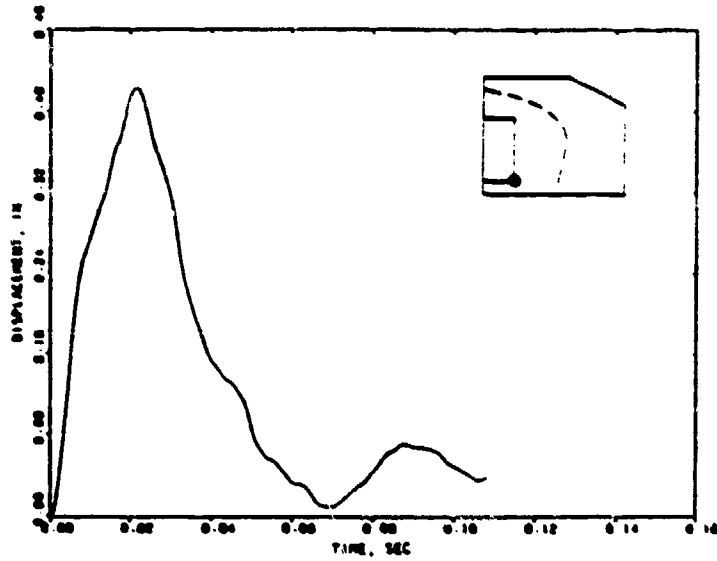


(c) Acceleration

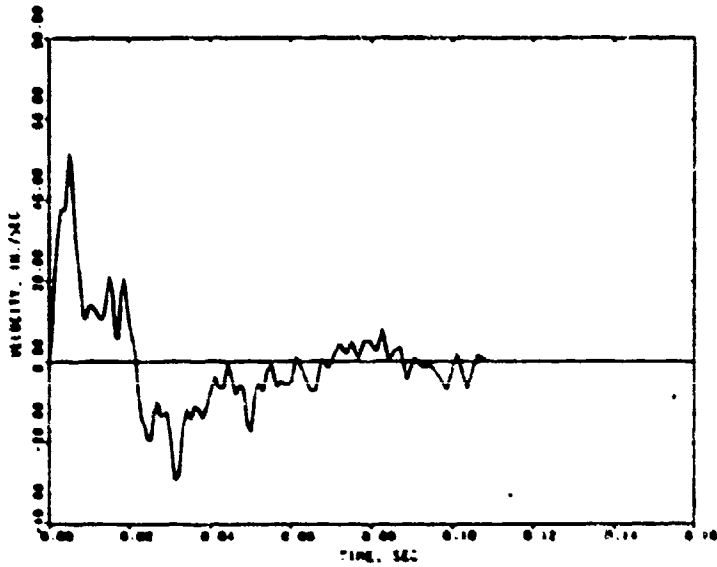
FIGURE 5-53. COMPUTED MOTION OF NORTHEAST IGLOG (ESKIMO II) AT NODE 105



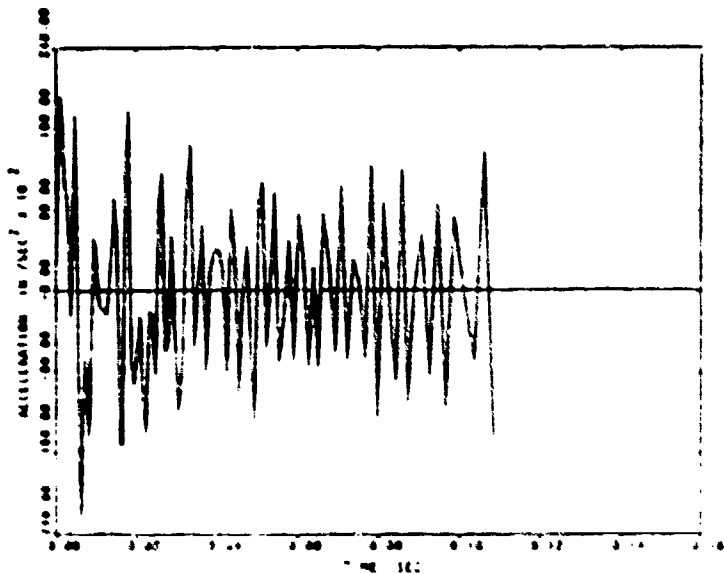
R-7556-1-4182



(a) Displacement



(b) Velocity

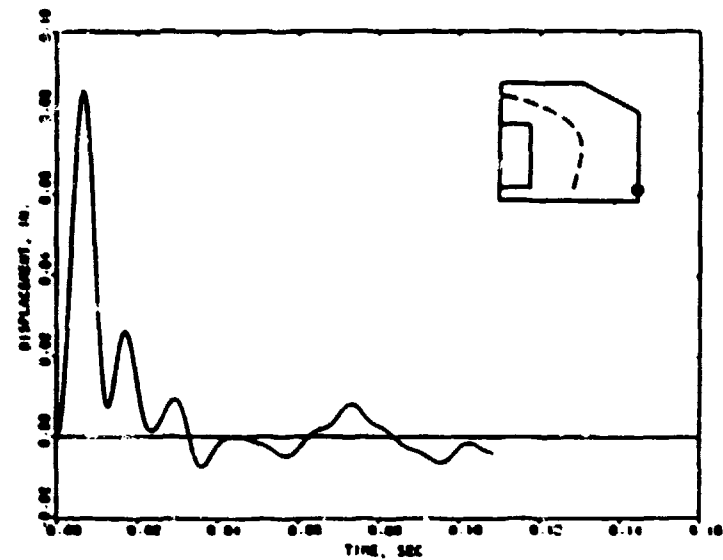


(c) Acceleration

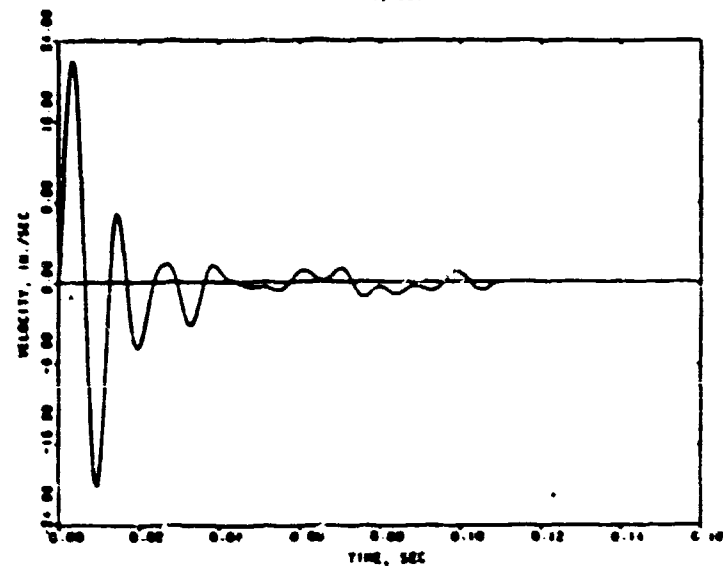
FIGURE 5-5-4. COMPUTED MOTION OF NORTHEAST IGLOO ESKIMO (1) AT NODE 100



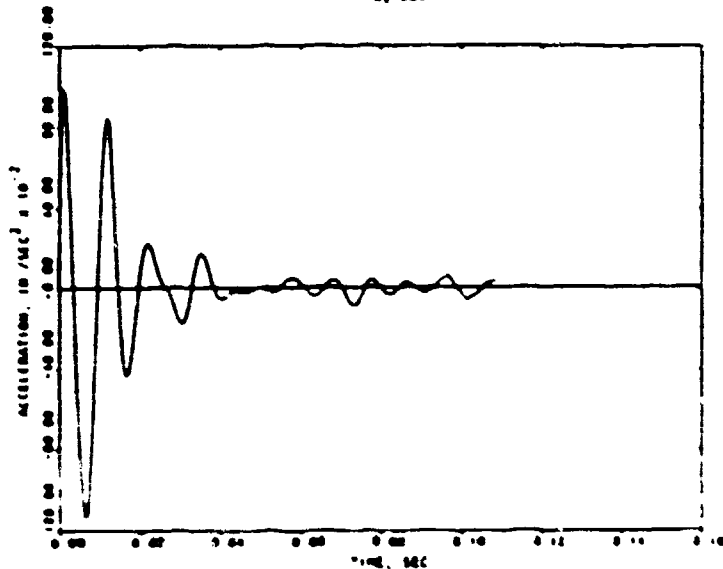
R-7556-1-4182



(a) Displacement



(b) Velocity



(c) Acceleration

FIGURE 5-55. COMPUTED MOTION OF NORTHEAST IGLOO (ESKIMO) AT NODE 115



R-7556-1-4182

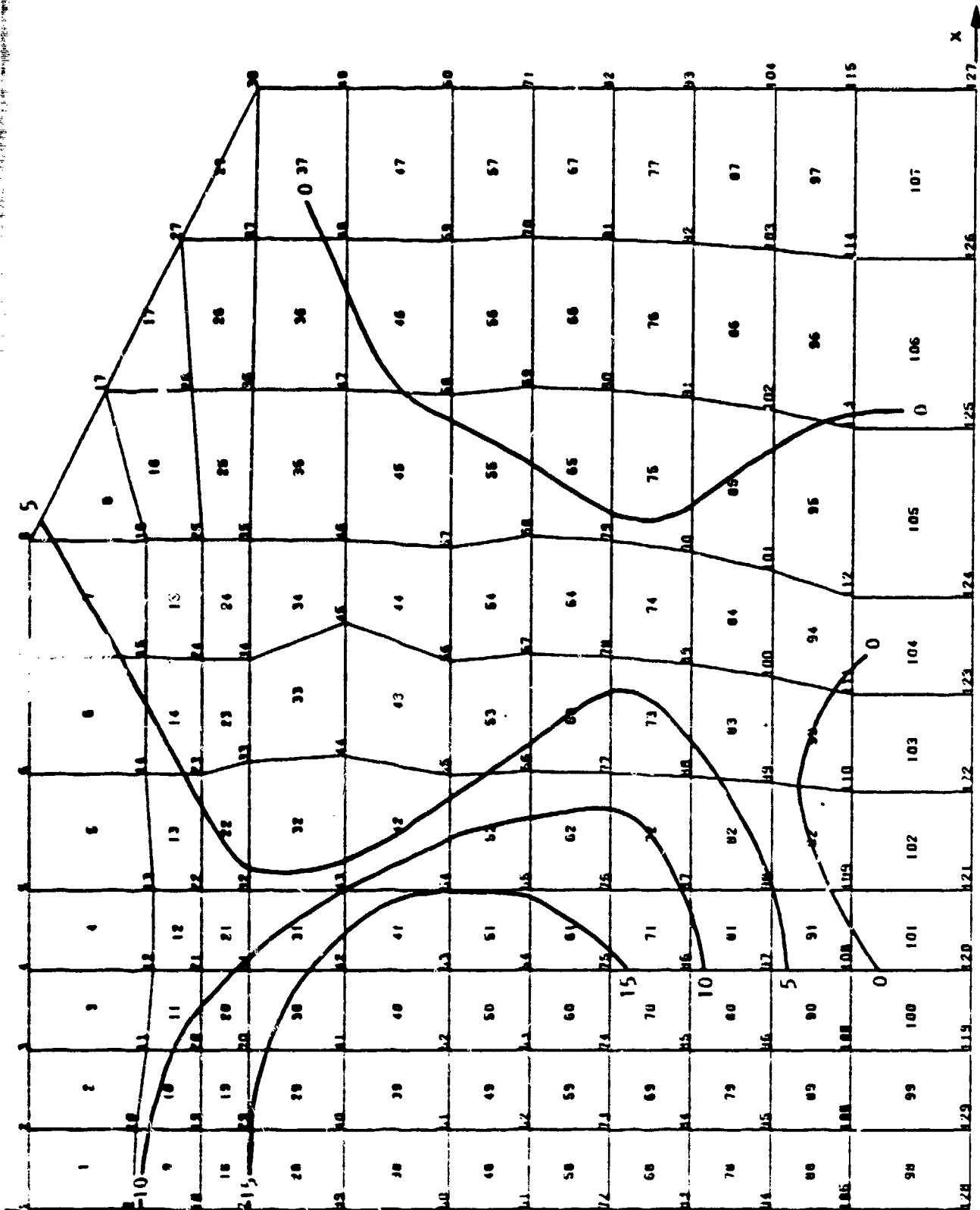


FIGURE 5-56. PERMANENT MOVEMENTS OF NORTHEAST HEADWALL OF ESKIMO 11 AS MEASURED (IN HUNDRETHS OF FEET)

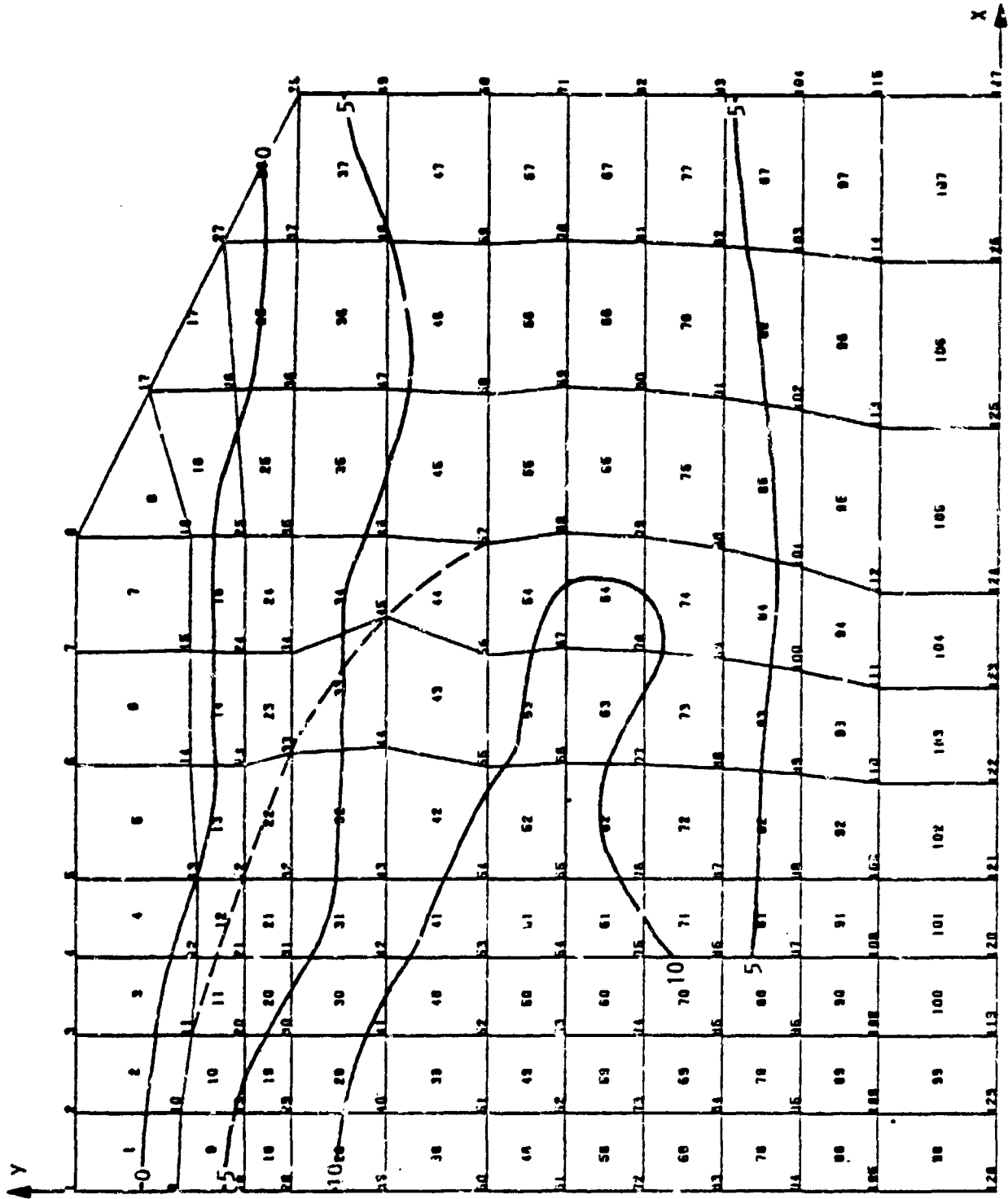
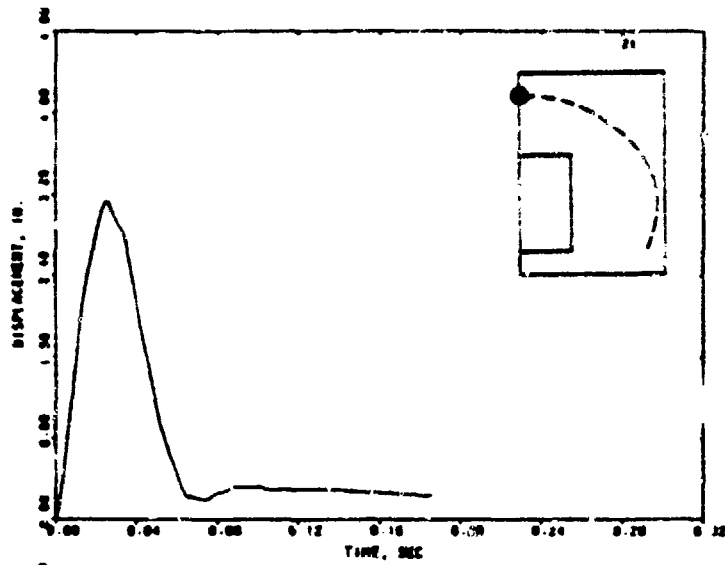


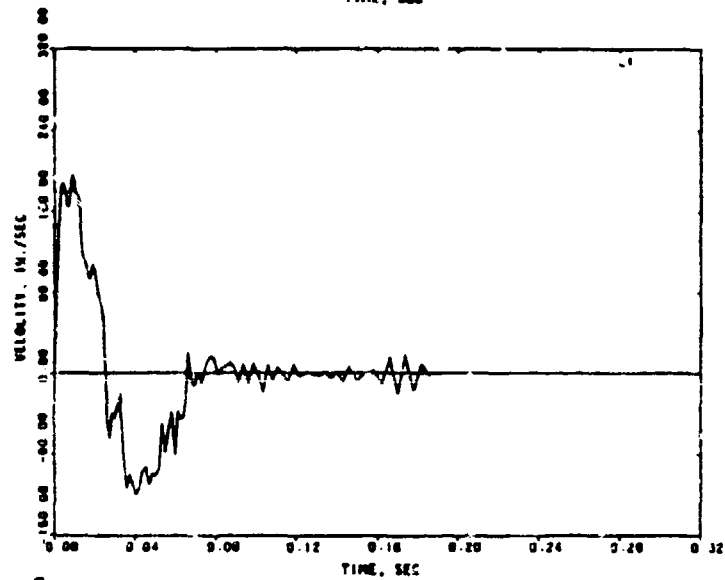
FIGURE 5-57. COMPUTED PERMANENT DISPLACEMENTS OF NORTHEAST HEADWALL OF ESKIMO III (IN HUNDRETHS OF FEET)



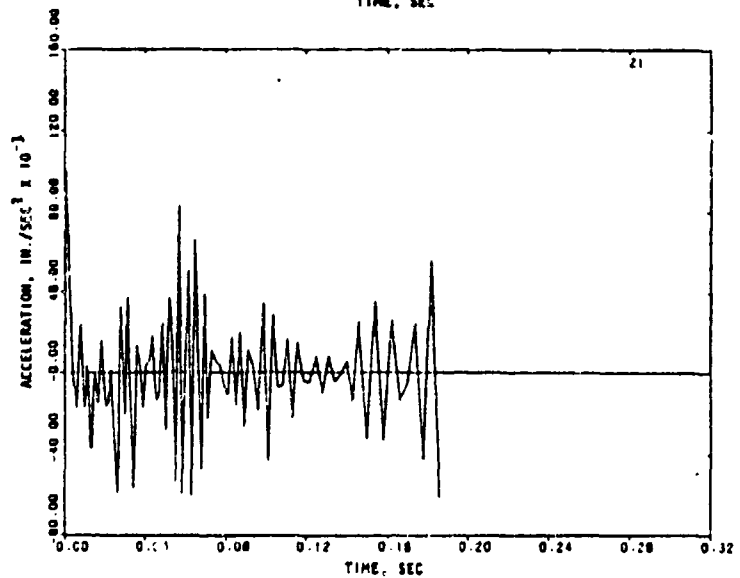
R-7556-1-4182



(a) Displacement



(b) Velocity

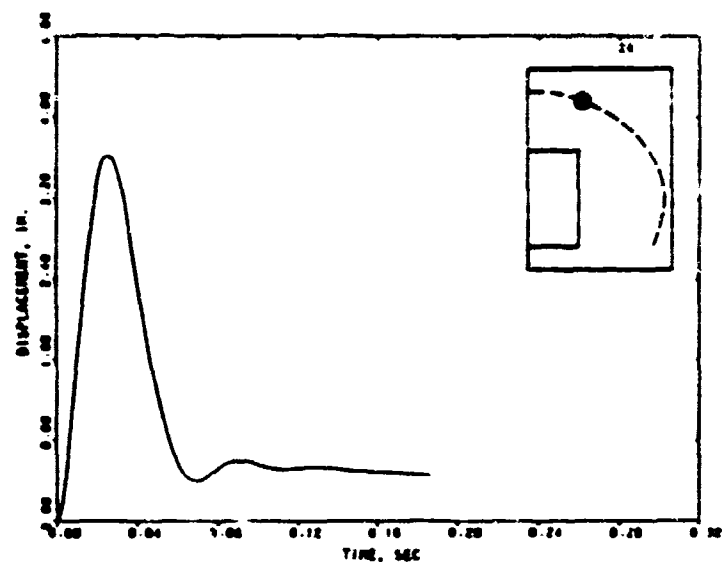


(c) Acceleration

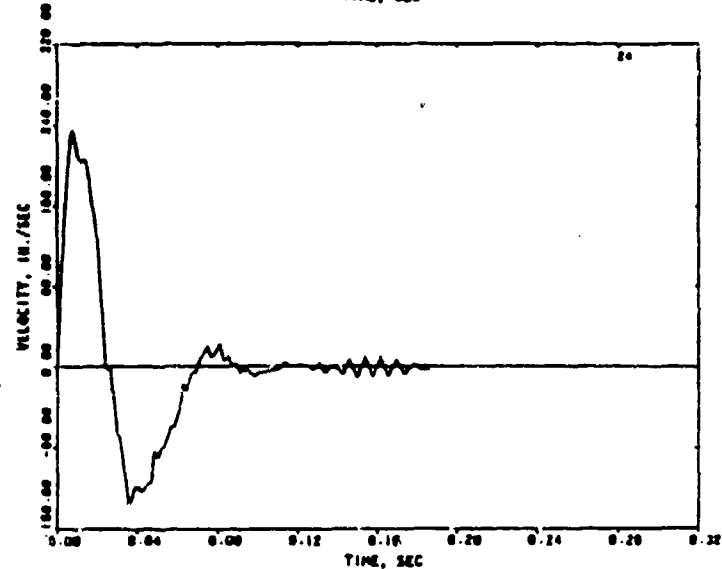
FIGURE 5-58. COMPUTED MOTION OF NORTHEAST IGL00 (ESKIMO IV) AT NODE 21



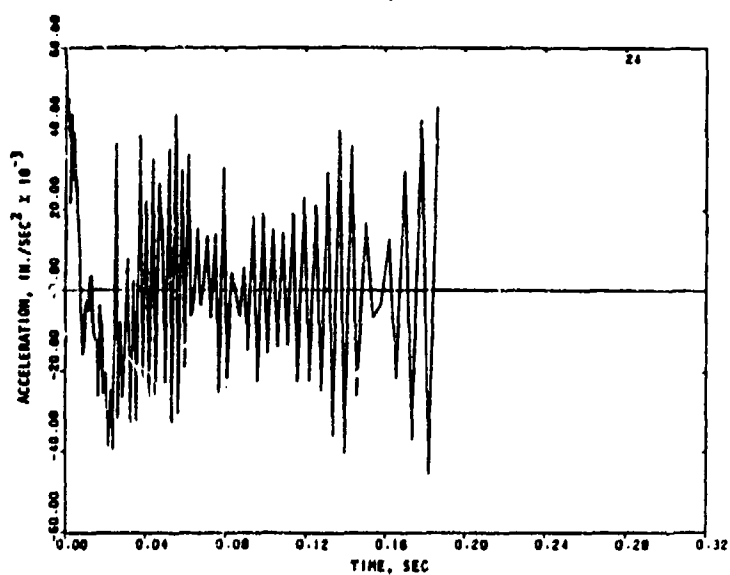
9-7556-1-4182



(a) Displacement

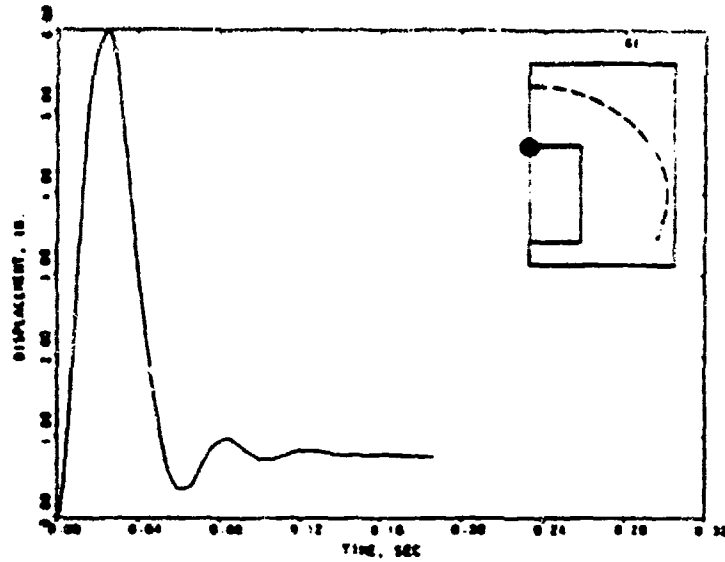


(b) Velocity

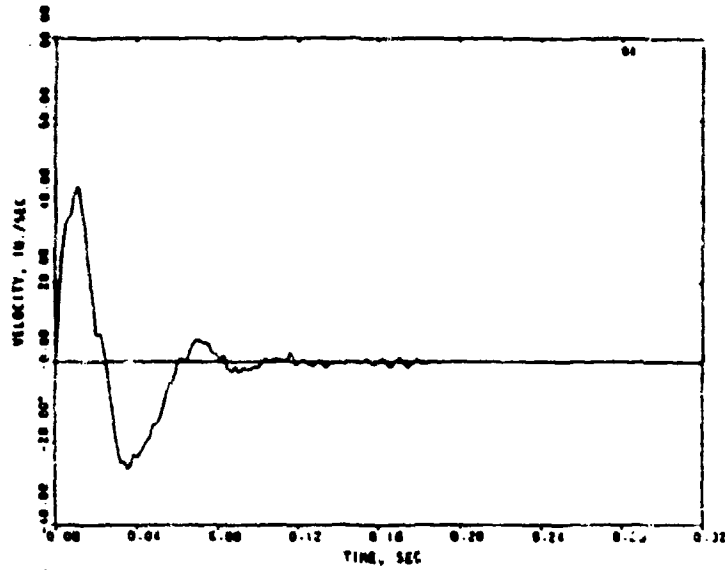


(c) Acceleration

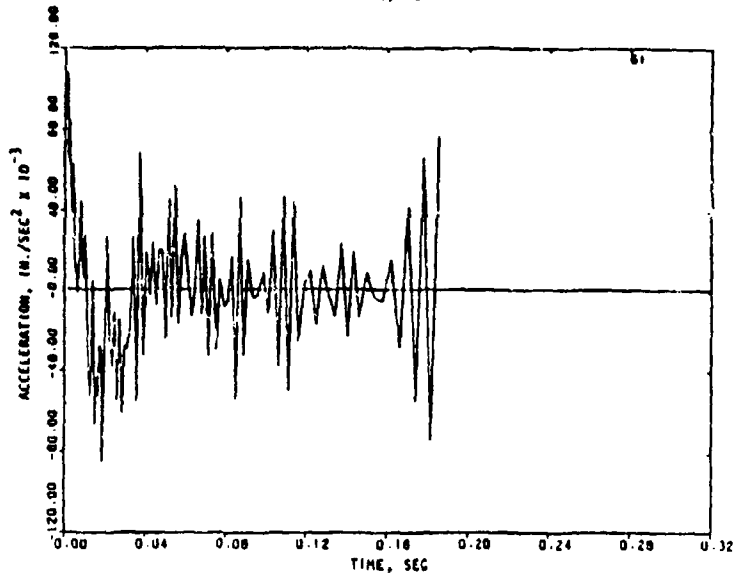
FIGURE 5-59. COMPUTED MOTION OF NORTHEAST IGLOO (ESKIMO IV) AT NODE 24



(a) Displacement

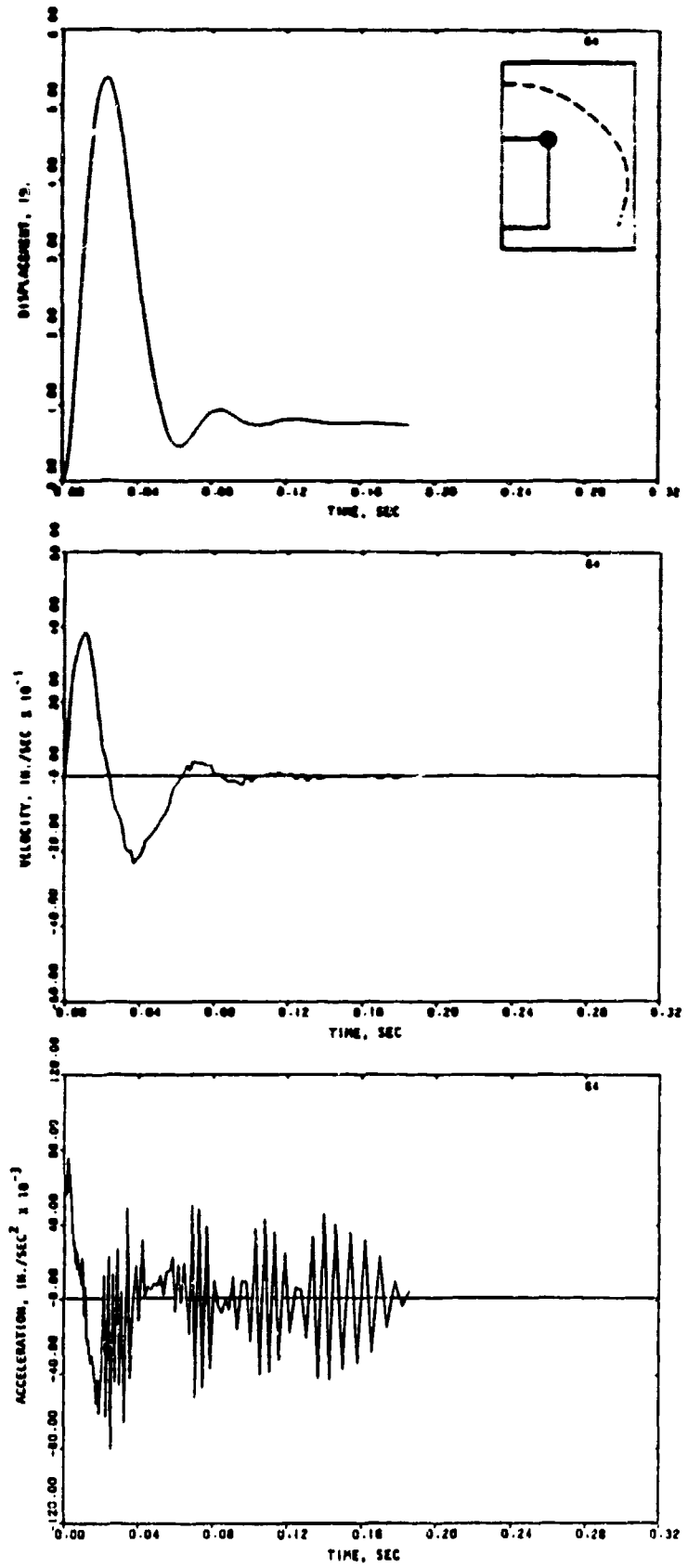


(b) Velocity



(c) Acceleration

FIGURE 5-60. COMPUTED MOTION OF NORTHEAST IGL00 (ESKIMO IV) AT NODE 61

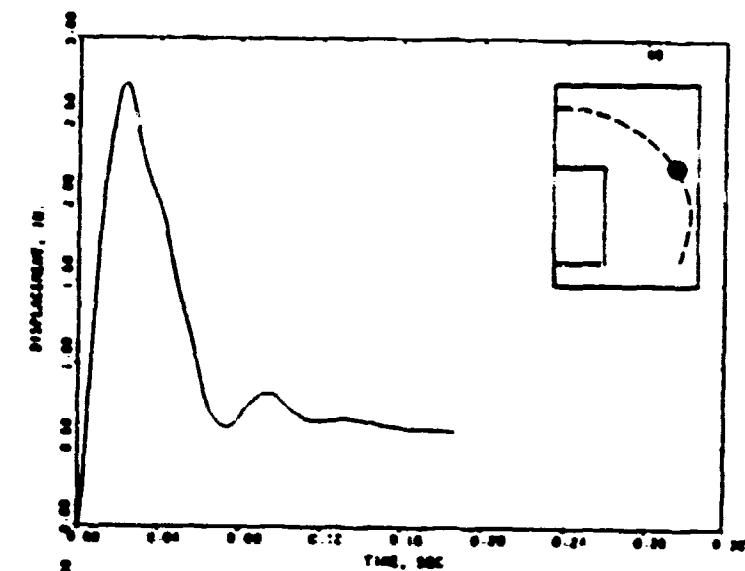


(a) Displacement

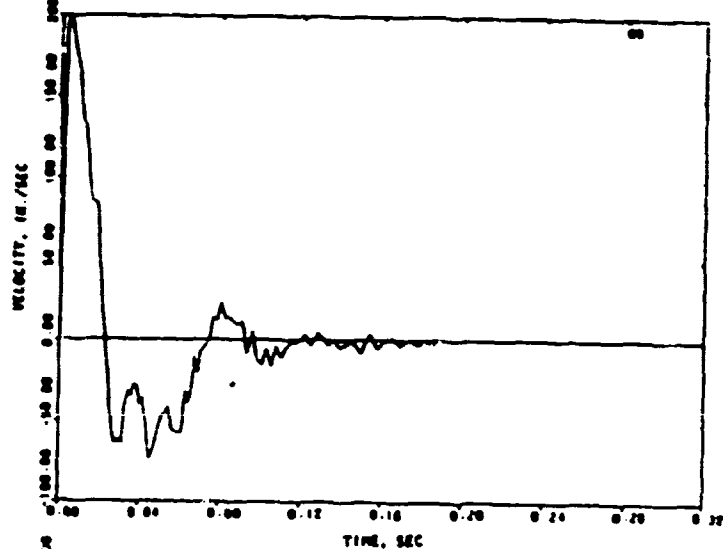
(b) Velocity

(c) Acceleration

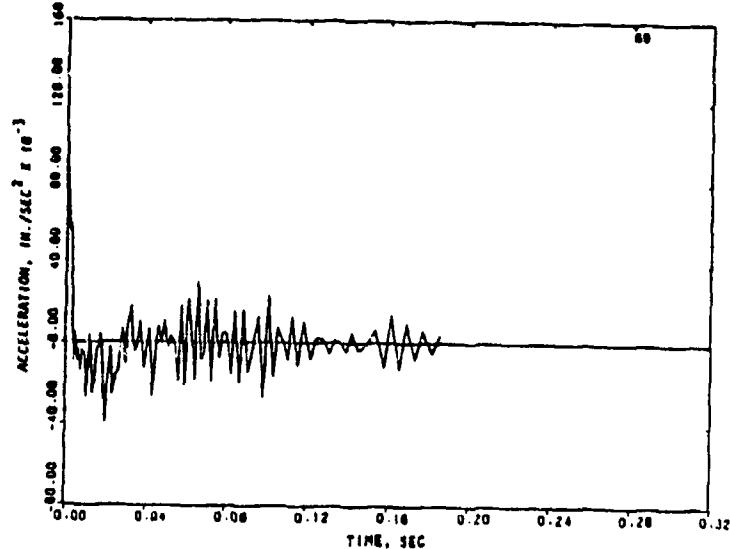
FIGURE 5-61. COMPUTED MOTION OF NORTHEAST IGLOO (ESKIMO IV) AT NODE 64



(a) Displacement

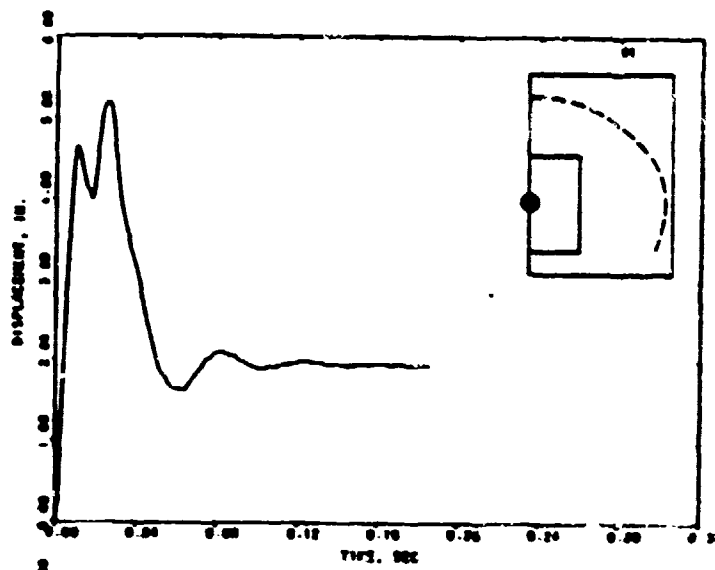


(b) Velocity

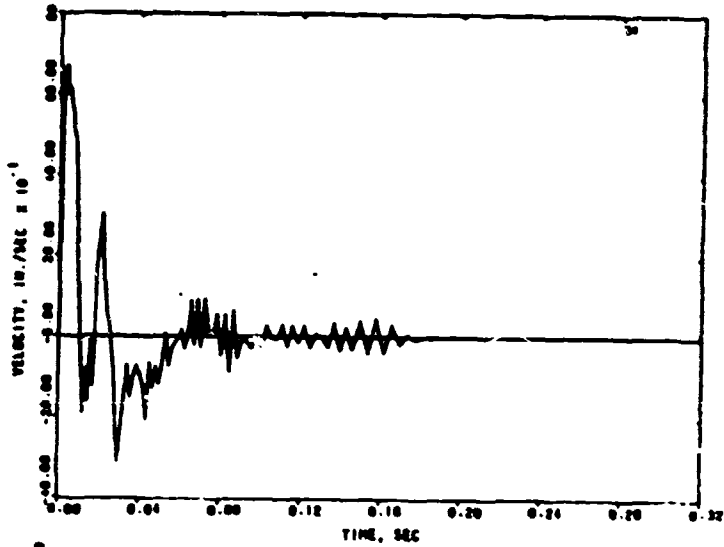


(c) Acceleration

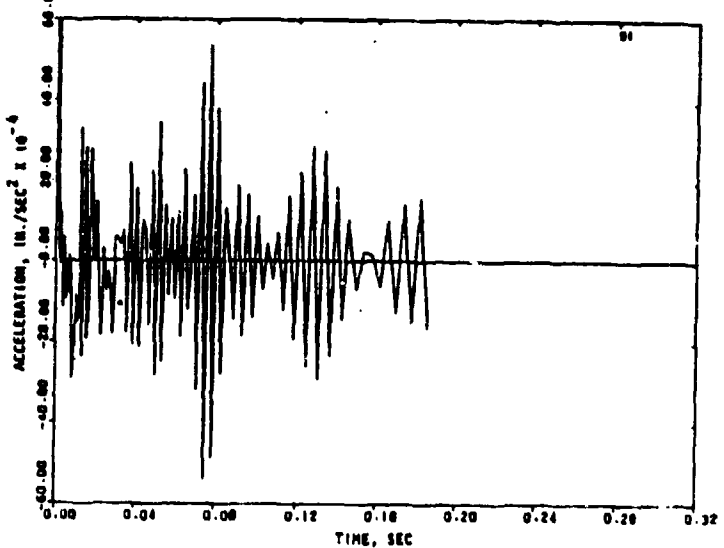
FIGURE 5-62. COMPUTED MOTION OF NORTHEAST IGLOO (ESKIMO IV) AT NODE 69



(a) Displacement

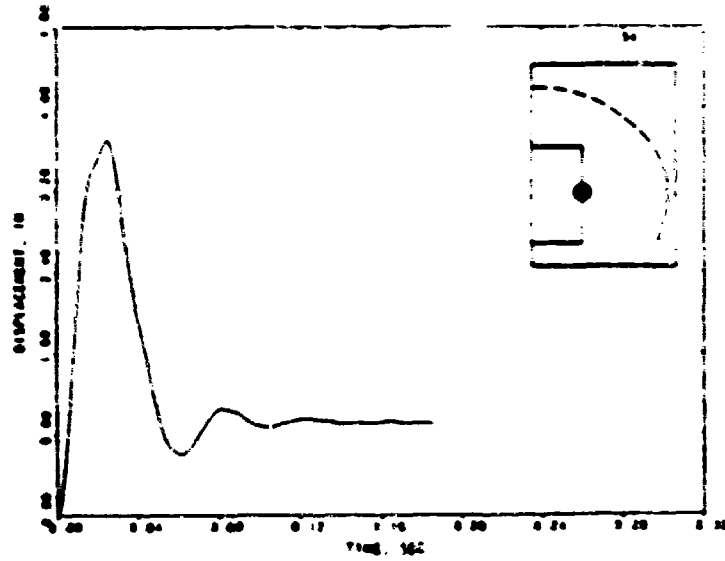


(b) Velocity

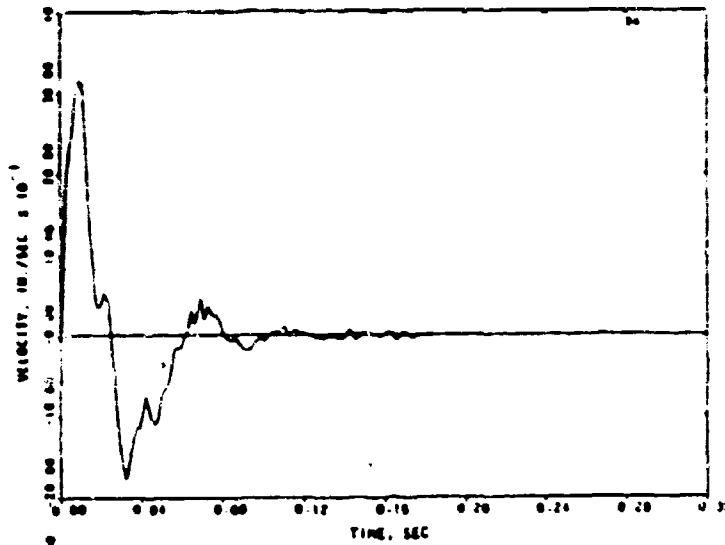


(c) Acceleration

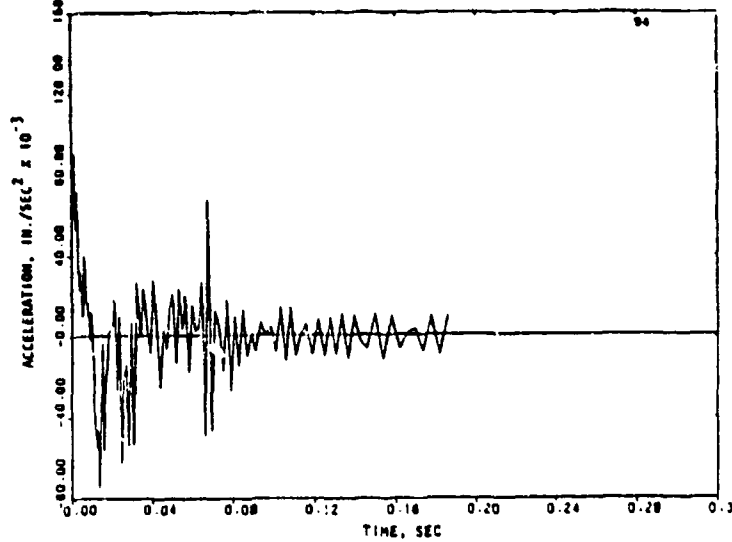
FIGURE 5-63. COMPUTED MOTION OF NORTHEAST IGLOO (ESKIMO IV) AT NODE 91



(a) Displacement

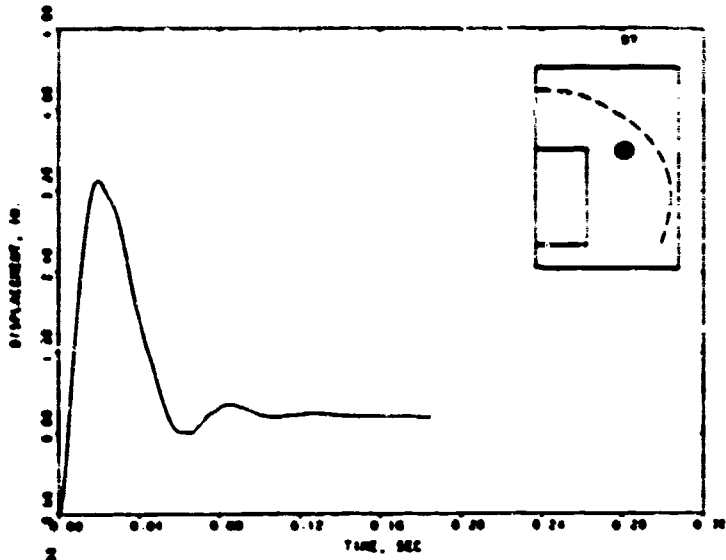


(b) Velocity

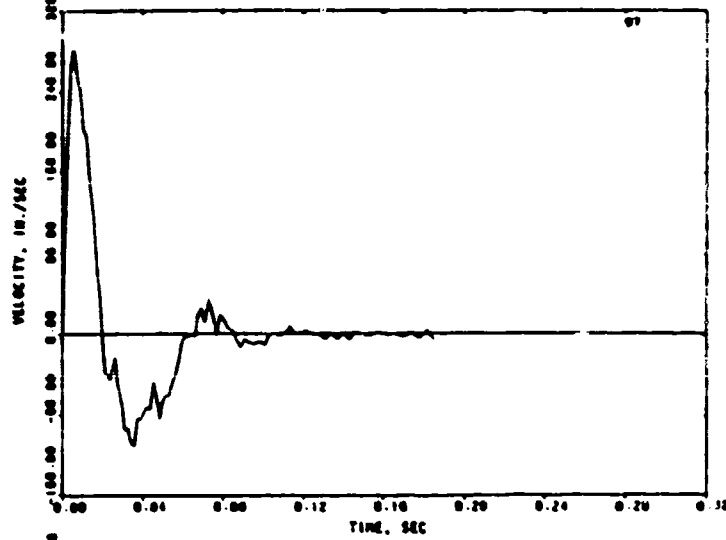


(c) Acceleration

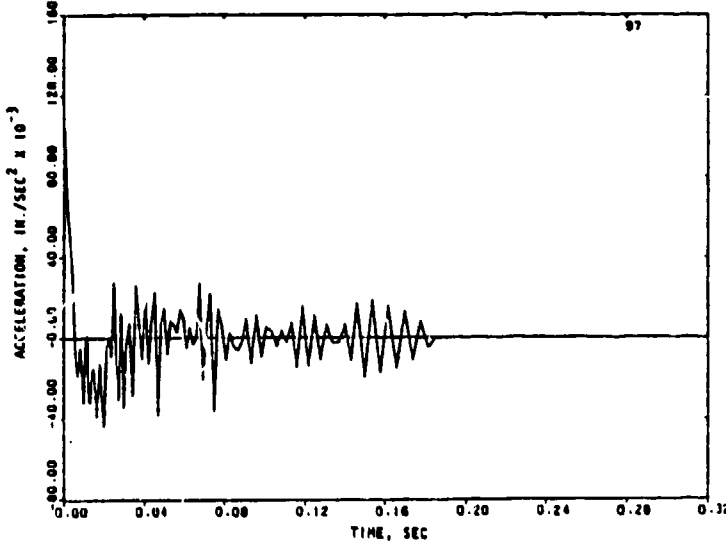
FIGURE 5-64. COMPUTED MOTION OF NORTHEAST IGLOO (ESKIMO IV) AT NODE 94



(a) Displacement



(b) Velocity

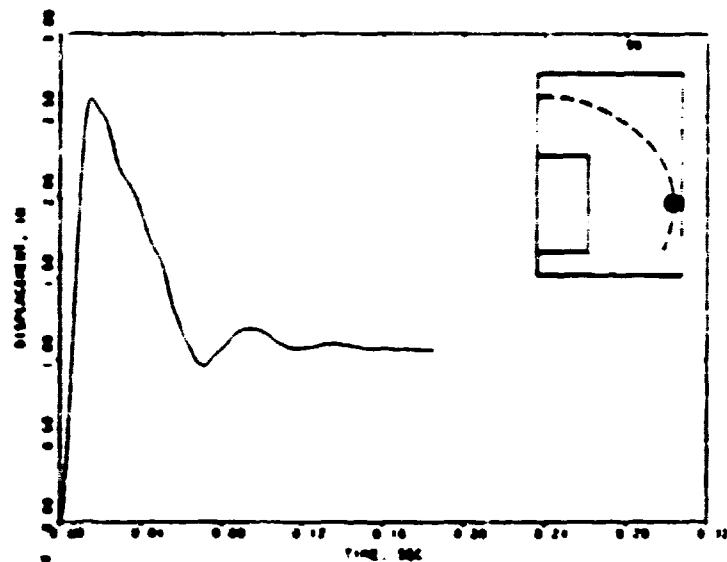


(c) Acceleration

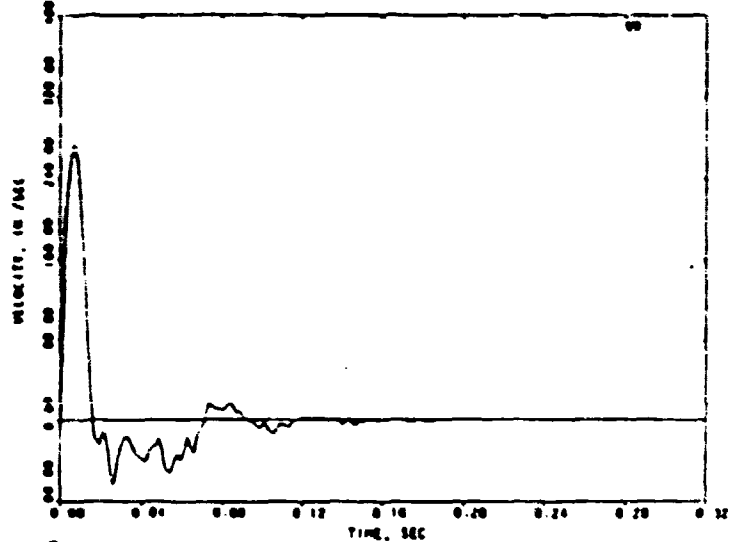
FIGURE 5-65. COMPUTED MOTION OF NORTHEAST IGL00 (ESKIMO IV) AT NODE 97



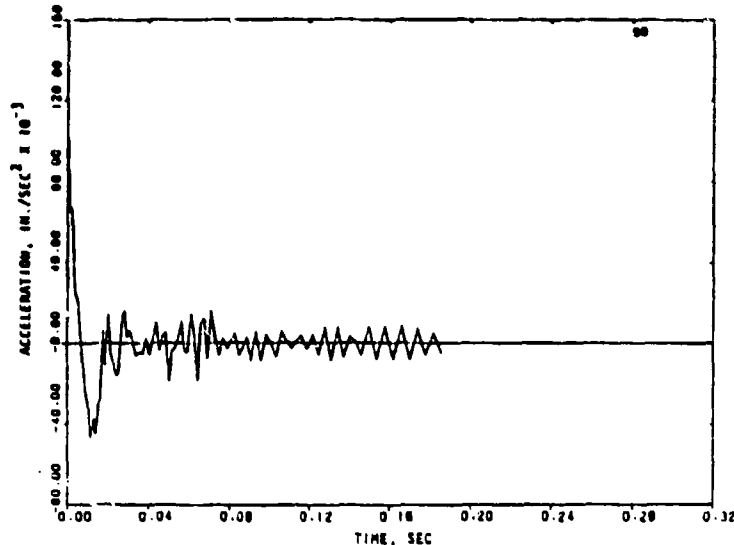
R-7556-1-4182



(a) Displacement

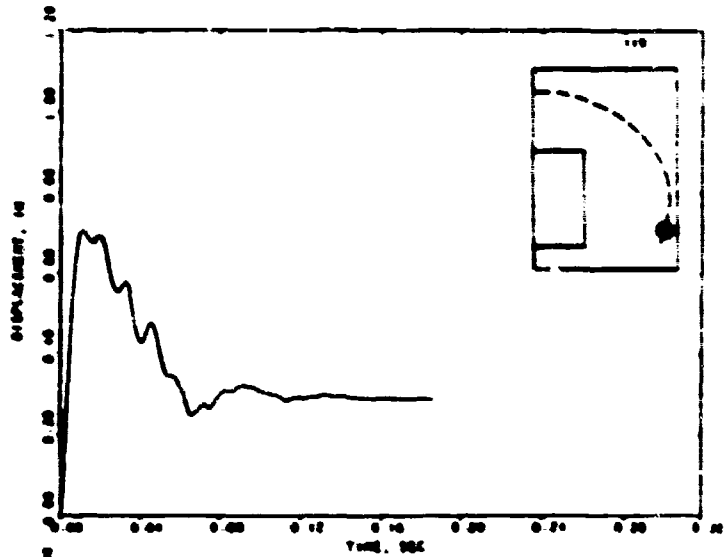


(b) Velocity

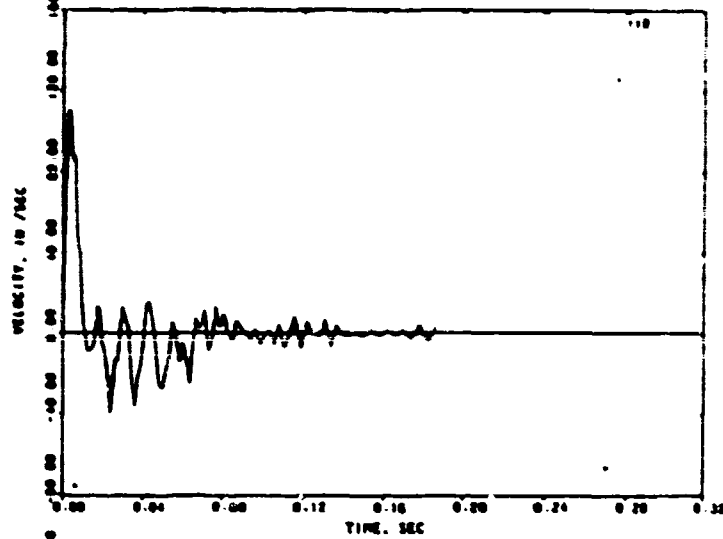


(c) Acceleration

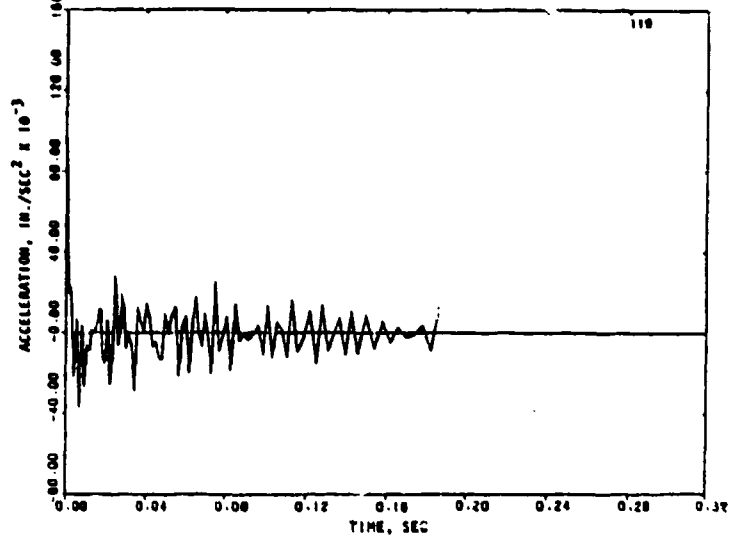
FIGURE 5-66. COMPUTED MOTION OF NORTHEAST IGL00 (ESKIMO IV) AT NODE 99



(a) Displacement:

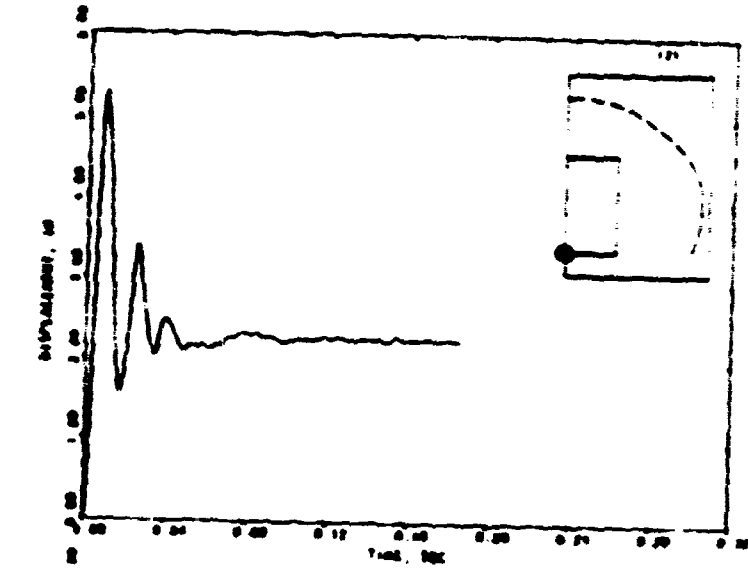


(b) Velocity

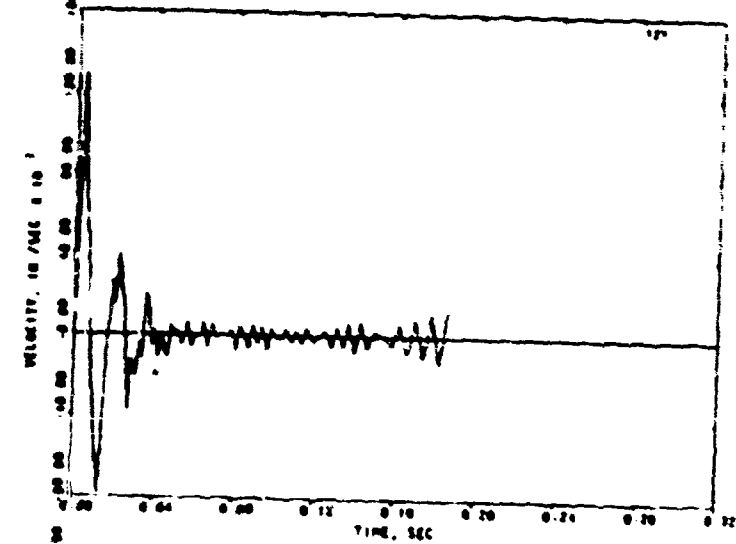


(c) Acceleration

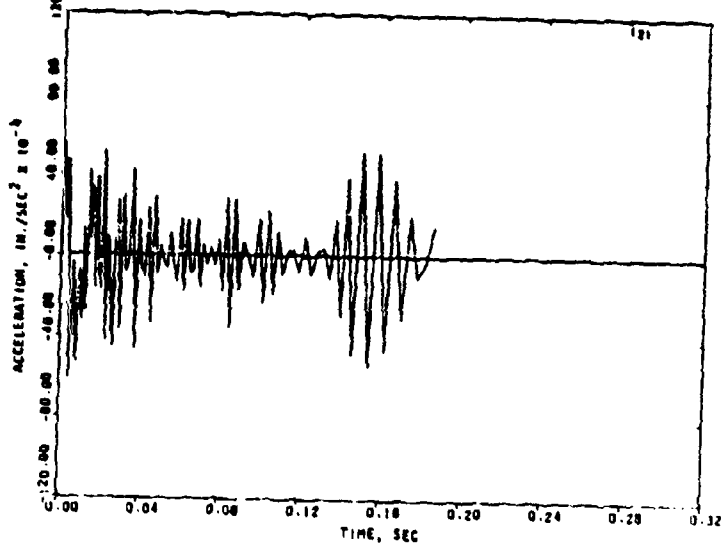
FIGURE 5-67. COMPUTED MOTION OF NORTHEAST IGL00 (ESKIMO IV) AT NODE 119



(a) Displacement

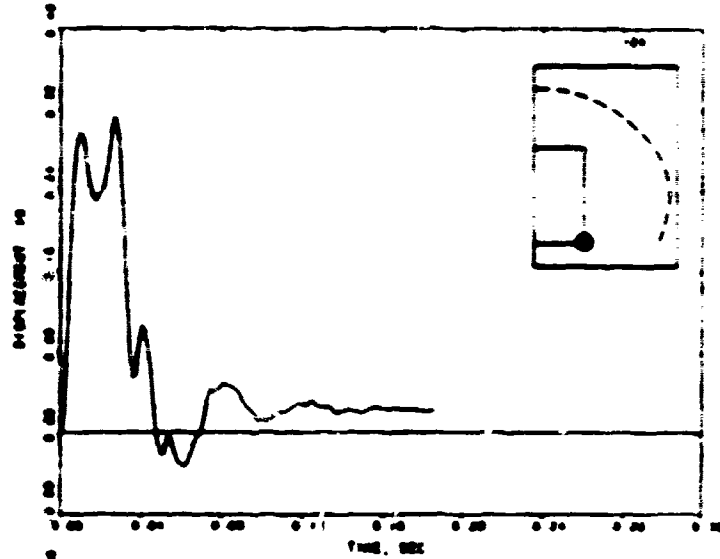


(b) Velocity

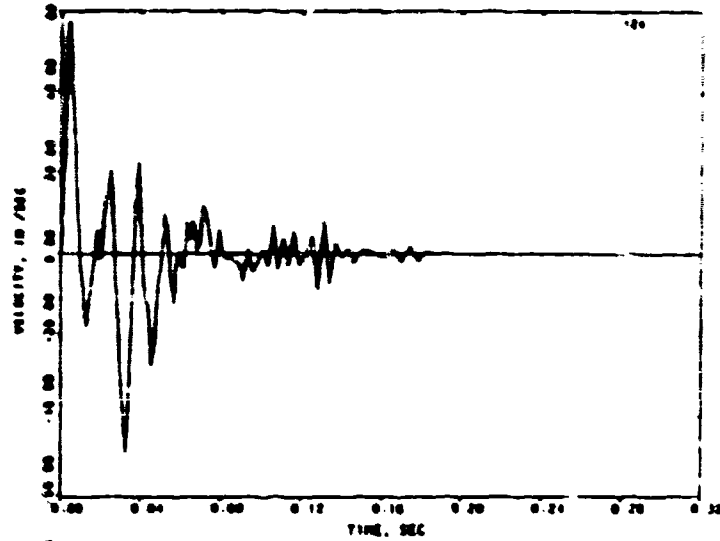


(c) Acceleration

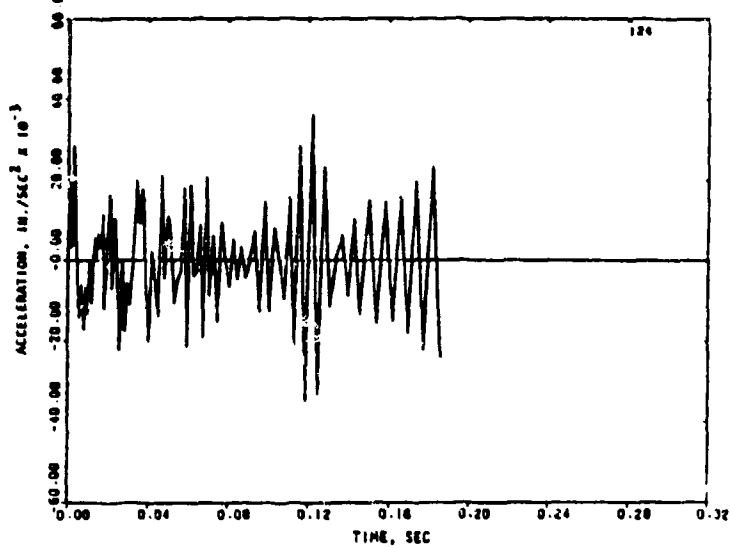
FIGURE 5-68. COMPUTED MOTION OF NORTHEAST IGLOO (ESKIMO IV) AT NODE 121



(a) Displacement



(b) Velocity



(c) Acceleration

FIGURE 5-69. COMPUTED MOTION OF NORTHEAST IGLOO (ESKIMO IV) AT NODE 124

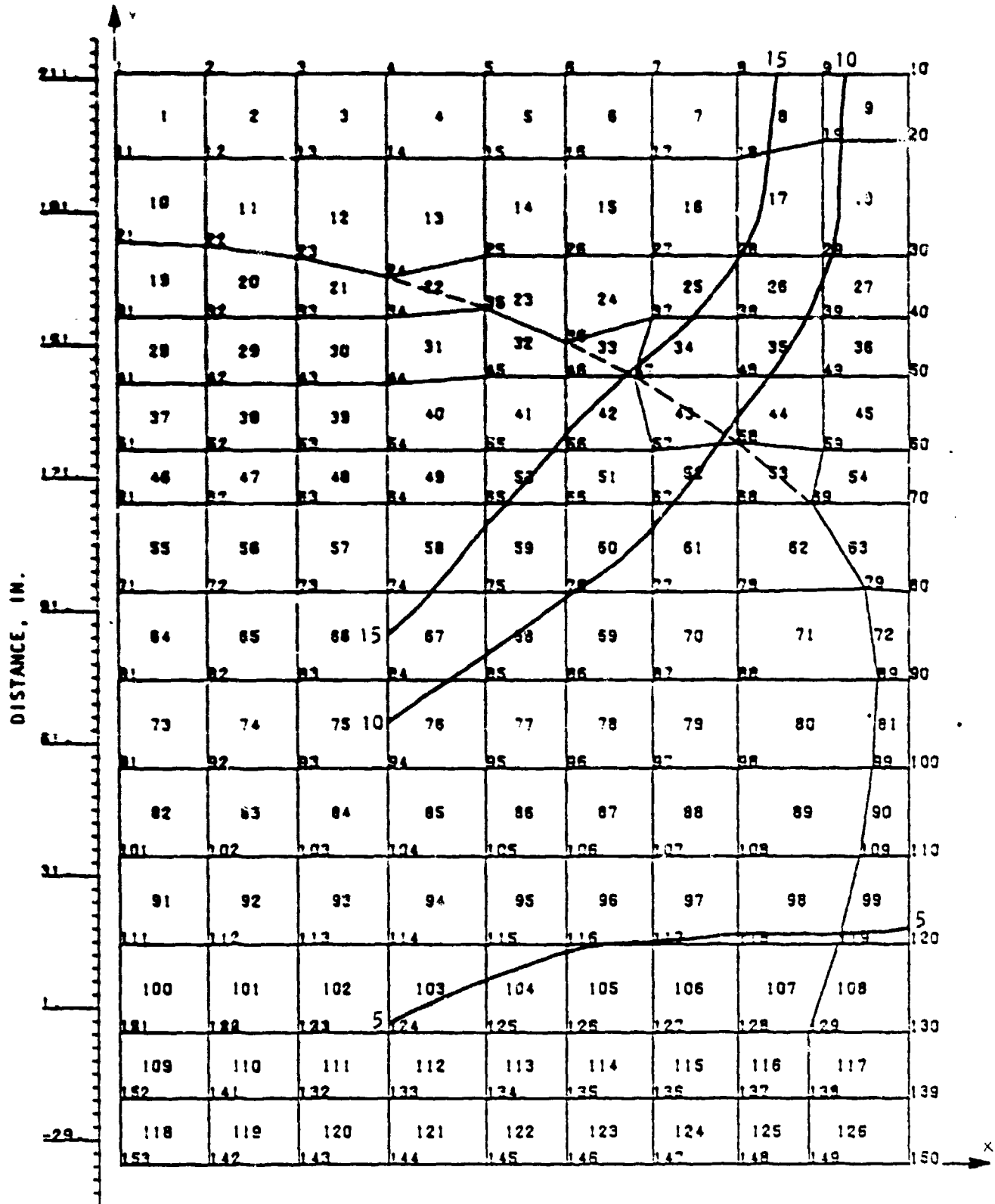


FIGURE 5-70. MEASURED PERMANENT DISPLACEMENT CONTOURS OF NORTHEAST HEADWALL OF ESKIMO IV (IN HUNDREDTHS OF FEET)

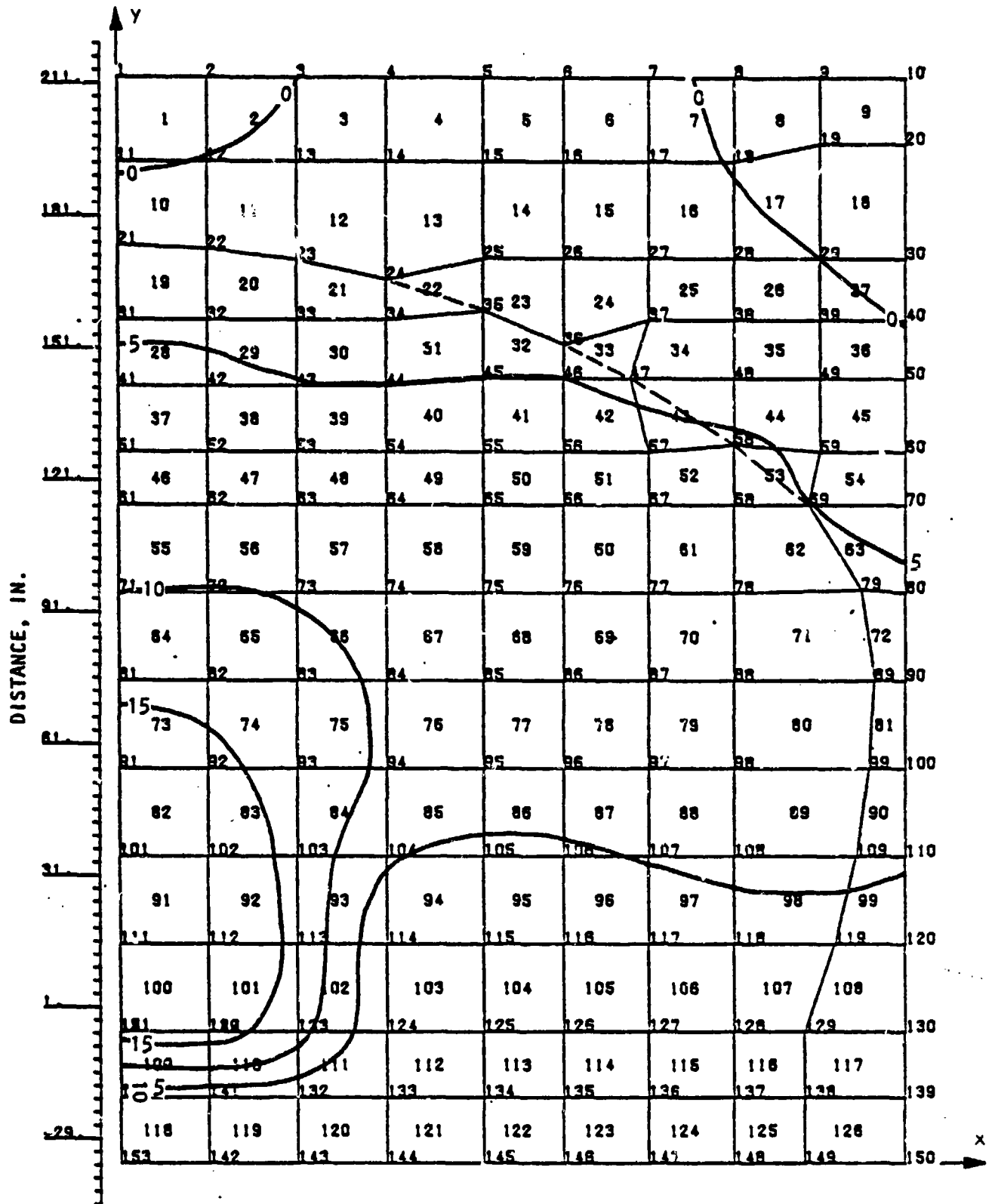


FIGURE 5-71. COMPUTED DISPLACEMENT CONTOURS OF NORTHEAST HEADWALL OF ESKIMO IV AT 158 MSEC (IN HUNDREDTHS OF FEET)

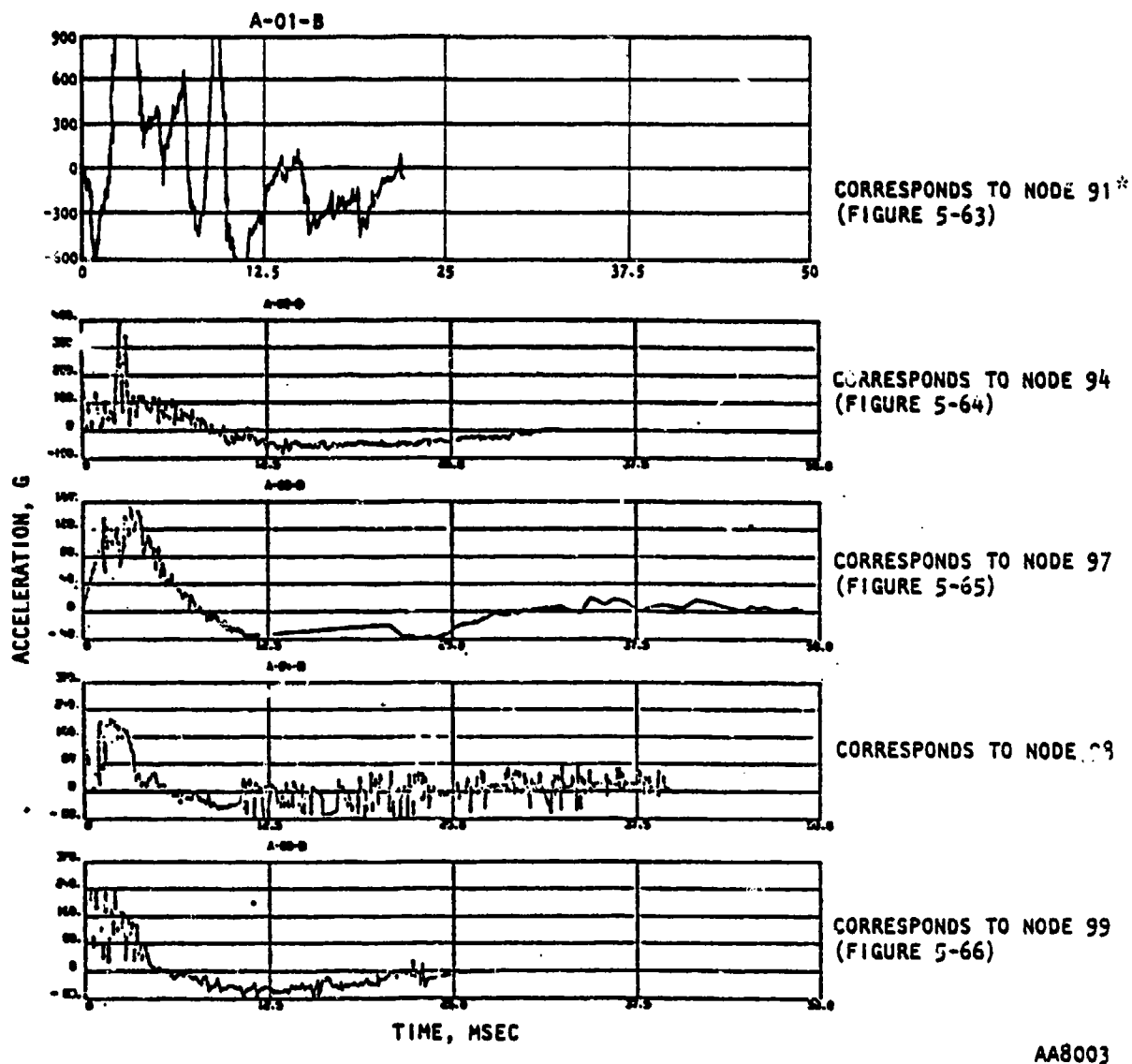
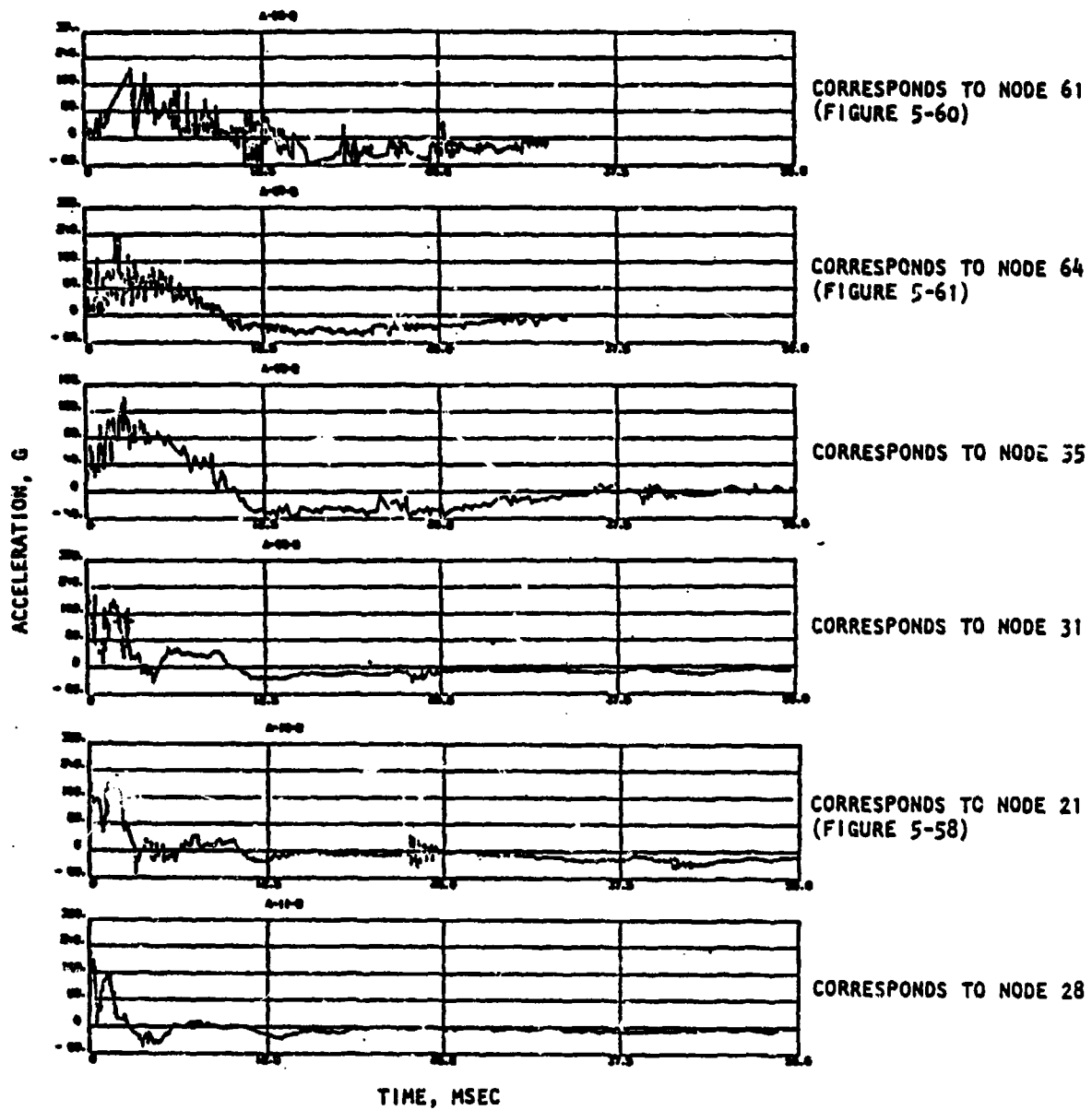


FIGURE 5-72. MEASURED ACCELERATION TIME HISTORIES OF NORTHEAST HE .LL OF ESKIMO IV (Ref. 6)

\*The motions at this gage exceeded its rating. Therefore, the record is not quite reliable.



R-7556-1-4182

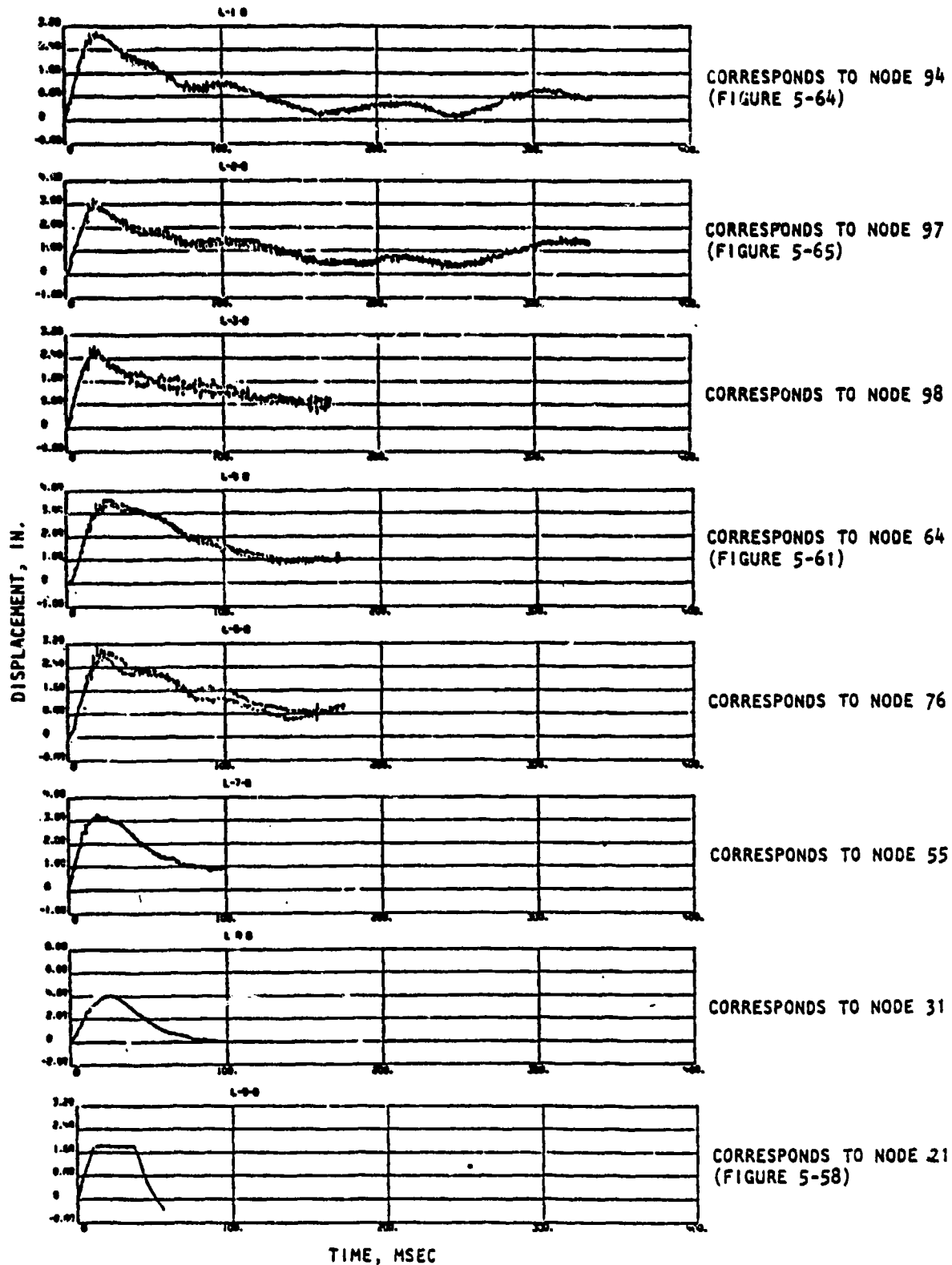


AA8004

FIGURE 5-72. (CONTINUED)



R-7556-1-4182



AA8002

FIGURE 5-73. MEASURED DISPLACEMENT TIME HISTORIES OF NORTHEAST HEADWALL IN ESKIMO IV (Ref. 6)



## SECTION 6

## CONCLUSIONS AND RECOMMENDATIONS

6.1 CONCLUSIONS

The present study consisted of dynamic analyses of magazine headwalls subjected to blast loadings in the ESKIMO tests. All the analyses were performed using the INSLAB code, a nonlinear finite element computer program. The computed results were compared with available test data. The following is a summary of conclusions of the study.

- a. The modified INSLAB computer program is capable of analytically predicting the behavior of the magazine headwalls used in the ESKIMO tests.
- b. The proposed nonlinear material model to represent the soil behind the headwalls appears to be satisfactory.
- c. The general behavior of the headwalls predicted by the calculations agreed well with the actual behavior of the headwalls in the tests.
- d. The results from the present analysis of the south and west headwalls in ESKIMO I, using the refined finite element mesh, show better agreement with the test results than those from the previous analysis.
- e. The analysis of the east headwall in the ESKIMO II test shows that (1) the computed maximum motions are much higher than those measured, and (2) the computed permanent displacement contours are similar in shape to those measured.

**Preceding page blank**



- f. The results of the analysis of the northeast headwall in the ESKIMO II test show that:
1. The computed maximum velocity above the doorway is much higher than that measured using the linear motion transducers.
  2. The computed maximum acceleration of the door is in good agreement with that measured using the accelerometers.
  3. The presence of the concrete beams around the doorway is effective in reducing the maximum displacements of the headwall.
  4. The biparting and sliding type of door is superior to the double-leaf and hinged type, for resisting the blast loads.
- g. The results of the analysis of the northeast headwall in the ESKIMO IV test indicated that:
1. The corrugated steel arch doesn't seem to provide any significant resistance to the motion of the headwall.
  2. The magnitudes and general shapes of the computed displacement time histories are in good agreement with those measured by the linear motion transducers.
  3. The computed acceleration time histories look somewhat different from those measured using the accelerometers; however, the computed maximum accelerations are in good agreement with those measured.



## 6.2 RECOMMENDATIONS

The analytical prediction capabilities exhibited by the present study have been satisfactory. However, there are certain aspects to the modeling of the headwall and door system that can improve the analytical prediction capabilities. The following is a summary of recommendations for improving the analytical prediction capabilities in order to reduce the dependence on the expensive, full-scale testing program.

- a. The present techniques for analyzing the headwall systems are not satisfactory when the doors are blown open. Therefore, the analytical methods should be improved to include the concept of breakable hinges. This would permit the calculation of true response of the headwall even after the doors are blow open.
- b. The parameters in the nonlinear soil models should be adjusted based on the test data available for the ESKIMO IV test. The resulting models are expected to better represent the backfill soils for improved analytical predictions.
- c. Detailed analysis of the test data for ESKIMO IV and comparison of the data with the results of the present analysis should be undertaken. This may include corrections to the data for drifts, etc., and also statistical analyses of the test data.
- d. Future tests should include a sufficient amount of instrumentation to produce data necessary to study the stress distribution in the headwall sections. This would include placing strain gages on reinforcing bars.



## SECTION 7

## REFERENCES

1. Weals, F.H. *ESKIMO I Magazine Separation Test*, NWC TP 5430. China Lake, CA: Naval Weapons Center, April 1973.
2. Ts'ao, H.S., et al. *Magazine Headwall Response to Explosive Blast*, R-7336-3284. El Segundo, CA: Agbabian Associates, January 1974.
3. *User's Guide for INSLAB Code*, U-7556-1-4001. El Segundo, CA: Agbabian Associates, September 1975.
4. Weals, F.H. *ESKIMO II Magazine Separation Test*, NWC TP 5557. China Lake, CA: Naval Weapons Center, September 1974.
5. Weals, F.H. *ESKIMO III Magazine Separation Test*, NWC TP 5771. China Lake, CA: Naval Weapons Center, February 1976.
6. Weals, F.H., and Wilson, C.H. *Preliminary Report, ESKIMO IV*. China Lake, CA: Naval Weapons Center, 1976.
7. Baker, W.E. *Explosions in Air*. Austin, TX: University of Texas Press, 1973.
8. *User's Guide for INSLAB Code*, R-6820-1580. Los Angeles: Agbabian-Jacobsen Associates, September 1970.
9. *Strength of Materials and Structural Elements*, Manual for Design of Structures to Resist the Effects of Atomic Weapons, EM1110-345-414. U.S. Army, Corps of Engineers, March 1957.
10. "IGL00 Door Test -- Modulus of Soil Reaction," unpublished memorandum. Washington, D.C.: Naval Weapons Center, Code 7036, October 1972.
11. Richart, F.E., Jr., et al. *Vibration of Soils and Foundation*. Englewood Cliffs, NJ: Prentice-Hall, 1970.
12. *User's Guide for TRI/SAC Code*, R-7128-4-2314. El Segundo, CA: Agbabian Associates, May 1972.
13. Wang, C.T. *Applied Elasticity*. New York: McGraw-Hill, 1953.

Preceding page blank



## APPENDIX A

## INCLUSION OF NONLINEAR SPRINGS IN INSLAB CODE

The response of the magazine headwall to blast loading is greatly influenced by the earth fill behind the headwall. The effect of the soil can best be incorporated in the two-dimensional headwall model by using a combination of damping elements and nonlinear (one-way) springs. Linear springs, which are already present in the existing INSLAB code, are inadequate for modeling the influence of the soil because they exert both pressures and tensile forces on the headwall and they tend toward a final displacement of zero. The properties of the nonlinear springs and the details of their incorporation in INSLAB are discussed herein.

Figure A-1 shows the load/deflection characteristics of the nonlinear springs. Two different spring constants,  $k_L$  and  $k_U$ , appropriate in the virgin loading zone (Zone 2) and the unloading/reloading zone (Zone 1) respectively, have been incorporated in such a way that after loading, equilibrium corresponds to a nonvanishing displacement,  $\delta_0$ . This equilibrium displacement is a function of  $\delta_{max}$ , the largest compressive displacement of the prior load history. Tensile spring forces are eliminated by using a spring constant of zero in "Zone 0," in which the displacement is on the tensile side of the equilibrium displacement.

The varying status of the nonlinear spring between Zones 0, 1, and 2 requires reformulation of the global stiffness matrix during transition from one zone to another. Furthermore, as shown in Table A-1, transition between zones usually requires an adjustment to the load vector. This is because the stiffness matrix is capable of accommodating only that portion of the incremental spring force that is proportional to the incremental displacement,  $\Delta\delta$ . Note that for a linear spring in which there is never any transition between zones, there is no need for a load vector adjustment.

**Preceding page blank**



NOTE:  $k_L$  = SPRING CONSTANT IN LOADING  
 $k_U$  = AN ARBITRARY STIFFNESS VALUE IN UNLOADING  
(CONTROLS THE PERMANENT DISPLACEMENT OF  
THE SPRING)

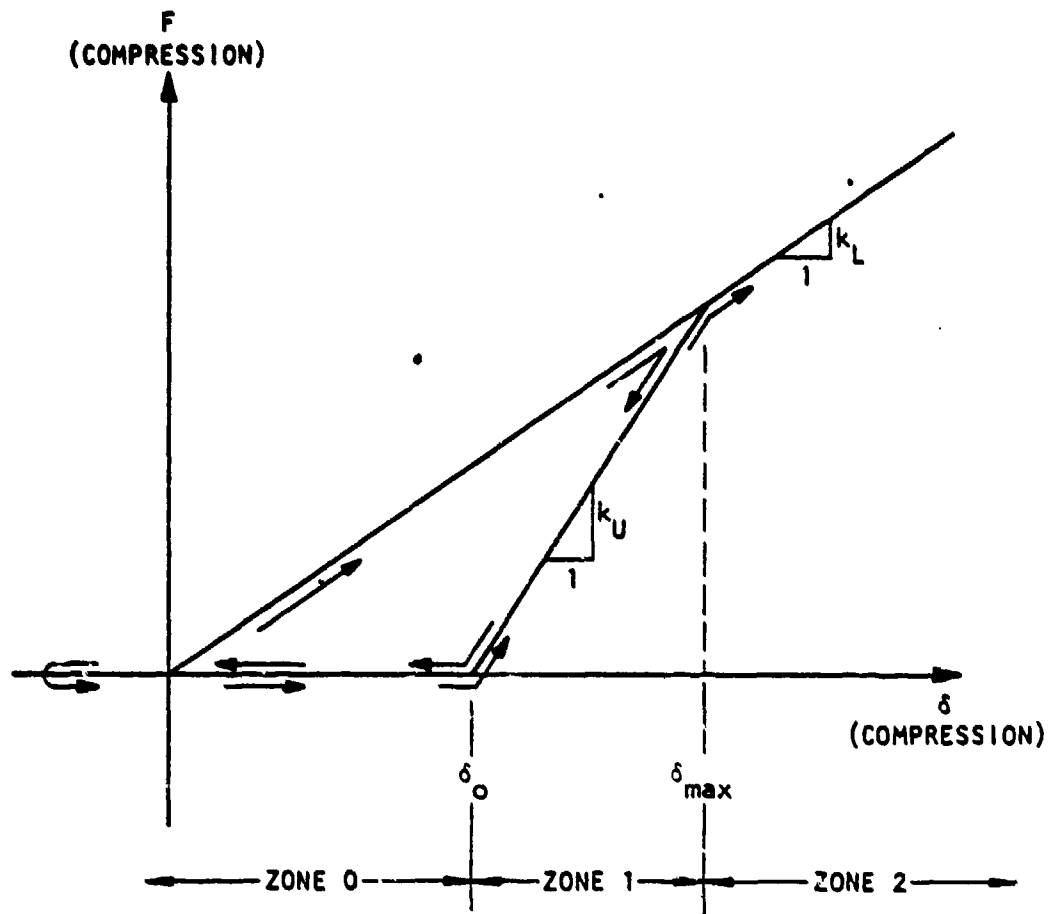


FIGURE A-1. LOAD/DEFLECTION CHARACTERISTICS OF NONLINEAR SPRINGS



TABLE A-1. ALLOCATION OF INCREMENTAL SPRING FORCE BETWEEN STIFFNESS MATRIX AND LOAD VECTOR

| Current Zone | Predicted Next Zone | Current Spring Force  | Predicted Next Spring Force  | $\Delta P$ , Predicted Increment in Spring Force                           | Included in Stiffness Matrix | Addition to Load Vector                                     |
|--------------|---------------------|---|--|--|------------------------------|---|
| 0            | 0                   | 0   | 0  | 0  | 0                            | 0   |
| 0            | 1                   | 0   | $k_U(\delta + \Delta\delta - \delta_0)$                                    | $k_U(\delta + \Delta\delta - \delta_0)$                                    | $k_U\Delta\delta$            | $k_U(\delta - \delta_0)$                                    |
| 1            | 0                   | $k_U(\delta - \delta_0)$                                    | 0  | $-k_U(\delta - \delta_0)$  | 0                            | $-k_U(\delta - \delta_0)$                                   |
| 1            | 1                   | $k_U(\delta - \delta_0)$                                    | $k_U(\delta + \Delta\delta - \delta_0)$                                    | $k_U\Delta\delta$  | $k_U\Delta\delta$            | 0   |
| 1            | 2                   | $k_U(\delta - \delta_0)$                                    | $k_U(\delta_{max} - \delta_0) + k_L(\delta + \Delta\delta - \delta_{max})$ | $k_U(\delta_{max} - \delta_0) + k_L(\delta + \Delta\delta - \delta_{max})$ | $k_L\Delta\delta$            | $k_U(\delta_{max} - \delta_0) + k_L(\delta - \delta_{max})$ |
| 2            | 1                   | $k_U(\delta_{max} - \delta_0)$                              | $k_U(\delta_{max} + \Delta\delta - \delta_0)$                              | $k_U\Delta\delta$  | $k_U\Delta\delta$            | 0   |
| 2            | 2                   | $k_U(\delta_{max} - \delta_0) + k_L(\delta - \delta_{max})$ | $k_U(\delta_{max} - \delta_0) + k_L(\delta + \Delta\delta - \delta_{max})$ | $k_L\Delta\delta$  | $k_L\Delta\delta$            | 0   |



Successful incorporation of the spring force (Table A-1) in the finite element model is dependent upon the ability to predict upcoming changes in zone. This is particularly important in the case of rebonding (transition from Zone 0 to Zone 1). In this case the spring constant changes from 0 to  $k_U$ . If this change in stiffness is not anticipated, calculation of the incremental displacement will proceed as if the spring constant remains 0 throughout the time interval. This will result in an excessively large displacement into Zones 1 or 2. By the time the spring force corresponding to this large displacement is included in the subsequent step, an increment of potential energy (spring deformation) has been erroneously added to the dynamic system. Cyclic repetition of this error causes unstable growth of oscillatory motion.

Using a truncated Taylor series expanded about time  $t$ , the displacement at the end of the time interval  $\Delta t$  can be estimated according to the formula

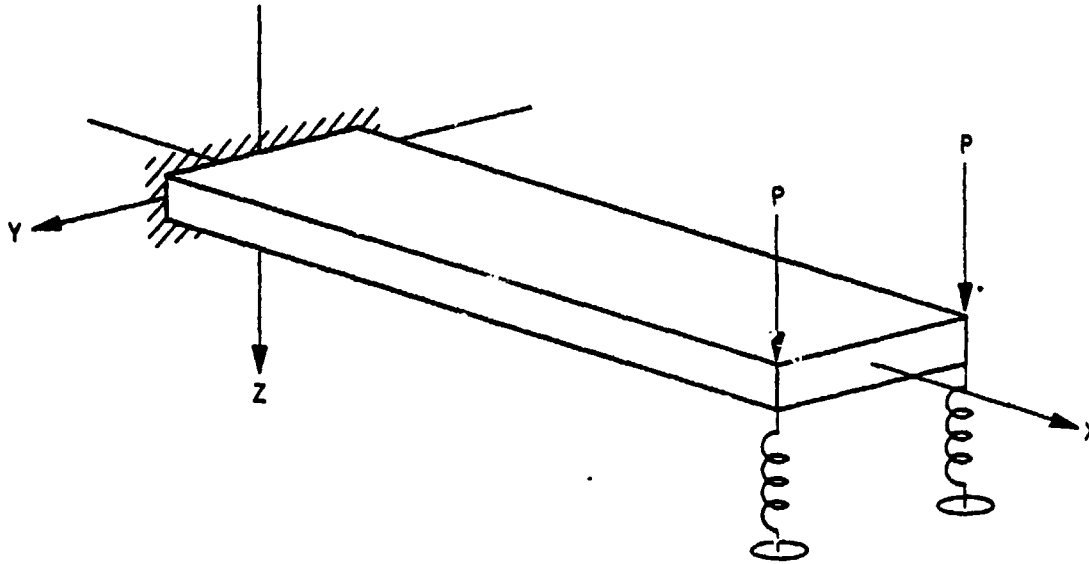
$$X(t + \Delta t) = X_t + \dot{X}_t \Delta t + \frac{1}{2} \ddot{X}_t (\Delta t)^2 \quad (A-1)$$

The accuracy of this estimate should improve with decreasing  $\Delta t$ . This forecasted future displacement is used to predict whether any changes in zone are to be anticipated. If so, a stiffness reformulation occurs during the next step, and the appropriate adjustment is incorporated in the load vector.

Figure A-2 shows the test problem that was used to check out the performance of the nonlinear spring. Some sample results of this test problem are shown in Figure A-3. Figure A-3a shows the time dependence of the load function,  $P$ , used in Case 1. The displacement of the end of the beam for this case is shown in Figure A-3b. The external load ( $= 2P$ ) deflects the beam until the nonlinear springs supply an equilibrating force. When the external load is relaxed, the nonlinear spring relaxes also. However, due to the high unloading spring constant, this relaxation of the spring occurs



R-7556-1-4182

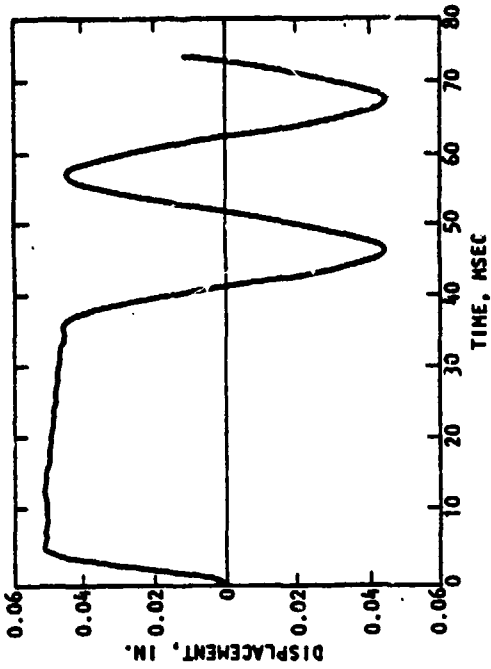


LENGTH = 10 IN.  
WIDTH = 1 IN.  
DEPTH = 0.2 IN.  
E =  $30 \times 10^6$  PSI  
 $\rho = 7.34 \times 10^{-4} \frac{\text{LB-SEC}^2}{\text{IN.}^4}$

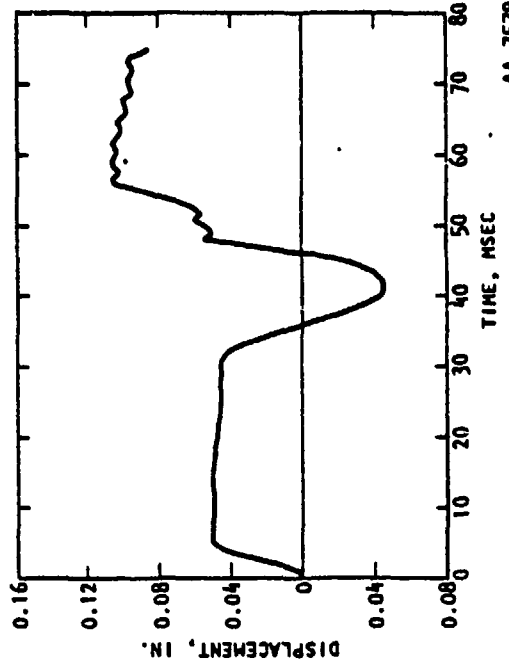
SPRING CONSTANTS

$k_L = 600$  LB/IN.  
 $k_U = 6000$  LB/IN.

FIGURE A-2. TEST PROBLEM USED TO CHECK OUT NONLINEAR SPRINGS

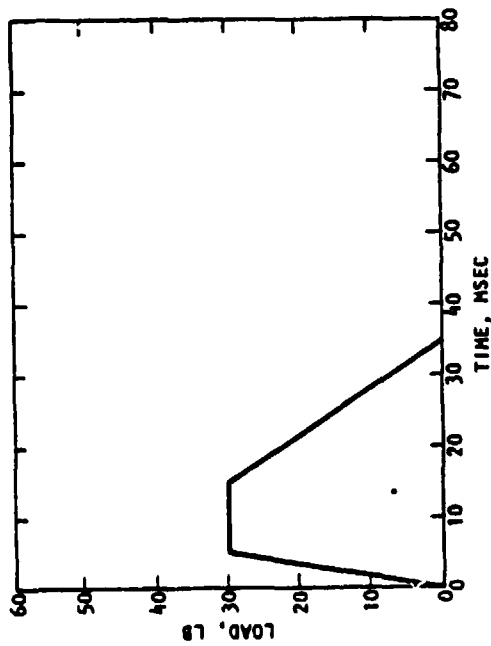


(b) Response at the end



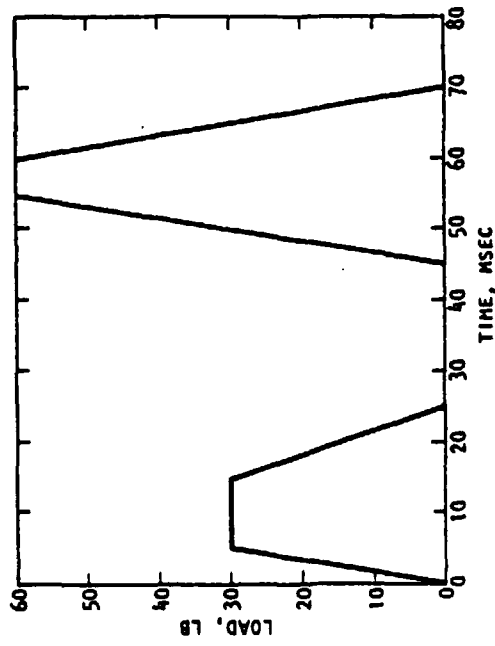
(b) Response at the end

AA 7579



(a) Load history

FIGURE A-3. SUMMARY OF NONLINEAR SPRINGS CHECKOUT RESULTS, CASE 1



(a) Load history

FIGURE A-4. SUMMARY OF NONLINEAR SPRINGS CHECKOUT RESULTS, CASE 2



with only a small recovery of displacement. When the external load has relaxed to the extent that the elasticity of the beam overcomes it, the beam debonds from the nonlinear spring and undergoes free vibration.

Figure A-4a shows the time dependence of the load function used in Case 2, which was designed to test rebonding. The results are shown in Figure A-4b. Debonding occurs at about 30 msec in this case, after which free vibration begins. The free vibration continues until the reapplication of external load at 45 msec. This external load and the inertia of the vibrating beam cause the beam to slam violently into the relaxed spring at the displacement  $\delta_0$  (see Fig. A-1). Temporary equilibrium is found in the vicinity of this displacement until the external load grows large enough to force the beam into Zone 2 of Figure A-1. At this point the stiffness reduces to the virgin loading value, allowing further displacement until a new equilibrium is reached.

The results of these two test cases indicated that the nonlinear spring is performing as intended. Both debonding and rebonding appear to be working correctly. Furthermore, the nonzero equilibrium displacement following a load cycle has been checked and found satisfactory. It is anticipated that these properties, when used in conjunction with dampers and/or concentrated masses, will prove satisfactory in modeling the effects of the soil behind the headwall.



## APPENDIX B

PROCEDURE FOR CALCULATING YIELD MOMENTS  
FOR A REINFORCED-CONCRETE SECTION

The yield moment of a reinforced-concrete cross section is defined as the moment that makes the steel in tension or the concrete in compression reach its yield limit. The reinforcement provided in the headwall section is governed by the former case; therefore, only the derivation for the under-reinforcement case (steel-in-tension yield) is described below.

A typical cross section of a reinforced-concrete section is shown in Figure B-1, and the strain diagram is shown in Figure B-2, where  $A_s$  and  $A'_s$  are the areas of the steel reinforcement in tension and compression, respectively. The strain level in tension steel is  $\epsilon_t$ , in concrete is  $\epsilon_c$ , and in compression steel is  $\epsilon'$ . The strains are related by the following formula:

$$\frac{\epsilon_t}{\epsilon_c} = - \frac{d - Kd}{Kd} = - \frac{1 - K}{K}$$
$$\frac{\epsilon'}{\epsilon_c} = - \frac{d' - Kd}{Kd} = - \frac{\frac{d'}{d} - K}{K} \quad (B-1)$$

The stresses in steel are as follows:

$$\sigma_s = - n \sigma_c \frac{1 - K}{K} = \text{stress in tension steel}$$
$$\sigma'_s = - n \sigma_c \frac{\frac{d'}{d} - K}{K} = \text{stress in compression steel} \quad (B-2)$$

where  $n = \frac{E_s}{E_c}$ , the ratio of modulus of elasticity of steel to concrete.

**Preceding page blank**

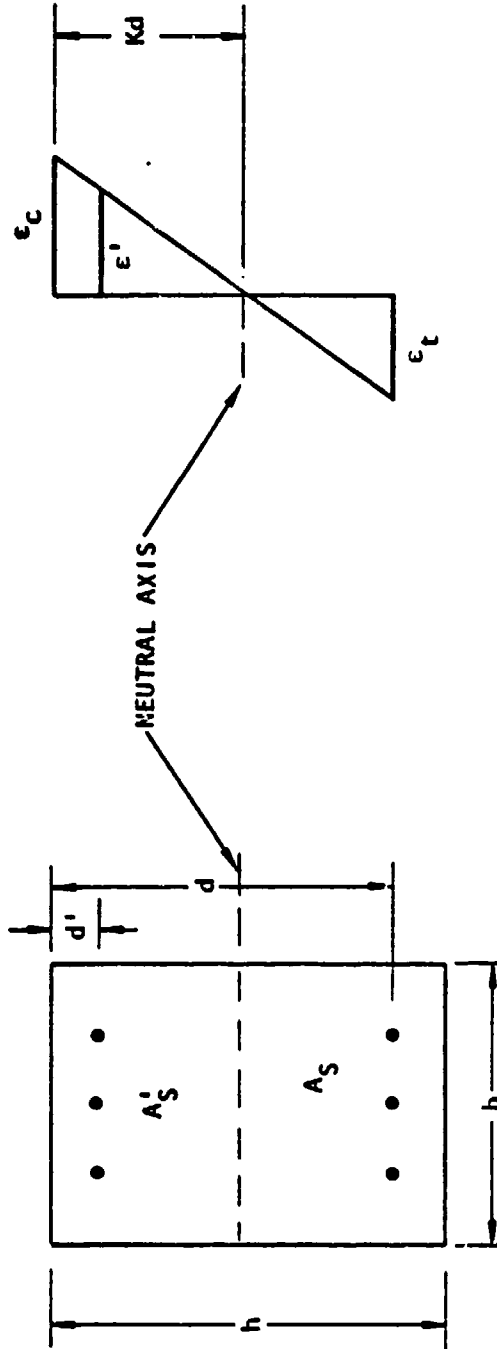


FIGURE B-1. A REINFORCED CONCRETE SECTION

FIGURE B-2. STRAIN DISTRIBUTION ACROSS THE SECTION



Denoting the area of steel as a fraction of the area of the concrete section, i.e.,

$$p = \frac{A_s}{bd}$$

$$p' = \frac{A_s'}{bd} \quad (B-3)$$

the equation of equilibrium becomes

$$\sigma_s A_s + j_s' A_s' + \frac{1}{2} \sigma_c Kbd = 0 \quad (B-4)$$

This can be rewritten after some arrangement into the form

$$K^2 + 2(np + np') K - (2np + 2np' \frac{d'}{d}) = 0$$

Therefore the solution of K becomes

$$K = \sqrt{(2np + 2np' \frac{d'}{d}) + (np + np')^2} - (np + np') \quad (B-5)$$

The yield moment for the underreinforcement case is

$$M = \sigma_s A_s (d - \frac{Kd}{3}) + \sigma_s' A_s' (d' - \frac{Kd}{3})$$

or

$$M = A_s j d \sigma_s \quad (B-6)$$



where

$$j = 1 - \frac{K}{3} + \frac{p'}{p} \frac{(\frac{d'}{d} - K) (\frac{d'}{d} - \frac{K}{3})}{1 - K} \quad (B-7)$$

If the solution of Equation B-5 is such that  $K > \frac{d'}{d}$ , then the stress in compression steel is

$$\sigma_s = 2n\sigma_c \frac{\frac{d'}{d} - K}{K} = 2 \frac{\frac{d'}{d} - K}{1 - K} \sigma_s \quad (B-8)$$

The equation of equilibrium for this case becomes

$$\sigma_s A_s + \sigma_s' A_s' + \frac{1}{2} \sigma_c Kbd - E_c \epsilon' A_s' = 0 \quad (B-9)$$

After some rearrangement, and the use of Equation B-3,  $K$  becomes

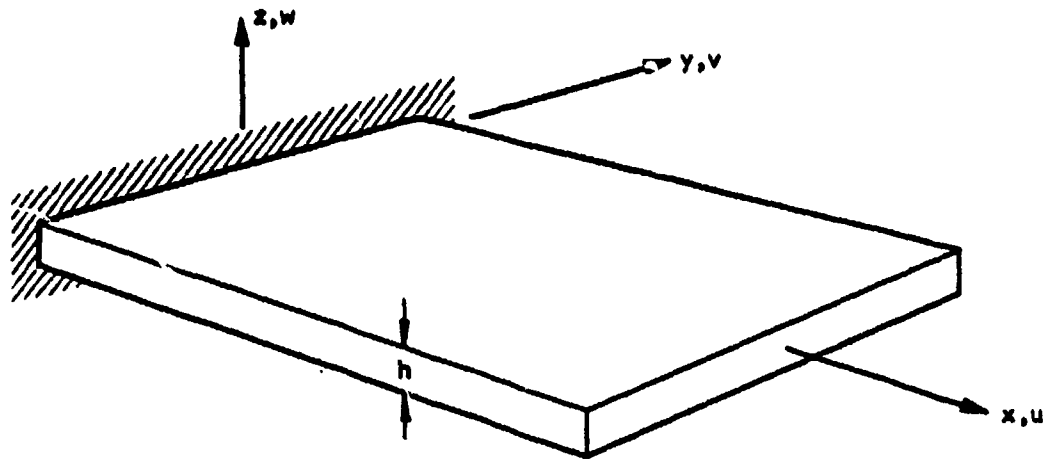
$$K = \sqrt{2[np + (2n - 1)p' \frac{d'}{d}] + [np + (2n - 1)p']^2} - [np + (2n - 1)p'] \quad (B-10)$$

The form of Equation B-6 remains the same except that for this case,  $j$  is defined as

$$j = 1 - \frac{K}{3} - \frac{(2n - 1)K - 2.1 \frac{d'}{d} p'}{n(1 - K)} \frac{p'}{p} (\frac{d'}{d} - \frac{K}{3}) \quad (B-11)$$



## APPENDIX C

PROCEDURE FOR COMPUTING EQUIVALENT MODULI  
FOR A REINFORCED CONCRETE SECTION

REINFORCED CONCRETE STRUCTURE

AA8240

Assume that the displacements in the reinforced concrete structure shown above are in the following form:

$$u(x,y,z) = - \frac{\partial W(x)}{\partial x} z = - W'(x) z$$

$$v(x,y,z) = 0$$

$$w(x,y,z) = W(x)$$

and the strains:

$$\epsilon_{xx} = - \frac{\partial^2 W(x)}{\partial x^2} z = - W''(x) z$$

$$\epsilon_{zz} = \epsilon_{yy} = \epsilon_{xz} = \epsilon_{xy} = \epsilon_{yz} = 0$$



Assuming that the vertical stress  $\sigma_{zz} = 0$

$$(\lambda+2G)\epsilon_{zz} + \lambda(\epsilon_{xx} + \epsilon_{yy}) = 0$$

$$\epsilon_{zz} = -\frac{\lambda}{\lambda+2G}(\epsilon_{xx} + \epsilon_{yy}) = \frac{\lambda}{\lambda+2G} W''(x)z$$

and

$$\begin{aligned}\sigma_{xx} &= (\lambda+2G)\epsilon_{xx} + \lambda\epsilon_{zz} \\ &= \left[ (\lambda+2G) - \frac{\lambda^2}{\lambda+2G} \right] \epsilon_{xx} = \frac{E}{(1-\nu^2)} \epsilon_{xx} = \frac{D}{I} \epsilon_{xx} \\ &= -\frac{D}{I} W''(x)z\end{aligned}$$

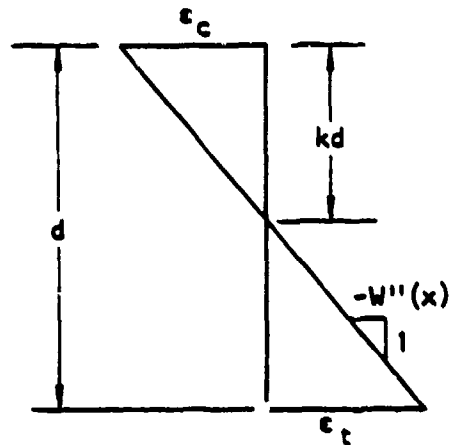
where

$$D = \frac{EI}{1-\nu^2}$$

Now the moment  $M_x$  is given by

$$M_x = -b \int_{-h/2}^{h/2} \sigma_{xx} z dz$$

$$M_x = \frac{bDW''(x)}{I} \int_{-h/2}^{h/2} z^2 dz = DW''(x)$$



STRAIN DISTRIBUTION

From the above strain distribution,

$$W''(x) = \frac{\epsilon_t}{(1-k)d}$$

$$\epsilon_t = (1-k)dW''(x)$$

Moment of the section is then given by

$$M = A_s j d \sigma_s = A_s j d E_s \epsilon_t$$

$$M = A_s j E_s (1-k) d^2 W''(x) = D W''(x)$$

Also

$$D = A_s j E_s (1-k) d^2 = \frac{E I}{(1-\nu^2)}$$

Therefore the effective  $E$  for the concrete section is given by

$$E = \frac{A_s j E_s (1-k) d^2 (1-\nu^2)}{I}$$